Potassium Nitrate Sorbitol Propellant

Experimental Investigation of Solid Propellant Characteristics

M. C. Olde

MSc Thesis Aerospace Engineering

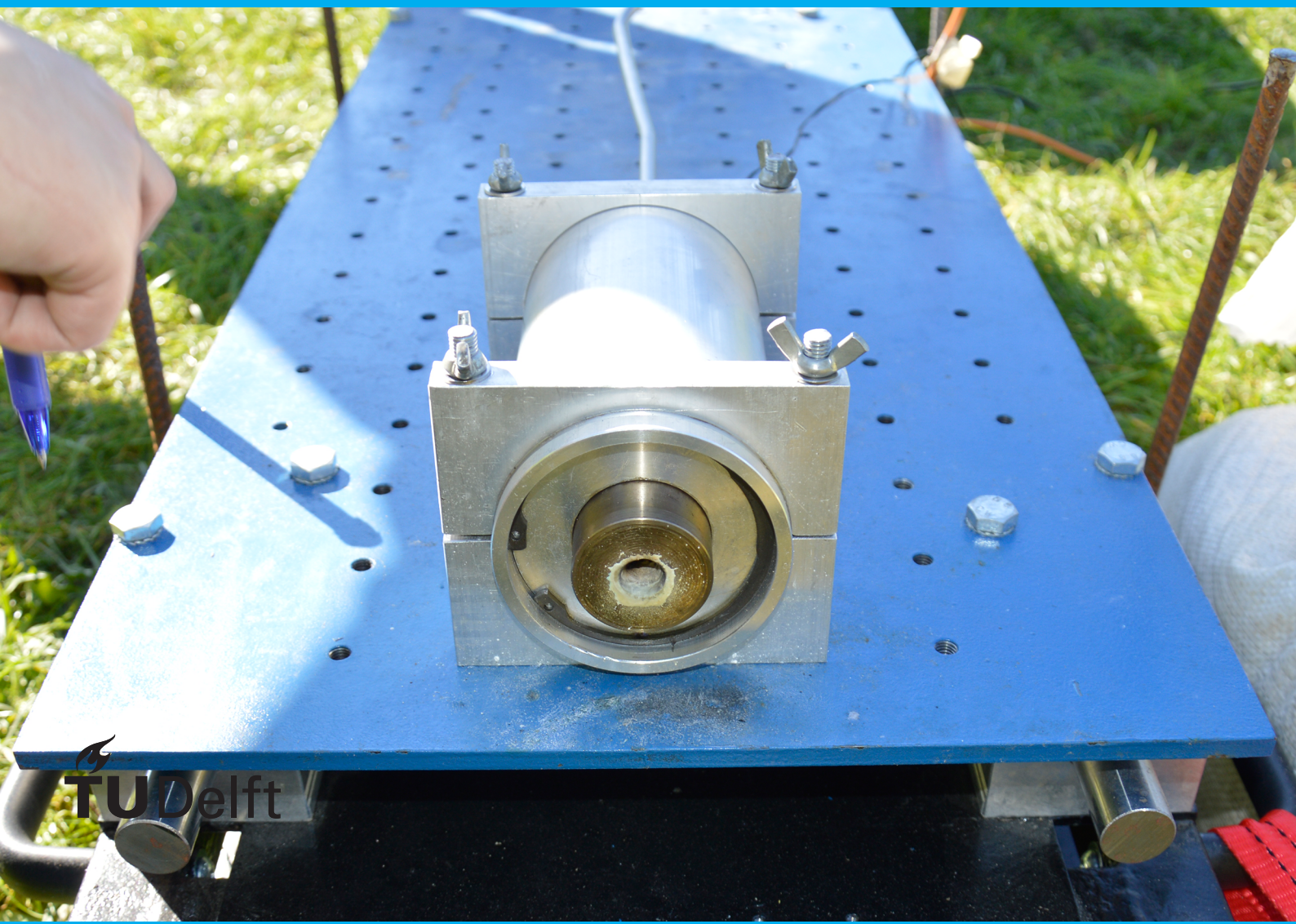

TU Delft

Potassium Nitrate Sorbitol Propellant

Experimental Investigation of Solid Propellant Characteristics

by

M. C. Olde

to obtain the degree of Master of Science
at the Delft University of Technology,
to be defended publicly on Tuesday April 30, 2019 at 14:00.

Student number:	4011058	
Project duration:	June, 2018 – April, 2019	
Thesis committee:	Prof. Dr. E.K.A. Gill,	TU Delft, Chair
	Ir. B. T. C. Zandbergen,	TU Delft, Supervisor
	Ir. R. Noomen,	TU Delft
	Dr. B. S. V. Jyoti,	TU Delft

An electronic version of this thesis is available at http://repository.tudelft.nl/.
Research data and resources of this thesis are available from the author via :
Martin_Olde@hotmail.com.

TU Delft

Summary

KNO_3-Sugar propellants, also known as rocket candy, form a group of simple, cheap and safe solid propellants that are used extensively in student and amateur rocketry communities. One of the most frequently used compositions is KNO_3-sorbitol (KNSB) with a typical 65/35 ratio by mass. This composition is used extensively by Delft Aerospace Rocket Engineering (DARE) for small experimental launches including the record-breaking flight of Stratos I in 2009 to 12.3 km altitude. However, KNSB propellant quality has been inconsistent: propellant density is occasionally below 85% in combination with large surface defects. Besides a very high grain rejection rate this has resulted in several explosive failures of new experimental motors in recent years.

These problems show that the current propellant manufacturing process is insufficiently understood and needs to be significantly improved. In addition the lack of propellant characterisation information challenges the design of new motors; large design margins and low chamber pressures are required, which limit theoretical motor performance. For DARE to improve on its solid propulsion there is therefore a need to investigate the KNSB propellant formulation and to develop means to investigate its ballistic properties. This thesis focuses first on improving the KNSB propellant manufacturing process and secondly on developing and validating a method for the determination of the ballistic properties.

To improve this propellant formulation several experiments were completed which focused on process steps used by several amateur researchers. The first experiment focused on the elimination of volatile components, mostly in the form of moisture, from the propellant mixture. A second experiment evaluated the (pre)heating of moulds and the application of mechanical pressure during curing to further increase propellant density and quality. These experiments required suitable definitions of propellant quality and methods to evaluate these. It was found that moisture, especially in sorbitol, caused the largest decline in propellant density with the application of vacuum the most effective method of removing this contamination. The addition of propellant compression and preheating of the moulds was found on the other hand to only marginally increase propellant density; however the developed tooling resulted in significant improvements in surface quality, geometrical accuracy and a reduction in grain defects.

Based on industry recommendations a Ballistics Evaluation Motor (BEM) was developed that allows determination of performance characteristics and steady regression behaviour over a large pressure range in a single test. Two KNSB propellant variations with different KNO_3 particle size distributions were tested with the BEM at varying ambient temperatures. Problems with the ignition of the fine composition resulted in misfires of the motor. After several changes to the igniter design resulted in more test failures, a Root Cause Analysis (RCA) was completed to identify the cause. This analysis showed that an unfavourable motor geometry, the fast burning igniter/primer mixture and the addition of a surfactant to the fine composition were likely candidates for the observed failures. A propellant ignition experiment was subsequently competed with small propellant samples of varying composition and primers which were ignited using an infrared laser. During this experiment it was determined that the surfactant was the most likely root cause of the misfires.

With the improved fine composition a total of 13 successful BEM tests were completed, which allowed the determination of motor performance and steady regression rates. I_{sp} up to 128 [s], c^* and C_f, were determined for both fine and coarse compositions. The steady regression rates were furthermore determined over a pressure range from 1.0 to 8.0 MPa for the coarse composition, and 1.0-4.0 MPa for the fine composition. These results were compared to KNSB strand burner results found in literature. Together these results validate the BEM design and the method developed to measure the ballistic properties of the KNSB propellant.

Both the obtained results in improving the propellant quality, understanding of its characteristics and the developed methods are a good step forward for DARE solid propulsion research. Several recommendations are however expected to improve the repeatability of BEM tests even further and might enable further, more advanced DARE research into solid propellant.

Preface

This thesis topic was chosen because I wanted to do something practical, however my history with solid propulsion goes back to long before the start of my thesis. I joined DARE's Solid propulsion team in 2016 after a large part of the team at that point had graduated or left. I joined forces with a few enthusiastic second and first year students and together we were going to build the largest solid rocket motor ever developed in DARE. This turned into an extensive introduction to failure analysis, as several failures left craters in the teams confidence. Undaunted by the challenges this led to several years of propellant research and rocket motor design during which I also became active as a safety officer for the society. Problems persisted but due to the interesting challenges, an not in the least my wonderful DARE colleagues, my enthusiasm grew. This led me to choosing the characterisation of solid propellants as my main research topic.

The study of solid propulsion at the TU Delft is however limited to the work in DARE. Looking outside DARE, it proved challenging to find a suitable thesis research project. Propellant ballistics information, a necessary first step for doing any solid propulsion related activities is hard to come by. This is not illogical, it involves extensive test campaigns and careful development of both the propellant manufacturing and its ballistic behaviour. Propellant manufacturing and ballistic information forms the core of the intellectual property for any solid propulsion company.

A solution was found in DARE's own KNO_3-Sorbitol propellant. It not particularly interesting to industry due to its low performance, but has over the years gathered an extensive amateur community. Notable is the work by Richard Nakka to whom I own considerable gratitude. KNO_3-Sorbitol propellant quality in DARE however was not up to spec, with large variations in quality and performance. There was an opportunity to solve several of the persistent Solid propulsion issues in DARE. On top of this it gave me the opportunity to freely share my results with the community and contribute to not only my engineering degree, but also to the work of all these people around the world working on their respective rocket motors and rockets.

Logically this work would not have been possible without support from family and friends, who keep surprising me with their interest in my rocket projects. Explicitly I would also like to thank the DARE safety officers; Felix Kuhnert, Jeije van den Wijngaart, Dion van Strydonck, Stijn Koehler and Tobias Knop for spending countless of days casting propellant and (mis)firing motors. In addition I would like to thank Jurriaan van Slingerland for his help during the laser experiments. Lastly there is of course the rest of DARE and the solid propulsion team in specific; I hope this works can make a difference for the future.

On a different note: my supervisor Barry Zandbergen has proved an excellent supervisor. He is someone who actually read the work I gave him and, after 100 odd pages, will still point out a spelling mistake or error in my calculations. This report was considerably improved by his numerous suggestions and our open discussions. On a similar note I would like to thanks Jyoti Botchu, who got involved in my project a few months after I started. I greatly appreciated the feedback and enthusiasm about my project. Also her practical experience with propellant chemistry proved invaluable when I simply could not get the system to work.

A final thanks is for my girlfriend, she has tolerated my incessant nerding over my rocket projects, but has also helped me persist during my years at the TU Delft. I am convinced this has left me a considerable better person.

M. C. Olde
Delft, April 2019

Glossary

3ME Delft University of Technology, faculty of Mechanical, Maritime and Materials Engineering

AN Ammonium Nitrate

AP Ammonium Perchlorate

APP Aerospace Propulsion Products B.V., a subsidiary of the Ariane Group

BEM Ballistics Evaluation Motor

$BKNO_3$ Boron – Potassium Nitrate

CP Command Post

CRH Critical Relative Humidity

DAQ Data Acquisition System

DARE Delft Aerospace Rocket Engineering

FEM Finite Element Analysis

K_2CO_3 Potassium Carbonate

KNDX KNO_3-Dextrose Propellant

KNO_3 Potassium Nitrate

KNSB KNO_3-Sorbitol Propellant

KNSU KNO_3-Sucrose Propellant

MEOP Main Engine Operating Pressure

NEM Net Explosive Mass

NERO NEderlandse vereniging voor Raket Onderzoek

NIST National Institute of Standards and Technology

NTC Nitro Cellulose

O/F Oxidiser to Fuel Ratio

PPE Personal Protective Equipment

PSD Particle Size Distribution

RCA Root Cause Analysis

RPA Rocket Propulsion Analysis, software package

RUD Rapid Unintended Disassembly, explosive failure

SRM Solid Rocket Motor

SRP Small Rocket Program, DARE first year project

STP Standard Temperature and Pressure

TRP Thermal Rocket Propulsion Practical

TU Delft Delft University of Technology

VRO Vlaamse Raket Organisatie

VSV Vliegtuigbouwkundige Studievereniging ’Leonardo Da Vinci’

List of Symbols

A_b	Burning Surface Area	[m^2]
A_e	Nozzle Exit Area	[m^2]
A_t	Nozzle Throat Area	[m^2]
A_f	Surface Area Flaws	[m^2]
A_{id}	Ideal Grain Surface Area	[m^2]
C_f^0	Characteristic Thrust Coeficient	[-]
C_f	Thrust Coeficient	[-]
F	Thrust	[N]
I_A	Surface Quality Index	[-]
I_ρ	Density Quality Index	[-]
I_{sp}	Propellant Specific Impulse	[s]
I_{tot}	Total Impulse	[Ns]
L	Grain Lenght	[m]
M_0	Sample Initial Mass	[kg]
M_{H2O}	Sample Moisture Content	[kg]
M_c	Motor Casing Mass	[kg]
M_{grain}	Mass of Grain	[kg]
M_{liner}	Mass of Liner	[kg]
M_{post}	Motor Burnout Weight	[kg]
M_{pre}	Motor Loaded Weight	[kg]
M_p	Vehicle Propellant Mass	[kg]
M_{res}	Propellant Residue Weight	[kg]
M_s	Sample Mass	[kg]
M_v	Vehicle Mass	[kg]
P_c	Chamber Pressure	[Pa]
P_e	Ambient Pressure	[Pa]
P_e	Nozzle Exhaust Pressure	[Pa]
P_{ref}	Burnrate Reference Pressure	[Pa]
P_{req}	Required Laser Power	[W]
P_{test}	Delivered Laser Power	[W]
R_{in}	Grain Port Radius	[m]
R_{out}	Grain Outside Radius	[m]
R	Specific Gas Constant	[J/kgK]
T_c	Chamber Temperature	[K]
T_f	Propellant Firing Temperature	[K]
T_{ref}	Reference Temperature, 273.15 [K]	[K]
V_c	Chamber Volume	[m^3]
V_{eff}	Effective Exhaust Velocity	[m/s]
Γ	van der Kerckhoven Constant	[-]
Φ	Radiant Flux	[W/m^2]
α	Moisture Reduction Rate	[1/s,1/days]
$\dot{m}$	massflow	[kg/s]
η_F	Nozzle Quality	[-]
η_b	Combustion Quality	[-]
γ	Adiabatic Index	[-]
ρ_{id}	Ideal Propellant Density	[kg/m^3]
ρ_l	Liner Linear Density	[kg/m]
ρ_p	Actual Propellant Density	[kg/m^3]
σ_r	Burnrate Fit Standard Deviation	[m/s]

ξ_{H2O}	Moisture Mass Fraction	[-]
ξ_{PM}	Propellant Mass Fraction	[-]
a, b, n	regression rate fitting constants	[m/s,m/s,-]
c^*	Characteristic Exhaust Velocity	[m/s]
e_{fit}	RMS Fitting Error	[-]
g_0	Standard Gravitational acceleration, 9.81 [m/s^2]	[m/s^2]
l_{liner}	Inhibitor Lenght	[m]
r	regression rate	[m/s]
t_0	Igniter Firing Time	[s]
t_b	Burn Time ($t_e - t_i$)	[s]
t_e	End of Burntime, Burnout	[s]
t_i	Start of Burntime	[s]
t_{id}	Ignition Delay	[s]
w	Burned Webb thickness	[kg]

Contents

1

Introduction

This MSc thesis describes the engineering process, developed methods, results and analysis of several experiments done on Potassium Nitrate - Sorbitol solid rocket propellant. This propellant has been extensively used by Delft Aerospace Rocket Engineering (DARE) a student rocket community connected to Delft University of Technology (TU Delft). Several standard motors have been developed in DARE which offer cheap reusable motors for launches of experimental rockets up to 1-2 [km]. The propellant, due to its relatively low performance has however never been thoroughly investigated in DARE, which has resulted, among others, in several test failures of experimental solid rocket motors (SRM)[56].

To identify the work needed to solve these problems a literature study was completed by the author in March 2018 [16]. The goal of this literature study was to determine what could be improved about the propellant formulation based on: a review of available data and research done in DARE, available research by other (amateur) researchers, and scientific literature. Potassium Nitrate - sugar propellants are widely used in the amateur community due to its low cost, use of nontoxic ingredients and simplicity. These sugar propellants have however seen limited use in the academic community as the performance is low compared to most commercially used solid propellants such as Ammonium Perchlorate (AP), Ammonium Nitrate (AN) or nitrocellulose (NTC) based propellants. The literature study resulted in a list of experiments to solve several of the issues that DARE had with their Potassium Nitrate-Sorbitol (KNSB) propellant. This MSc thesis describes several of those experiments and the methods developed to determine propellant ballistic properties.

The first two chapters of this thesis could together be considered the introduction as they provide some insight into propellant manufacturing and characterisation of the KNSB propellant and ingredients. These properties provide an essential framework preliminary to the two main parts of this thesis which describe in detail the experiments done.

In this chapter; first in section 1.1 the research context and the summary of results of the literature study are presented. Secondly the research goal and research questions are provided in section 1.3. In section 1.4 the potential gains are shown by comparing trajectories of a DARE rocket under development to the gains that might be achieved.

1.1. Research Context

Although performance of KNO_3-sugar propellant is typically low compared to commercially used propellants (an I_{sp} of around 110-130 [s] compared to 220-250 [s] respectively [19],[63]) it has several interesting properties that make it ideal for small scale and amateur experimentation. Examples of work on KNO_3-sugar propellants are the extensive work by Richard Nakka [63],[12] and work done by for instance the NEderlandse vereniging voor Raket Onderzoek (NERO) or the Vlaamse vereniging voor Raket Onderzoek (VRO). Additionally several larger projects have also started the use KNO_3-sugar propellants; getting optimal performance from this simple propellant is exactly the reason why, for instance, Sugar Shot to Space was formed [69].

In academics small motors based on KNO_3-sugar propellant were used to study base flow interaction inside a supersonic wind tunnel at the TU Delft [3]. Additionally the propellant is used frequently for demonstrations and student practicals [57]. KNO_3-sugar propellant is one of the few experimental propellants allowed on Tripoli launch events, one of the large international rocketry associations [59].

1.1.1. Solid Rocket Motors

Solid rocket motors (SRM) consist of pressure vessels partially filled with solid rocket propellants. During combustion the exposed grain surfaces burn inward to produce hot gasses. These combustion gasses are accelerated through a nozzle in order to produce thrust. The lack of moving parts makes the solid rocket motor easier to operate than liquid or hybrid propulsion systems. As a solid motor cannot generally be controlled after ignition, the grain geometry is carefully designed to produce the desirable pressure and thrust behaviour while balancing other design requirements. A typical solid rocket motor is shown in figure 1.1.

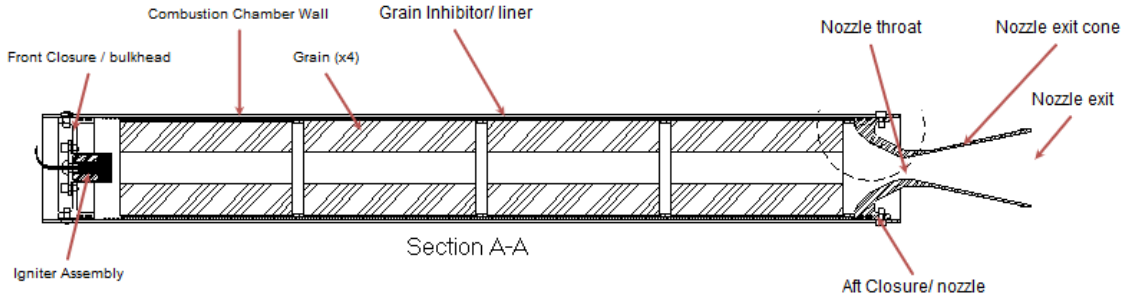

Figure 1.1: A typical amateur rocket motor as adapted from *Richard Nakka* and also in use in DARE.

As shown in figure 1.1 several propellant grains are loaded in a cylindrical pressure vessel closed on one end by a pressure bulkhead (including possibly an igniter assembly) and closed at the other end by a converging/ diverging nozzle. Propellant with density ρ_p [kg/m^3] burns perpendicular to the grain surface A_b [m^2] with regression rate r (typically several [mm/s]). The hot gasses are then accelerated in the nozzle where thermal energy is converted to linear momentum. Mass flow from the burning areas integrated over the motor volume V_c [m^3]is described by equation 1.1.

$$\dot{m} = \int_{V_c} \rho_p A_b(s) r(s) ds \tag{1.1}$$

Accepting significant simplifications from reality, especially with respect to the ignition transient and burnout behaviour, the rocket motor can be described by reasonably simple models [20, 24]. However central to the design of any solid rocket motor is the propellant characterisation data which includes, for a specified manufacturing method: propellant combustion data, regression rates information, density, handling information and ageing characteristics. Combustion of solid propellants includes complex reactions as the propellant goes from the solid to gaseous phases. Analytical models of this process are still hardly able to predict this process even in the rarest of cases. The empirical nature of most of this data and the sensitivity with respect to the manufacturing method makes propellant characterisation an expensive and time consuming effort [20].

1.1.2. Potassium Nitrate Sugar Propellants

The most popular Potassium Nitrate - Sugar propellants typically consist of KNO_3 powder that is suspended in a matrix of sugar with a mixture ratio around 65/35 by mass. The relatively high ignition temperature (in excess of 300 [°C]) allows the heating of the sugar to a slurry at around 110-185 [°C] after which it is cast in a desirable shape. After cooling the propellant forms hard, somewhat brittle grains that can be used in solid rocket motors. Commonly used sugars are for instance Sucrose and Dextrose. Sorbitol ($C_6H_14O_6$) is a poly alcohol that is typically used as a sugar replacement in candy

or soft drinks. The mixtures of KNO_3-Sucrose, KNO_3-Dextrose or KNO_3-Sorbitol are typically abbreviated to KNSU, KNDX and KNSB respectively. Although specific impulse of KNSB is several seconds lower than with the other sugars, several practical aspects make it a commonly used variation. Sorbitol does not caramelise giving it an effectively infinite pot life. In addition the lower melting temperature of Sorbitol (110 [°C]) versus for instance sucrose 185 [°C] [46] adds a significant safety margin when making the propellant.

The use of KNSB propellants by ”amateurs” is a trade between low risk, low toxicity and above all availability of the constituents on one hand, and a substantial loss in performance on the other [16]. The primary advantage of KNSB propellant compared to commercially used AN or AP propellants are thus the following:

- *Accessibility:* The compounds, especially the oxidizer, are available in relatively large quantities from the food industry.
- *Safety:* The propellant has a relatively high ignition temperature (in excess of 300 [°C]) and does not involve toxic substances, which makes it a relatively safe propellant to work with.
- *Cost:* The cost of KNO_3 and Sorbitol is significantly lower at about $3,50$ [€/kg] compared to around 25 [€/kg] for AN or AP propellants [61].
- *Simplicity:* The production of small grains of KNSB propellant is straightforward utilising standard kitchen appliances [65, 68]. For most commercial, composite propellants special vacuum chambers and industrial mixing equipment is necessary [20].

The biggest drawbacks are the following:

- *Performance:* The thermodynamic ideal performance, assuming no losses, is only around 160 [s], [63] of I_{sp} compared to around $220 - 250$ [s] of I_{sp} for other, better performing industrial propellants [19].
- *2-phase losses:* About 40 % of exhaust products is in the form of liquid droplets of potassium carbonate (K_2CO_3) which do not perform expansion work in the nozzle, are not accelerated as easily and do not readily release thermal energy to the surrounding gasses. This loss factor accounts for a loss of at least 30 seconds of I_{sp} from the theoretical 160 [s]. [63]
- *Susceptibility to Defects:* The propellant is cast around 120 degrees Celsius and shrinks when it cools down to room temperature [65, 68]. This can cause significant thermal stresses. Additionally after curing the propellant is relatively brittle which makes the propellant susceptible to handling and thermal shocks resulting in cracks and subsequent engine failure.

1.1.3. Delft Aerospace Rocket Engineering

Delft Aerospace Rocket Engineering is one of the largest student rocketry societies in the world. It consists of 150+ (under) graduate students that work on all aspects of rocket science including but not limited to propulsion, structures, electronics, recovery systems and operations. The society was founded in 2001 as a committee under the Vliegtuigbouwkundige Vereniging ’Leonardo Da Vinci’ (VSV), the association for aerospace engineering students at Delft University of Technology (TU Delft). The society has been a separate legal entity since 2010.

University support that includes access to offices and workshops, affordable tuition, and a conductive legal framework have allowed DARE to independently organise multiple launches every year. Next to this DARE is one of the only student societies that has launched rockets from multiple international launch sites. DARE has on occasion held the (European) altitude record with Stratos I (2009, 12.3 km) and Stratos II (2015, 21.5 km). The current aim is, in competition with a large number of other (under) graduate groups around the world, to be the first student team to reach space [52]. To this end Stratos III shown in figure 1.2 was launched from Spain in the summer of 2018. As this rocket did not reach the intended altitude Stratos IV, a design iteration of Stratos III, is planned for a space attempt in summer 2019.

As a student team DARE has contributed to several scientific publications. Most of this research was performed as part of MSc graduation work performed at DARE. This means that for MSc students

Figure 1.2: Stratos III launch crew with rocket in the summer of 2018. Courtesy to Jurriaan Brobbel.

practical propulsion and rocket flight experiments are possible even though the aerospace faculty itself does not have large scale rocket propulsion programs. On one hand this offers the students a relative flexibility as DARE has over the years acquired its own measurement equipment and hardware, and students can produce their own components, which means that design modifications can be made rapidly at limited expense. On the other hand all scientific work in DARE is performed within the constraints and limitations of a student organisation without access to professional chemical laboratories or test facilities.

1.2. Review of Past Research

As was mentioned several standard motors with KNSB have been developed in DARE which are routinely used for flight tests of small experimental rockets. Several larger motors up to 15 [kNs] were developed with this solid propellant which led, among others, to the successful launch of Stratos I, a two stage sounding rocket that broke the student altitude record in 2009 [21]. Subsequent developments in DARE with KNSB propellant have however shown that insufficient knowledge exists within DARE to reliably design and build larger KNSB rocket motors [11] [56].

The review of DARE's current KNSB propulsion technology indicates that performance of most DARE SRM's is below the I_{sp} performance reported by other authors[16]. Theoretical performance is generally well described with isentropic relations when corrected for 2-phase losses due to condensed K_2CO_3. The ideal sea level I_{sp}, corrected for 2-phase losses at the main engine oeprating pressure (MEOP) of 2.0 [MPa] is 110 [s] and increases to 126 [s] at 6.895 [MPa] (1000 [Psi]). However several tests conducted in DARE [21] and by other amateur researchers [63] [60] have suggested performance up to 130 [s], slightly above the estimated maximum.

A first important conclusion from the literature study is that for DARE to perform academic research on their propulsion systems the quality of reporting, design traceability and configuration control needs to be significantly improved. In the thesis work of both [21] and [11] key numbers, technical drawings or used sources where missing that made it impossible to reproduce parts of their work or reliably take their designs to continue research.

In conclusion to the literature study a research program was proposed with KNSB propellant that can be categorised into three categories; improved quality of the propellant, improved propellant characterisation and improved motor performance, of which the first two topics were investigated during this thesis. Large experimental rocket motor's in DARE have a very high failure rate which is expected to be solved largely with enhanced propellant quality through changes in the production process and increased understanding of propellant properties. Secondly overall motor performance can be increased by narrowing the required design safety factors (typically between 3-5) and increasing the motor operating pressure. This requires the development of a ballistics evaluation method to investigate the propellant performance and propellant regression rate as function of the chamber pressure and propellant temperature. In summary the following conclusions were drawn in the literature study [16] and can be seen as the starting point for this thesis:

1. *Improved propellant quality:,* is key to increasing the reliability and repeatability of DARE solid rocket motors. The current heritage manufacturing method of KNSB propellant is from 2011 [68] but results in large variations in propellant density and high (>30-50%) propellant rejection rates due to voids, cracks or other deviations in grain geometry. An comparative study was performed of the propellant manufacturing strategies by several other amateur researchers, which identified three specific process steps in combination with changes in tooling. In addition acceptance criteria were proposed to evaluate manufactured grains. The focus of the casting research is the following:

   (a) *Propellant Density,* The density of grains is often below 85% of the theoretical value (1841 [kg/m^3]) while other researchers report densities between 95-98%. Besides a possible link between grain quality and propellant density, the low propellant density requires larger, heavier motors to achieve the desirable altitudes and velocities. Several potential causes such as thermal contraction and contamination with volatile components such as moisture were identified. Similarly solutions were found in the work of other amateur researchers such as the application of vacuum, preheating of casting moulds and application of mechanical compression. It needs to be understood why the current KNSB density is so poor for propellant made in DARE and how this can be prevented.

   (b) *Propellant Quality,* Large defects result in a very high rejection rate for DARE propellant grains and, in case of poor quality control, a high risk of motor failures. It needs to be understood what manufacturing steps need to be controlled to obtain the desired propellant quality. This requires more insight into the current manufacturing process and suitable definitions of grain quality and propellant formulation so that suitable checks can be made before motor firing.

2. *Improved propellant characterisation,* is a blanket term for many of the propellant specific properties that define its behaviour inside the motor environment. This typically includes items such as the specific impulse, characteristic velocity and the propellant burnrate as function of chamber pressure and propellant temperature. The steady burn rate of a solid propellant describes the speed at which a propellant surface combusts inward. Due to the high complexity of the thermodynamic and chemical processes involved this needs to be determined experimentally. Furthermore, as the regression rate determines to a large extend the mass transfer inside the rocket motor the accurate determination is key to predicting motor thrust and operating pressure [19]. A method therefore needs to be developed to measure motor performance and the steady regression rate of solid propellants under the desired operating conditions. The focus of the ballistics research is the following:

   (a) *Accurate Performance Predictions.* As was mentioned the performance of KNSB motors agrees reasonably well with isentropic models such as found in [19, 24] assuming some empirical constants for combustion and nozzle efficiency. Various ways exist to measure the motor performance with the most common the ballistics evaluation motor (BEM) [4]. Other methods, such as the strand burner allow measurement of some of the ballistic properties but are less representative of the actual motor environment.

   (b) *Steady Regression Rate,* As mentioned the regression rate of propellants is an empirical property that is a function of propellant formulation, chamber pressure and propellant temperature. [21], [63] and [6] all provide relations for the propellant burnrate of KNSB propellant

however it is unclear how well these agree with the current DARE KNSB composition or what uncertainty might still be expected.

A progressive burning BEM was found in literature that allows the measurement of the steady regression rate over a large pressure range in a single test [10]. This trades the required number of tests and amount of necessary hardware for a possible reduction in measurement accuracy. A review of other KNSB motors suggest that operating pressures between 2-7.5 [MPa] would be a desirable range while firing temperatures between 0-30 [°C] might be realistically encountered.

Together these steps will allow DARE to significantly improve on its propellant formulation, making the motors more reliable while reducing the amount of rejected grains. In addition it would allow DARE to significantly increase the performance of its KNSB motors through a reduction of the design safety margins, increase in propellant mass for a given motor, and an increase in motor chamber pressure.

1.3. Research Design

This MSc thesis project aims to provide DARE, the scientific community, and (amateur) rocket engineers with the experimental data to reliably design KNSB solid rocket motors by performing several characterisation experiments and by thoroughly investigating the formulation of the KNSB propellant. Key problem areas include: low propellant density and missing or incomplete propellant characterisation data such as the propellant burnrate. This leads to the inability to accurately predict performance of the solid rocket motor designed in DARE.

To improve KNSB propellant formulation through a thorough investigation of the KNSB propellant manufacturing method and the determination of several key propellant properties such as the burnrate and the measurement of KNSB propellant performance.

Sub goals defined for this thesis are:

- To provide DARE and the (amateur) research community with the recommended production method for KNSB propellant by combining practices and recommendations from DARE and the (amateur) research community.
- To provide DARE and the (amateur) research community with a complete and validated data set of KNSB propellant, that allows them to design and build reliable, high performance KNSB based solid rocket motors, by experimental investigation and analysis of the KNSB propellant.
- To develop a ballistics research motor that allows the determination of KNSB propellant performance and regression rates as function of the motor environment by designing, building, testing and analysing a BEM system and data regression method.

1.3.1. Research Questions

A proposal for the research questions was made in the Thesis proposal, the questions below were adapted from this list. This involved changes that were made to the research plan due to time constraints but also new research directions and experiments that were not foreseen at the start of the project.

1. What is the most effective manufacturing method for KNSB propellant to obtain good quality propellant grains with a reject rate below 5%, a density larger than 95% of theoretical, and consistent ballistic behaviour?

   (a) How should the KNSB formulation be described to achieve the desired propellant quality and consistent firing results?
   (b) Of the various out-gassing strategies: application of vacuum [55], sustained heating [63] [6] or storage with desiccant [63] what is the effect on known impurities (H_2O) on the KNSB propellant and how does it affect propellant quality and density?
   (c) Does preheating the moulds similar to [63] positively affect propellant quality?
   (d) What is the effect of applying mechanical compression and what is its effect on propellant density and quality?

2. What are the performance and burnrate characteristics of KNSB propellant?
   (a) What is the measured performance of KNSB rocket motors and how is this influenced by propellant composition and chamber pressure?
   (b) How well is KNSB propellant performance predicted by chemical equilibrium tools such as RPA [50] and what corrections should be used when designing KNSB motors?
   (c) How accurate are the burn rate properties measured by [63],[6], and how well do they describe the DARE KNSB propellant inside the SRM environment?
   (d) What are the ignition and combustion characteristics of KNSB propellant and how are they affected by the propellant composition?
   (e) What are the performance and burnrate characteristics of KNSB propellant?

3. Can a linearly progressive ballistics evaluation motor be used to determine the KNSB propellant characteristics and how does this method compare to other ballistic analysis methods?
   (a) What repeatability in terms of performance and regression rates is found for BEM tests and what drives the reproducability?
   (b) How does the result compare to strand-burner results from other authors?

As this thesis study revolves around KNSB propellant an important first step is a description of the propellant formulation including the used ingredients and process steps used in DARE. This can be seen as part of the introduction and constitutes chapter 2. With the addition of a section on working safety and performance this chapter aims to provide a complete overview of the KNSB propellant formulation.

Two casting experiments are subsequently performed to look at the three proposed changes to the KNSB production method and come to an improved propellant manufacturing. The first experiment described in chapter 3 is to investigate moisture contamination in the KNSB propellant and compare strategies to remove this. Strategies that will be evaluated are the application of vacuum on the molten propellant, storage with desiccant and continued heating of the propellant mixture. The out-gassing methods are then compared in terms of their success of removing moisture but also with respect to practical aspects.

A second experiment, described in chapter 4 consists of applying mechanical compression to and preheating of casting moulds to further improve propellant density and quality. The resulting grains of the second experiment will subsequently be used to evaluate the quality criteria proposed during the literature study.

Lastly the performance and regression experiments are described in part II, chapters 5 and 6. This is closely tied to the development of the ballistic evaluation motor BEM for which the detailed design is described in more detail in appendix E. Ignition problems during its development prompted changes to the BEM igniter which culminated in a laser ignition experiment described in chapter 5. With these problems solved a number of KNSB grains were fired with the BEM at varying chamber pressure and grain temperature. With this data the performance and regression rates was estimated of the KNSB propellant. Furthermore the grains produced with the developed production method provided validation for the method and give further insight into the propellant formulation and motor repeatability.

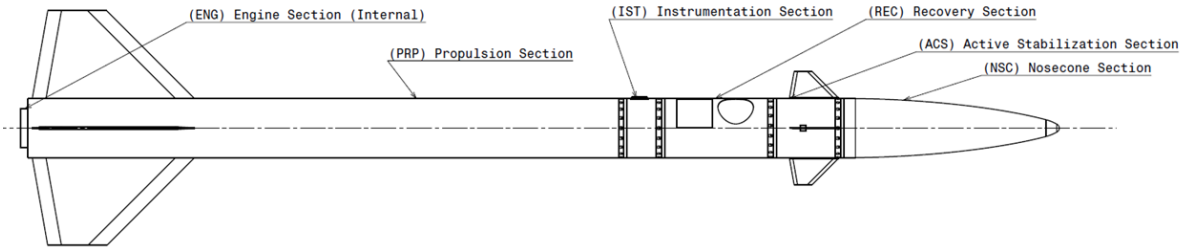

Figure 1.3: Aether reference vehicle under development by DARE which is to demonstrate supersonic attitude control, a high speed recovery system and a new KNSB based propulsion system.

1.4. Conceptual Rocket Model

As was described in the literature study the proposed research offers the possibility to significantly improve the performance of DARE solid propulsion. Although the KNSB propellant has a relatively low performance compared to DARE's hybrid motors (200-220 [s] of I_{sp} [52]) the benefits of solid motors, especially for smaller research projects is considerable. In this thesis several improvements to the KNSB formulation are investigated such as:

1. *Increase in the propellant density,* which is currently occasionally below 85% compared to the theoretical value of 1841 [kg/m^3] while work from other amateur researchers suggest that densities of 95-98% are possible.

2. *Increase in chamber pressure,* which for current DARE motors is between 1.5-2.8 [MPa] due to the limited burnrate information available on the DARE KNSB formulation. At higher chamber pressures and higher nozzle expansion ratios the specific impulse increases considerably. At the same time shorter burn times will reduce gravity losses, increasing maximum velocities reached.

3. *Decrease in engineering margins,* would allow lighter motors to be developed. Currently in DARE solid rocket motor casing have safety factors of 2-3 on the maximum expected operating pressure which is calculated with a 25% margin. If the maximum operating pressure is more accurately predicted and repeatably demonstrated during static firings the uncertainty could be reduced perhaps to 5% and the safety factors to 1.5.

To evaluate these changes a rocket model developed for the coarse WB46060, *Engineering Optimisation* is used to estimate the maximum altitude and flight velocity reached in terms of these improvements. This is based on the Aether supersonic demonstrator vehicle under development in DARE and shown in figure 1.3. It should be kept in mind that potential improvements in reliability are difficult to quantify in terms of altitude or velocity reached.

Five cases will be evaluated; 1) the nominal case with the current technology, 2) a case with the nominal propellant density increased to 95%, 3) with the nominal chamber pressure at 7 [MPa] instead of 2.5 [MPa], 4) with the casing design load case decreased from $P_c \times 130\% \times 2$ to $P_c \times 105\% \times 1.5$, and 5) with the combination of all of the above.

Maximum flight velocity and altitude is estimated using a simple trajectory model developed for engineering optimisation [15] that accounts for drag and gravity losses. The trajectory assumes a 2D flight solving the equation of motion along the flight path and for the flight path angle ($\gamma_0 = 85$ [°]). Constant parameters and simulation results are provided in table 1.1. The motor is assumed to be filled with propellant for approximately 80% of its volume with the casing weight being determined purely by hoop stress of the aluminium pressure vessel and an additional 2.5 [kg] for nozzle and forward bulkhead. Grain design is such that approximately neutral burning Bates grains are used with a variation of around 10% between $P_{c,max}$ and $\bar{P_c}$. In addition the motor performance assumes a combustion and nozzle quality of 0.9 [-] both which are similar to the values reported in literature. Together the empty vehicle mass M_v, empty motor mass M_c and propellant mass M_p constitute the takeoff weight of the vehicle in [kg].

		case (1)	case (2)		case (3)		case 4)		case (5)	
variable	unit	value		Δ[%]		Δ[%]		Δ[%]		Δ[%]
Vehicle Mass	[kg]	38								
Casing Mass	[kg]	6.65	6.64	120	15.58	234	5	75	10.17	153
Propellant Mass	[kg]	33.09	36.99	112	33.09	100	33.09	100	36.99	112
Takeoff Mass	[kg]	77.75	81.63	105	86.67	111	76.09	98	85.16	110
Burnout Mass	[kg]	44.66	44.64	100	53.58	120	43	96	48.17	108
Burn time	[s]	6.01	6.0	100	4.84	81	6.01	100	4.82	80
$P_{c,max}$	[MPa]	2.48	2.48	100	7.24	81	2.48	100	7.28	80
A_e/A_t	[-]	4.78	4.78	100	11.28	236	4.78	100	11.28	236
$\bar{I_{tot}}$	[kNs]	36.0	40.2	112	40.42	112	35.98	100	45.2	125.6
$\bar{I_{sp}}$	[s]	111	111	100	124	112	111	100	125	112
v_{max}	[m/s]	422	452	107	430	102	429	102	492	117
h_{max}	[km]	5.84	6.11	105	5.98	102	5.85	100	6.36	109

Table 1.1: Estimated effect of propellant improvements on a reference vehicle's performance. (1) Nominal performance, (2) increased propellant density, 85% to 95%, (3) increased chamber pressure 2.5 [MPa] to 7.5 [MPa], (4) reduced casing safety margins 2.6 to 1.575 and (5) combined improvements.

It can be seen in table that increasing propellant density, motor performance through a higher chamber pressure, and decreasing the safety margins combined can increase the final flight velocity by 17% compared to the nominal design. A large portion of the performance increase due to the higher chamber pressure ends up in the increased chamber mass which means that the design chamber pressure could be optimised more closely to obtain the maximum flight velocity. In addition even though the total motor empty mass decreases by 25% it has only a marginal effect on the total launch weight. As such it is to be expected that a lighter, minimal diameter rocket would see considerably larger improvements in maximum flight velocity.

Lastly the substantial increase in reliability by increasing propellant density and improving the propellant characterisation data is not reflected by the simulations; with the test failures over the last few years it is to be expected that even without the performance increases it is worth wile to improve the KNSB propellant formulation.

2

Potassium Nitrate-Sorbitol Propellant

As this thesis revolves around the formulation of Potassium Nitrate (KNO_3) Sorbitol ($C_6H_{14}O_6$) propellant, this chapter is used to describe the propellant formulation used. This includes a short overview of the propellant performance and ideal combustion characteristics, a description of the ingredients used in this study and a step by step explanation of the manufacturing steps as used in DARE. This chapter is to introduce the base manufacturing steps for KNSB propellant as it was at the start of this thesis with references to how this formulation was improved during this thesis. This allows the subsequent chapters to focus directly on the experiments done with KNSB propellant and collects all formulation information into a single chapter.

In section 2.1 the basic performance parameters are provided including a brief discussion on the propellant mixture ratio. Subsequently in section 2.2 the ingredient selection followed by propellant manufacturing in section 2.3 is discussed. In the last section safety is discussed briefly.

2.1. Propellant Theoretical Performance

The primary goal of a (solid) rocket propellant is to deliver thrust [N] by expelling a high velocity exhaust. As the propellant itself needs to be accelerated with the vehicle the most often used measure of propellant performance is in terms of specific impulse $I_{sp,is}$ [s] given in equation 2.1 with a further separation between the characteristic velocity c_{is}^* [m/s] which is a measure of combustion performance excluding the effect of the nozzle, which contribution is given by the thrust coefficient $C_{f,is}$ [-]. In this work the subscript 'is' is used to denote ideal isentropic performance.

To determine the quality of a system typically a nozzle quality $\eta_F = C_f/C_{f,is}$ [-] and combustion quality, $\eta_b = c^*/c_{is}^*$ are used to describe the ratios of realised performance to ideal isentropic performance.

$$I_{sp,is} = \frac{V_{eff,is}}{g_0} = \frac{1}{g_0} c_{is}^* C_{f,is} = \frac{1}{g_0} \frac{P_c A_t}{\dot{m}} \cdot \frac{F_{is}}{P_c A_t} \tag{2.1}$$

c_{th}^* [m/s] can be calculated with equation 2.2. In this equation Γ [-] is the van Kerckhoven function, R and T_c the specific heat [J/kgK] and combustion temperature [K] respectively. On the left hand side P_c, A_t and $\dot{m}$ are the chamber pressure [Pa], nozzle throat area [m^2] and mass-flow [kg/s], all instantaneous values.

$$c_{is}^* = \frac{1}{\Gamma}\sqrt{RT_c} = \frac{P_c A_t}{\dot{m}} \tag{2.2}$$

The nozzle thrust coefficient is given in equation 2.3. A distinction is made between the characteristic thrust coefficient, C_f° and thrust coefficient C_f corrected for pressure thrust. When $P_e = P_a$, the case of ideal expansion, $C_f^\circ = C_f$, while the case with $P_a = 0$ gives vacuum performance. The characteristic thrust coefficient is subsequently given in equation 2.4.

$$C_{f,is} = C_{f,is}^0 + \left(\frac{P_e - P_a}{P_c}\right)\frac{A_e}{A_t} = \frac{F_t}{P_c A_t} \tag{2.3}$$

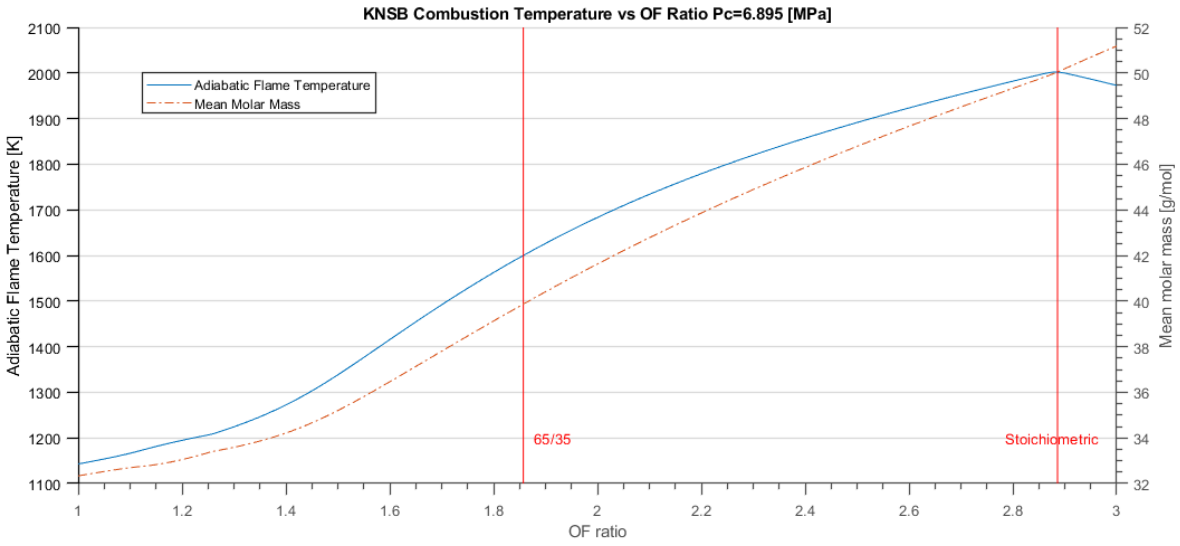

Figure 2.1: Adiabatic flame temperature and mean molar mass of reaction products for KNSB propellant as function of mixture ratio.

$$C_{f,is}^{0} = \Gamma \sqrt{\frac{2\gamma}{\gamma - 1}\left(1 - \left(\frac{P_e}{P_c}\right)^{\frac{\gamma-1}{\gamma}}\right)} \tag{2.4}$$

KNSB propellant is generally made with a 65/35 ratio by mass which is equal to an O/F ratio of approximately 1.857 [-]. The stoichiometric ratio is:

$$26\,KNO_3 + 5\,C_6H_{14}O_6 \longrightarrow 17\,CO_2 + 35\,H_2O + 13\,K_2CO_3 + 13\,N_2$$

With KNO_3 and Sorbitol molar masses equal to 101.103 [g/mol] and 182.171 [g/mol] respectively this is equal to an O/F ratio of 2.8859 (≈74/26) [-]. Rocket motor exhausts typically consist of many other (partial) reaction products such as CO, OH and H_2. In addition, although the combustion temperature might be higher at the stoichiometric ratio, the lower mean molar mass, and especially the lower quantity of condensed K_2CO_3 generally increases specific impulse [20] at lower O/F ratios. An additional reason why KNSB propellant is used at a 65/35 ratio is that a lower solid loading with KNO_3 particles is generally favourable for the rheological properties of the mixture (makes it pourable).

Combustion Analysis with RPA [50] shows that the 65/35 ratio is at the start of a maximum impulse plateau but at a lower combustion temperature which is favourable for motor thermal design. Combustion temperature and ideal specific impulse from RPA [50] as function of O/F ratio is shown in figures 2.1 and 2.2. A more extensive summary of the propellant properties including tabulated chemical properties is provided in appendix A. As could already be somewhat expected from equation 2.4, at a fixed O/F ratio of 1.857 [-] performance can be increased with increasing chamber pressure and the expansion ratio. KNSB isentropic performance as function of chamber pressure is shown in figure 2.3

2.2. Ingredient Selection

Both KNO_3 and Sorbitol are acquired via Brentagg [41] in 25 [kg] bags of industry grade quality but are produced by Azoty Chorzow and Tereos Syral Belgium NV respectively. It is important that the ingredients are kept free from contamination, which is why they are stored in sealed drums after opening. During this thesis study two variations of the KNSB propellant were tested, with coarse and fine KNO_3 powder roughly similar to compositions used by Gudnason [6] and Nakka [63].

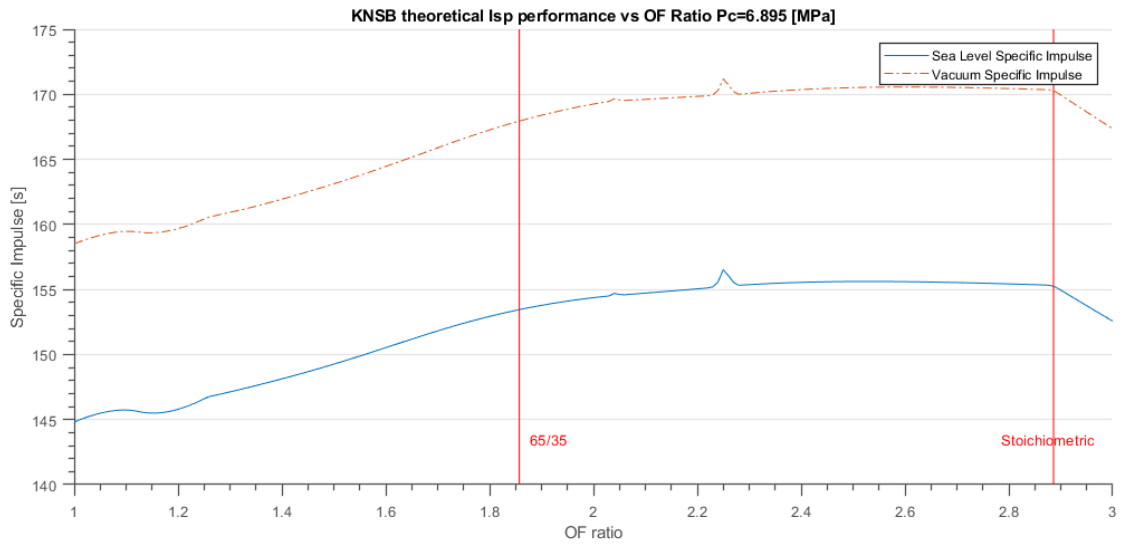

Figure 2.2: Sea level ($P_a = 0.1$ [MPa]) and vacuum performance for KNSB propellant as function of mixture ratio. The spike at an O/F of 2.25 is due to a numerical error in the C_f estimate in RPA, T_c, M_{mol} and c^* rise monotonously.

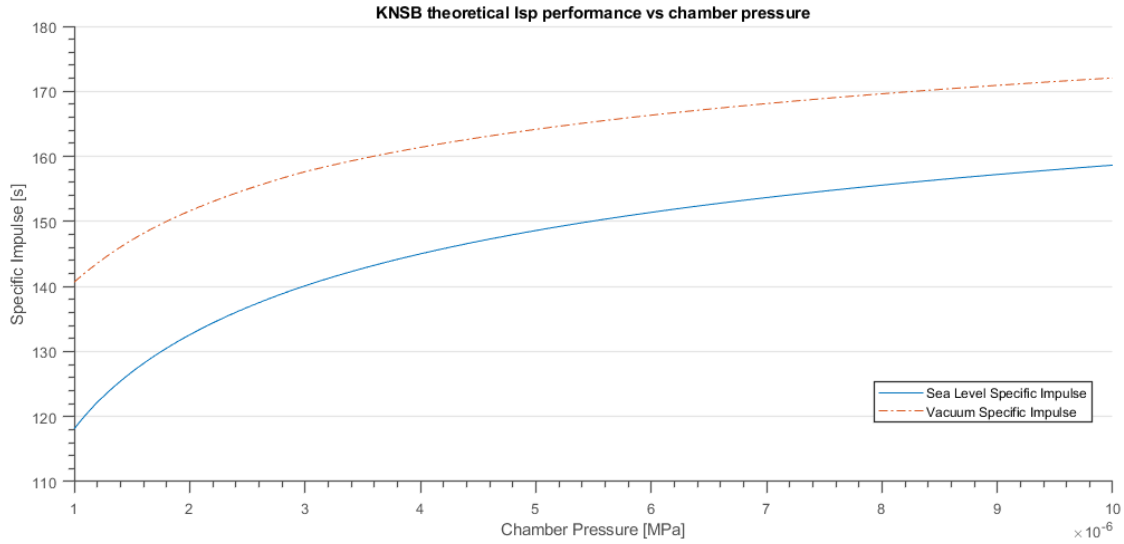

Figure 2.3: Sea level ($P_a = 0.1$ [MPa]) and vacuum I_{sp} performance for KNSB propellant with an 65/35 O/F ratio as function of chamber pressure.

The solid ingredients, fine KNO_3, coarse KNO_3, and sorbitol are shown in figure 2.4, which were produced with the KEYENCE VHX-5000 digital microscope[1].

2.2.1. Potassium Nitrate

KNO_3 or salpeter is a white crystalline powder commonly used as a preservation agent in the food industry or fertiliser in agriculture. It is not poisonous unless ingested in large quantities. Potassium Nitrate works as an oxidising agent but needs the addition of a fuel to combust, contrary to some other commonly used oxidisers. It is therefore classified as class 5.1 oxidising agent and considered less hazardous than for instance Ammonium Perchlorate (AP) which is considered a class 1.3 or 1.1 explosive substance depending on the particle sizes. It is readily soluble in water. Some basic characteristics are provided in table 2.1 which is taken from appendix A. Note that KNO_3 does not have a well defined boiling point as decomposition occurs $KNO_3 \longrightarrow KNO_2 + O$ before this point [37].

Property	Unit	Value	Note
Formula	[-]	KNO_3	Crystalline white solid
Purity	[%]	99,5	
Additives	[%]	0,5–1,0	SiO_2, Anti-Caking Agent
M_{mol}	[g/mol]	101.103	
T_d	[°C]	400	Decomposition ($KNO_3 \rightarrow KNO_2$+O)
T_f	[°C]	337	Fusion Temperature
ρ_s	[kg/m³]	2109	Density at STP

Table 2.1: KNO_3 Properties

An important part of designing composite solid propellants is the selection of the particle sizes for the various ingredients as they have a large impact on combustion and regression properties but also several manufacturing characteristics such as mixture viscosity. It is not uncommon for AP composite propellants to have bi- or even tri- model particle size distributions [14, 16] to achieve desirable propellant properties. The two primary blends of KNO_3 PSD are:

- *Coarse KNO_3,* as obtained from Brentagg [44]. This is the default distribution in DARE. As obtained particle sizes were also reported by Magnus Gudnasson [6]. A close up photo of the coarse particles is shown in figure 2.4.
- *Fine KNO_3,* machined from coarse KNO_3 using a hammer mill and a 100 [μm] filter. A close up photo of the fine particles is shown in figure 2.4. [63] uses a similarly machined particle size distribution with a sub 100 [μ m] average particle size for his motors and reports higher combustion qualities and higher regression rates as primary reasons for its use. KNO_3 is prepared from, as obtained, coarse particle size distributions using a coffee grinder by [63].

During this thesis study all experiments were produced from a total of three bags by the same manufacturer one of these bags was machined in its entirety to create approximately 23 [kg] of fine KNO_3.

2.2.2. Sorbitol

Sorbitol is an artificial sweetener that is used in a considerable amount of food products instead of sugar. It is a poly alcohol that is delivered as a 'fluffy' white powder. An important benefit of sorbitol over the use of other sugar propellants is the lack of caramelization (the breakdown of sugars at temperature). A second benefit is the low melting point (94-110 [°C]) depending on the amount of hydration and impurities. It is reported [63] that KNSB is also less brittle than for instance KNSU. The higher $-OH$ content does result in a lower combustion temperature and lower theoretical performance compared

[1] A large thanks to Technician Sander van Asperen, 3ME department of Material Science Engineering - Microstructures

(a) Microscope image of coarse, as obtained KNO_3.

(b) Regular photo of coarse, as obtained KNO_3.

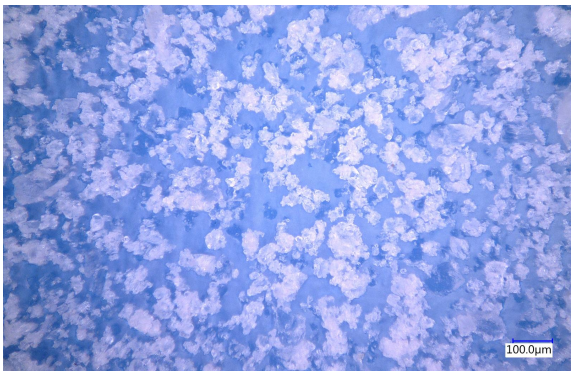

(c) Microscope image of fine, milled KNO_3.

(d) Regular photo of fine, milled KNO_3.

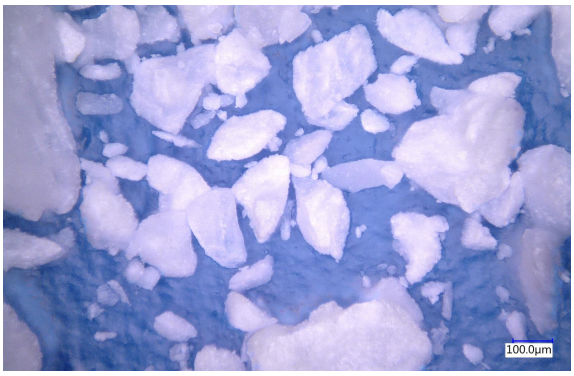

(e) Microscope image of Sorbitol as obtained.

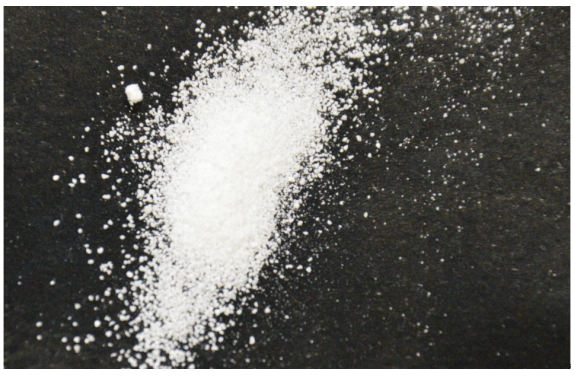

(f) Regular photo of Sorbitol as obtained.

Figure 2.4: KNO_3 and Sorbitol samples.

to other sugar propellants. An additional drawback, which was not fully understood until the casting experiments of part I, is the very high susceptibility to moisture, especially under the humid conditions encountered in the Netherlands that can easily be in excess of 75 % ciritcal relative humidity (CRH). A short summary of sorbitol properties is provided in table 2.2.

Property	Unit	Value	Note
Formula	[-]	$C_6H_{14}O_6$	Soft White Powder
Purity	[%]	>= 97.0	
Additives	[-]		none listed.
M_{mol}	[g/mol]	182.171	
T_b	[°C]	295	Boiling Point
T_f	[°C]	111	Melting Point (95 for hydrate)
ρ_s	[kg/m³]	1489	Density at STP

Table 2.2: Sorbitol Properties

2.2.3. Particle Size Distributions

As the two particle sizes used in this study are central to this study the particle size distributions were measured directly for most production batches using an Microtrac S3500 laser diffraction analyser at 3ME[2]. This system characterises the particle sizes by passing small (<1[g]) samples trough a laser beam.

The measurements from the first batches taken from the KNO_3 after mixing are shown in figures 2.6 and 2.5 and were repeated three times to verify the repeatability of the measurement. Characteristics such as the mean, minimal (10%) and maximal (95%) percentile sizes are given in table 2.3. As a comparison also the particle size distribution of the sorbitol was measured. As the sorbitol melts during propellant preparation this has only marginal influence on the propellant composition. For reference Richard Nakka estimated his particle size distribution to be 60-125 [μm] average [63] with an optical method, while Gudnason [6] finds a particle size distribution with 10% <150 [μm], the median 50% <330 [μm] and 95% <900 [μm]. This means that both distributions agree well with the distributions used in this study.

What became clear during the thesis study is that measuring particle size distributions, and especially assuring that the measured sample is representative for the whole is a scientific field/ black art in and of itself. The elongated tails of the distributions are for instance believed to be caused by particles sticking together and distort the distributions somewhat. Similarly distinctions should be made between fraction of particles by mass or fraction of the total number of particles (there is approximately a x^3 relation between these). In this study particle sizes are defined in terms of particle fractions.

2.2.4. Additives

Although various additives have been used in combination with KNO_3-sugar propellants for instance to enhance the burnrate, during this study only one additive was used together with KNSB propellant. Early during experiments with the manufacturing of fine KNSB propellant it was found that the mixture was too viscous to allow effective pouring into the moulds. Scooping, as suggested by Nakka [63] resulted in relatively large surface defects. A solution was found in the addition of small quantities of surfactant; sodium laureth sulfate (concentrated soap, acquired from *jojoli.nl*, CAS 68891-38-3) as used by [58] and [63]. The effect of surfactant on the ignition and combustion properties of (fine) KNSB propellant is investigated and discussed in detail in chapter 5.

[2]A large thanks to Technician Michel van den Brink, 3ME department of Process and Energy

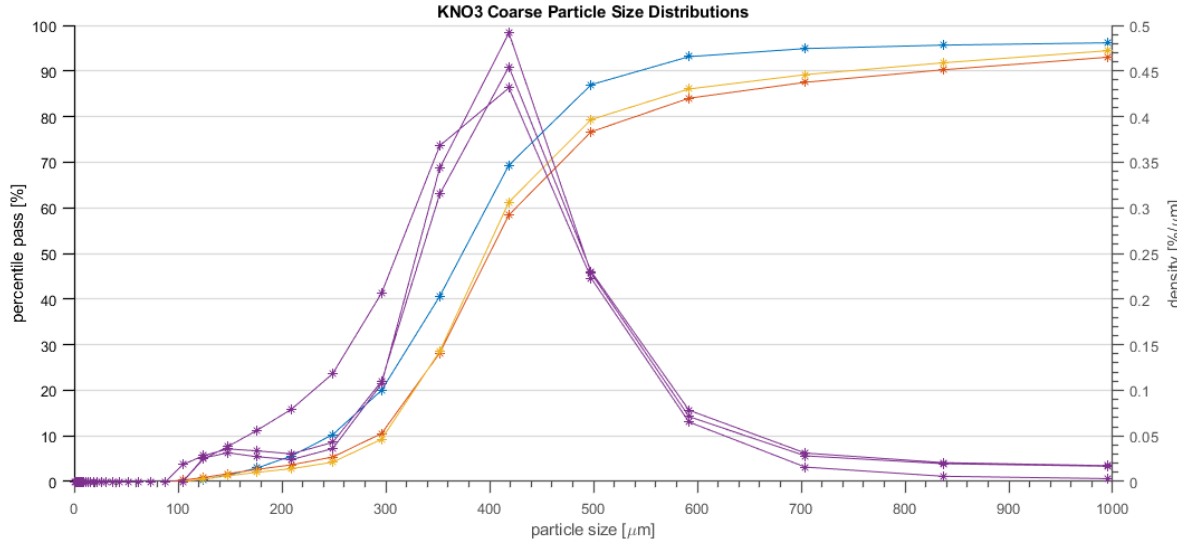

Figure 2.5: Coarse particle size distribution and density functions for samples from 05-09-2018.

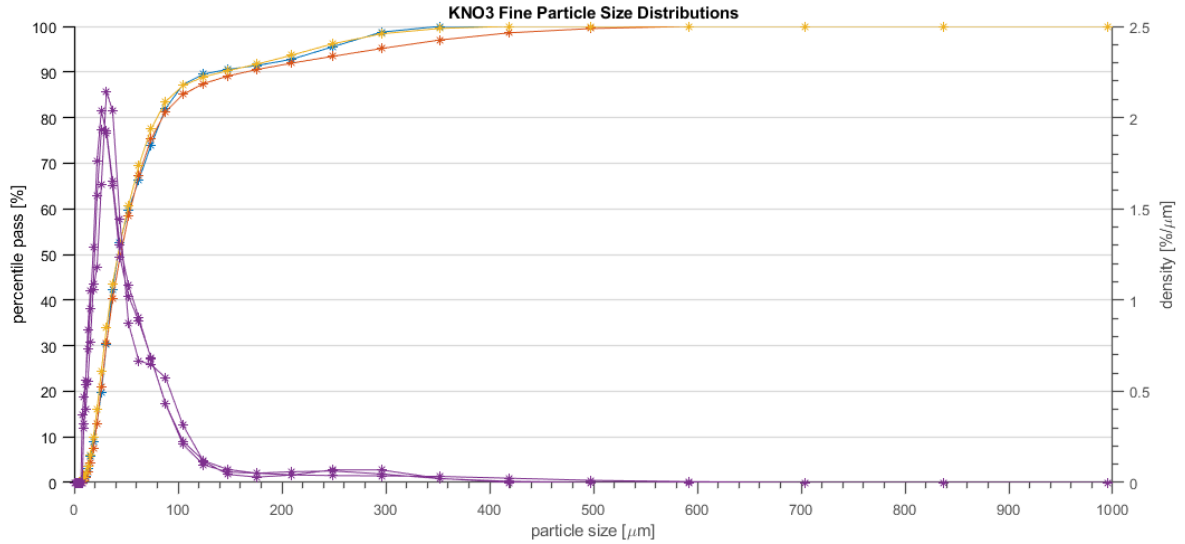

Figure 2.6: Fine particle size distribution and density functions for samples from 27-06-2018.

Batch	Type	Date	Mean [μm]	<10% [μm]	<95% [μm]	note
1	KNO_3 Coarse	05-09-2018	376.9	246.9	716.2	
2	KNO_3 Coarse	05-09-2018	435.8	292.8	1145	
3	KNO_3 Coarse	05-09-2018	421.4	298.8	1040	
1-3	**Mean**	05-09-2018	**411.4**$\pm$30.7	**279.5**	**967.1**	
10	KNO_3 Coarse	25-09-2018	371.1	252.5	844.7	
11	KNO_3 Coarse	09-10-2018	310	176.8	876.7	
15	KNO_3 Coarse	07-01-2019	290.7	151.3	480.6	
7	KNO_3 fine	27-06-2018	53.03	19.56	241.9	manufacture
8	KNO_3 fine	27-06-2018	51.43	19.22	219.1	„
9	KNO_3 fine	27-06-2018	55.67	20.26	291.8	„
7-9	**Mean**	27-06-2018	**53.37**$\pm$2.14	**19.68**	**250.93**	
12	KNO_3 fine	25-09-2018	51.27	18.61	229.8	
13	KNO_3 fine	28-11-2018	69.40	18.04	340.7	Laser Ignition
14	KNO_3 fine	07-01-2019	60.58	17.93	329.4	
4	Sorbitol	05-09-2018	276.1	116.6	1134	
5	Sorbitol	05-09-2018	263.4	107.8	877.2	
6	Sorbitol	05-09-2018	546.8	124.6	1330	
7-9	**Mean**	05-09-2018	**362.1**$\pm$8.403	**116.3**	**1113.7**	

Table 2.3: KNO_3 and Sorbitol Particle Size Distribution Characteristics

Amounts added were determined in drops/100 [g] of propellant supplied with a squeezable transfer pipette. The average weight per drop, based on 6 measurements of 50 drops each was $\mu = 0.0263$ [g] with $\sigma = 0.0016$ [g]. This results in on average 0.079/100 [g/g] and with a standard batch of 6 [kg] (see next section) in the addition of 4.75 [g] of surfactant per [kg].

2.3. Improved Propellant Manufacturing

When propellant production was reviewed for the literature study [16], the DARE heritage production manual for KNSB, written by Hein Olthof [68] in 2011, included nine steps including 'passive' activities such as propellant curing. Based on a literature and process descriptions from many other sources [60],[63],[70] and [54] further improvements were selected for investigation with respect to tooling and production. The effect of these changes on propellant quality and density is the main topic for the first two experiments in chapter 3 and 4.

In this section the heritage and improved manufacturing method are described side by side to allow easy comparison and to provide the baseline manufacturing method as used for experiments in chapters 5 and 6 including changes due to the lessons learned. This spoils some of the conclusions of following chapters but gathers the overall description of the KNSB formulation in a single place. In subsection 2.3.1 the tooling and equipment is described, thereafter in 2.3.2 both methods are discussed.

2.3.1. Equipment

Measurement equipment used during this thesis during production of propellant and special tools are provided in table 2.4. Heritage equipment was not listed specifically although the scales are most likely similar as they have been part of the lab inventory for approximately 10 years. Generic equipment such as hex keys are left out to keep the list concise and as, in many cases, the supplier could not be established. Heritage casting moulds consisted of vertical PVC tubes of the desired dimensions with

type	Product	Supplier	Range	Accuracy
Measurement Equipment				
Scales	FNR 225594	Metler Toledo	0-16 [kg]	1 [g]
Calipers	NA	Mitutoyo	0-150 [mm]	0.05 [mm]
IR Thermometer	2276-20	Milwaukee	-30 to 800 [°C]	1.5% rel [°C]
Tools				
Induction cooker	CR6505	CAMRY	1.5[kw]	200 [W]
Vacuum Pump	VE 115	Best Value Vacs	5 [Pa]	5 [Pa]

Table 2.4: Casting equipment used during the production of KNSB propellant.

aluminium mandrels placed after propellant casting and fixed in place with tape. Grains were cut to their final dimensions with a circular saw. The inprecise placement of the mandrel occasionally resulted in variations in radial web thickness and voids. Similarly trimming quality and length variations were highly dependent on operator experience [16].

An updated casting mould is developed on the basis of designs from [60] and [55] who recommended spring compression as a method of increasing propellant density and quality. In addition several other tooling changes were incorporated to increase the manufacturing accuracy and yield of DARE KNO_3 manufacturing. The moulds include:

- *Spring compression,* to increase KNO_3 packing density and eliminate voids and defects due to thermal contraction during propellant curing.
- *Machined Components,* to create grains with high surface finishes and an accurate concentric geometry.
- *Grain Separation Features,* that ensure that grain damage during post processing are minimised.

The mould design is shown in figure 2.7. A further design descriptions including calculations, bill of materials and drawings is available in appendix F.

2.3.2. Method

The KNSB production steps are provided below with the a flowchart of both the heritage and improved process in figure 2.8. The main difference between heritage and improved manufacturing method resides in the addition of two addition process steps (no 6. application of vacuum, and no. 8 application of compression) and changes in tooling. A description of the steps is provided below with accompanying pictures of the production steps in figure 2.9.

1. *Ingredient Preparation,* Ingredients are stored dry in sealed blue containers. Powders are used as obtained from the supplier while fine KNO_3 was milled with a rotary hammer mill at the start of the project.
2. *Mould Preparation,* For all grains to be a cast a mould is prepared beforehand (refer to section 2.3.1 and appendix F. The bottom plate and mandrel are greased thinly (0.1-0.2 [mm]) on all sides

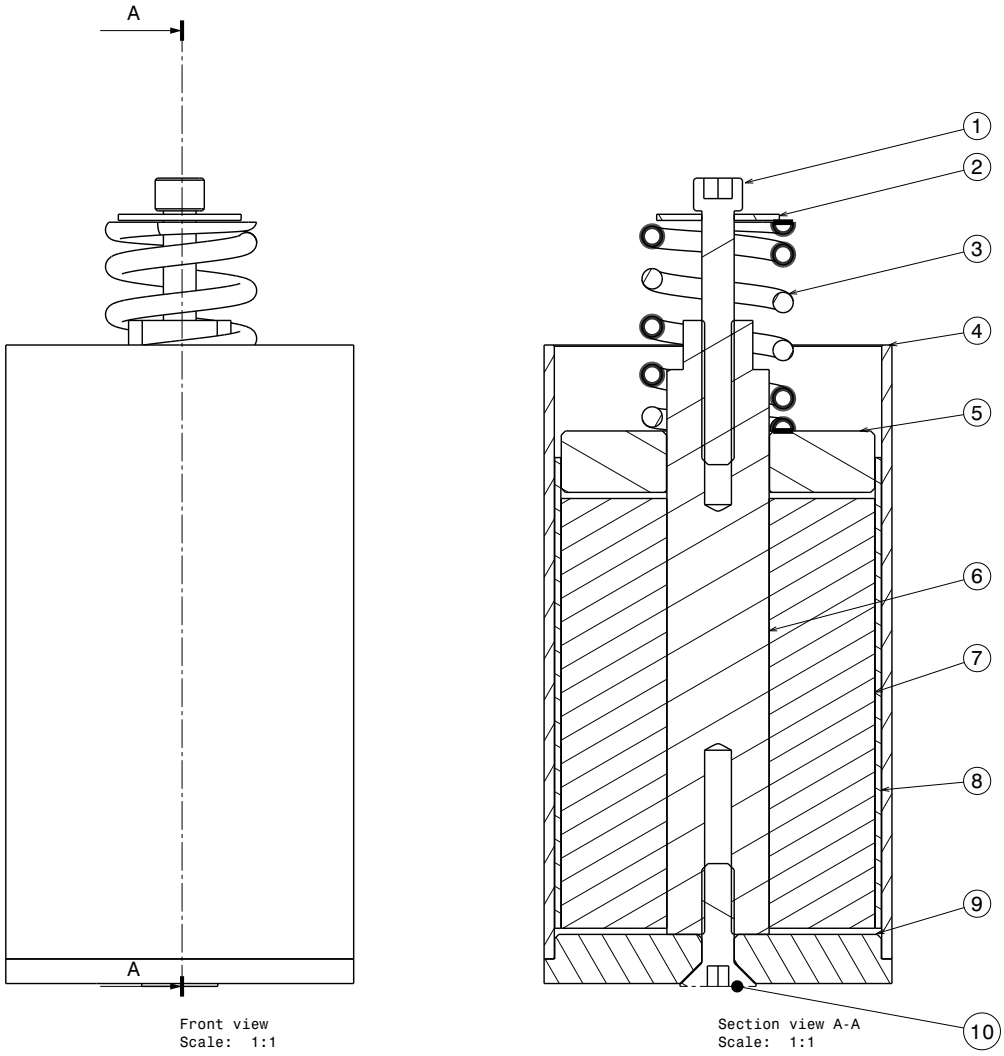

Figure 2.7: Casting Equipment with BEM propellant grain. (1) 70mm M8 Hex, (2)35mm×1.5mm M8 Washer, (3) FIBRO compression spring, (4) Aluminium Mould Tube, (5) Aluminium Plunger, (6) Aluminium Mandrel, (7) BEM Grain, (8) Cardboard inhibitor tube, (9) Aluminium base, (10) 30mm M8 countersunk Hex.

exposed to the propellant with high temperature SKF bearing grease. The plunger is greased on all sides including the M8 thread (refer to step 10). Cardboard liners receive a production code including the date of manufacture, mould number, coarse or fine, and a sequential number. Moulds are assembled without plunger but with the cardboard liners pressed down into the moulds.

3. *Weighing of ingredients,* is sequentially done for both KNO_3 and sorbitol weighed to form a batch of 2 [kg] ± 5 [g] pre-mix. Only one drum is open at a time to prevent cross-contamination. The ingredients are poured through a coarse sieve into a 10 liter stainless steel cooking pot to breakup any lumps.
4. *Mixing of Ingredients,* is done with a wooden spatula by hand for several minutes to form a homogeneous mixture. Stirring will further happen during the heating and casting phase up to a total amount of 20-30 minutes.
5. *Heating of Propellant Mixture,* is done on two induction cooking plates (CAMRY CR6505). Temperature is measured approximately every 3 minutes using an infrared thermometer to within ± 3 [°C] as there is, even under continuous stirring, some temperature variations throughout the propellant. When the propellant has reached 125 ± 3 [°C] either another 2 [kg] batch of premix is

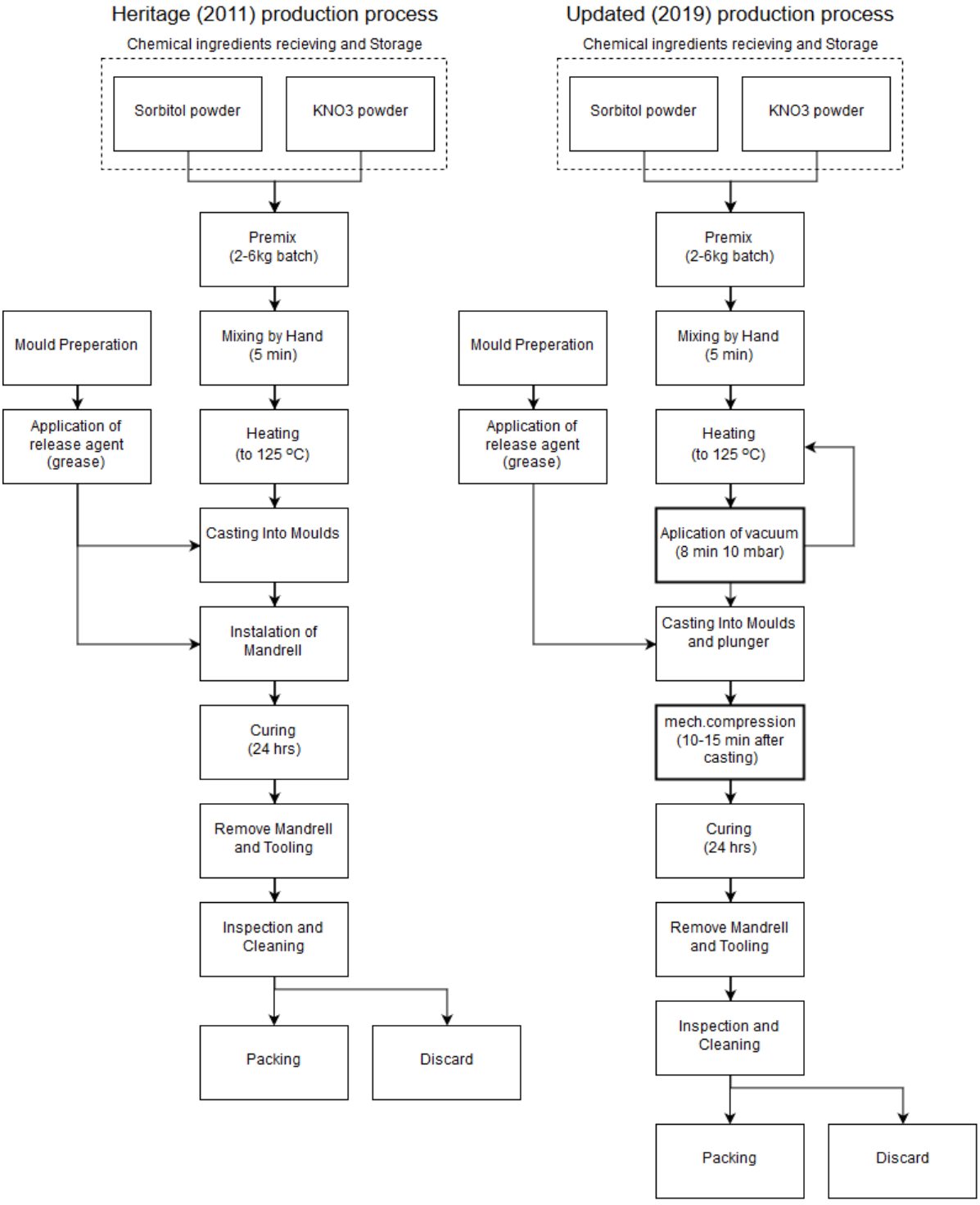

Figure 2.8: Heritage (2011) and improved production process for KNSB propellant with the new process steps shown in bold.

added up to a maximum total of 6 [kg] or the propellant heating is completed. This is done to allow easy stirring of the partially molten mixture. For fine KNSB propellant 3 [drops/100g] of surfactant are added using a squeezable transfer pipette.

6. *(Application of Vacuum),* was found to be the most effective method of removing moisture and other volatile components from the molten mixture. The pot is removed from the induction plate and a 25 [mm] thick acrylic lid is placed on the pot. Using a vacuum pump a vacuum is created that seals the rubber gasket and lowers pot pressure to < 10 [mbar] for 8 minutes. A needle valve is used by the operator to assure the propellant does not enter the vacuum system hose. This is done by manually increasing pot pressure which limits expansion of the mixture.
7. *Casting of Heated Mixture,* the scale is placed on the ground and covered in sheets of paper. The mould, plunger, bolt, nut and spring are placed on the scale and mould empty weight is recorded. Scales are tared. When the propellant is at the desired temperature of 125 ± 3 [°C], two people cast the propellant up to the required weight (for the BEM 758 ± 10 [g], the variance is mainly due to operator experience). Cast propellant weight is recorded. The plunger spring and bolt is placed and pressed down by hand.
8. *(Application of compression),* after the propellant has cooled for approximately 15 minutes the springs are compressed by $4 - 5$ [mm] to a compression force of 630-780 [N], equal to approximately 1.7-1.9 [bar] (relative). Small leaks (<2 [g]) around the plunger are sometimes observed.
9. *Curing of Propellant Grains,* is done at room temperature for up to 24 [hrs]. During this time compression results in a spring extension of approximately 1.5-2 [mm] due to thermal contraction.
10. *Mold Separation and Cleaning,* differs considerably between the heritage and improved method. Traditionally the mandrels are removed by hand after which grains are cleaned and inspected. Grains of sufficient quality are subsequently cut with a circular saw to form multiple Bates grains of the desired length.

    The improved process is completed in several steps with some ”of the shelf” tooling to aid the process. First all bolts and the springs are removed. Afterwards the mould base is removed using a blunt screwdriver and mallet. In the third step the mandrel is removed by hand or, if not possible due to friction, using a sufficiently long tube, threaded rod, washer and nut; this allows the mandrel to be drawn through the plunger without much effort. Subsequently the grain is pressed from the aluminium tube. In the last step the cardboard inhibitor is cut away up to the desired length (typically the propellant surface plus 3 [mm] and removed by application of force in the M8 threaded connection of the plunger.
11. *Post Processing,* is done by first cleaning the grain of any residual grease and propellant residues such as might be on the outside of the cardboard inhibitor. Grains are visually inspected and grains with flaws are discarded. The grain is weighed and all relevant dimensions are recorded. Grains are sealed in plastic bags with a small paper sachets filled with $CaCl_2$ desiccator. They are subsequently packed in cardboard storage boxes and stored at room conditions.

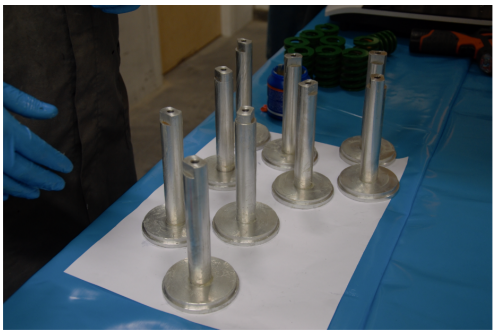

(a) Casting moulds are prepared.

(b) Ingredients are weighed.

(c) Ingredients are mixed to form premix.

(d) Premix is heated.

(e) Vacuum is applied.

(f) Propellant is cast.

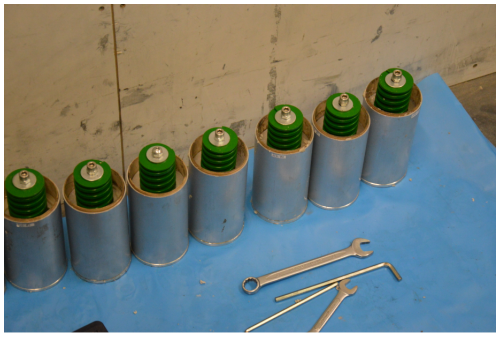

(g) Propellant cures under compression.

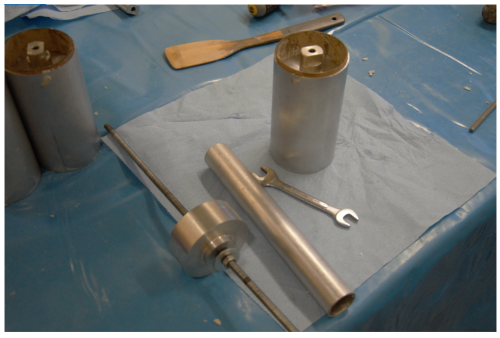

(h) Mandrel is removed.

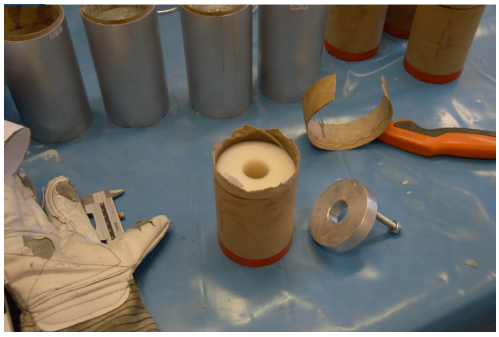

(i) Plunger is removed.

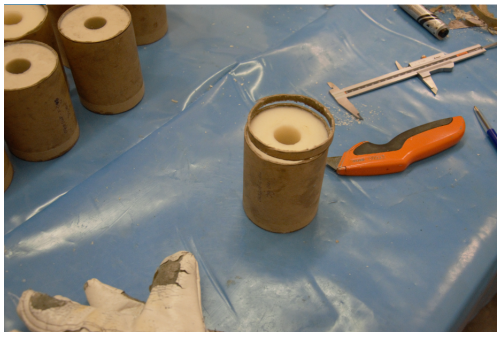

(j) grain is cleaned and trimmed.

Figure 2.9: Propellant preparation steps.

2.4. Working Safety

Production and testing with energetic materials needs to be carefully considered to assure safety of people and property. Besides the obvious premature ignition of propellant there are several other risks that warrant attention. These risks and their mitigation are briefly discussed below. In addition the reader is referred to appendix E which includes a much more detailed safety assessment of the BEM system as part of the overall design description which was used for the design safety review by the DARE safety board.

In this section first the guiding principles are provided under which DARE works with energetic materials and conducts its experiments. In the last two sections the risks associated with propellant manufacturing and solid motor testing are briefly discussed.

2.4.1. Guiding Principles

The fact that DARE is able to design, build, test and fly large rocket motors and rockets is only possible due to continued diligence with respect to safety. DARE has acquired some extensive experience in testing rocket motors, such as those used in this thesis, that have also on occasion failed. Starting point for any activity is:

> Safety of (DARE) personnel, external people, the general public and their property shall have the highest priority and shall be considered with care during all DARE's activities.

This means that for any safety critical operation (and those are conservatively defined) a review is made of the risks associated with that activity. Based on these risks a mitigation strategy is formulated that can include simple measures such as the use of Personal Protective Equipment (PPE), or occasionally more stringent requirements such as minimum safety distances from a test setup.

In DARE a safety board which consists of experienced senior members is responsible for the evaluation of the risks analysis and mitigation strategies. An independent safety officer is assigned to attend any safety critical activity and in that capacity verify that the mitigation strategies are followed and that the test is performed safely. For this thesis project all work with energetic materials such as propellant manufacturing and motor tests was conducted under supervision of a DARE safety officer.

2.4.2. Propellant Preparation

The accidental ignition of propellant is the most obvious risk however not the most likely. Generally the room used for preparation is clean with double, easily accessible exits. In addition the manufacturing is done by at minimum three people, including the DARE safety officer. PPE are worn such as lab-coats, safety shoes, leather gloves and glasses. Fire extinguishers and a bucket of water (both as extinguishing medium and for disposal of scraps) are available at the exit. The most important risks are provided below:

1. *Ignition of propellant,* can lead to rapid deflagration or explosive action which can result in significant damage or injury. A large benefit of the KNSB propellant is its high initiation temperature and very low susceptibility to electric or mechanical ignition. To eliminate any further risk during manufacturing, possible ignition sources are removed. The process furthermore assures that bulk ingredients are kept pure.

2. *Molten propellant,* can cause serious second degree burns when in contact with the skin directly or via hot equipment. To limit this risk the pots are only ever filled up to 2/3 and are always handled with two hands. To limit this risk even further leather gloves and long-sleeved lab coats are worn.

3. *Work with fine particles,* can cause irritation to the respiratory tract when inhaled. Only the milled, fine KNO_3 is fine enough to become airborne during mixing. The risk is minimised by the use of suitable dust masks for those involved.

2.4.3. Testing

During rocket motor testing there are three key hazards that need to be taken into account: unintended ignition of a motor during preparations, a pressure wave hazard due to motor failure and a shrapnel hazard due to motor failure. As any propellant test in DARE is experimental, the mitigation strategies focus primarily on limiting the effect of a worst case failure instead of prevention.

1. *Unintended ignition of a motor during preparation,* can lead to significant damage or injury when unconstrained. To prevent the worst case outcome the pressure vessel is only closed when the motor is fully constrained in the test bench, this results at most in propellant deflagration at ambient pressure without the risk of fast moving shrapnel. After the motor is constrained the last step involves placing the igniter which is done with minimal crew and a firing system with redundant keys in the hands of the safety officer.

2. *Pressure wave hazard,* that could lead to permanent hearing damage to spectators or public. In case of motor failure the high pressure vessel could create a shock wave. As this sound dispersion is difficult to predict minimum safety distances to the system shall be maintained during a test. Worst case sound-levels, assuming a perfect hemispherical isentropic pressure wave is 150 dB with hearing protection or 140 dB without. These sound levels dictate the minimum required safety distance during firing.

3. *Shrapnel hazard,* can similarly lead to serious injury or damage to property. In case of motor failure or pressure vessel rupture mechanical components can be ejected at velocities upward of 30 [m/s]. The primary method is that the pressure vessel is safe by design as a single failure mode is incorporated that results in predictable shrapnel dispersion. A further mitigation is a heavy wooden shrapnel box and sand bags that minimise the scattering of components. Similar to the pressure wave hazard sufficient distances are observed in unshielded directions.

I

Propellant Casting Research

3

Out-gassing Experiment

Two experiments were proposed in the thesis proposal [17]: 1) to investigate moisture contamination in the KNSB propellant and how to remove this and 2) applying mechanical compression and preheating of casting moulds to further improve propellant density. This chapter discusses the experiment goals, experiment design, result and analysis of the first experiment and is drawn together from two documents a test plan and test report that were written at an earlier stage of the thesis project.

Moisture is an often cited cause of under performance of sugar propellants as both KNO_3 and Sorbitol are hygroscopic [63]. In addition Motsyk [11] reported moisture as the root cause for a loss in I_{sp} by as much as 25 [s]. As the propellant is cast at around 100 [°C] it could cause some of the observed porosity and density problems. it is therefore decided to systematically introduce a contamination of moisture in KNSB propellant samples. This will allow quantifying the effect of the out-gassing strategies against known contamination levels and possibly allow the determination of the baseline moisture level.

To streamline the description of the experiments performed in this thesis the next four chapters will all follow a similar structure. First he test goals for this chapter: out gassing experiment are provided. Subsequently the experiment design is discussed including the analysis method, variables and experiment protocol. Afterwards the measurement and analysis results are provided and discussed. The chapter will conclude with conclusions and recommendations.

3.1. Experiment Goals and Success Criteria

At the highest level the goal of this experiment is to answer the following: *What is the most effective manufacturing method for KNSB propellant to obtain good quality propellant grains with a reject rate below 5% a density larger than 95% of theoretical?* Moisture and other volatile impurities could have a large impact on this quality which is why this is investigated directly. The experimental goals are:

1. Quantify the effect of out-gassing strategies on propellant quality. The methods to be investigated are:
   (a) Application of vacuum [55].
   (b) Sustained heating [63] [6].
   (c) storage with desiccant [63].
2. Determine the best production technique for KNSB propellant grains for the BEM with respect to achieved quality and effort.

It is at this point difficult to estimate to what an extend the methods work and if an effect can be measured with available equipment. The ingredients are in principle obtained in anhydrous form, however are exposed briefly to air during production. In addition the stirring could introduce gas into the mixture that needs to be removed.

The success criteria for this experiment are the following:

1. Successful determination of the effect of the various out-gassing strategies on KNSB propellant and the contamination with moisture.
2. Partial validation of the casting procedures for BEM propellant grains.

Additionally the following secondary objectives are defined:

1. Experience gained with the various out-gassing methods for future use during KNSB preparation.

The suspension criteria are provided below. These denote conditions under which the test campaign will be halted until the problems have been resolved.

1. An unacceptable risk to the involved personnel, critical equipment, general public or their property.
2. Any indication that success criteria as defined in this section can no longer be met.

3.2. Experiment Design

The propellant, baseline equipment and the heritage propellant manufacturing method are defined in chapter 2. For this experiment only coarse KNO_3 was used without added surfactant. A challenge in this experiment is that a trade needs to be made between the available resources (time, available casting moulds) and the (statistical) reproducability of results. In addition many of the applied methods are highly equipment dependent which makes it difficult to generalise the measurement results to an optimal production strategy.

As was discussed in previous section the effect of out-gassing/ moisture reduction strategies on propellant quality is investigated. The three strategies that are considered are:

1. *Application of vacuum [55].* By applying a vacuum gasses and liquids, enclosed in the molten propellant, will merge to form large bubbles that can more easily escape the propellant mixture. [55] applies several vacuum cycles but is unclear about the duration, as such it is recommended to start with 1 minute cycles. In addition it is expected that propellant temperature, through the mixtures viscosity may affect the release of bubbles, this should therefore be monitored.
2. *Sustained heating [63] [6].* By sustained heating the entrapped moisture will evaporate and similar to the application of vacuum more easily escape the propellant mixture. [6] continues heating the propellant for 25-30 minutes to release trapped gasses. However as the experimental time needs to be limited it is suggested to start with 2 minute intervals.
3. *Storage with desiccant [63].* Desiccant is a very hygroscopic substance that removes moisture from the surrounding air. When stored in a closed box together with the premix it draws moisture from the propellant constituents. Nakka [63] suggests storage for at least 24 hours.

Analysis with *RPA* [50], indicates that a 50 [g/kg] contamination with water results in a loss of I_{sp} of around 1.5 [s]. For this experiment batches will be contaminated with 25 and 50 [g/kg]. This is a trade between a plausible contamination level while still easily measured with the available scales. Note that the moisture is added to baseline moisture quantity in the ingredients which is not a priory known. This means that care needs to be taken to define the contamination as fraction of propellant dry mass or as fraction 'as obtained' premix. To measure the effect of the various strategies of the same propellant it is proposed to measure propellant weight from the several propellant batches of 250 grams each before and after applying the various strategies. The amount of mass removed compared to the two control batches will be taken as a measure of the methods effectiveness.

The experiment logic for this experiment is shown in figure 3.1. A 4 [kg] initial batch of propellant is produced as specified in the experiment protocol. This dry premix is mixed thoroughly by hand until an homogeneous batch is produced. The 4 [kg] of premix is then split into 4 separate containers. Two containers are stored with known quantities of water, two containers are stored dry.

The 1 [kg] containers are afterwards stirred and weighed again to confirm the water uptake. They are again split to form four 250 [g] batches for a total of 16 on which the out-gassing strategies will be applied at regular intervals alternated with weight measurements. This is expected to result in a steady

weight decrease per sample, as function of the duration that a specific method was applied and initial moisture content. A comparison between strategies will indicate the effect of the various strategies on propellant composition.

Initially the plan was to measure propellant density and quality 250 g propellant samples to measure propellant density and quality. This approach was discarded as the surfaces of the respective propellant samples made determination of the volume impossible. To still determine the effect of out gassing on propellant quality (and meet experiment objectives) two batches of propellant grains were compared that were produced for a Stratos I booster motor [21]. These grains were produced with identical manufacturing method with the addition of vacuum on the molten premix as this was found to be the most effective method of reducing volatile compounds from the mixture.

3.2.1. Method

The effectiveness of the methods will be discussed based on three parameters:

- The overall moisture reduction at the end of the experiment expressed in [g] per 100 [g] initial sample.
- The estimated slope, α, and estimated starting moisture content, in both [g/100g] and as a mass fraction ξ_{H2O}.
- The practical lessons learned and evaluation of the various methods.

the mass reduction is calculated as fraction of remaining mass $M_s(t)$ or moisture $M_{H2O}(t)$ divided by the sample starting mass M_0 including initial moisture denoted by [ξ_{PM}] and [ξ_{H2O}] respectively . This is given in equation 3.1. Alternatively multiplication with 100[g] yields a more intuitive number either as [g] remaining out of 100 [g] premix, or as [g] moisture per 100[g] premix. As example the added moisture to EXA-50 is $^{50}/_{1000+50} = 0.0476$ or 4.76 [g]/100[g].

$$\xi_{PM}(t) = \frac{M_s(t)}{M_0} \tag{3.1}$$

$$\xi_{H2O}(t) = \frac{M_{H2O}(t)}{M_0} = \frac{M_0 - M_s(t)}{M_0} \tag{3.2}$$

A nonlinear function fit is used for all cases with the exception of the control group which was measured only twice and thus does not allow meaningful regression. This is a straight forward least squares fit with two model constants, ξ_{H2O} and α. For the application of vacuum and continued heating (methods 1 and 2) the variable, t, is in [s]. For method 3, the storage with desiccant the variable, t, is in [days]. The model choice is given in equation 3.3 and based on a models for a standard chemical reactor [2] where the flow from a control volume is linearly depended on its concentration. E.g. when flushing dye from a well mixed volume of water.

$$F(\xi_{H2O}, \alpha, t) = \xi_{PM}(t) = 1 + \xi_{H2O}(0)\left(e^{\alpha t} - 1\right) \tag{3.3}$$

Uncertainty and reproducability of the experiment is primarily defined by four aspects:

1. Possible errors of the test procedure such as measuring with or without a spoon or the introduction of additional contamination due to a high relative humidity in the room.
2. Measurement uncertainty and the low amount of measurements. One example is the measurement accuracy of 1 [g] for the Metler Toledo Scales. An other example the uncertainty in the time that a certain method was applied. This was estimated for method 1, 2 and the control group 0 to ± 20 seconds as it took a few seconds for the propellant to be transferred from heating plate to scales. For method 3 this is estimated at 5 minutes but when compared to the experiment duration a significantly smaller relative uncertainty.
3. Hardware and sample variations. Although care was taken that similar equipment was used and that samples were created from the same source at the same time. The fact that the setup was

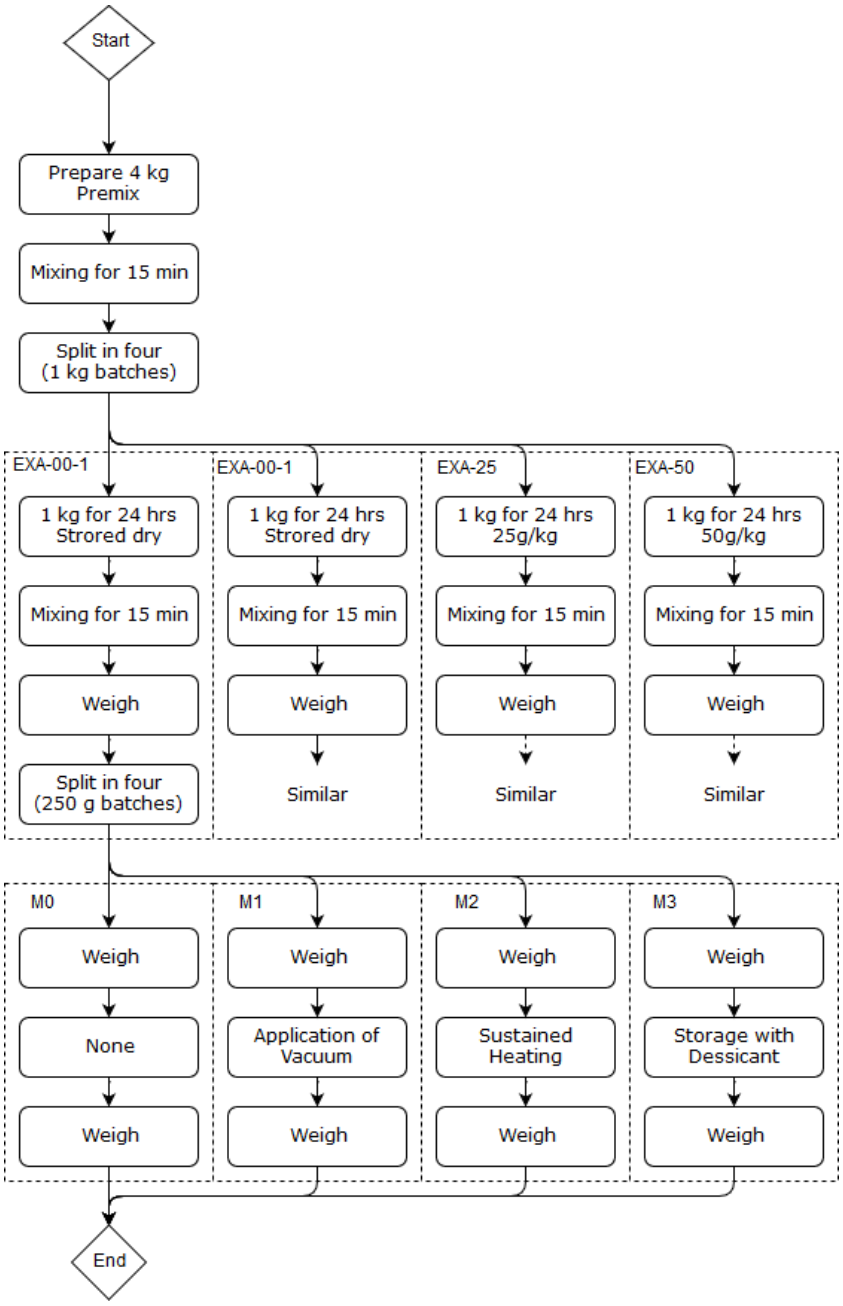

Figure 3.1: Test logic for the out gassing experiment.

rebuilt on several days with a different people does not rule out slight variations. Similarly the precise mixture ratio (both chemical, with respect to the PSD and with respect to contamination from stirring or from the air) could not be ascertained with absolute certainty.

4. The choice of the model, even though based on reasonable assumptions of the underlying physics is not derived from first principles as this is considered well beyond the scope of this thesis experiment. In addition this model neglects clear variables such as propellant temperature (which is neither constant or uniform) or for instance vacuum pressure.

RMS Fitting error, as provided in row 10 of table 3.7, is evaluated separately and is given by equation 3.4.

$$e_{fit} = \sqrt{\frac{1}{n}\sum_{n}\left(y_n - F(x_n)\right)^2} \tag{3.4}$$

3.2.2. Experiment Variables

Besides a single continuous variable, sample mass, and the general observations there are several control variables that will be controlled as much as possible during the experiment. The control variables

Variable	name	Range	Accuracy
M	Sample Mass	≈0-250 [g]	$\pm$ 0.5 [g]
T_{IF}	Sample Temperature (Infrared)	≈15-130 [°C]	$\pm$ 0.5 [°C]

Table 3.1: Experimental Variables

during the test are the following:

- *Propellant Composition,* will be fixed at 65% KNO_3 and 35% Sorbitol by mass with an accuracy of 1 gram in 1000 gram (determined by the accuracy of the scales). Course KNO_3 will be used to limit experiment variables.
- *Propellant homogeneity* will be controlled by mixing the entire propellant batch for 15 minutes before starting the experiment. After splitting the batches they will be stirred for an additional 15 minutes.
- *Initial Propellant Moisture Content* will be controlled by using the same propellant sources for the entire experiment and controlling exposure of the samples with airtight containers.
- *Process Control* will be assured by closely following the casting procedures. Specifically the following points will controlled:

  1. Casting temperature at 125-130 [$^{\circ}C$] (measured to within 0.5 degrees) by infrared thermometer.
  2. Duration of all process steps will be recorded by stopwatch.
  3. Equipment will be used sequentially and will be thoroughly cleaned between sets.

3.3. Experimental Setup

The casting room set up is shown in figure 3.2. The data acquisition system was used for experiment part B during which the National Instruments C-RIO and laptop was used to measure temperature.

3.3.1. Protocol

The experiment protocol is provided in appendix B.1 and was designed based on the heritage production process [68] with modifications to measure the desired quantities. The process and equipment was described in more detail in chapter 2. Several deviations arose during the experiment and are discussed below with their motivation.

Figure 3.2: Casting Room Setup with Compact RIO used in propellant casting experiment in chapter 4.

1. *(Step A17-A18)* Water uptake by the samples, EXA-25 and EXA-50 was found to be significantly slower than the expected 24 hrs proposed in the test plan. Instead the samples were stored for about two months (in part due to the Stratos III launch campaign in July). Total container mass in that time remained constant and all moisture (measured to within 0.1 g with a pocket scale (Holex Pocket Scale) was transferred to the premix during that time.
2. Based on feedback during the test readiness review it was decided to have two control groups during the experiment, these are =named EXA-00-1 and EXA-00-2 both with no added moisture compared to EXA-25 and EXA-50
3. *(Parts E-G)* As no liners were used with these samples the plungers were left out of the experiment as the propellant would flow around the plungers. This caused a slightly uneven propellant surface which made measuring propellant density difficult. Instead to quantify the effect of moisture reduction on actual grain density/ quality use was made of two batches of propellant cast on a different date. These are discusses in section 3.4.4.
4. *(Part E)* The measurements on the desiccant that were measured 8 [hrs],16 [hrs] and 24 [hrs] after preparation showed no changes and were subsequently abandoned for a month due to other experiment activities. It was found after a month that a moisture decrease had happened, however the measurement frequency was significantly limited due to this change.
5. *(Part E)* After the first results from EXA-25 and EXA-50 the expected effect of adding desiccant to the EXA-00 batches was a slight sample weight loss over several weeks with an expected weight loss very close to, or below the measurement accuracy of the scales. It was thus decided to skip experiments EXA-00-1 M3 and EXA-00-2 M3.

3.3.2. Identification of Samples

The proposed test samples are listed in table 3.2. Each sample gets a reference code to maintain traceability. The code 'EXA' denotes the experiment with the subsequent number the amount of moisture added per [kg] propellant and the repetition of the specific test conditions if applicable. M1, M2 and M3 denote the applied method, application of vacuum, continued heating, and storage with desiccant respectively. M0 is the control group. The last number denotes the repetition of the specific test conditions. These codes will be used in reporting of the results and analysis.

no	Test-id	Water [g/kg]	Method
1	EXA-00-1-M0	0	Control
2	EXA-00-1-M1	0	Vacuum
3	EXA-00-1-M2	0	Heating
4	EXA-00-1-M3	0	Desiccant
5	EXA-00-1-M0	0	Control
6	EXA-00-2-M1	0	Vacuum
7	EXA-00-2-M2	0	Heating
8	EXA-00-2-M3	0	Desiccant
9	EXA-25-M0-1	25	Control
10	EXA-25-M1	25	Vacuum
11	EXA-25-M2	25	Heating
12	EXA-25-M3	25	Desiccant
13	EXA-50-M0	50	Control
14	EXA-50-M1	50	Vacuum
15	EXA-50-M2	50	Heating
16	EXA-50-M3	50	Desiccant

Table 3.2: Proposed test matrix for investigation of out gassing strategies.

3.4. Results

For the Out-Gassing experiment samples were prepared on 08-06-2018, the out-gassing experiment was subsequently performed between 29-08-2018 and 06-09-2018 (with the exception of the measurements on the samples with desiccant). Ambient temperature in the room was 19-21 [°C]. Humidity was between 85 and 93 % on the days of the experiments due to intermittent heavy rains[1] but not measured directly in the production room. The prepared batches (EXA-25 and EXA-50) in their respective storage containers are shown in figure 3.3, the control batches were stored in similar containers but without the paper cups holding the added moisture. The added moisture was measured with 0.1 [g] accuracy, the propellant mixture ratio was accurate to within 1 [g] out of 1000 [g].

[1] weatheronline.co.uk

Figure 3.3: The two prepared premix batches with added moisture. Measured quantities (25g/kg and 50g/kg) of moisture were placed in the cups.

3.4.1. Measurement Results

The results for the Out-Gassing Experiment is shown in tables 3.3, 3.4, 3.5 and 3.6. The measurements and their units are provided in the rows with the different methods (M1,M2,M3 and M0) shown in the columns. First the container weight before and after storage with the cups containing moisture. The final batch weight is the total premix before division into the separate 250 [g] samples. Casting jig and jig empty weight is provided for some samples that were cast after completing the respective methods. Pot empty weight subsequently is the empty weight of the pot before each sample was placed.

Pot weight varies depending on the spoon weight (a few gram stuck to the spoon) and if the vacuum lid was included. A slight disparity exists between some sample weights + empty pot weight as not all propellant could always be perfectly transferred to the heating pot and the spoon was not always included in the pot empty weight.

Weights were measured at the start of every step with the total weight (sample+pot). Subsequently for every step the sample weight, approximate time and propellant temperature are recorded. For vacuum this is denoted as minutes (+1m) while for heating and control the time was used.

Table 3.3: Out-Gassing Experiment 0 g/kg

EXA-00-1		M1 (Vac)	M2 (Heat)	M3 (Desc)	M0 (Control)
Container Weight before	[g]	1097			
Container Weight after	[g]	1097			
Batch Weight	[g]	1000			
Sample Weight	[g]	250	250	250	250
Casting Jig	[#]	J9	J4		J5

Continued on next page

Continued from previous page

EXA-00-1		M1 (Vac)	M2 (Heat)	M3 (Desc)	M0 (Control)
Jig Empty Weight	[g]		593		590
Pot Empty Weight	[g]	941	941		655
step 0 -	[g]	1214/1213	1213		905
		10:49	11:33		11:50
	[° C]	125	131		125
step 1 -	[g]	1212	1213		905
		+1m	121/128		
			11:37		
step 2 -	[g]	1212	1212		
		+1m	11:41		
			110		
step 3 -	[g]	1212	1212		
		+1m	11:45		
			128		
step 4 -	[g]	1212(a)			
		+3			
		11:17			

(a) Experiment terminated due to unchanging sample mass.

Table 3.4: Out-Gassing Experiment 0 g/kg

EXA-00-2		M1 (Vac)	M2 (Heat)	M3 (Desc)	M0 (Control)
Container Weight before	[g]	1097			
Container Weight after	[g]	1097			
Batch Weight	[g]	1000			
Sample Weight	[g]	250	250	250	250
Casting Jig	[#]	NA	NA	NA	NA
Jig Empty Weight	[g]				
Pot Empty Weight	[g]	965	660		660
step 0 -	[g]	1215	905		905
		12:11	15:27		15:44
	[° C]	140(a)		125	125
step 1 -	[g]	1213	905		904
		12:24	15:27		15:47
		+1M	125		
step 2 -	[g]	1213	905		

Continued on next page

Continued from previous page

EXA-00-2		M1 (Vac)	M2 (Heat)	M3 (Desc)	M0 (Control)
		12:26 +1M	15:29 121		
step 3 -	[g]	1213(b) 12:26 +1M	905 15:32 108		
step 4 -	[g]	1212 +3M	904 15:34 138		

(a) accidentally overheated to 140 [° C]

(b) Pot was reheated from 106-126 [°C].

Table 3.5: Out-Gassing Experiment 25 g/kg

EXA-25		M1 (Vac)	M2 (Heat)	M3 (Desc)	M0 (Control)
Container Weight before	[g]	1130			
Container Weight after	[g]	1130			
Batch Weight	[g]	1021			
Sample Weight	[g]	255	255	255	255
Casting Jig Jig Empty Weight	[#] [g]	J3 593	J1 597	 500 (e)	J7 596
Pot Empty Weight	[g]	941	633		633
step 0 -	[g] [° C]	1196 13:15 125	888 13:50 03-09-18	287 (f) 15:05	910 14:19 125
step 1 -	[g]	1193 13:20 +1m (a)	886 13:55	287 23:45 03-09-18	908 14:22
step 2 -	[g]	1192 13:23 +1m	885/911 13:58 (c)	287 10:45 04-09-2018	
step 3 -	[g]	1190 13:26 +1m	909 14:03 (d)	287 20:35 04-09-2018	
step 4 -	[g]	1190 13:33 +1m (b)	908 14:06 (d)	281 25-09-18	

Continued on next page

Continued from previous page

EXA-25		M1 (Vac)	M2 (Heat)	M3 (Desc)	M0 (Control)
step 5 -	[g]	1188 13:38 +1m			
step 6 -	[g]	1188 13:40 +3.12m			

(a) Not below 200 [mbar], otherwise around 10 [mbar], moisture from boil-off wiped off with paper.

(b) Pot was reheated to 140 [°C].

(c) Spoon added to weight measurement (855 wh=911 with)

(d) Sample accidentally overheated to 155-160 [°C]

(e) amount of fresh CaCl desiccant added to the batch

(f) sample weight together with (open) storage box

Table 3.6: Out-Gassing Experiment 50 g/kg

EXA-50		M1 (Vac)	M2 (Heat)	M3 (Desc)	M0 (Control)
Container Weight before	[g]	1156			
Container Weight after	[g]	1156			
Batch Weight	[g]	1048			
Sample Weight	[g]	255	255	255	255
Casting Jig Jig Empty Weight	[#] [g]	J8	NA	NA	NA
Pot Empty Weight	[g]	942	660	500(d)	660
step 0 -	[g] [° C]	1224 14:55 125	914 15:28 120	287(e) 15:05 03/09/18	915 15:53 125
step 1 -	[g]	1222 14:59 +1m (a)	906 15:36	287(e) 23:45 03-09-18	912 15:57
step 2 -	[g]	1218 15:02 +1m	903 15:42 (c)	286 10:45 04-09-2018	
step 3 -	[g]	1214 15:05 +1m (b)	902 15:45	286 20:35 04-09-18	
step 4 -	[g]	1211 15:13		275	

Continued on next page

Continued from previous page

EXA-50		M1 (Vac)	M2 (Heat)	M3 (Desc)	M0 (Control)
		+1m		25-09-18	
step 5 -	[g]	1210 15:24 +3:21			

(a) Not below 200 [mbar], otherwise around 10 [mbar], moisture from boil-off wiped off with paper.

(b) Pot was reheated to 130 [°C].

(c) Sample accidentally overheated to 150-165 [°C]

(d) amount of fresh CaCl Desiccant added to the batch

(e) sample weight together with (open) storage box

3.4.2. Observations

During the experiment a number of observations were made:

1. General
   (a) Thorough stirring of the propellant was done however this did not eliminate all temperature uncertainty throughout the premix pot. The infrared thermometer measured at the liquid level and variations of ± 2 degrees were observed even after stirring.
   (b) The smaller pot which was used did not work well with the set-temperature function of the heating plates (induction), see figure 3.4a. In addition the smaller than usual samples (≈ 250 [g] compared to 2 [kg] or more) melted relatively quickly. This resulted in overheating several times, these instances are noted in the tables. No changes (colour/ smell/ viscosity) were observed to the propellant which stayed below reported decomposition/ boiling temperatures (refer to appendix A) so the experiment was continued.
   (c) A small uncertainty was introduced in the earliest batches based on whether the spoon was included in the initial weight measurement as propellant tended to stick to it. Measurements were afterwards corrected for this error.
   (d) During application of the vacuum the propellant expands 2-4 times in volume and looked a little like rising bread dough. The vacuum pot was barely large enough for this. A needle valve was used to control the vacuum which reduced the initial vacuum to 100-200 [mbar]. This prevented the propellant to be sucked into the hose/ vacuum pump.
   (e) The propellant lost a lot of heat during the vacuum process (likely due to the low sample weight and the latent heat from evaporation of the water) and the method did not work when the propellant was below 110 [° C] due to the substantial increase in viscosity. This therefore needs to be controlled when applying a vacuum to the molten propellant.
2. EXA-00
   (a) During heating of the regular propellant batches, much smaller bubbles (barely visible to the naked eye) were observed. It can be concluded that indeed a little moisture is present in every propellant batch. In Addition heating to 125 degrees does indeed already result in some boil-off of volatile components.
3. EXA-25
   (a) Propellant Premix felt relatively dry to the touch.
   (b) Some lumps had formed, these were broken up with the sieve.

(a) The propellant samples on the induction hotplate with thermostat active.

(b) The moisture condensed against the vacuum pot lid in EXA-50.

Figure 3.4: Pictures from experiment A: out-gassing methods

(c) Violent boiling was observed both during initial heating (upwards of 100 [° C]) and especially the first time vacuum was applied. This is quite distinct from the nominal propellant where this was not observed (EXA-00 or other historical batches). During the first vacuum cycle the moisture condensed against the vacuum pot lid, this was subsequently wiped of with paper.

4. EXA-50

(a) Propellant Premix felt like saturated wet sand, was very sticky. Similar to EXA-25 lumps were observed in the premix.

(b) Similar to EXA-25 sieving was attempted, however was unsuccessful. Instead the remaining premix was mixed by hand and divided over the sample containers.

(c) Similar to EXA-25 violent boiling was observed during heating and during the first time vacuum was applied. During the first vacuum cycle the moisture condensed against the vacuum pot lid, this was subsequently wiped of with paper. See figure 3.4b.

3.4.3. Analysis

Analysis results are provided in table 3.7. The various samples are given in separate columns with overall weight, weight loss and total application time given in the first three rows. The resulting mass fractions are provided in the next two rows. Fitting constants and the RMS error is given in the subsequent three rows. In the last three rows the estimated amount of moisture at the start of the experiment is calculated from the fitting constants, the added moisture is provided, and the removed moisture is presented. This shows both how good the fitting estimate is and how much moisture was actually removed during the experiment.

As can be seen in table 3.7 the predictions based on the function fits are really good for M(1) but

Table 3.7: EXA Analysis Results

Batch		EXA-00-1			EXA-00-2			EXA-25				EXA-50			
Method		M1	M2	M0	M1	M2	M0	M1	M2	M3	M0	M1	M2	M3	M0
Initial wt	[g]	250	249	250	250	245	250	255	254	255	255	255	254	255	255
End wt	[g]	248	248	250	247	249	249	247	248	249	253	241	242	243	252
total duration	[s]/[days]	540	720	240	540	780	240	492	960	22.2(d)	180	741	1020	22.29d)	240
$\xi_{PM}(t = end)$	[-]	0.992	0.996	1	0.988	0.996	0.996	0.9686	0.9764	0.9765	0.9922	0.9451	0.9528	0.9529	0.9882
$\xi_{H2O}(t = 0)$	[-]	0.0080	0.0552		0.0130	0.0929		0.0339	0.2598	0.0423		0.0692	0.0587	0.0631	
$1 - \xi_{H2O}(t = 0)$	[-]	0.9920	0.9448		0.9870	0.9071		0.9661	0.7402	0.9577		0.9308	0.9413	0.9369	
α	[1/s] [1/days]	0.0060	0.0001		0.0063	0.0000		0.0061	0.0001	0.0368		0.0042	0.0016	0.0616	
η_F, RMS	[-]	0.0018	0.0009		0.0006	0.0012		0.0018	0.0002	0.0011		0.0048	0.0000	0.0007	
Added moisture	[g/100g]	0	0	0	0	0	0	2.5	2.5	2.5	5.0	5.0	5.0	5.0	5.0
Estimated moisture	[g/100g]	0.8	(5)		1.3	(9.2)		3.4	(25)	4.2		6.9	5.9	6.3	
Removed Moisture	[g/100g]	0.8	0.4	0	1.2	0.4	0.4	3.1	2.4	2.4	0.08	5.5	4.7	4.7	1.2

are off for M(2). The baseline moisture level in the premix is consistently estimated to be between 1-2 grams/100g even when comparing different methods, which can be readily explained by variations in humidity and exposure to room conditions. Application of vacuum seems to be the most effective method, removing the most moisture from the propellant in the shortest amount of time. It is however still quite comparable with the effect of sustained heating on the propellants moisture content which requires less equipment but careful control of propellant temperature. Lastly it can be clearly seen that if the constituents are not fully dry, which was the case in this experiment, just heating the propellant to its casting temperature which (at 250 grams, 1.5 kW) takes about 3 minutes is insufficient to get rid of all contamination.

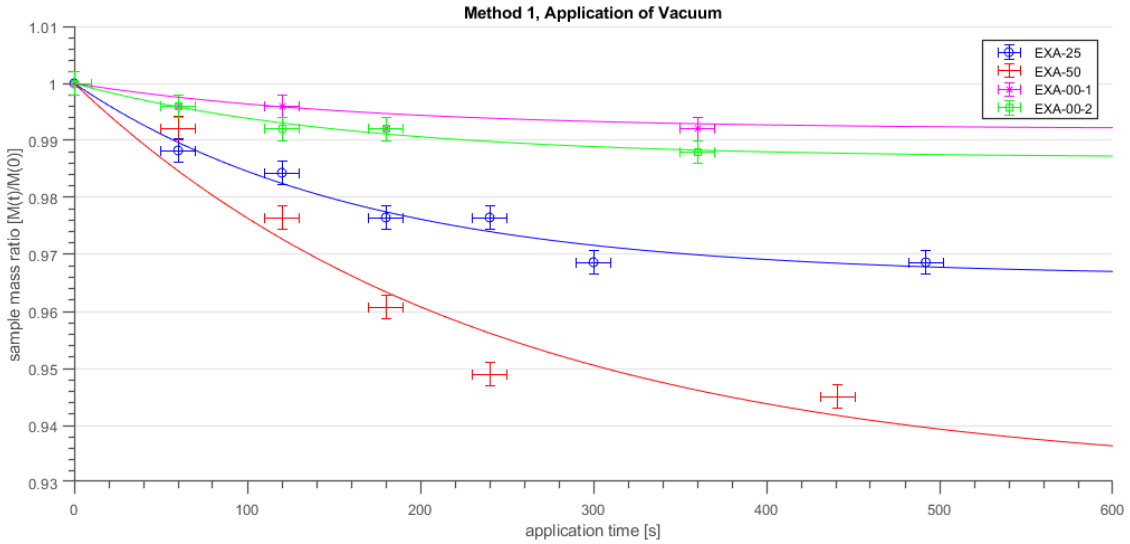

Figure 3.5: Application of vacuum on molten propellant. Mass fraction as function of time in seconds. Measurements with measurement errors and the least squares fit.

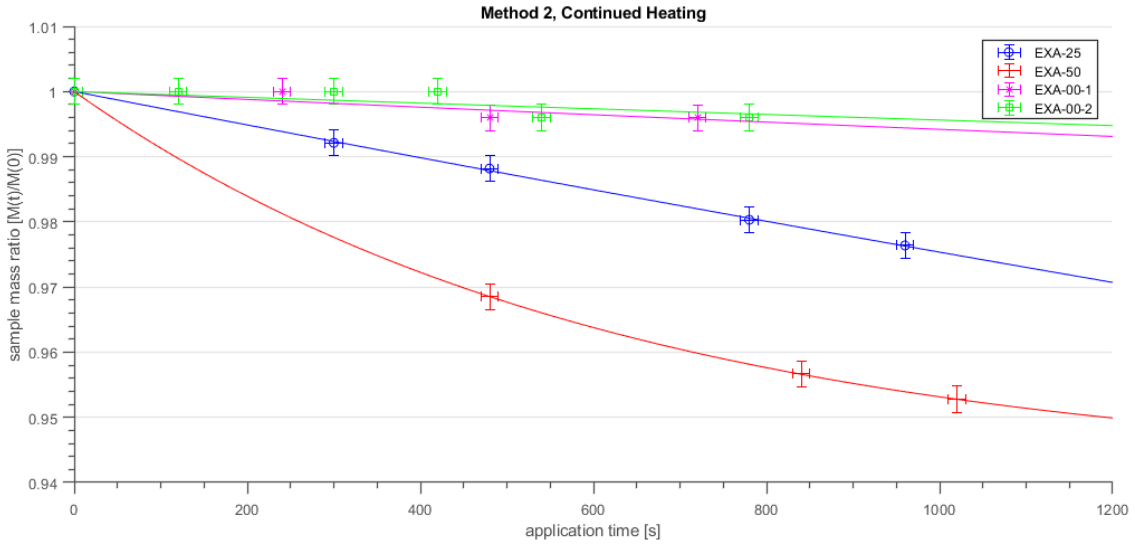

Figure 3.6: Application of continued heating on molten propellant. Mass fraction as function of time in seconds. Measurements with measurement errors and the least squares fit.

Method 1, Application of Vacuum

Presented in a different way in figure 3.5 the model follows the decrease in moisture content very

well. In addition, with method 1, the application of vacuum, the total amount of moisture removed coincides well with the expected moisture content. The moisture reduction rate is 0.006 [1/s] for EXA-00-1, EXA-00-2 and EXA-25. EXA-50 is a bit of an outlier, but still close with a reduction rate of 0.0042 [1/s].

Several aspects of this method were not included in the process such as variations of the propellant temperature (sometimes in the order of 20 degrees) and pressure (which ran close to 200 [mbar] during the first minute that vacuum was applied on EXA-50. It was observed that below 110 degrees the boil-off was significantly reduced as the propellant got more viscous and the propellant was reheated several times. The removal of latent heat during boil off reduced temperature fairly rapidly for EXA-50 reducing the effectively of the method. This can therefore also easily explain the reduced rate for EXA-50 compared to the other batches.

Method 2, Continued Heating

In figure 3.6 the data and trends are shown for method 2, continued heating. Although the model fits the data quite well (fitting error is 0.12 [g/100g] or lower) the overall trend does not show the expected exponential behaviour. This is supported by the total amount of moisture compared to the amount estimated for the various batches with method 1. The estimated value from method 2 varies considerably and is well outside the realistic ranges for EXA-00-1, EXA-00-2 and EXA-25 (shown between brackets).

When comparing the total amount of moisture removed during the experiment, the expected amount of moisture based on method 1, and predicted moisture quantities, it also seems that the experiment was not continued long enough to stabilise sample weights. Extrapolating the observed trends it can be expected that reduction would end at around 1200-1400 [s] or 20-23 minutes which agrees with propellant prepared by Gudnason [6]. This could have also resulted in more repeatable estimates of total moisture content.

Method 3, Storage with Desiccant

The samples stored with the desiccant follows the trend similar to the application of vacuum (higher moisture content results in a faster reduction rate). Several additional measurements are needed to support a more thorough analysis which was hampered by the fact that it was not known how long the process would take. (Note that the initial test plan, assumed the effect to be in the range of 24 hours.) Overall it can be concluded that the method works well but at a completely different time scale than M(1) and M(2)

3.4.4. Investigation Between Moisture and Propellant Density

From the experiment it was clear that moisture was present in the base ingredients however a relation between propellant quality and density and the moisture content was not yet established. To answer this question several grains were analysed which were produced for the DARE launch day on October 25th and 26th. These grains consisted of two sets of regular 80 mm grains which were cast without compression and trimmed afterwards to their final dimensions with the method described in section 2.3.2 [68].

One set was cast with moisture reduction through the application of vacuum for eight minutes and one set was cast without the application of vacuum. The resulting densities are shown in table 3.4.4 and the conclusion is clear; the inclusion of moisture decreases the propellant density from 1749 [kg/m^3] to as much as 1531 [kg/m^3]. Both sets of grains are shown in figure 3.7 The high porosity is clearly visible in the grains that were cast with propellant which was not put under vacuum, the other grains do not show these defects.

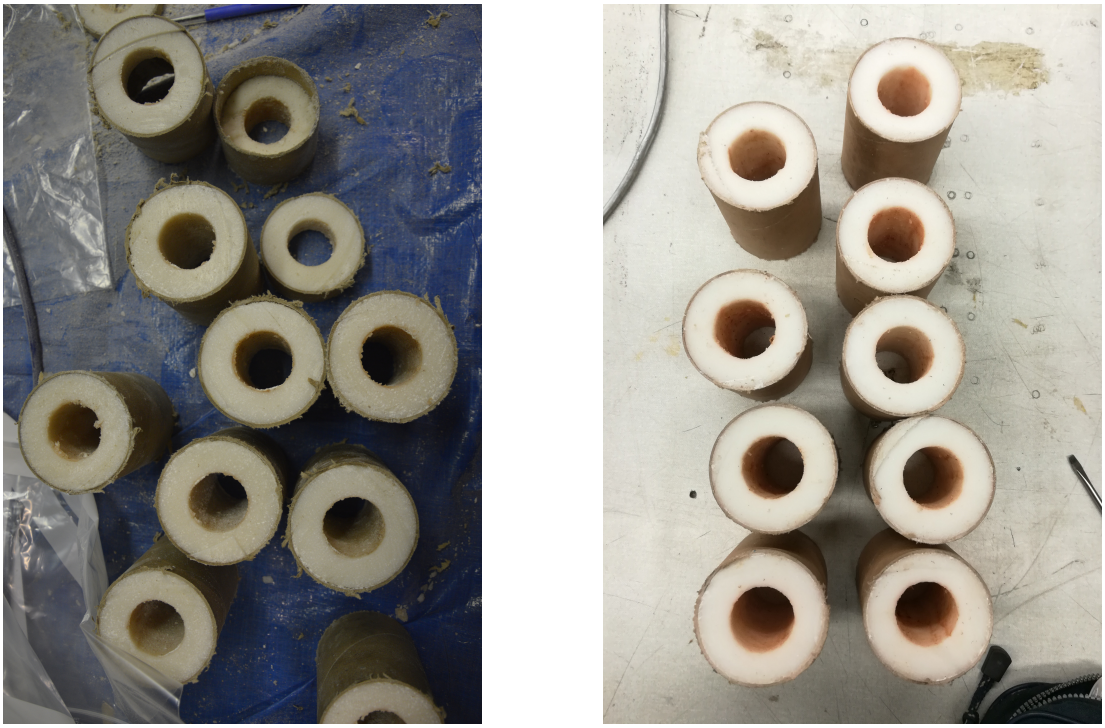

(a) Stratos I 80 mm grains produced with a surplus of moisture.

(b) Stratos I 80 mm grains produced after application of vacuum.

Figure 3.7: Stratos I booster grains

Property	unit	Without Vacuum	With Vacuum
Average Grain Mass	[g]	475	541
Average Liner Weight	[g/mm]	257	257
Number of Grains	[-]	8	9
Mean Propellant Density	[kg/m^3]	1531	1749
σ_ρ	[kg/m^3]	15.5	18.7
Mean Density Ratio	[-]	0.83	0.95
σ_{DR}	[-]	0.0084	0.010

With this result it can be clearly concluded that the low densities seen in earlier DARE projects [16] can be explained by the high relative humidity and the use of sorbitol that has been exposed to outside conditions.

3.5. Discussion

The experiment demonstrated that considerable moisture is present in the propellant and that it is responsible for the low propellant density. The application of vacuum was found to be the most effective method to reduce this moisture although relatively comparable to continued heating of the propellant. It was furthermore found that 1-2% of moisture is present even in the 'dry' ingredients.

It was found during analysis of the experiment that both Sorbitol and KNO_3 are hygroscopic. However especially the hygroscopicity of sorbitol is of particular concern. Upward from 60% RH the moisture content of sorbitol grows essentially unlimited (refer to appendix A). When combined with the relative humidity during the experiments (up to 93% during the out gassing experiment and up to 79% during the casting experiments from the next chapter) a cumulative exposure of an hour is already expected to

lead to significant contamination with moisture, which is further demonstrated by the variation between EXA-00-1 and EXA-00-2. KNO_3 on the other hand has a hygroscopicity that is reported significantly lower with only about 0.03% water uptake in 80% relative humidity over 50 days [7]. The sorbitol stored and used in DARE thus is the most likely source of the moisture contamination. It is recommended that sorbitol is stored in absolutely airtight containers, and a suitable out-gassing method is used during manufacture .

Analysis during this experiment was complicated by the difficulty in estimating the effects of the various strategies when designing the experiment. Several aspects of the methods were not included in the process such as variations of the propellant temperature (sometimes in the order of 20 degrees) and pressure (which ran close to 200 [mbar] during the first minute that vacuum was applied on EXA-50). It was further observed that below 110 degrees the boil-off of samples was significantly reduced as the propellant got more viscous. To compensate the propellant was reheated several times. The removal of latent heat during boil off reduced temperature fairly rapidly for EXA-50 further reducing the effectively of the method. This can therefore also easily explain the reduced rate for EXA-50 compared to the other batches.

The application of vacuum appears to be explained well by concentration difference as the driving mechanism. For regular boiling the proposed model works less well which could be explained by a different driving mechanism such as heat transfer inside the propellant. The moisture reduction would then fit a linear trend assuming a constant power from the heating plate. The large fluctuations in propellant temperature point towards a possible improvement of this method but also show the limitations of current casting equipment; it is sufficient for heating large propellant batches to an approximate temperature but less useful for maintaining a precise propellant temperature.

Similarly large improvements could be made to the desiccator system which would improve the effectiveness of the desiccant. The current design only allowed limited circulation of gasses inside the boxes. In addition many commercial desiccators apply a vacuum to aid the process. Lastly it is noted that scaling up this process to significant quantities (more than several [kg] at a time) is expected to be unpractical.

3.6. Conclusion and Recommendations

What is clear is that ingredients in DARE can have moisture quantities upwards of 1-2% by mass depending on the ingredient source, and how long it has been stored. Sorbitol at DARE is in principle stored dry in an airtight container however with current usage the sorbitol can cumulatively be exposed to room conditions for multiple hours before it is used making propellant. Together with its high hygroscopicity [36] this explains in part the moisture content measured in the experiments. It is recommended to control the moisture uptake if possible by stressing the importance of proper storage, looking for a method to measure the base moisture content of sorbitol before use, and by application of vacuum as an additional process step.

It was proven during this experiment that the KNSB propellant density is mainly reduced by contamination with water of the premix/ingredients. This was contrary to initial expectations as can be seen in for instance the estimated stroke when the casting jigs were designed (upwards of 10 [mm], see appendix F). Casting the propellant in the Netherlands with on average very high humidity and a room that generally has one door open to the outside leads to easy contamination of the propellant. It is clear from the work of other researchers such as [60] that, as they work under dryer conditions, a specific moisture reduction strategy is of less importance as long as ingredients are stored dry.

3.6.1. Evaluation of Out-Gassing Strategies

Several methods for actively reducing moisture content were compared. Of these the application of vacuum (<10 [mbar]) on molten propellant is the most effective, A contamination of 1-2 [g] H_2O/100 [g] is removed in 6 to 8 minutes. In addition there is clear visual feedback on the process compared to for instance sustained heating. It is a method that can also be considered when using different sugars such as sucrose or dextrose that generally are much more constrained in their pot life due to caramelization.

The sustained heating of KNSB propellant was showed to be inferior to the application of vacuum. Although the KNSB propellant is considered to have a near unlimited pot life, the application time, which can be in excess of 25-30 minutes is prohibitive. In addition, depending on the heating equipment and amount of propellant being prepared it is a process more prone to overheating. With suitable equipment the method does work.

The storage of ingredients with desiccant is on paper the slowest method. Even so several large benefits make it worth considering. Moisture reduction with desiccant can take over 60-70 days with the current desiccator design. When comparing it to the application of vacuum it is likely an unpractical method for large batches of ingredients. The method should however be strongly considered for several reasons. Bulk storage of the separate ingredients with small containers of desiccant can assure the dryness of ingredients, limiting the problem altogether. Adding desiccant to the bulk ingredients takes very little effort and can be done prior to mixing the ingredients.

Lastly it can be established that simply heating the propellant to the desirable casting temperature is an insufficient way of reducing the moisture quantity of the propellant grains.

3.6.2. Evaluation of Experiment Goals

The experimental goals are:

1. **MET** *Quantify the effect of out-gassing strategies on propellant quality,*
   Various methods were compared and the effect on contamination with moisture was measured in terms of duration and weight decreased. Furthermore insight was gained into the base moisture quantity in the (initially presumed dry) ingredients and this was linked to an increase in propellant porosity and a simultaneous decrease in propellant density.
2. **PARTIALLY MET** *Determine the best production technique for KNSB propellant grains for the BEM with respect to achieved quality and effort.*
   With the new insight it is recommended to change the production process with the application of vacuum on the molten premix. Furthermore it stresses the importance of maintaining dry ingredients and it is recommended to investigate of direct measurement of moisture content of the bulk ingredients is possible.

No complete BEM grains were produced in this experiment and as such the goal is considered partially met as the propellant quality and density was already substantially improved.

In conclusion the focus of this experiment was primarily on two aspects on KNSB propellant manufacturing: to figure out how to increase propellant density to for DARE acceptable levels, and how to improve the overall propellant quality to the point that grains can be cast with minimal spares. This experiment has substantially improved both and in addition provided significantly more practical insight in the KNSB propellant. Although the experiment could be improved further with the new insight, the limitations of current DARE casting equipment (temperature control) and facilities (humidity) make further improvements challenging with only a limited reward until such improvements can be made.

4

Propellant Casting Experiment

Although a density increase was achieved already with the moisture reduction strategies described in the previous chapter, two key techniques still needed to be evaluated. The application of mechanical compression and preheating of moulds before casting. In addition the tooling changes need to be validated before the regression experiments of later chapters. Before the experiment results from chapter 3, thermal contraction was believed to account for a large part of the reported density problems. Similarly heated moulds could reduce the cooling rate of propellant directly after casting, potentially leading to density and quality increases. In this experiment it is investigated if these methods can increase propellant density beyond the results obtained with the application of vacuum.

Besides the problematic propellant density at the start of this thesis, the high propellant geometrical variations, cutting losses and high rejection rate of grains were identified as area's of improvement [16]. Where improvements in propellant density are expected to alleviate these problems somewhat, there is still a lot of improvement possible. Important here is a less subjective definition of propellant quality that includes but is not limited to the propellant density alone. A crack might not lead to measurable propellant density variations but could still result in motor failure.

Similar to the previous chapter first the experiment goals will be provided together with the success criteria. The experiment design is provided which includes a description of the propellant quality which is provided as part of the method description. These were adapted from proposal made in the literature study [16]. Experiment results are provided in section 4.4. Those results are then discussed and concluded in section 4.4.2 and 4.6 respectively.

4.1. Experiment Goals and Success Criteria

A first addition to the propellant manufacturing is the application of vacuum on the liquid propellant. In extension to the goals provided in chapter 3 the following test goals are defined:

1. Quantify the effect of mechanical pressure and preheating of moulds on propellant quality.
2. Determine the best production technique for KNSB propellant grains for the BEM with respect to achieved quality and effort.

Additionally the following secondary objectives are to be met:

1. Gather data about cooling and compression rates of BEM propellant grains.
2. Gain experience with the manufacturing of BEM propellant grains using the designed tooling.
3. Create sufficient grains to be used in the thermal conditioning experiments of the regression experiment from chapter 6.
4. Evaluate the grain quality criteria (refer to section 4.2.1) for acceptance of KNSB grains.

The formal success criteria for this experiment are the following:

1. Successful determination of the effect of compression and preheating the moulds on propellant quality.
2. Successful validation of the casting procedures for BEM propellant grains.

Additionally the following secondary criteria are defined:

1. Successful collection of thermal and compression data during the curing of KNSB grains.
2. Successful production of at least 6 grains that meet the acceptance criteria as defined in section 4.2.1. These grains are to be used in the thermal conditioning tests and BEM tests.

The suspension criteria are provided below. These denote conditions under which the test campaign will be halted until the problems have been resolved.

1. An unacceptable risk to the involved personnel, critical equipment, general public or 3rd party property.
2. Failure of a propellant grain to meet the quality assurance criteria as defined in section 4.2.1 without a clear root cause.
3. Any indication that success criteria as defined in this section can no longer be met.

4.2. Experiment Design

During this experiment the effects of preheating moulds and adding mechanical compression are investigated. The strategies considered for this experiment are:

1. *Preheated casting equipment.* By preheating the casting equipment to 100 °C the propellant has a more uniform cooling rate. This allows the propellant to settle more evenly and could results in a higher quality grain. Ambient temperature, pre-casting mould temperature and propellant temperature will be recorded.
2. *Applying mechanical pressure to the propellant after casting.* Mashek [60] recommends compression forces equal to 25 Psi (1.7 bar). Based on reported results this will increase propellant quality to 95-99 % of the theoretical value (1841 [kg/m^3].)

Six grains will be cast.Two grains are cast with heated moulds and compression, two grains are cast with only compression and two grains are cast with only the plunger in place. As compression has been established most firmly in literature the approach with only heating of the casting moulds is omitted.

Propellant is prepared from a single batch of premix and grains will be cast in quick succession. Afterwards the grains are checked with the quality criteria outlined in section 4.2.1. Two grains, one with both compression and heating and one with only compression will have embedded thermocouples to register the propellant temperature during the curing process. In addition measurements will be taken of the spring compression to indicate the contraction and compression force during the casting process.

4.2.1. Propellant Quality Criteria

The proposed quality assurance requirements are provided below. These were adapted from chapter 4 in [16].

The first batch of propellant grains for the BEM will determine the standard that other grains will be compared to. The initial set of grains will thus consist also of a trial run without accurate numbers on expected propellant density and typical surface consistency. Criteria BEM-QA-1.1 to BEM-QA-1.3 are therefore initially based mainly on comparison to earlier DARE propellant production methodologies without the changes and representative numbers from literature. The criteria are expected to be improved as more experience is gained.

- BEM-QA-1_1 Solid Propellant grain acceptance shall be determined based on the following indicators:
  - BEM-QA-1.1_1 Ingredient sources shall be of similar purity from a known supplier.

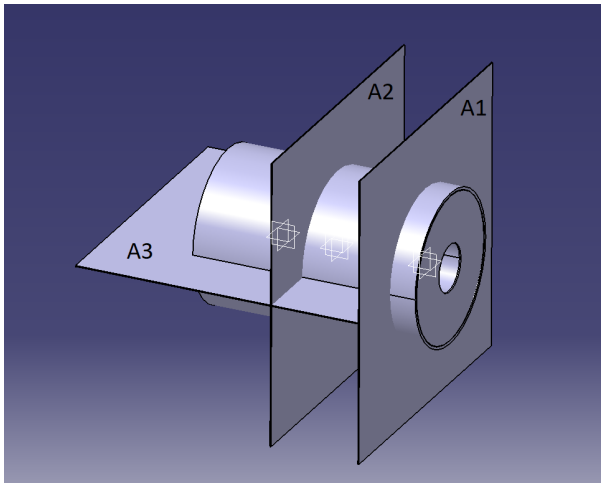

Figure 4.1: Nominal grain cutting planes (A1, A2 and A3)

  - BEM-QA-1.2_1 The KNO_3 PSD shall be measured and not deviate more than [TBD] from the propellant characterization data.
  - BEM-QA-1.3_1 Production shall follow established procedures such as defined in chapter 2.
  - BEM-QA-1.4_1 No errors or flaws shall be identified that change the propellant surface area by more than 5 [%].
  - BEM-QA-1.5_1 Propellant density shall be larger than 95 [%] of theoretical.
  - BEM-QA-1.6_1 Grain geometric dimensions shall be within $+0/-0.5$ [mm] for the outside diameter and within ± 1 [mm] on other dimensions as defined in appendix E.
  - BEM-QA-1.7_1 Appearance of the propellant shall be consistent with earlier grains (e.g. visual inspection and experience).

- BEM-QA-2_1 For production changes a test grain shall be subject to general and destructive inspection:
  - BEM-QA-2.1_1 The test grain shall meet general grain acceptance criteria (BEM-QA-1).
  - BEM-QA-2.2_1 The test grain shall be cut 3 times as specified in drawing 4.1.
  - BEM-QA-2.3_1 The grain slices shall have no flaws other than from machining and have a uniform bond with the inhibitor material.

To facilitate qualitative analysis the propellant quality is further expressed as indices with 0 very poor and 1 indicating perfect quality. Propellant density is then expressed via equation 4.1 with $\rho_{id} = 1841$ [kg/m^3] [16].

$$I_\rho = \frac{\rho_{grain}}{\rho_{id}} = \frac{M_{grain} - M_{liner}}{\pi L(R_{out}^2 - R_{in}^2)\rho_{id}} \tag{4.1}$$

Macroscopic surface quality is expressed via equation 4.2 with $A_{0,id}$ and A_{flaws} the nominal exposed surface area and additional surface area due to flaws respectively in [m^2]. The nominal burning surface area is provided from geometric calculations. The surface areas of flaws can be estimated from basic geometric objects such as the surface of a hemisphere. The error made by this method is expected to be sufficient for quantitative analysis as long as it is kept consistent between grains.

$$I_A = \frac{A_{b,id}}{A_{b,id} + A_{flaws}} \tag{4.2}$$

Variable	name	Range	Accuracy
M	Sample Mass	≈0-250 [g]	± 0.5 [g]
X	Sample Compression distance	≈0-5 [mm]	± 0.05 [mm]
T_{TC}	Sample Temperature (TC)	≈15-125 [°C]	± 1 [°C]
T_{IF}	Sample Temperature (Infrared)	≈15-125 [°C]	± 0.5 [°C]

Table 4.1: Measured Variables

4.2.2. Experiment Variables

The experimental variables are compression to 1.7 bar of mechanical pressure and heating to around 90 °C for the experiment. The measured quality are the propellant quality as expressed in the density and surface quality as outlined in section 4.2.1. Measured variables are provided in table 4.1

Control variables during the test are, similar to chapter 3, the following:

- *Propellant Composition,* will be fixed at 65% KNO_3 and 35% Sorbitol by mass with an accuracy of 1 gram in 1000 gram (determined by the accuracy of the scales).
- *Propellant homogeneity* will be controlled by thoroughly mixing the entire propellant batch before starting the experiment.
- *Process Control* will be assured by closely following the casting procedures. Specifically the following points will controlled:

  1. Casting temperature (to within 0.5 degrees) by infrared thermometer.
  2. Duration of all process steps will be recorded by stopwatch together with a time-lapse from a camera.
  3. Equipment will be identical and will be thoroughly cleaned between tests.

It is expected that the largest increase in propellant density will be achieved by both heating the moulds and applying mechanical pressure. It is expected that density index I_ρ of the uncompressed propellant will be around 0.85-0.9 in line with DARE experience, only compressed grains are expected to have a density ratio around 0.95. Grains that are heated and compressed are expected to have densities around 0.95-0.99.

Propellant surfaces are expected to be vastly increased leading to rejection rates below (9/10) depending on operator experience.

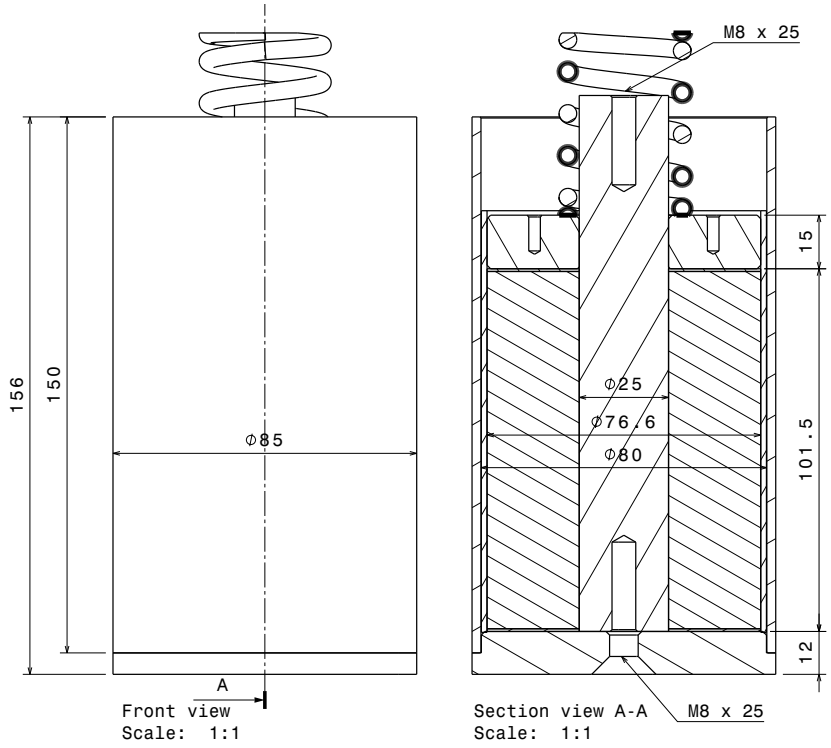

Figure 4.2: Developed Casting mould with BEM grain (refer to appendix E.)

4.3. Experimental Setup

The propellant grains to be produced will be similar to BEM grains. A drawing with the dimensions of the grain and casting mould is provided in figure 4.2. Besides the equipment provided in chapter 2 a National Instruments C-RIO and laptop were used (refer to figure 3.2 to measure the propellant using K-type thermocouples (RS-Pro) at a measurement frequency of 10 [Hz].

4.3.1. Protocol

The experiment protocol is provided in appendix B.2. Similar to the first experiment, the heritage manufacturing method was used as described in 2. Deviations that were taken from the experiment protocol are the following:

A first iteration of this experiment was performed on 06/09/2018. Although the casting process worked well it was found that due to in-proper tolerances (after the redesign) of the liners caused the plungers to get stuck during compression. One of these grains is shown in figure 4.3.

A second iteration of the experiment was performed on 09/10/2018. For the compression experiment the propellant samples were made and cast on the 09/10/2018 and removed the following morning on 11/09/2018 around 13:30. Temperature was recorded during the night. Ambient temperature in the room varied between 14 and 22 [°C]. Relative humidity was between 70% and 79%. [1]

With the results from the session on 06/09/2018 as reference it was decided to remove the uncompressed grains from the experiment as the expected results would be uneven grains with large surface defects as shown in figure 4.3. Instead the grains UC-1 and UC-2 were compressed similar to CC-1T and CC-2 but not pre-heated with similar updates in grain identification.

The entire propellant batch was made from 2×2 [kg] batches of premix and 1×1.1 [kg] batch of

[1] weatheronline.co.uk

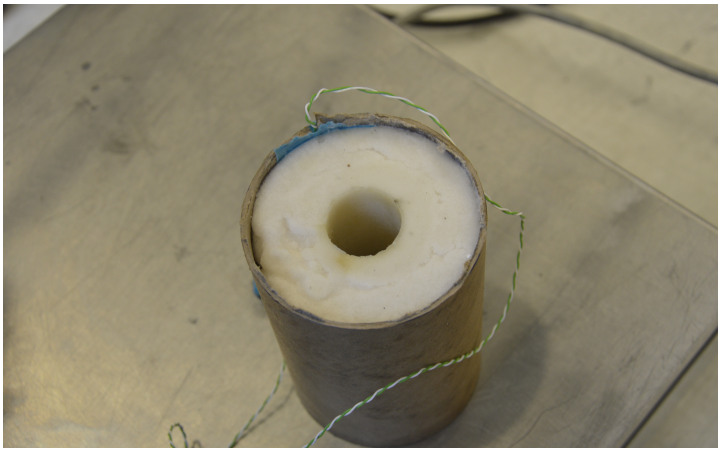

Figure 4.3: Grain produced during the first try of the experiment on 06/09/2018 showing large surface defects due to problems with plunger tolerances.

premix with some left premix from an earlier experiment that same day. This was molten as a single 5,3 [kg] propellant batch that was thoroughly mixed by hand to eliminate any between grain variations. As the grains could not be cast simultaneously the propellant mix was reheated to 125 ± 1 [° C] for every grain.

As the propellant batch was much bigger than during the first experiment a new vacuum pot was developed and build. This consisted of one of the regular 10 [L] propellant pans together with a laser cut 25 mm acrylic plate, a rubber seal and an adapter similar to the smaller vacuum lid. This vacuum pot was tested before use and shown to be sufficiently airtight. The vacuum was applied for a total of 8:15 minutes resulting in a total propellant weight loss of 4 [g].

4.3.2. Identification of Grains

The identifiers will follow a different structure than the samples from the outgassing experiment. The first letter after the code 'EXB' denotes compressed denoted with (C), or uncompressed denoted with (U). The second letter will denote whether the mould was hot (H) or cold (C). The number denotes the repetitions of the test conditions this can include a (T) if thermocouples are present. The experiment matrix is shown in figure 4.2.

no	Test-id	Compression	Preheated	Thermocouples
1	EXB-CC-1	yes	no	no
2	EXB-CC-2	yes	no	no
3	EXB-CC-3T	yes	no	yes
4	EXB-CC-4	yes	no	no
5	EXB-CH-1T	yes	yes	yes
6	EXA-CH-2	yes	yes	no

Table 4.2: Proposed test matrix for investigation of compression and heating strategies.

4.4. Results

The manual measurements taken during the experiment are shown in table 4.3. Geometric values are defined as in figure 6.6a. Measurement accuracy was 1[g] for all weight measurements and 0.05 [mm] for all geometric dimensions. Due to the frayed edges of the cardboard after cleaning and trimming the inhibitor length was a little less accurate. Similarly it was difficult to define exactly the outer propellant diameter as the diffusion into the cardboard was difficult to estimate. This was solved by measuring the dimensions of a grain cut with the propellant saw as part of the quality check.

Compression force is determined by measuring the compression of the springs. In relaxed state these measure 65 [mm] with a spring constant of 156.0 [N/mm]. This results at a length of 61 and 59 in a compression force of 624 [N] and 936 [N] respectively. Divided by the grain surface and neglecting any friction this equals a mechanical pressure of 0.154 and 0.231 [MPa] respectively. Baseline compression was thus set to approximately 60 [mm] resulting in a pressure of 0.193 [MPa], a little over the design pressure of 0.17 [MPa] to account for expansion and friction losses.

Table 4.3: Compression Experiment

EXB		CC-1	CC-2	CC-3T	CC-4	CH-1T	CH-2
Order of Casting	[-]	3	4	5	6	1	2
Compression		✓	✓	✓	✓	✓	✓
Preheated Mould						✓	✓
Thermo-couples				✓		✓	
Propellant Production							
Total Premix weight	[g]	5100 (a)					
Total Molten Weight	[g]	5328					
After Vacuum	[g]	5326 (b)					
Casting Jig		01	02	03	04	05	06
Jig Empty Weight	[g]	1109	1115	1134	1133	1116	1111
Propellant Mass	[g]	754	758	760	759	768	756
Mould Temperature	[° C]	ambient				78	75(c)
Time	[hh:ss]	21:27	21:32	21:35	21:41	21:17	21:21
Casting temperature	[° C]	126	125	124.7	125.8	125	124
Propellant Curing							
Time	[hh:ss]	21:48	21:51	21:52	21:53	21:46	21:47
Uncompressed	[mm]	65					
Compression	[mm]	59.58	60.35	59.6	60.2	59.8	60.25
Time	[hh:ss]	22:31					
Initial Compression	[mm]	60.8	60.7	60.3	61	60.9	61.35
Reset Compression	[mm]	59.9	59.8	59.6	59.5	59.85	59.95
Time	[hh:ss]	23:42					
Compression	[mm]	60.35	59.95	59.8	59.9	60.0	60.3

Continued on next page

Continued from previous page

EXB		CC-1	CC-2	CC-3T	CC-4	CH-1T	CH-2
Time	[hh:ss]	13:34					
Compression	[mm]	60.3	60.0	59.8	59.9	60.0	60.3
Total Stroke	[mm]	1.40	0.55	0.90	1.20	1.20	1.45
Remarks	[-]	(d)	(d)		(d)	(e)	(e)
Grain Quality Measurements							
Final Assy Weight	[g]	1861	1873	1896	1889	1852	1853
Grain Mass after trimming	[g]	783	792	796	790	797	777
Inhibitor Length	[mm]	109.95	112.8	116.4	113.5	111.0	108.2
Inhibitor mass	[g]	36.2	37.1	38.3	37.3	36.5	35.6
Propellant Length	[mm]	105.6	107.9	109.15	110.6	106.15	104.65
Grain Outer Diameter	[mm]	79.85	79.8	79.9	79.9	79.9	79.9
Propellant Outer Diameter	[mm]	75.9 (f)					
Inhibitor Diffusion	[mm]	0.4 (g)					
Propellant Core Diameter	[mm]	24.8	24.9	24.7	24.95	24.8	24.8
Est. Area of Defects	[mm^2]	0	0	6	3	0	0
Max Propellant Density	[kg/m^3]	1750	1733	1716	1686	1773	1753
Min Propellant Density	[kg/m^3]	1709	1693	1676	1646	1732	1712
Grain Quality Indices							
Propellant Density Ratio	[-]	0.95/ 0.93	0.94/ 0.92	0.93/ 0.91	0.91/ 0.90	0.96/ 0.94	0.95/ 0.93
Propellant Defect Ratio	[-]	$\approx 0\%$	$\approx 0\%$	<1%	<1%	$\approx 0\%$	$\approx 0\%$

(a) Some error as remaining propellant of a previous batch was not included.

(b) Vacuum was applied for a total of 8 minutes 15 seconds.

(c) Extrapolated from thermocouple data from CH-1T

(d) Applied compression led to small propellant beads on top of plunger.

(e) Pure Sorbitol was pressed from bottom of grain.

(f) Measurements taken from sawed propellant grain averaged from 4 distinct measurements.

Thermal data was gathered from 5 thermocouples, two placed on the CC-3T two on CH-1T. One Thermocouple measured the ambient reference temperature in the room. The location of the thermocouples is shown in photo 4.4. The location for both sensors was 50 [mm] from the bottom of the liner. The thermocouples inside were located at 17 ± 0.5 [mm] from the cardboard edge.

The thermal data gathered during the night and subsequent morning is shown in figure 4.5 and 4.6. Timing uncertainty is around 2 minutes based on the recorded duration of certain production steps. A sensor connection error occurred (between 21:30 and 21:55) with the CH-1T thermocouple mounted externally to the grain. This was detected and corrected after roughly 25 minutes.

Figure 4.4: Thermocouple Placement inside the grain.

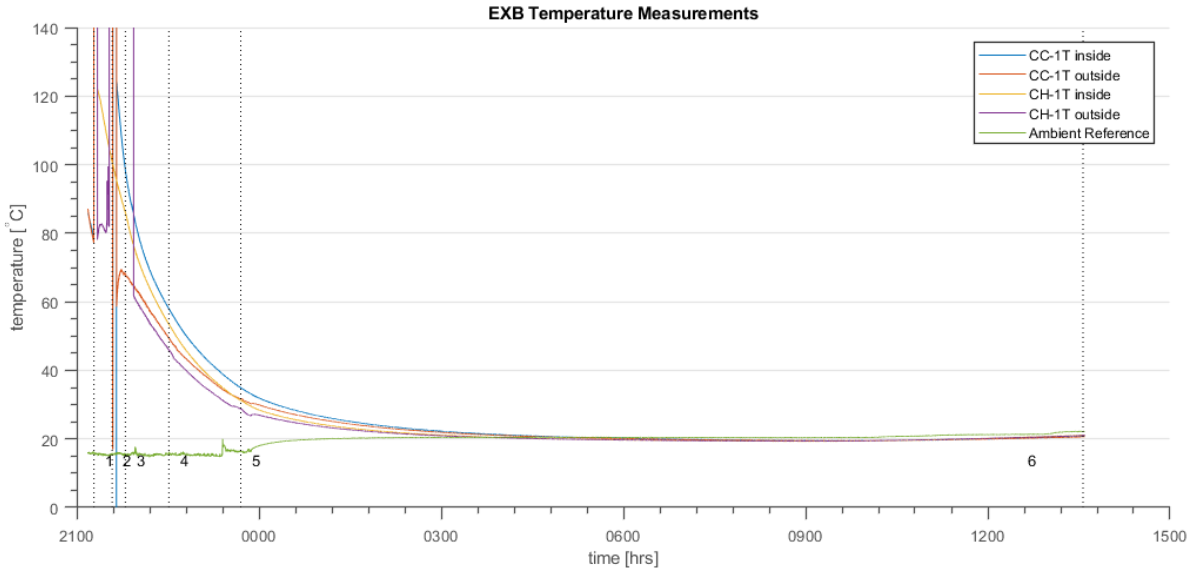

Figure 4.5: Thermal data obtained during experiment part B. Vertical black lines denote the following events: (1) casting CH-1T, (2) casting CC-1T, (3) compression applied, (4) compression measurement compression reset, (5) compression measurement, (6) compression measurement and end of experiment.

4.4.1. Observations

During the experiment several additional observations were made:

1. Propellant Preparation

    - During Vacuuming of the propellant it was found that the current pot volume (approximately 8 [l]) was insufficient to directly apply the full vacuum (10 [mbar]) on the entire 5.3 [kg] as the propellant would expand into the vacuum hose. This was solved by reducing the vacuum with a needle valve similar to the EXA-25/ EXA-50 batches from the out gassing experiment. Expansion was in this way actively limited to just below the lid. After most bubbles had collapsed the pressure was further reduced to the intended 10 [mbar] after about 2 minutes. The temperature drop during this period was only 3 [$^{\circ}C$] from 125 to 122 [$^{\circ}C$].
    - The weight difference between total premix weight, molten weight and the remaining weight after vacuum shows a decrease of only 4 [g] resulting in a net moisture quantity of $^{4}/_{5332} \approx$

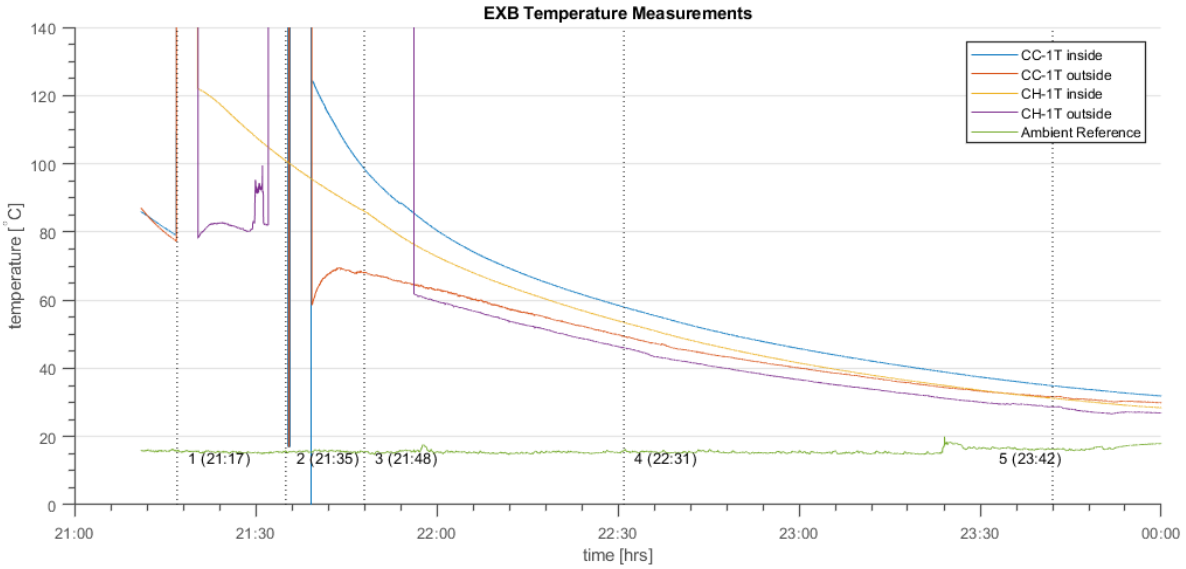

Figure 4.6: Thermal data obtained during experiment part B. Vertical black lines denote the following events: (1) casting CH-1T, (2) casting CC-1T, (3) compression applied, (4) compression measurement, (5) compression measurement.

0.075% this is considerably less than the the results obtained in the out-gassing experiment.

2. Casting

   - Casting temperature was measured with an infrared thermometer. Although measurement accuracy was 0.1 [°C], the propellant wasn't uniformly heated. This resulted in actual measurement inaccuracies of around 3 [°C] dependent on how vigorously the propellant was stirred. As vigorous stirring potentially introduces more air bubbles into the mixture this inaccuracy was accepted during the experiment.
   - Casting has become relatively routine during the experiment resulting in relatively short cycle times between grains of around 3 minutes. As the preheated moulds were cooling down relatively quickly (see figure 4.6) it was decided to fist cast CH-1T and CH-2. Afterwards the remaining grains were cast in sequence.

3. Compression Measurements

   - In figure 4.5 it can be clearly seen that room temperature is influenced by the open door, which was opened for ventilation reasons, during casting activities up to roughly 00:00. Afterwards the door is closed and room temperature stabilises at around 20 degrees until the next morning when the sun warms up the room slightly.
   - During compression small beads of propellant were observed on top of the grains CC-1, CC-2 and CC-3, similarly with the two preheated moulds, CH-1T and CH-2, pure sorbitol was pressed around the plungers. This is shown in figure 4.7. This explains in part the larger compression stroke measured on several of the other grains. Although the volume of propellant lost could not be measured the observed amounts did coincide roughly with measured discrepancies. A comparison of the cast weight and measured weight is performed in the subsequent section.
   - As the grains were cast sequentially the compression was applied only after 20 minutes for UC-1 to CC-2 and 26 and 29 minutes for CH-1T and CH-2. Thermal data shows that the propellant at that time was still fluid for all grains. This is also clear from the propellant beads pressed from the grains mentioned in the previous comments. It cannot however be ruled out that this timing could be further fine-tuned in future casting sessions. In addition the full crystallisation of sorbitol only happens over a few days as the propellant retains a soft, rubber like, state even after it has attained room temperature.

4. Grain Post Processing

   - Grain surface quality was the highest ever observed in DARE with surface finishes very close to plastic and (almost) no gaps, bubbles or other defects.
   - Although the base of the casting moulds came of easily, the plugs were relatively difficult to remove from the grains. This was solved in the end by using an aluminum 40 ⌀ [mm] tube of sufficient length and M8 threaded rod. The plugs were subsequently removed at leisure by drawing them through the plunger. After plugs were extracted 1/3 from the mould most could be removed fully by hand.
   - Trimming the cardboard was done by hand which resulted in some slightly frayed edges. This reduced the measurement certainty on the length of the cardboard liners to ± 0.5 [mm].
   - Propellant outer diameter was difficult to determine from the cast grains directly as propellant diffuses slightly into the cardboard. A better measurement was taken from the cut grain.

Figure 4.7: Propellant pressed from the grains. Grain order is reversed to table 4.3.

4.4.2. Analysis

For the experiment on compression, the thermal data for both heated and non pre-heated grains are shown in figures 4.5 and 4.6. To aid in analysis three additional figures are presented. In figure 4.8 the thermal data is shifted so that casting times of both CC-1T and UC-1T coincide with T=00:00 [hrs:min] relative. In figure 4.9 and 4.10 the compression data is superimposed on top of the temperature data.

When comparing compression data for the six grains it is evident that the grains that had reported leaks (all except CC-1T) had, on average also larger compression strokes. Based on the mass difference, assuming the maximum uniform density, the resulting stroke correction is provided in table 4.4.

Table 4.4: Compression Experiment, correction for leaks

EXB		CC-1	CC-2	CC-3T	CC-4	CH-1T	CH-2
Cast Propellant Mass	[g]	754	758	760	759	768	756
Grain Mass after trimming	[g]	783	792	796	790	797	777
Inhibitor mass	[g]	34.0	34.9	36.0	35.1	34.3	33.5
Grain Propellant Mass	[g]	754	758	760	759	768	756
Mass difference	[g]	5.0	0.87	0	4.1	5.3	12.5
Max Propellant Density	[kg/m^3]	1750	1733	1716	1686	1773	1753
Propellant Cross section	[m^2]	0.0041					
Correction	[mm]	0.70	0.12	0	0.59	0.73	1.73
Measured Stroke	[mm]	1.40	0.55	0.90	1.20	1.20	1.45
Corrected Stroke	[mm]	0.70	0.43	0.90	0.61	0.47	-0.28

In table 4.4 it can be seen that with this correction the actual strokes are closer together with the overall compression between 0.43 and 0.90 compared to 0.55-1.45 for the non corrected stroke. It seems however that the last grain, CH-2, has a measurement error as the correction leads to a negative stroke: the propellant effectively got longer during the cooling. The difference in compression data can therefore not readily be explain by looking at the mass difference. Most likely a measurement error with the cast propellant (some propellant was spilled on the scales or a different bolt or washer was weighed along with the propellant).

When comparing compression with respect to the cooling of the grains it must be noted that all non-preheated moulds where compressed between 21 and 12 minutes after casting. For the preheated moulds this was between 29 and 26 minutes. This results in temperatures at compression between 91,1 [$^\circ C$] (CC-3T) and 85,8 [$^\circ C$] (CC-1) for the non-preheated moulds. For the preheated moulds this temperature is 91,2 [$^\circ C$] (CH-2) and 88.0 [$^\circ C$] (CH-1T). It can be seen that the grains with the lowest density were cast last and were therefore still warmer when compression was applied. Similarly the preheated grains show that the highest density is obtained for the grain where compression was applied latest.

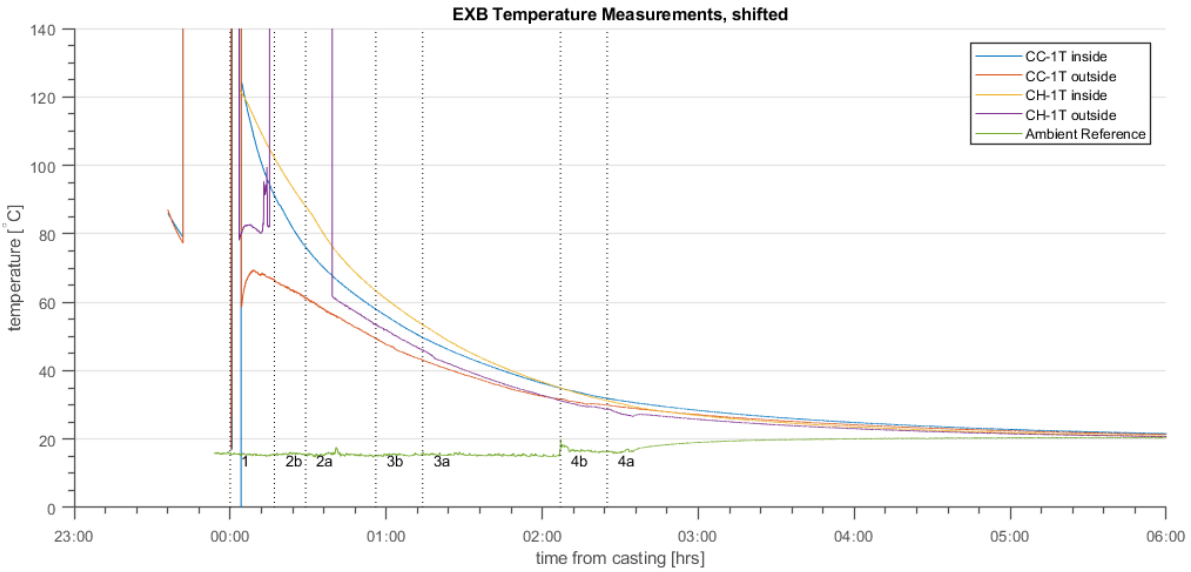

Figure 4.8: Thermal data shown with all major events shifted so that casting times of CH-1T and CC-3T coincide with T=00:00. Vertical black lines denote the following events: (1) casting CH-1T, (2) casting CC-3T, (3) compression applied, (4) compression measurement.

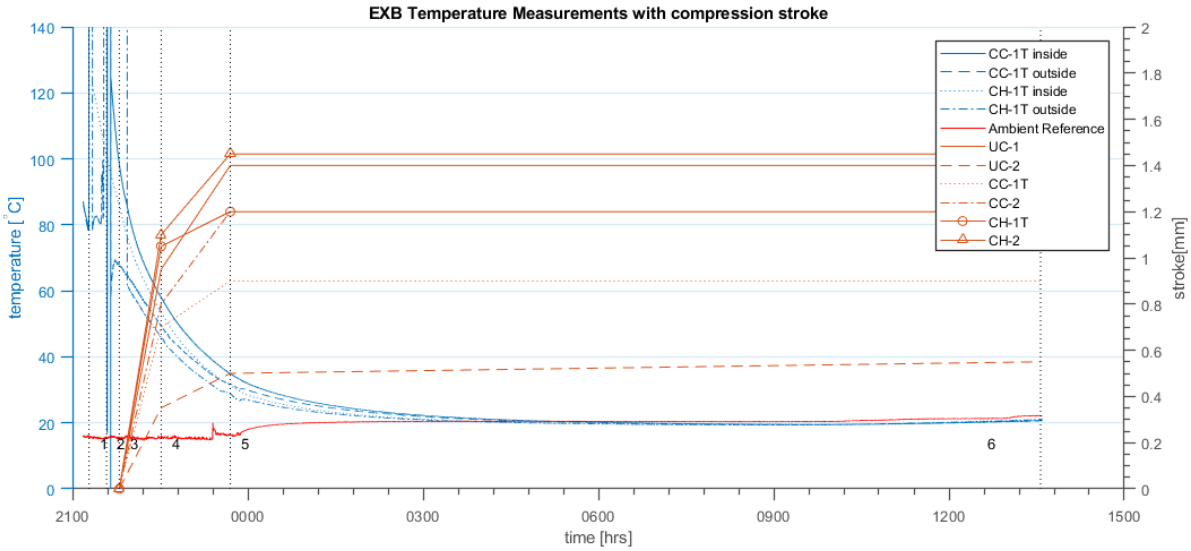

Figure 4.9: Thermal data obtained during experiment part B shown in blue. Vertical black lines denote the following events: (1) casting CH-1T, (2) casting CC-3T, (3) compression applied, (4) compression measurement, (5) compression measurement and (6) compression experiment and end of experiment. Measured (uncorrected) cumulative stroke shown in orange.

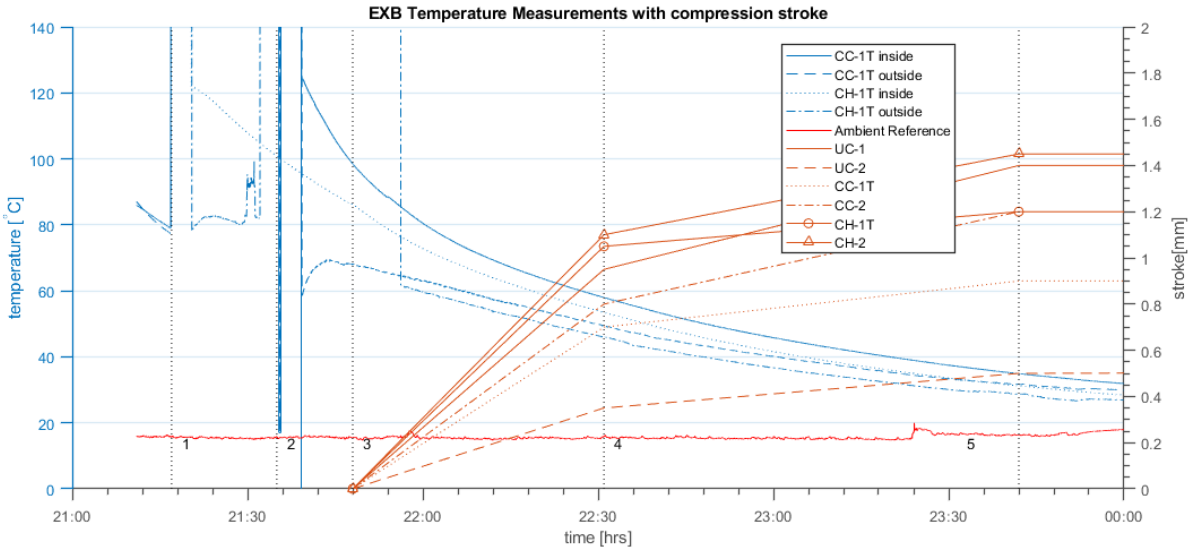

Figure 4.10: Thermal data obtained during experiment part B shown in blue. Vertical black lines denote the following events: (1) casting CH-1T, (2) casting CC-3T, (3) compression applied, (4) compression measurement, (5) compression measurement. Measured (uncorrected) cumulative stroke shown in orange.

4.4.3. Grain Acceptance

The grain acceptance criteria as provided in section 4.2.1 are provided below and are evaluated based on the propellant produced in this experiment.

BEM-QA-1_1 *Solid Propellant grain acceptance shall be determined based on the following indicators:*

- BEM-QA-1.1_1 *Ingredient sources shall be of similar purity from a known supplier.*
  DARE standard supplier was used and defines the standard. Technical/ food grade KNO_3 and Sorbitol with purity in excess of 99,5 and 97 % respectively: refer to chapter 2. Moisture removal was not as effective or ingredient source was drier resulting in a lower amount of moisture removed. The effect of composition variations on ballistic performance needs to be established to define limits.

  It is recommended to investigate reproducability of ballistic properties to define limits on ingredient purity.

- BEM-QA-1.2_1 *The KNO_3 PSD shall be measured and not deviate more than [TBD] from the propellant characterisation data.*
  Measured as part of characterisation. KNO_3 PSD provided in section 2.2.3. Similar to ingredient purity it is not known what the effect is of PSD on motor performance.

  It is recommended to investigate reproducability of ballistic properties to define limits on ingredient purity.

- BEM-QA-1.3_1*Production shall follow established procedures such as defined in chapter 2.*
  It was found that specifications on ”pot life”, the time between heating and casting was ill defined. Similarly the time between casting and applying compression was not well defined and should be considered for the future. This limit is now set tentatively at 15 minutes. Other exceptions as part of the experiment are noted.

- BEM-QA-1.4_1 *No errors or flaws shall be identified that change the propellant surface area by more than (estimated) 5 [%] from the grain as from the technical drawing.*

  Grain surface quality almost flawless for all grains. Initial port area (in [mm^2] is calculated based on the actual length of grains as given in equation 4.3 to eliminate a small error due to changing liner thickness. In addition this eliminates a implicit dependency on the density of the propellant which is primarily expressed in variations of propellant grain length and mass.

$$\eta_A = \frac{A_{flaw}}{A_b(0)} = \frac{A_{flaw}}{2\pi R_{in} \cdot L_g} = \frac{A_{flaw}}{8.7 \cdot 10^3} \tag{4.3}$$

  Results are provided in table 4.3 and show that propellant grains have little to no defects (below 1%).

- BEM-QA-1.5_1 *Propellant density shall be larger than 95 [%] of theoretical.*
  The density of the propellant is calculated with equation specified in 4.1. Liner weight was subtracted from the propellant grain. Based on measurements of 3 different liners the weight was found to be 0.328 [g/mm]. The calculation results are provided in table 4.3.

  This requirement is not met for all grains although a good improvement is made compared to the propellant density obtained in earlier DARE work. Only preheated grains CH-1T and CH-2 and ambient cast grain CC-1 meet minimum density requirement of 0.95 %. looking at the very good surface qualities the density the requirement of 95% could be slightly relaxed. On the other hand maturity could further increase density of future batches.

  It is recommended to test the grains slightly below the density ratio of 95% and establish if this has a marked difference on ballistic properties.

- BEM-QA-1.6_1 *Grain geometric dimensions shall be within* $+0/-0.5$ *[mm] for the outside diameter and within* ± 1 *[mm] on other dimensions as defined in appendix E.*

  Requirements met for all radial dimension and could be constrained much further with the current tooling. Grain length variations are beyond 1%. Original grain dimensions were however set for perfect density, not corrected for increased liner thickness and does not account for any propellant leaks (resulting in slight variations of propellant mass). When this is taken into account a 95% density propellant grain with a propellant mass of 755 [g] would result in a grain length of 107 [mm]. It is therefore recommended to relax this requirement and avoid conflicting requirements.

  It is recommended to relax the requirement on propellant grain length to 107$\pm$3 [mm] based on motor geometrical constraints and margins on operating pressure for the intended motor.

- BEM-QA-1.7_1 *Appearance of the propellant shall be consistent with earlier grains (e.g. visual inspection and experience).*

  Better than expected. Defines future standards.

BEM-QA-2_1 *For production changes a test grain shall be subject to general and destructive inspection:*

- BEM-QA-2.1_1*The test grain shall meet general grain acceptance criteria (BEM-QA-1).*

  Verified, grain CH-2 meets general acceptance requirements (density and area).

- BEM-QA-2.2_1*The test grain shall be cut 3 times as specified.*
  This was completed.

- BEM-QA-2.3_1*The grain slices shall have no flaws other than from machining and have a uniform bond with the inhibitor material.*

  Propellant was defect free with surface scratches traced back to cutting operation. Inhibitor bond was very good with diffusion of up to 0.4 [mm] into the cardboard. This was less than the estimated 0.6-0.9 [mm] measured at the frayed cardboard edge of other propellant grains. As this is a more accurate measurement the value was updated in table 4.3.

  Similarly the propellant-inhibitor bond was checked and found, based on several separate measurements to be roughly 75,9 [mm] $\varnothing$, coinciding with liner thickness as measured before casting (2.0 mm). Similar to the diffusion this value was taken as standard value for all grains.

4.5. Discussion

The propellant density was found to only marginally increase by applying compression to the propellant. When the experiment was designed it was expected that a considerable part of the density decrease would be due to thermal contraction however during this experiment it was found that the effect was limited to 1-2% with a similar variation as measured with the heritage production method (see section 3.4.4). It can not be fully ruled out that the applied vacuum was not as effective as with previous experiments reducing the measured density increase somewhat.

When comparing the difference between heated moulds and moulds at ambient temperature there is a small difference in density which could be explained by the temperature distribution inside the grain when compression was applied. Although measured temperatures are fairly similar between preheated and ambient moulds, it is expected that the internal temperature distribution has larger variations. Especially the large thermal mass of the aluminium core is expected to affect this significantly with the effect more pronounced for grains with smaller web thicknesses. It is questionable whether this outweighs the current effort needed to heat moulds prior to casting as no oven is directly available for casting and the thermal storage box that was acquired for these experiments has a limited volume.

The surface quality is almost perfect for all propellant grains with only minute surface defects. In addition the geometric variations are very small. This is a marked improvement over the grain surface quality of heritage DARE propellant grains which often had considerable defects and large geometry variations. This is a large benefit of the developed tooling and propellant casting with compression: the surface quality is vastly improved. Lastly it eliminates a large production step compared to DARE's traditional propellant production as the propellant does not need to be cut with a circular saw after casting.

Quality criteria were evaluated for the produced propellant grains. In general the steps appear to be sufficient to eliminate faulty grains by recording the ingredients and checking that procedures were consistently followed. The absolute demonstration of the quality check however closely ties into the required ballistic behaviour. With respect to the evaluation of criteria BEM-QA-1.1_1 and BEM-QA-1.2_1 it was found that at this point no suitable requirements exist for 'ingredient purity' or deviations of particle size distributions. It is therefore recommended to evaluate this as part of the steady regression experiments used during this thesis or perhaps as part of future research. Similarly it could be considered for large projects to cast BEM grains from the same propellant batch and fire these as part of the propellant quality check. Similar practices exist with strand-burners and BEM systems in industry [20].

4.6. Conclusion and Recommendations

It has been shown in this experiment that propellant made with both heated moulds and unheated moulds can result in near to perfect surface qualities and densities over 95%. However this point has not been reliably met as several grains have densities slightly below the minimal (but somewhat arbitrarily set) required propellant density of 95%. This could be due some errors in the process or limited operator experience. The compression stroke of the conservatively measured 0.4-0.9 [mm] can only explain an improvement in density of 0.36-0.8% (assuming a 107 [mm] long, 95% density grain). The uncertainty in this measurement. Based on the evaluation of quality criteria it is recommended to evaluate BEM reproducability to define composition limits. In addition it is recommended to test grains that fall a little short of the 95% density ratio to establish if the threshold should be re-evaluated.

Added compression improves surface quality significantly to the point where generally all grains are flawless. Although equipment is slightly more complex it reduces overall propellant production time significantly by eliminating the need to cut the propellant with a saw. Preheating the moulds on the other hand improves density somewhat but no effect was found with respect to the surface quality. It does allow the operator a little more time before compression needs to be applied. However, with proper procedures, this effect is expected to be limited compared to the effort of heating the equipment before casting. It is very likely that the preheating becomes more important for smaller grains where the thermal mass of the mandrel is much larger compared to the propellant. It is therefore recommended to first investigate further density increases through maturing of the production process.

4.6.1. Evaluation of Casting Process and Tooling

The casting moulds that were developed for this thesis study proved to significantly improve propellant surface qualities and geometrical accuracy of the propellant grains. With several manufacturing errors (improper tolerances on plungers) solved after a first casting iteration grain rejects based on geometric or surface defects have been fully eliminated.

It was found that the easiest method for removing the grains from the moulds was through the use of several additional tools such as an aluminium tube that fit over the mandrel and a length of threaded rod. These components will be added to the tooling inventory and were included in the process description in chapter 2. Significantly more time than expected was necessary for the production of inhibitor tubes. These cardboard tubes saw several iterations as part of these casting experiments. The best solution was the production of tubes from slightly larger 90 [mm] ∅ tubes.

The casting procedure was tested and several productions steps such as the time between casting and compression were added to the procedure. In addition the changes in tooling were evaluated and significant experience gained in the production of (BEM) grains with the new procedure. Even with the improved formulation experience in execution and evaluation remains important. Together it can be determined that, with a small margin, both the developed casting equipment and improved production process produce the desired propellant quality necessary for the BEM experiments of subsequent chapter.

4.6.2. Evaluation of Propellant Quality Criteria

The propellant quality criteria were evaluated and several changes were proposed. This involves relaxing the requirement on grain length as this conflicted with the accepted propellant density variations. The propellant surface quality and geometrical accuracy has increased to the point that analysis is straightforward and can be easily applied.

Lastly it is recommended to evaluate the acceptance criteria further with respect to ballistic performance. Several criteria such as those on ingredient purity or particle size distributions are not yet useful as tolerances are not yet defined and will likely be driven by the ballistic properties. To facilitate this the current PSD and ingredient sources were recorded for this experiment but will only become quantifiable when more test results are available.

4.6.3. Evaluation of Experiment Goals

the following test goals were set for the current experiment:

1. **PARTIALLY MET** *Quantify the effect of mechanical pressure and preheating of moulds on propellant quality.*
   Only a small increase in propellant density could be determined compared to the results from chapter 3. Surface qualities are on the other hand significantly improved by the improved tooling which includes mechanical compression. Uncertainties in the effect of the vacuum applied to the the propellant mixture make a precise determination of the increase in density inconclusive. It is as such recommended to closely evaluate future propellant grains and see if density (variations) become smaller with the maturity of the system or if variations persist.
2. **MET** *Determine the best production technique for KNSB propellant grains for the BEM with respect to achieved quality and effort.*
   In terms of production steps, surface quality and geometrical accuracy, the improved propellant formulation was found to significantly improve propellant quality while eliminating the machining of the propellant grains.

Additionally the following secondary objectives are to be met:

1. **PARTIALLY MET** *Gather data about cooling and compression rates of BEM propellant grains.*
   Data was gathered on the compression and thermal history during curing of the propellant grains. Compression stroke was complicated by propellant leakage around the plunger. The compression measurements could be refined however the limited effect on propellant density limits the benefits of future study.
2. **MET** *Gain experience with the manufacturing of BEM propellant grains using the designed tooling.*
   Through the two iterations most of the teething troubles have been eliminated from the tooling and casting process. Changes were made to the inhibitors and tooling and method used for removing grains from the moulds. Together they have significantly reduced the grain rejection rates based on surface or geometrical variations. Several grains were produced with propellant densities slightly below the initial goal of 95% density however ballistic tests should be used to evaluate if this criteria can be relaxed to reduce grain rejection rates further without compromising on ballistic performance.
3. **MET** *Create sufficient grains to be used in the thermal conditioning experiments of the regression experiment from chapter 6.*
   Two grains with embedded thermocouples were produced and can be used for thermal conditioning experiments.
4. **MET** *Evaluate the grain quality criteria (refer to section 4.2.1) for acceptance of KNSB grains.*
   The developed quality criteria were evaluated with respect to the produced propellant grains. Two modifications were proposed to reduce conflicting requirements. In addition it was found that for several measures, most notably on ingredient purity and PSD deviations, ballistic properties will have to be measured to define limits.

II

Propellant Regression Research

5

Laser Ignition Experiment

After the propellant casting experiments from chapters 3 and 4 an experiment was designed to determine the ballistic behaviour of both fine and coarse KNO_3 propellant under representative motor conditions. During the first of these BEM experiments it proved impossible to ignite the fine KNSB mixture. For the BEM system the igniter design was based on standard DARE practices which consists of a electric match, a small (≈ 1 [g]) commercially available black-powder charge in combination with an ignition primer painted on the exposed propellant surfaces. Several solutions were tried to increase energy transfer to the propellant grain using a trial and error method however these solutions proved ultimately unsuccessful. After a total of 9 misfires this prompted a more thorough root cause analysis and experiment focused solely on the ignition characteristics of the KNSB propellant.

This experiment, discussed in this chapter, was designed to study ignition of KNSB propellant samples outside the BEM environment. An opportunity was found to use a Nd:YAG infrared laser at the TU Delft faculty of 3ME[1]. This laser setup allowed the delivery of a finite and controlled impetus to the propellant surface and allows direct observation of the propellant samples during ignition and combustion. The goal of this experiment was first to find the root cause of the observed ignition failures and in addition bridge the gap in knowledge on KNSB ignition behaviour.

In contrast to the chapter 3 and 4 first the BEM root cause analysis will be discussed. Subsequently the test goals and success criteria will be defined. The experiment setup and samples under test are provided in section 5.3 followed by the results and discussion. In the conclusion the solution is provided that allowed the BEM experiment to be completed. In addition the area's of improvement are identified to support future laser combustion experiments.

5.1. Root Cause Analysis

To organise the the failure investigation a root cause analysis (RCA) was performed on the ignition failures (misfires) of the BEM system. This root cause is briefly discussed in this section and consists of a description of the BEM and the ignition train. Second the failure is described including any observations made that might aid the investigation. The RCA method consists of the identification of possible causes and looking for supporting proof or a rebuttal of these causes until a root cause has been defined. This analysis can consist of tests and and experiments to gather more evidence. The method was derived from methods used at Aerospace Propulsion Products B.V. (APP).

5.1.1. Description of the BEM Ignition Environment

The Ballistic Evaluation Motor (BEM) developed for this thesis is a core burner with around 760 grams of propellant per grain. The design is shown in figure 5.1. The nozzle geometry is variable between tests and adapted for the different propellant types and design operating pressures. The grain is inhibited

[1]Department of material science (Research group Joining and Additive Manufacturing). The author would specifically like to thank Jurriaan Slingerland and Professor Ian Richardson

on front and back by 1.5 [mm] cardboard disks and high temperature silicon glue. The outside of the grain is inhibited by a bonded cardboard tube. Nominal design operating pressure is 2-7.5 MPa with the design failure pressure via nozzle shear out between 11 MPa (yield) and 14 MPa (rupture) (refer to appendix E for a detailed design description.).

The propellant that resulted in the misfires was the fine Potassium Nitrate- Sorbitol propellant composition with a 65/35 mixture ratio by mass. Propellant density was between 95%-97% of the theoretical density. A surfactant (Sodium Laureth Sulfate) was added (6 drops equal to 0.16 [g] /100 [g] of dry ingredients) to improve rheological properties of the fine composition. Grains were stored in sealed plastic bags at dry indoor conditions prior to motor installation and firing.

Ignition is achieved by an electric match (squib) glued in a drilled out M12 bolt. This ignites a 0.8-1 gram black powder charge (Swiss No.2) sealed in the bolt with cotton wool. Subsequently ignition of the exposed propellant surface is achieved by ignition of an ignition primer in the form of a Nitrocellulose/ fine black powder paint. This DARE standard ignition primer is a combination of 0.3 [g] nitrocellulose (NTC) (Vectan ball 10, smokeless powder) dissolved in acetone, and 4 [g] of fine black powder (ground Swiss poudre no. 2). This is liberally applied to grain port (around 2 grams) and left to dry before installation into the motor.

After the first set of failures (end of September) it was a more energetic primer coating was used. The coating was improved with Titanium powder (99.1% pure `pyropowders.de`, sub 100 [μm] particle sizes) to the following recipe: 1 grams of NTC to 8 grams of fine black powder, 0.8 grams of additional KNO3 and 1.2 grams of Ti-powder. This recipe coincides with several Roman candle mixtures found in online sources. The titanium, besides a theoretical flame temperature that is somewhat higher than of black powder alone was also thought to increase heat transfer by direct impingement of burning metal particles with the propellant surface. Two other solutions were further implemented in the field such as: application of coarse KNSB shards in the central port (3 gram) and closing of the nozzle with tape (resulting in a burst pressure at 8 bar). Also these tests resulted in misfires. The coarse KNSB shards left K_2CO_3 deposits confirming that combustion took place inside the motor. These shards were however kept relatively small as there was a concern of the shards blocking the motor nozzle.

5.1.2. Description of the BEM Misfires

At the moment of igniter firing the motor builds up pressure as the ignition charge is consumed. During successful BEM firings the propellant then starts combustion 1-2 seconds after firing. For misfires this first pressure spike is also seen, but ignition of the main propellant charge fails. Further observations are:

1. Post-test inspection showed that the primary ignition change and all ignition primer were fully consumed. The propellant looked slightly caramelised but clean and showed no other signs of degradation.
2. Surface qualities of the grains as cast are similar to plastic, very smooth and generally flawless.
3. Open air test of the igniter together with the motor geometry (refer to figure 5.1) shows that the impingement point of the black powder and ignition flame likely occurs towards the nozzle end of the grain.
4. On several grains that were not fired the primer coating was found to detach from the smooth propellant surface. This is increased by the evaporating acetone which causes the coating to shrink resulting in cracks in the primer surface.

5.1.3. Analysis

Possible root causes are provided below. They are briefly discussed and arguments in support (+) or against (-) them are provided.

1. Ignition train causes insufficient heat transfer to the propellant grain.
   (a) (+) All coating and igniter material is consumed during misfires.

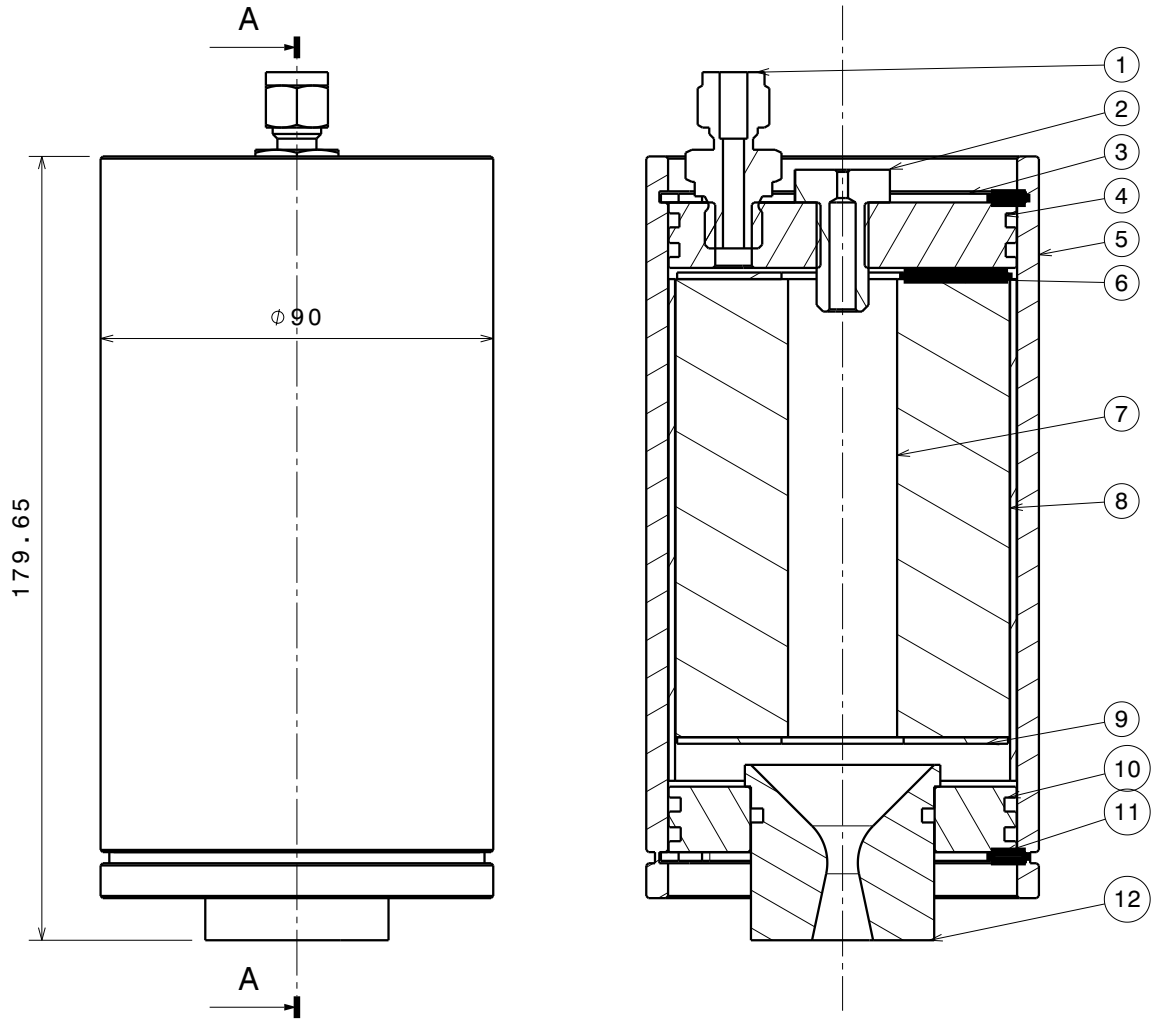

Figure 5.1: Ballistic Evaluation Motor BEM used during experiment.(1) Swagelock RS-4 Adapter to pressure sensor. (2) M12 Igniter Bolt with Dowdy seal, (3) Aluminium Casing, (4) Circlip, (5) Forward Closure, (6) Cardboard Inhibitor Disk, (7) Propellant Grain, (8) Cardboard Inhibitor Tube, (9) Cardboard Inhibitor Disk, (10) Aft Closure, (11) Circlip, (12) Steel Nozzle.

   (b) (+) Grain surface is slightly discoloured but otherwise smooth.
   (c) (+) Ignition spikes fast, however motor only fully ignites two seconds after firing.
   (d) (-) Coarse motors were successfully fired with this configuration.

2. Ignition material is ejected from motor before effective heat transfer can occur
   (a) (+) A visible flame is seen during firing of the igniter.
   (b) (+) Ignition coating does not adhere well to the propellant.
   (c) (-) Pressure spike indicates significant combustion inside the motor.
   (d) (-) Coarse motors were successfully fired with this configuration.

3. The propellant does not burn
   (a) (-) The propellant was ignited in open air with a propane torch without problem.
   (b) (-) Propellant sources are identical to the coarse KNSB propellant that does not exhibit similar ignition problems.
   (c) (+) Milling of the KNO_3 and the application of the surfactant are the main differences between the coarse and fine KNSB propellants.

Based on anecdotal evidence from several sources it appears that ignition of KNSB is a two-step process. First the surface caramelises / liquefies which requires significant heat input. Subsequently a flame and mass flow from an ignition source starts combustion of the propellant which then spreads along the surface. This theory explains both the ignition delay observed in KNSB firings and the observed difficulty to achieve ignition with a fast burning ignition system.

After consultation with Richard Nakka [64] it was confirmed that the surfactant was reported (both by Nakka and Scott Jolley [58]) to suppress ignition in KNSB propellant. Nakka strongly recommends using less surfactant (to about 2 drops or 0.05 [g]/100 [g]). Upon review of the coating/ primer mixture it was suggested that added titanium powder actually takes up energy and does not make the ignition mixture burn hotter, instead it reduces the thermal flux due to it high melting point. It was further proposed to switch to a slower burning gelled mixture of black powder, sorbitol and isopropyl alcohol to improve surface adhesion. It was theorised that the lower burnrate would create a higher thermal input to the propellant surface.

5.1.4. preliminary Conclusion

The following causes are likely to contribute to the observed failures:

1. *A disadvantageous igniter/ grain geometry.* There are no sharp corners or vortex inducing locations in the BEM design which would normally create a hot spot from which full combustion is achieved.
2. *Insufficient sustained heat flux from the ignition primer/coating.* The baseline nitrocellulose-black powder coating burns very fast compared too many other proposed compositions. In addition it is considered that the added Ti-powder does not significantly increase the heat output of the coating primer.
3. *Inhibiting effects from the surfactant.* The surfactant was found in several reported experiments to adversely affect the ignition characteristics of KNSB propellant. In addition the amounts used in this study were larger than those recommended by [64].
4. *Other Composition Differences between fine and coarse KNSB.* As also the KNO_3 PSD was dissimilar other propellant differences could not be ruled out.

The disadvantageous geometry is very likely a strong contributing factor however, as the coarse KNSB propellant was fired successfully, an insufficient condition to inhibit ignition. As the root cause analysis is at this stage not fully conclusive it is proposed to investigate the ignition characteristics of propellant directly focusing on propellant variations with fine and coarse KNO_3, variations in the amount of surfactant, and the effects on ignition of different ignition primer compositions.

5.2. Experiment Goal and Success Criteria

As described in the introduction ignition of the fine KNSB composition resulted in several misfires. The root cause analysis resulted in several probable causes for this behaviour. Specifically it was suggested that a surfactant (Sodium Laureth Sulfate), used to improve the rheological properties of the propellant for casting, made ignition more difficult although other composition variations could not be ruled out in the preliminary analysis. In addition it was suggested that better ignition results might be obtained with different primer compositions.

The RCA discussion was complicated by the lack of qualitative knowledge surrounding ignition of the KNSB propellant compositions leading to guesswork as to the underlying mechanisms. With the limited amount of time between experiment conception and the planned date of the test, and novelty of the laser ignition method, the test goal was intentionally kept relatively simple and primarily focused on qualitative analysis. The test goals are:

- Determine if there are any differences between the ignition of coarse, fine KNSB compositions and if this is adversely affected by the surfactant.
- Gain insight in the ignition process of KNSB propellant and how this might be improved with the addition of an ignition primer.

The success criteria for this experiment are the following:

1. Successfully establish the root cause of the BEM misfires.
2. Determine what primer coatings result in the most effective ignition of KNSB propellant.

Similar to previous experiments the following suspension criteria will be observed. These denote conditions under which the test campaign will be halted until the problems have been resolved.

1. An unacceptable risk to the involved personnel, critical equipment, general public or their property.
2. By decision of the lab technician, Jurriaan Slingerland.
3. Any indication that success criteria as defined in this section can no longer be met.

5.3. Experiment Design

The use of lasers to investigate propellant ignition has a relatively long history as it allows the delivery of well defined energy fluxes to the propellant surface compared to other methods such as resistance wires, shock tubes or arc-furnaces[8]. Especially the benefit of selecting the radiant heat flux [W/cm^2] independent of pressure, propellant firing temperature and chemical environment around the propellant sample supports the methods popularity. It is specifically stated that ignition studies are complicated as it is an inherently transient state where different authors maintain different criteria for ignition and key concepts are not unambiguously defined between studies [8].

As at this stage no suitable metric exists to determine the onset of sustained ignition, the experiment relies on visual observations of the propellant samples using camera's and operator observations. In addition a thermal imager is used to measure sample surface temperature which might identify the moment of runaway thermal decomposition. Expected thermal events of the KNSB propellant are the melting point of sorbitol at 100-110 [°], boiling point of sorbitol at 295 [°], melting temperature of KNO_3 at 337 [°] and decomposition of $KNO_3 \longrightarrow KNO_2 + O$ at 400 [°] [37]. (Refer for an overview of the ingredient and propellant chemical properties to appendix A). Reactions with atmospheric oxygen could introduce additional energy into the system but are likely to occur beyond the boiling point of sorbitol. Adiabatic flame temperature at ambient pressure is 1440 [K] [50], but due to thermal losses expected flame temperature is estimated anywhere between 700-1440 [K]. From these values it is expected that thermal runaway will occur somewhere between 350-400 [°].

Studies of ignition of PBAN AP based composite propellant by radiant flux shows ignition to be achieved in 100-1000 [ms] for radiant fluxes of 10 [cal/cm^{2}s] ≈ 42 [W/cm^2][8]. As this is around the lower limit of the welding laser it was decided to make the propellant samples larger than 1 [cm^2]. At the same time the propellant sample mass was to be kept around 3 [g] excluding ignition primer. The

final sample design was a circular pellet of 16 [mm] ⌀ with a height of 8 [mm]. The 16 [mm] sample diameter results in a sample surface area of 2.011 [cm^2] providing a range in indecent flux from approximately 25 [W/cm^2] up to 1500 [W/cm^2] by placing the sample outside the focus of the beam.

It proved hard to find literature sources for the optical reflectance, transmittance or absorbance of

no.	PSD	Surf	Primer
1-3	Coarse	-	-
2-6	Fine	-	-
7-9	Fine	2 drops/100g	-
10-12	Fine	6 drops/100g	-
13-15	Coarse	-	P1
16-18	Coarse	-	P2
19-21	Fine	-	P1
22-24	Fine	-	P2
25-27	Coarse	-	P3
28-30	Fine	-	P3

Table 5.1: Proposed test conditions for the laser ignition experiment.

sorbitol and KNO_3.These values provide the difference in radiant energy that is reflected, transmitted or absorbed by the material/ material surface. NIST [26] provided spectra only going up to 26 [μm], it is however expected that both materials are relatively transparent, potentially resulting in only a small fraction of the indecent energy flux heating the desired propellant surface, leading to internal heating of the sample or scattering of the laser light through the room. A first step in the experiment should therefore consist of the calibration of laser power. This is explained in section 5.4.2.

As only a limited time was available for the experiment the samples are ranked by priority. Of each sample listed in table 5.1 three repetitions will be made. Coarse and fine KNSB samples will be fired with subsequently the fine composition with 2 and 6 drops/100 [g] (0.053 [g/100g] and 0.158 [g/ 100g] of surfactant each. Three primer coatings, indicated by P1-P3, will be tested and are provided in table 5.2. For simplicity samples are referred to by simple sequential numbering.

no	Composition	Solvent	Note
P1	BP(2) / NTC(0.3)	Acetone	DARE Heritage
P2	Charcoal(0.6/ KNO_3(1.4)	Isopropyl Alcohol	
P3	BP (2)/ NTC (0.3)/ Ti(0.7)	Acetone	Upgraded mixture

Table 5.2: Primer coatings tested during the ignition experiment

5.4. Experiment Setup

The system available for the experiment is a laser welding setup shown in figures 5.2a and 5.2b . It provides continuous output power from 50 [w] up to 3 [kW] at a wavelength of 1064 [nm] (near infrared) which is supplied to the room via a fibre-optic cable (yellow cable in figure 5.2a). The laser objective (HAAS-Laser 22-24-01-AY) with a focal distance of 159 [mm] from the objective reference plane at a beam width of maximum 23 [°]. 3-axis can be independently set for the laser objective (X,Y,Z) in addition to the elevation angle of the beam. Ventilation of exhaust products is provided by a welding exhaust hood which provides positive suction and which can be placed close to the propellant sample.

The (expensive) laser optics were protected by pressurised gas that was blown perpendicular to the protective glass cover.

The setup design needed to assure the flux delivered was well defined. This involved determining the illuminated surface area, a method of aligning the optics to the sample of interest and finding the propellant optical response to the radiant flux. The beam geometry is shown in figure 5.3. Calculations to align the beam with the sample surface resulted in the distances as shown in figure 5.3 with the sample placed beyond the focal point to increase the distance from the sensitive laser optics. A schematic of the setup is shown in figure 5.4. Imaging was performed by two cameras (JVC and GoPro) capable of recording at 60 [fps]. Thermal data is gathered by a TESTO thermal imager that estimates temperature from radiometric recordings.

5.4.1. Sample Preparation

Identical samples received sequential roman numbers which were marked with a permanent marker on the back of each sample. The different amounts of surfactant were further identified with dots on the side of the sample; no dot for no added surfactant, 2 dots for 2 drops of surfactant/ 100 [g], 3 dots for 6 drops of surfactant per 100 [g].

A total of 18 coarse and 18 fine KNSB samples were produced. In addition 9 fine samples were produced with both 2 drops and 6 drops per 100/[g] propellant each from propellant batches of 100 [g] total. This means that both a larger than typical uncertainty had to be accepted on mixture composition and surfactant quantity than in the BEM grains which were produced in 6 [kg] batches. The samples were cast in preheated aluminium moulds (≈ 60 [°C] shown in figure 5.5a. These samples were left to cure for 24 hours sealed inside a plastic bag with a bag of $NaCl_2$ desiccant. Coating was applied with a small brush and was left to dry for around 10 minutes to limit exposure to moisture.

5.4.2. Protocol

It was requested to test the setup first with half size samples. The first full size sample test was designed to estimate the radiant yield (temperature rise of the propellant sample per radiant joule delivered). To this end the TESTO 890 thermal imager was used to measure the approximate propellant surface temperature after a short, low power laser pulse (50 [W], 0.1 [s]). This is then linearly extrapolated to find the desired power level for achieving 350 [°C] in approximately 1 second.

The test protocol for the experiment laser ignition method is found in appendix B.5. First four samples are designed for safety and power level check. These samples are designated a-d in the test matrix.

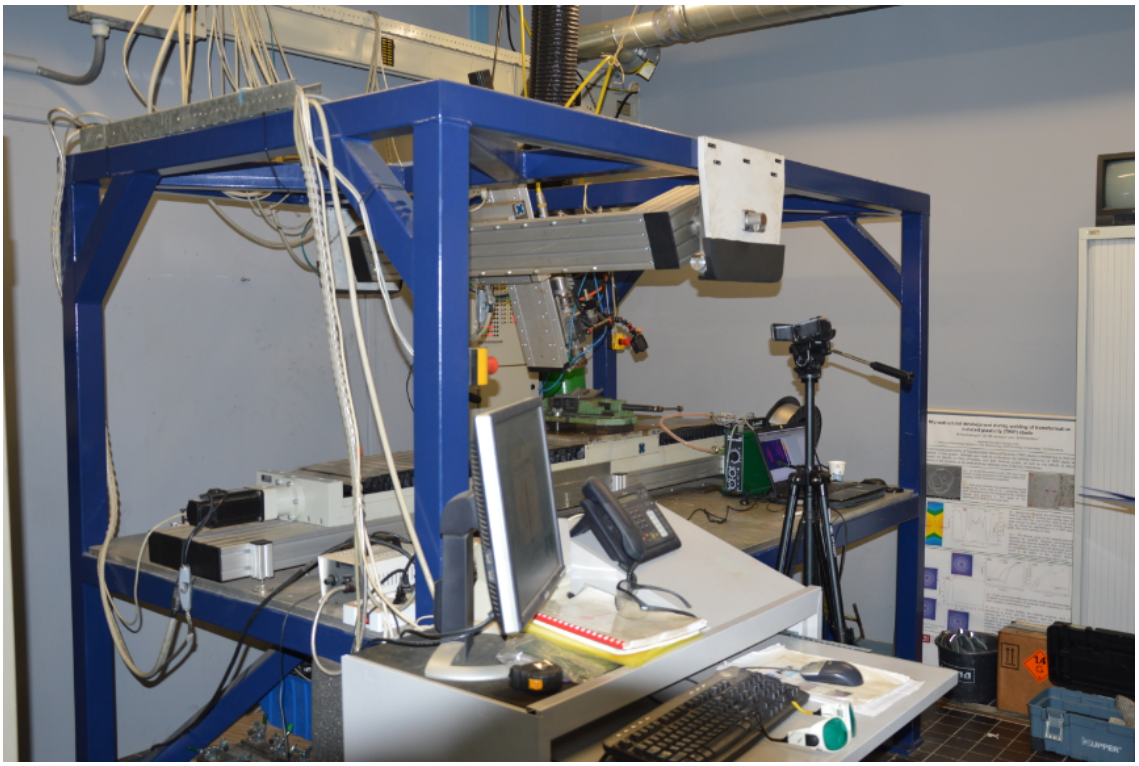

(a) Laser welding setup made available for the laser ignition experiment.

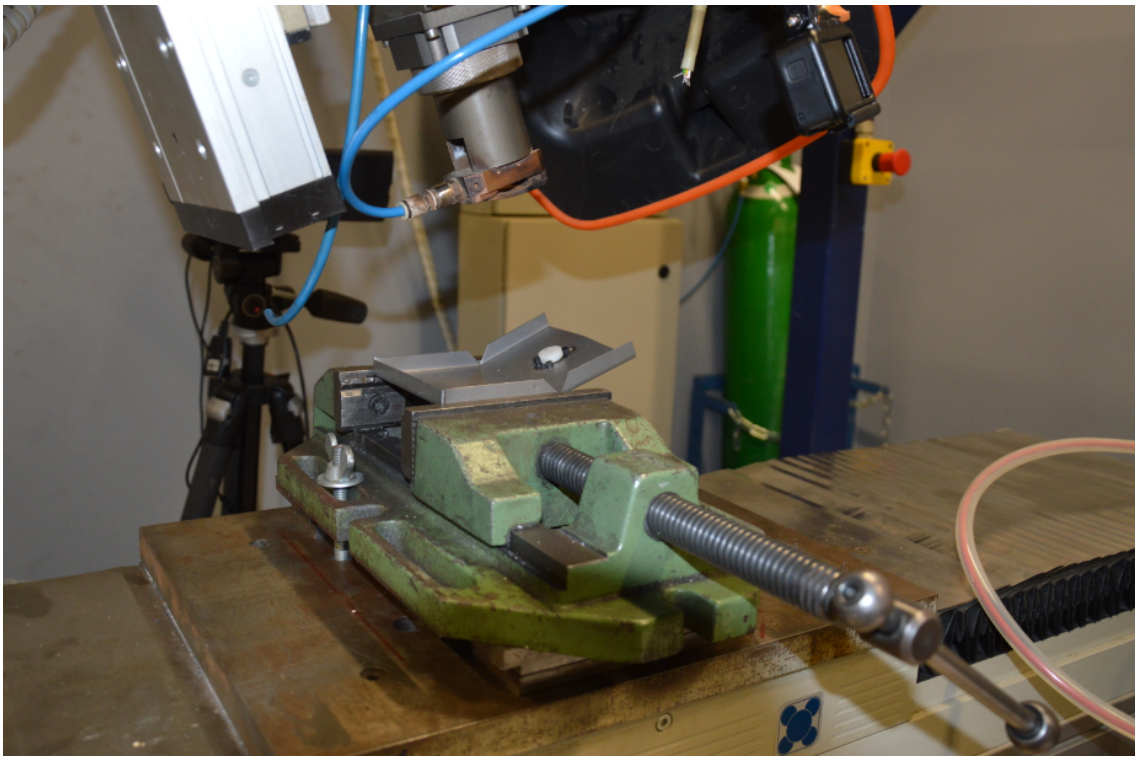

(b) Close up of sample holder (with sample) for the laser ignition experiment.

Figure 5.2: Experimental setup used during the ignition experiment.

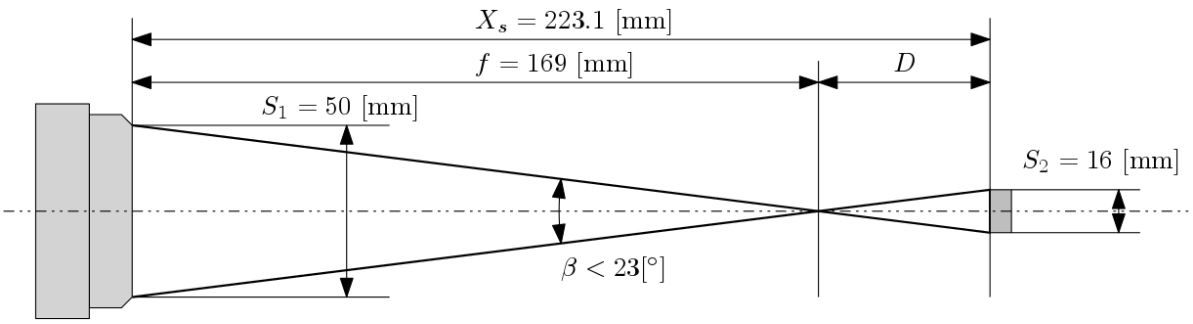

Figure 5.3: Beam geometry

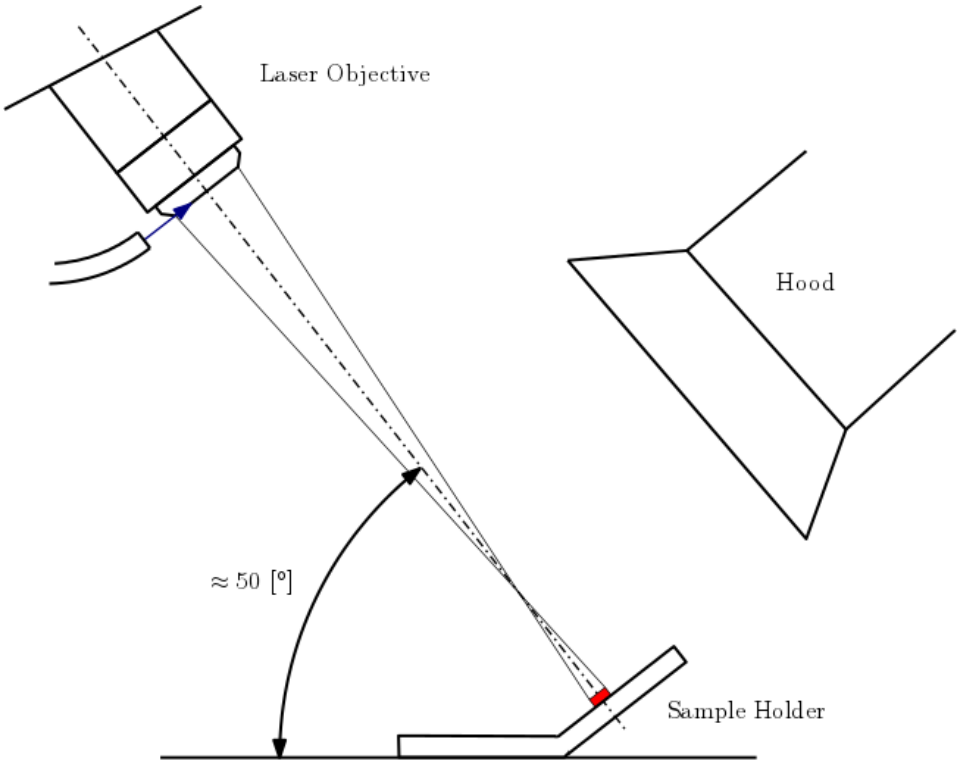

Figure 5.4: Setup Schematic

(a) Cast propellant samples in the aluminium moulds.

(b) Coated samples packed and numbered.

Figure 5.5: Propellant samples prepared for experiment D: laser ignition.

5.5. Results

Sample							Test Conditions		
no.	ID	Comp.	Surf.	Prim.	∅[mm]	Wt.[g]	time	P [W]	Φ [W/cm^2]
a	II	Coarse	-	-	15.95	1.9	11:30	2500	1250
b	XVII	Coarse	-	-	15.75	1.8	11:45	2500	1250
c	IV	Coarse	-	-	16.00	2.6	11:45	2500	1250
1	XV	Coarse	-	-	16.05	2.7	11:54	2500	1250
2	X	Coarse	-	-	16.00	2.7	11:58	2500	1250
3	VIII	Coarse	-	-	16.00	2.6	12:01	2500	1250
4	III	Fine	-	-	16.00	2.8		2500	1250
5	VII	Fine	-	-	15.95	2.9	12:11	2500	1250
6	XIV	Fine	-	-	15.95	2.9	12:15	2500	1250
7	IV	Fine	2	-	16.25	2.5	12:59	2500	1250
8	V	Fine	2	-	16.00	2.5	13:02	2500	1250
9	II	Fine	2	-	15.85	2.5	13:08	2500	1250
10	VI	Fine	6	-	16.00	2.5	13:12	2500	1250
11	III	Fine	6	-	15.9	2.6	13:16	2500	1250
12	V	Fine	6	-	16.00	2.6	13:20	2500	1250
13	I	Coarse	-	P1	15.95	2.7		200	100
14	V	Coarse	-	P1	16.00	2.7		50	25
15	XII	Coarse	-	P1	16.00	2.6		50	25
16	VI	Coarse	-	P3	16.05	2.8		50	25
17	XIV	Coarse	-	P3	16.00	2.7		50	25
18	IX	Coarse	-	P3	16.1	2.8		50	25
25	VII	Coarse	-	P2	16.05	2.7	14:17	50	25
26	III	Coarse	-	P2	15.95	2.7	14:20	50	25
27	XIII	Coarse	-	P2	16.05	2.8	14:21	50	25

Table 5.3: Test results for investigation of the steady burn rate.

The laser ignition experiment was completed on 10-12-2018. The pilot laser was not working as such alignment of the beam proved difficult, similarly the distance to the focal point could only be approximately determined with an estimated uncertainty of ± 2 [mm]. Measured focus distance to the approximate sample surface was determined to be 221 [mm], indicating that the beam was expanded slightly larger than the sample. In the end uncertainty in beam location and beam width at focal point resulted in a beam width at the sample surface estimated to be ± 20 [%] and approximately 2 [mm] offset to side of the propellant surface.

As laser alignment took longer than anticipated the fine composition with the various ignition primers (samples 19-24 and 28-30) were left out limiting the total amount of tests to 20 samples fired. An overview of the experiment is provided in table 5.3.

The calibration test was at a power level of 50 [w] for one second. The resulting temperature curve (measured at location of maximum temperature) is shown in figure 5.6a. Calculation of the desired

temperature after one second, $\Delta T \approx 350$ [°C] is done with simple interpolation shown in equation 5.1.

$$P_{req} = \frac{P_{test} t_{test} * \Delta T_{req}}{T_{test,max} - T_{amb}} = \frac{50[\text{W}] \cdot 1[\text{s}] \cdot 350[^{\circ}\text{C}]}{89.5[^{\circ}\text{C}] - 21.6[^{\circ}\text{C}]} = 257[\text{W}] \tag{5.1}$$

An error was made during the experiment where the TESTO thermal data was read out and final sample temperature taken instead of the maximum spot temperature. This resulted in a estimated $T_{test,max} - T_{amb} = 7.4$ [°C] which resulted in an estimated required power level of 2.5 [kW]; this meant that the ignition of all uncoated samples occurred within 0.1 [s] instead of the desired 1 [s].

Radiant flux Φ [W/cm^2] is calculated by dividing the applied power by the surface area (≈ 2 [cm^2]). During this experiment radiant fluxes have been used between approximately 25 [W/cm^2] and 1500 [W/cm^2] with the largest uncertainty due to the actual illuminated area and the actual beam coherence.

A total of 20 samples were ignited using the laser with 19 samples achieving full combustion. One sample (no. 12) with 6 drops of surfactant extinguished after the laser was turned off. Example thermal measurements from samples 2 (coarse), 5 (fine, no surfactant) and 12 (extinguished) are shown in figure 5.6b. It can be seen that propellant surface temperature rises nearly instantaneously with the measured flame temperature significantly lower once the burning surface is no longer visible. The adiabatic flame temperature is much higher than the observed maximum between 350-450 [°C]. The lower temperature plateau occurs when the burning surface area is no longer directly measured as the propellant burns away.

Surface temperature measurements for the samples with coatings P1,P2 and P3 are shown in figure 5.6c and give higher measured surface temperatures. Samples that were coated with nitrocellulose/ black powder showed faster ignition but thermal graphs show a slight igniting delay that was not observed for the coating based on KNO3/charcoal only. Several observations and a comparison between the different cases is made of the ignition and flame structure of the propellant samples which are provided in the next section.

5.5.1. Observations

During the experiment the following observations were made:

1. Investigation of fine and coarse propellant samples with and without surfactant,
   (a) As was mentioned the alignment of the laser beam was imperfect. This offset of the beam on the test sample illuminated by the beam is shown in figure 5.7g.
   (b) Self extinction was observed in a single fine sample (no. 12) The extinguished surface became soft and formed a liquid layer on top of the sample as shown in figure 5.7b. However also in the other samples with large quantities of surfactant (10-11) initially a clear flame (shown image has adjusted brightness) was visible as shown in figure 5.7a. The lack of particles in this flame indicating a low amount of KNO_3 or K_2CO_3.
   (c) Fine and coarse sample combustion showed considerably difference in the flame structure. In coarse combustion 5.7c particles are visible in the flame and continue combustion as part of the flame indicated by their brightness, while the fine propellant showed a smooth uniform flame front 5.7d. KNO_3 at the burning surface was visibly the brightest and likely hottest location in the flame. The flame front for both fine and coarse propellant shown in figures 5.7f and 5.7e respectively.
   (d) Side way flame spreading was observed to be much slower than internal combustion. For fine and coarse propellant the samples combust from inside out. It can however not be ruled out that this is due to partial heating of inside of the propellant samples.
   (e) For the coarse KNO_3 propellant it was observed that the glowing KNO_3 particles transformed into the similar hollow deposits also found inside the BEM during post firing inspection (refer to chaper 6). With decomposition of KNO_3 likely happening directly at the particle surface. In contrast the fine propellant burned significantly cleaner leaving much less deposits after combustion, mirroring observation during inspection of the BEM tests with fine KNSB propellant.

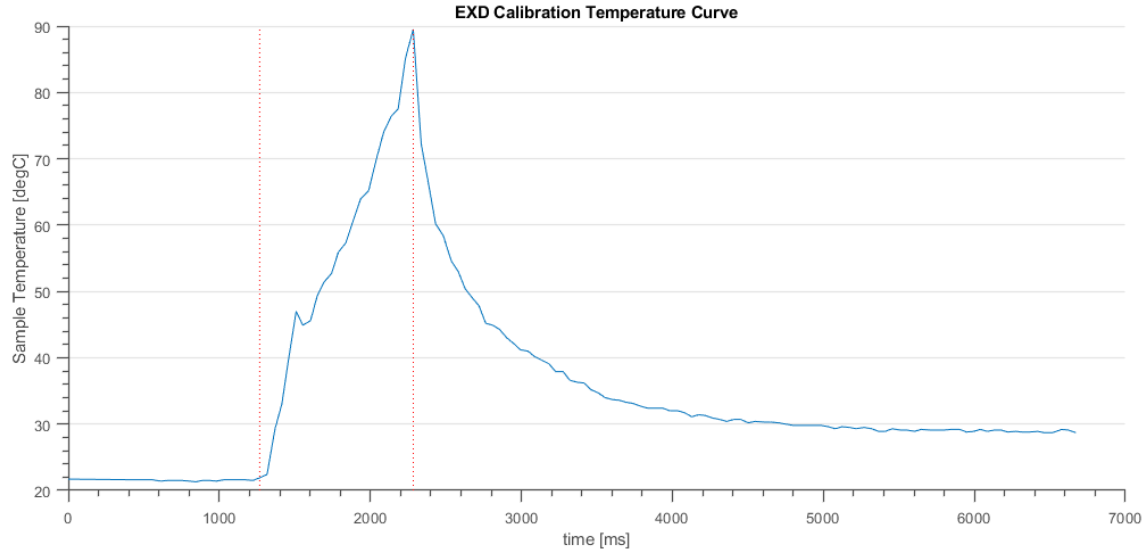

(a) Sample temperature increase with 50 [w], 1 [s] pulse width reaching 89.5 [°C]. This measurement was used to estimate the surface temperature as function of input power.

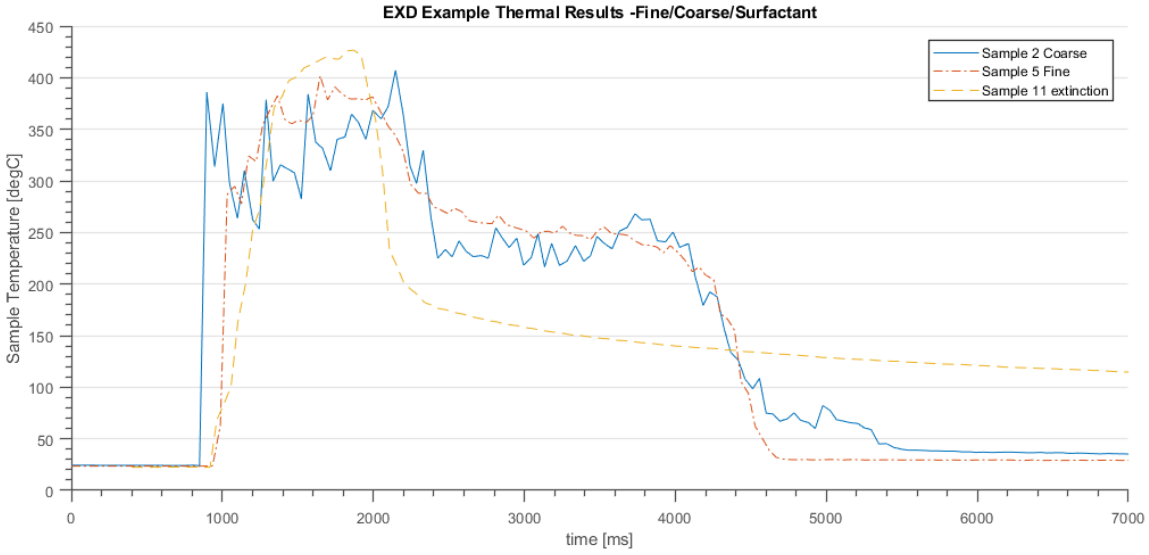

(b) Burning surface temperature measurements for samples 2 (Coarse), 5 (fine) and 12 (fine, 6 drops of surfactant, self extinguished). Radiant flux at 1250 [w/cm^2]

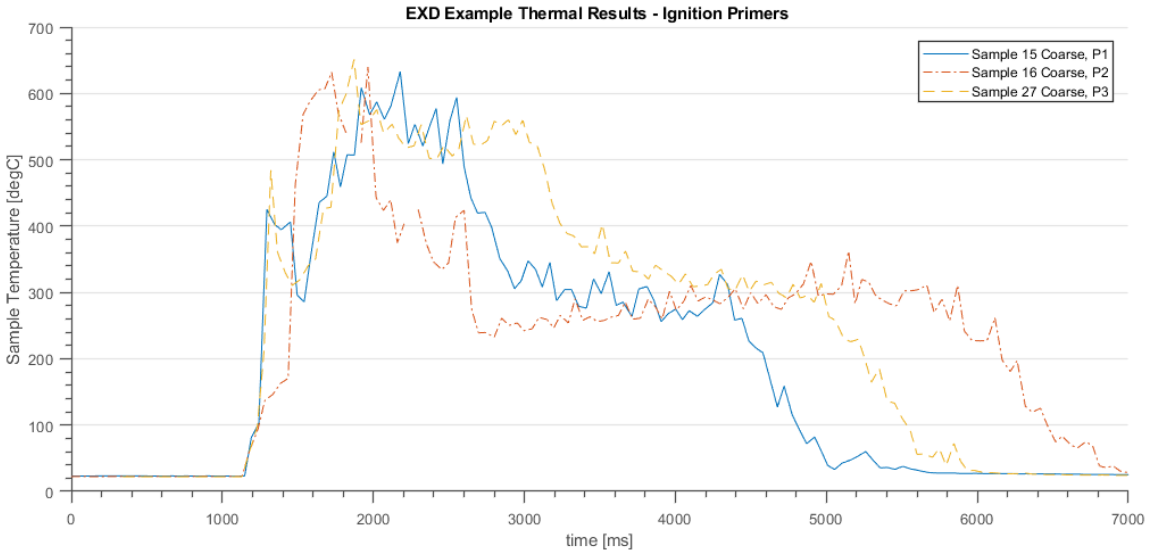

(c) Burning surface temperature measurements for samples 15 (coarse P1), 16 (coarse P2) and 27 (coarse P3), Radiant flux at 25 [w/cm^2]

Figure 5.6: Example surface thermal measurements made during the laser experiment using the TESTO thermal imager system.

2. Investigation into ignition primers

   (a) Even at the significantly reduced power level ignition occurred relatively fast over the entire propellant surface. For the heritage mixture P1:BP/NTC near instantaneous ignition was observed across the entire surface at 200 [w]. (no 13).

   (b) Ignition for the P2:charcoal/KNO_3 mixture was considerably slower. A visible deterioration occurred where the surface became darker shortly before ignition. Flame-spreading for this coating seemed to occur below the primer surface.

   (c) Similar to P2:Charcoal/KNO_3, P1:BP/NTC in one case seemed to ignite below the propellant surface as could be seen in figure 5.8a.

   (d) The Titanium coating P3:BP/NTC/Ti, did not appear to improve ignition of the sample although bright sparks were observed to scatter around the sample.

5.6. Discussion

5.6.1. Investigation of fine and coarse propellant samples with and without surfactant

Extinction was observed for sample 12 which has a high quantity of surfactant (6 drops, equal to approximately 0.16 [g/100g] propellant. The flame that was observed while the sample was illuminated by laser showed considerable differences to the flame structure of other samples (fine, coarse, fine with two drops) as it was a less turbulent clear flame compared to the other samples. The other experiment repetitions with same experiment conditions (10-11) showed the same initial flame structure. This could be explained by a lack of KNO_3 present in the flame either as the solid particles remain stuck at the propellant surface or because the KNO_3 particles do not attain the necessary temperature to start decomposition. As the propellant with 6 drops was ignited successfully and proceeded to burnout for 2/3 samples and full BEM grains ignited with a blowtorch, it seems that primarily the initial ignition is affected and the effect of the surfactant becomes less once steady combustion is attained.

As no other clear differences were found in the ignition behaviour of the other (fine, coarse, fine with two drops) samples this result strongly supports the surfactant as key inhibiting ingredient. Based on observations the ignition of the propellant surface follows the following phases: rapid gasification in selected locations; a gaseous flame (likely with little KNO_3) after which several local initiation points grow from inside outward.

Combustion for coarse propellant showed similarities to the combustion structure of AP composite propellants [24]: the relatively faster decomposition of the binder dislodges oxidiser particles which then continue combustion in the flame, this could be explained by the significantly lower boiling point of sorbitol (295 [°C]) compared to the decomposition temperature of KNO_3 [°C]. The small size of the fine KNO_3 particles prevented direct observation of this behaviour although the observed flame was translucent which suggests that at least some condensed particulate was present.

Temperature measurements were reviewed however neither the initial temperature rise and absolute magnitude appears to represent the actual decomposition. Maximum measured temperatures of the samples was between 250-450 [°C]. As this is around or even below the minimum decomposition temperatures of the propellant it is expected that flame temperature was incorrectly measured. This could be explained by partial transparency of the flame, or specific thermal wavelengths distorting the estimation of the peak temperature. This measurement can likely be improved by moving the camera closer to the sample, however it is recommend to first investigate proper calibration or use equipment better suited to the task.

5.6.2. Investigation into ignition primers

When comparing the ignition behaviour of coarse samples coated with ignition primers it was found that the compositions P1 and P3 ignited faster than P2 which agreed with expectations. This is likely due to the low ignition temperature of nitrocellulose (auto ignition at 170 [°C]) or due to the lack of sulphur

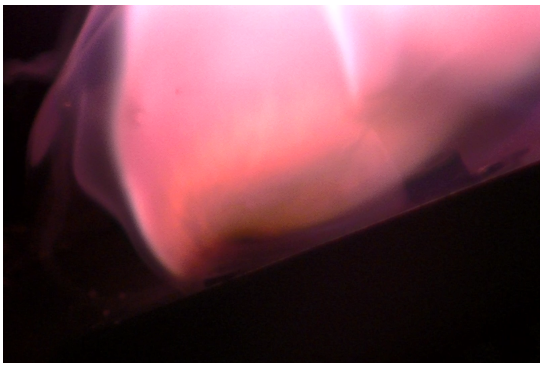

(a) Flame structure during ignition of the fine composition with 6 drops of surfactant (no 11).

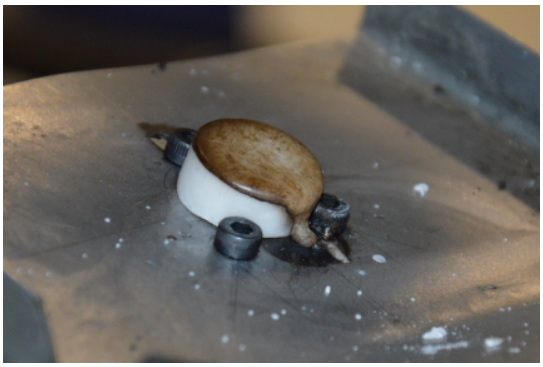

(b) Extinguished propellant (no 12) sample with molten propellant surface.

(c) Coarse Propellant flame structure with a more turbulent luminous flame showing uneven regression at the sample edge.

(d) Fine propellant showing more even regression with a smooth edge at which combustion occurs.

(e) Coarse Propellant flame structure showing significant active particles at the burning surface.

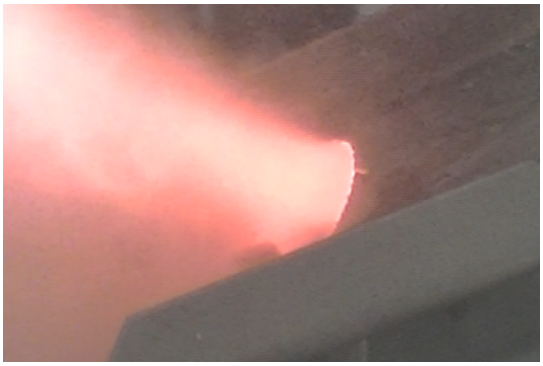

(f) Fine flame front with similar active region thinner and more evenly distributed.

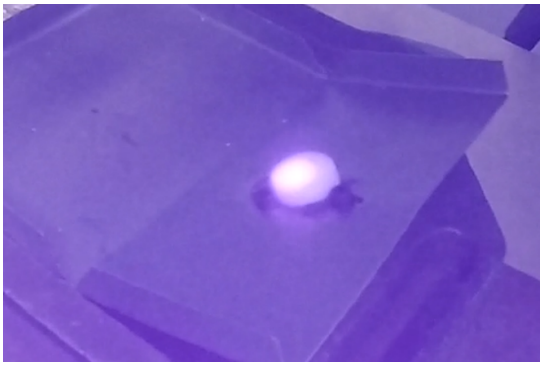

(g) Beam showing slight off-centre beam alignment.

(h) Uneven ignition at very high indecent flux.

Figure 5.7: Propellant samples prepared for experiment D: laser ignition.

(a) Ignition of the coating (P2) showing ignition to start below the surface.

(b) Instantaneous ignition (P1) across a large part of the surface.

Figure 5.8: Propellant samples prepared for experiment D: laser ignition.

(on of the ingredients in black powder) in the composition. In black powder, the sulphur decomposition is the lowest temperature (150 [°C]), and partially catalytic, decomposition to occur [7].

Maximum measured temperatures were also much higher for the coated samples even though radiant flux (25 [W/cm^2] was a small fraction of that used with uncoated samples. This is likely due to the presence of carbon in all primer mixtures which is specifically noted for its optical activity in infrared. This would increase the absorbance and emissions both resulting in efficient ignition and high measured surface temperatures. Although the slower ignition of the samples with P2 might be desirable, the slow flame spreading might also hamper efficient ignition of the full motor. It is recommended to further investigate the various ignition primers with the laser experiment, but also to test these different coatings in the BEM and compare the differences under the representative motor environment to reach a full conclusion.

5.7. Conclusion and Recommendations

A new method was piloted during this experiment which allows direct study of the flame structure and combustion characteristics of solid propellants. First and foremost the experiment goal was to identify any differences between propellant samples with and without surfactant, with fine or coarse particle size distributions and between the different ignition primers.

The extinction of fine propellant samples with six drops or 0.16 [g/100g] of surfactant indicate that this is the most likely cause of the observed misfires. Differences were observed in the flame structure of fine (with and without 2 drops or 0.05 [g/100g] surfactant) and coarse samples however this did not appear to affect the ignition characteristics. In conclusion to the RCA it is recommended to lower the surfactant quantity to below 2 drops per 100 [g] and confirm if ignition can be achieved with the BEM.

5.7.1. Evaluation of Ignition and Combustion Behaviour

Investigation Into the Effect of Surfactant

Several lesson were learned in the course of this experiment. It was found that surfactant indeed affects ignition of the propellant. As a mixture with large quantities of surfactant ignites, sorbitol quickly evaporates and combusts with a smooth flame likely aided by atmospheric oxygen. The surfactant then subsequently limits the decomposition or diffusion of KNO_3 or its decomposition products. Ignition subsequently halts when the laser source is removed and sorbitol is no longer supplied. The extinction of the fine surfactant composition was clearly seen in sample 12 which extinguished, but similar flame structures were also seen in samples 10 and 11. Samples with a limited amount of surfactant did not exhibit this slow burning flame structure instead igniting in a similar way as the nominal samples without surfactant.

The flame structure of both fine and coarse propellant showed several noticeable differences. Com-

bustion for the propellant appears to occur primarily at the propellant surface. In the coarse propellant frequently oxidiser particles are separated from the surface. This suggests a possible correlation between motor efficiency (c^*, or η_b) and particle size distributions. For the fine propellant the active region was much reduced and typically found to be only a few tenths of [mm] thick. Fine propellant similarly appeared to combust more evenly and perpendicular with less irregularities at the propellant surface.

Investigation Into the Effect of Ignition Primer

Three different coatings were tested, both the heritage NTC coating (P1) and improved coating with titanium powder (P3) led to rapid ignition of the propellant surface while the KNO_3/Charcoal/Isopropyl Alcohol mixture (P2) showed relatively slow degradation, this is however not necessarily bad as the heritage composition results in very sharp pressure buildup inside the BEM environment. For several of the ignited samples the flame front appeared to spread below the propellant primer mixture. It was however clear that the addition of an ignition primer significantly reduced the required energy needed to get the propellant to ignite. This is very likely amplified by charcoal in all three primers.

Analysis of the surface temperatures showed that fast burning primers P1 and P3 showed two stage ignition of the samples while the second primer P2, was slightly slower and did not exhibit this behaviour. This is likely caused by the lower initiation temperatures of nitrocellulose or black powder. It can be concluded that the application of a primer is an essential part of the ignition train in KNSB solid rocket motors due to the significant increase in heat transfer. It is however unclear if ignition with any of the three compositions. On one hand the slower burning composition P2 could increase the total heat input by burning slower, on the other hand the faster compositions (P2, P3) are likely to cause faster flame spreading in the motor creating a more predictable pressure rise. With the clear results with the added surfactant it is recommended to first try the BEM with the heritage primer mixture and reduced surfactant quantities before changing the ignition primer.

5.7.2. Evaluation Of Experiment Method

A new method was developed for investigating the ignition and combustion behaviour of solid propellants at ambient conditions. Several measurements however can be significantly improved and are likely to increase the quantitative results of the experimental method.

As limited experience existed with the laser ignition setup it is recommended to come to a more complete process for alignment of the beam and determining the radiant flux on the propellant sample. The method for determining the required power level of the laser functioned, however the calibration error points to deficiencies in the experimental method. This error was primarily due to inexperience with the TESTO camera and the lack of knowledge on the propellant reflectively, by comparison AP propellants are fully opaque, while sorbitol has an absorbance <20% below 20 [nm]. With the results from this thesis a better estimate can be made of the desired power levels, in addition it is recommended to become better acquainted with the measurement equipment before the test and work out the steps to a higher level in the procedures. If a new ignition experiment is conducted it is further recommended to develop a sturdier sample mounting stand that allows more accurate positioning of the samples and is less prone to damage by the laser.

Low spatial resolution and frame rates of the thermographic camera (10 [fps]) made it difficult to see the propellant decomposition happen at the propellant surface. The effects and regions of interest were smaller than initially anticipated. As could be seen in figure 5.7f the region of interest is in the sub [mm] range and reactions occur fast. It is therefore recommended to reduce power levels and move the camera closer to the samples to improve the resolution of the phenomenon of interest. Lastly it was found that thermal measurements of the flames where inaccurate, it is recommended to investigate improved calibration or different measurement techniques (camera's, thermocouples) to improve measurement quality.

It proved difficult to quantify the point of ignition based on observations of the thermal or video recordings. Before this experiment is performed a second time, it is recommended to investigate in literature methods used for these experiments in industry. In addition a good understanding of the propellant chemistry and its thermal decomposition could aid in interpreting the measurement results.

5.7.3. Evaluation of experiment Goals

The following experiment goals were set during the experiment:

- **MET** *Determine if there are any differences between the ignition of coarse, fine KNSB compositions and if this is adversely affected by the surfactant.* High quantities of surfactant were identified as the most probable root cause, differences in ignition behaviour between fine and coarse samples or fine with smaller quantities of surfactant were not observed. It is recommended to fire the fine composition with lower amounts of surfactant (below two drops or 0.05 [g/100g]) in the BEM system and validate the findings of the root cause analysis.
- **Partially MET** *Gain insight in the ignition process of KNSB propellant and how this might be improved with the addition of an ignition primer.* Insight was gained in the difference between coated and uncoated samples but it proved difficult to compare the the different primers and evaluate their effect on the propellant inside the BEM environment.

In conclusion insight was gained in the ignition behaviour and flame structure of KNSB propellant with noticeable differences between coarse and fine propellant compositions. It was indeed confirmed that the addition of surfactant, especially at ratios at or above 6 drops, or 0.16 [g] per [100g] propellant adversely affects ignition. A clear benefit between the various ignition primers was not discovered although the KNO_3/Charcoal mixture burned slower which is likely caused by absence of sulphur or nitrocellulose, which decomposes at relatively lower temperature than KNO_3/ charcoal alone. The experiment proved that laser ignition can be a valuable measurement technique and recommendations were made to develop this method further.

6

Steady Regression Experiment

With the propellant density and quality problems solved in chapters 3 and 4 the the propellant steady regression behaviour and combustion characteristics are the next step to characterise the KNSB propellant. These properties provide the link between the propellant formulation and ballistic behaviour and thus allow a confirmation that propellant produced in a certain batch, even as equipment or ingredient sources might change, meets the required ballistic performance.

To this end a ballistic evaluation motor was developed that allows measurement of propellant performance under varying pressure and temperature conditions. In addition a method was developed that estimates propellant regression behaviour from the measured quantities such as chamber pressure and grain geometry. This experiment method will be put to the test in this chapter and refined together with the investigation of the KNSB propellant properties.

First the experiment goals and success criteria will be provided in 6.1. Subsequently the section on experiment design will go into detail about the theory and relations behind the determination of the propellant performance and regression rate. This will include a sensitivity analysis on the basis of simulated sensor input. In section 6.5 the BEM is discussed in more detail although its design is discussed in much larger detail, including the requirements, (Ballistic) design, safety and load analysis in appendix E. In section 6.6 the data of in total 13 successful firings is present and the performance and regression rates calculated. These results are subsequently discussed and compared to values found in literature in the discussion, section 6.9 where also the developed BEM system and measurement method will be evaluated. The chapter is subsequently concluded in section 6.10 where recommendations will be made for future ballistics research.

6.1. Experiment Goals and Success Criteria

As provided in the introduction the first goal of this experiment is to determine the ballistic behaviour of the KNSB propellant by measuring the steady regression rate for KNSB propellant with both fine and course KNO_3 particle size distributions (PSD), and by determining propellant performance in terms of characteristic velocity,c^*, thrust coeficient, C_f, and specific impulse I_{sp}. A second important goal is to evaluate the BEM system as a means to measure these ballistic properties. Besides the overall test goals the success and suspension criteria are provided below. The test objectives are the following:

- Determination of the steady regression rate for both fine and course KNSB propellant as function of chamber pressure and propellant initial temperature.
- Confirmation of the similarity between the propellant from this study and those used by Nakka [63] and Gudnason [6].
- Determination of characteristic velocity, thrust coefficient and specific impulse for KNSB propellant.
- Development and demonstration of an experimental method for determining the propellant steady burnrate.

- Establish, evaluate and suggest improvements for increasing the repeatability of DARE solid rocket motors.

The success criteria to be observed during the tests are the following:

1. Determination of the KNSB propellant steady regression rate for fine and course KNO_3 PSD over the pressure range of 2.0-7.5 $\pm$ 0.5 [MPa] and the temperature range of 0-30 $\pm$ 5 [°C].
2. Determination of the characteristic velocity,c^*, thrust coefficient, C_f, and specific impulse, I_{sp}, for at least six motors.

The suspension criteria are provided below. These denote conditions under which the test campaign will be halted until the problems have been resolved.

1. An unacceptable risk to the involved personnel, critical equipment, general public or 3rd party property.
2. Any (RUD) event that results in the loss of non consumable hardware (e.g. propellant is considered a consumable).
3. Any indication that success criteria as defined in this section can no longer be met.

6.2. Experiment Design

The determination of propellant ballistic properties is achieved by testing propellant samples under representative conditions. In industry various designs exist to achieve this end with strand burners and sub-scale (compared to missiles or launchers) ballistic evaluation motors [19]. Strand burners are generally cheaper and easier to operate but ballistic evaluation motors offer a more representative operating condition in terms of gas and thermal environment. In modern propellant laboratories these methods coexist and are used together to evaluate the propellant ballistic performance [4].

Based on literature review a progressive burning, (pressure increases over the duration of the test) BEM design was chosen. Based on the experiment requirements, safety and operational requirements this motor, shown in figure 5.1, was developed for this thesis. A more extended summary of the design and design process is available in appendix E.

Propellant grains are ignited and, based on thrust, pressure, geometric, and mass measurements the propellant behaviour is established. In this section the models and methods used to determine propellant ballistic performance is described. First the theory on motor performance is expanded in section 6.3 and the methods are discussed. Subsequently the steady regression rate is similarly described and the analysis methods evaluated.

Several motors will be assembled in the lab excluding the igniter and forward closure which are, for safety reasons (refer to section 2.4), installed shortly before firing. Measurements will be taken of grains and motor hardware. A total of 2 load tests (with lower design pressure, to verify the design operating pressure) will be completed. Subsequently, for both propellant variations, at least three motors will be fired at ambient conditions and two at cold conditions for a total of 12 tests. As the tests are planned for September 2018, grains will be thermally conditioned to achieve firing temperatures below 5 degrees. Thermal conditioning will be considered as part of the equipment calibration activities. During the test pressure, thrust and thermal data will be gathered. Subsequently motors are disassembled and again relevant motor measurements are taken.

6.2.1. Experiment Variables

During the test two discrete variables and a single continuous variable will be investigated. The variables are provided in table 6.1. The control variables that will be specifically controlled are discussed below. The listed accuracy in table 6.1 is the accuracy is with respect to the experimental range of interest, not the required measurement accuracy which is below 1% of the measurement range as determined during sensor calibration C. E.g. it is expected that the chamber pressure will not precisely be between 2-7,5 [MPa] as this is directly depended on the to be determined burn rate. Instead the aim is

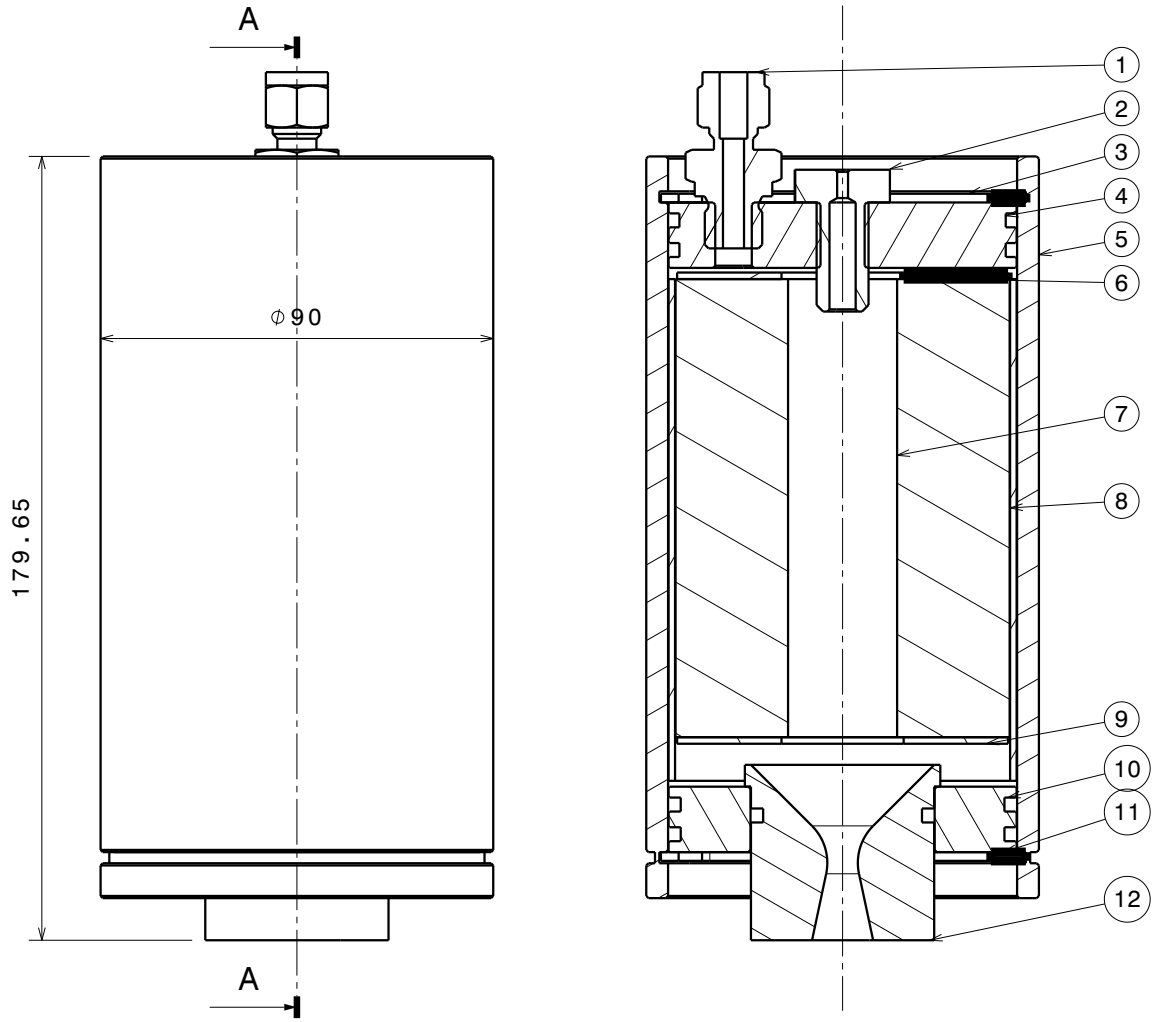

Figure 6.1: Ballistic Evaluation Motor BEM used during experiment.(1) Swagelock RS-4 Adapter to pressure sensor. (2) M12 Igniter Bolt with Dowdy seal, (3) Aluminium Casing, (4) Circlip, (5) Forward Closure, (6) Cardboard Inhibitor Disk, (7) Propellant Grain, (8) Cardboard Inhibitor Tube, (9) Cardboard Inhibitor Disk, (10) Aft Closure, (11) Circlip, (12) Steel Nozzle.

Variable	name	Range	Accuracy
P_c	Chamber Pressure	2-7.5 [MPa]	$\pm$ 0.5 [MPa]
T_0	Propellant Temperature (C,A,H)	0-30 [°C]	$\pm$ 5 [°C]
D_m	KNO_3 PSD mean diameter (F,C)	100, 350 [μm]	$\pm$ 50 [μm]

Table 6.1: Experimental Variables

to measure it over the range 2-7,5 [MPa] where the actually realised pressure range might be slightly more or less (± 0.5 [MPa].

The control variables that receive specific scrutiny during the test are the following:

- *Propellant Composition* will be fixed at 65% KNO_3 and 35% Sorbitol by mass through the manufacturing process.
- *Grain Surface Quality* will be controlled through the manufacturing process and the quality check in accordance to the quality criteria outlined in chapter 4.
- *Grain Density* will be controlled through the manufacturing process by increasing the propellant density ratio to above 93% in accordance to the quality criteria outlined in chapter 4.
- *Gas Flow Velocity* will be controlled through the design port to throat area larger than the recommended ratio of $\left(\frac{4}{3}\right)^2 = 1.778$ [-] [23]. ($\approx 9 - 13$ [-])
- *Ignition Charge* all motors will be ignited with similar 1.0 [g]'s of black powder together with 1 [g] of ignition primer, these will be constructed from the same batches to assure consistency between tests.
- *Nozzle Geometry* as the fine (F) and course (C) propellant variants are expected to produce different burn rates the nozzle geometry has to be changed to achieve the desired pressure range. Nozzle geometry will be kept with equal convergence/ divergence angles and nozzle throat radii produced on an accurate CNC mill. The nozzle throat diameter will be measured before and after the test with an accuracy of ± 0.05 [mm] or better.
- *Grain Geometry* is to be kept constant, however small production differences cannot be ruled out. The analysis will be adapted for these variations on a case by case basis. As such general dimensional differences will be tolerated, measurement accuracy will be ± 0.05 [mm].

Lastly the geometrical BEM dimensions, environmental conditions (ambient pressure, temperature and weather) will be noted to assure similarity between tests.

6.2.2. Identification of Equipment Under Test

The proposed tests are listed in table 6.2. Test identifier 'EXC' determines the experiment, 'C' or 'F' denotes whether Fine or Course KNO_3 was used. The numbers denote the repetition of the test configuration. In case of test failure (such as a misfire) the test identifier will not be reused.

As shown in table 6.2 for both fine and coarse compositions a load test will be performed with a lower nominal operating pressure by increasing the nozzle size. These load tests will be used to verify the design works as intended while observing a larger effective margin of safety to the maximum operating pressure. Afterwards ambient tests will be repeated 3 times while two conditioned tests will be performed. This is limited by the size of thermal conditioning box available for the experiment. As the tests were planned for the start of September the expected ambient temperature is well above the cold conditioning temperature allowing a suitable ΔT between ambient and cold firing temperatures.

no	test-id	PSD	P_c [Mpa]	T_0 [°C]
1	EXC-C-01	Course	1.5-5.5	≈25
2	EXC-C-02	Course	2.0-7.5	≈25
3	EXC-C-03	Course	2.0-7.5	≈25
4	EXC-C-04	Course	2.0-7.5	≈25
5	EXC-C-05	Course	2.0-7.5	≈5
6	EXC-C-06	Course	2.0-7.5	≈5
7	EXC-F-01	Fine	1.5-5.5	≈25
8	EXC-F-02	Fine	2.0-7.5	≈25
9	EXC-F-03	Fine	2.0-7.5	≈25
10	EXC-F-04	Fine	2.0-7.5	≈25
11	EXC-F-05	Fine	2.0-7.5	≈5
12	EXC-F-06	Fine	2.0-7.5	≈5

Table 6.2: Proposed test matrix for investigation of the steady burn rate.

6.3. Determination of Motor Performance

A first step in measuring motor performance is in determining specific impulse, I_{sp} [s], characteristic velocity, c^* [m/s] and nozzle coefficient C_f [-] for the motors under test. The measured c^* [m/s] specifically is used in determining also the steady regression rate of the propellant in section 6.8. Together these values provide insight into the achieved exhaust velocity and possible areas of improvement of the propellant and motor.

As stated in in the introduction, performance of a rocket motor is expressed specifically through the comparison between the ideal and experimental values of c^* (equation 2.2) and C_f (equation 2.3) with the resulting efficiency's η_b and η_f [-] as ratios between achieved and ideal performance. For any combination of chamber pressure P_c [Pa], ambient pressure P_e [Pa] and expansion ratio A_e/A_t [-] a distinction is made between two cases: ideal isentropic rocket performance, denoted by subscript (is) and the measured performance based on BEM experimental data which is denoted with subscript (x).

In this thesis frozen flow is assumed with chemical properties of the reaction products taken at chamber conditions (infinite area chamber) as estimated by RPA [50]. The standard (65/35) chemical composition will be assumed at a fixed initial temperature of 293.15 [K]. Furthermore, in this study no time was available to combine loss models such as described in [1] to attempt to predict the quality factors from propellant or motor specifications, as such, only a comparison to literature values is made in the analysis of results.

6.3.1. Method

Experimentally determining $I_{sp,x}$, c^*_x and $C_{f,x}$ is challenging as various values need to be estimated such as the instantaneous nozzle throat area and mass flow. In this section first the method is provided with which the values for c^*_x and $C_{f,x}$ are calculated for the BEM tests, subsequently the sensitivity is analysed that estimates the effect of these key assumptions.

It is important to note that, as the BEM is designed around a progressive burn-profile, that the flow is only optimally expanded at one design pressure (around 2 [MPa], $A_e/A_t = 4$). Based on the evaluated quality factors an estimate is made for nozzle performance assuming the ideal sea level expansion ratio ($P_e = 0.1$ [MPa]) at ambient $P_e = P_a$ and vacuum $P_a = 0$ [Pa] conditions. These results therefore provide a first validation case of the maximum achievable and theoretical I_{sp} that might be achieved and can be

used as starting point for the future. Even so various loss factors do shift with expansion ratio (refer to [1]) and therefore this first analysis does not provide a full characterisation of the maximum achievable I_{sp} performance.

Experimental values used are quasi steady state pressure and thrust data filtered using a $k = 200$ moving average filter (at $f = 1000$ [Hz] sampling frequency this is equal to an 0.2 [s] wide averaging window). Integrated properties were simple cumulative sums as the numerical integration error is significantly smaller than the other experimental errors.

System average specific impulse, $I_{sp,x}$

Although less useful a value then for a neutral burning BEM, the time averaged specific impulse $\bar{I_{sp,x}}$ is calculated with equation 6.1. An instantaneous value of $I_{sp,x}$ is calculated with equation 6.2. This does mean that, as the average characteristic velocity is used, this is an approximation for the true instantaneous I_{sp} (as function of chamber pressure). This is however expected to be more accurate than when you using a constant mass flow estimate such as during earlier analysis [16].

$$\bar{I_{sp,x}} = \frac{1}{g_0}\frac{\int_{t_b} F(t)dt}{\int_{t_b} \dot{m}(t)dt} = \frac{I_{tot}}{g_0 \Delta M} \tag{6.1}$$

$$I_{sp,x} = \frac{1}{g_0}\bar{c_x^*}C_{f,x} \tag{6.2}$$

The boundaries of t_b for calculating c^* is the chamber pressure exceeding 0.2 [MPa] (absolute), thus assuring the flow is choked ($P_c/P_a \approx 1.6$). A more extended discussion on the definition of burn time and the effect on the calculated propellant properties can be found in section 6.4.2.

Experimental Determination of $\bar{c_x^*}$

As the instantaneous mass flow cannot be directly measured, a test average value is calculated. This ignores the fact that both the theoretical c_{is}^* and combustion quality η_b generally increase slightly with chamber pressure. The loaded propellant mass ΔM [kg] will be used, in contrast to the ΔM expelled (loaded-burnout weight) as it is a more representative measure of propellant performance. An analysis of this choice is made in the next section. To obtain test average values the right hand side of equation 2.2 is used and integrated over the entire burn. $\bar{c_x^*}$ [m/s] is defined in equation 6.3.

$$\bar{c_x^*} = \frac{\int_{t_b} A_t(t)P_c(t)dt}{\int_{t_b} \dot{m}(t)dt} = \frac{1}{\Delta M}\int_{t_b} A_t(t)P_c(t)dt \tag{6.3}$$

Experimental Determination of $C_{f,x}$

The experimental thrust coefficient $C_{f,x}$ can be determined using the right hand side of equation 2.3. As both thrust F and chamber pressure P_c are directly measurable quantities an instantaneous value can be determined. A first analysis is made with the constant (initial) throat area A_t, while a refinement is made to include variations in nozzle throat area due to erosion or deposits.

$$C_{f,x}^0 = C_{f,x} - \left(\frac{P_e - P_a}{P_c}\right)\frac{A_e}{A_t} = \frac{F_t}{P_c A_t} - \left(\frac{P_e - P_a}{P_c}\right)\frac{A_e}{A_t} \tag{6.4}$$

As all motors use the same expansion ratio $A_e/A_t = 4$ the theoretical thrust coefficients are approximately constant for all motors with deviations only due to changing chemical equilibrium and changes in pressure thrust. Correcting for this difference, the characteristic thrust coefficients can be easily compared.

A challenge for determining the characteristic thrust coefficients C_f^0 is determination of the exhaust pressure. To this end the area equation from [24] (page 52) needs to be inverted.

6.3.2. Sensitivity Discussion

As mentioned several explicit choices are made that will influence the experimental values for $\bar{c_x^*}$, $C_{f,x}$ and $I_{sp,x}$. To get an estimate of the design influence of these choices the various choices are separately considered in this section.

1. *Choices for ΔM [kg]:*

   (a) ΔM_1 defined as the propellant mass in the propellant grain after correction for the weight of the liner (used for calculating the propellant density), see equation 6.5.

   $$\Delta M_1 = M_{grain} - \rho_{liner} l_{liner} \tag{6.5}$$

   (b) ΔM_2 defined as the mass difference before and after firing, with or without a correction for the condensed propellant residues (K_2CO_3) found in the chamber and weighed independently. See equation 6.7.

   $$\Delta M_2 = M_{pre} - M_{post} \tag{6.6}$$

   $$\Delta M_{2,res} = M_{pre} - M_{post} - M_{res} \tag{6.7}$$

   This choice will be evaluated as part of the results and discussion in this chapter. ΔM_1 is the preferred option as it is a more representative value for propellant performance. ΔM_2 is however likely the most often used value by amateur researchers as it is easier to relate to rocket performance.

2. *Choices for A_t [m^2].* Four different definitions were considered of increasing complexity.

   (a) $A_t(0)$ as constant initial value

   (b) $\bar{A_t}$ as time averaged mean

   (c) $A_t(t)$ as a linear function of time (over t_b)

   (d) $A_t(\dot{m})$ as a linear function of expelled mass (estimated via simulation)

   (e) $R_t(\dot{m})$ as a linear function of expelled mass, resulting in a quadratic equation for $A_t(\dot{m})$ (estimated via simulation)

   It was observed during past firings of KNSB propellant motors [57] that nozzle area's tend to decrease as deposits form on the nozzle. The deposits found were almost perfectly smooth suggesting an even buildup of slag reducing the throat/exit area by 10-20% during the test. Such an area reduction can have a large effect on measured performance and regression rates. The measured performance will be calculated in terms of the constant initial throat, for more thorough analysis the other options are also considered.

3. *Shifting expansion ratio.*: As next to A_t also the nozzle exit area A_e contracts during the test a different exhaust velocity, exit pressure and therefore thrust could be measured. It is assumed that the formation of deposits in time is the same for both nozzle throat and exit. For the calculation of $C_{f,x}^{\circ}$ and P_e the area ratio is assumed constant at 4 [-] however this choice will also be evaluated.

6.4. Determination of the Steady Regression Rate

The steady burnrate r (typically) [mm/s] is defined as the propellant regression velocity as function of chamber pressure P_c [Pa] and the propellant initial temperature T_f [19]. As the regression rate is fundamentally limited by the reaction rate or thermal quasi-equilibrium at the burning surface area, the phenomenon is highly dependent on propellant composition, propellant properties and the chamber environment. An empirical relation for the propellant burnrate is given in equation 6.8 [16] in which a, b and n are model constants that are fitted to the data, T_{ref} the reference temperature and P_{ref} is the reference pressure taken in this study equal to be 273.15 [K] and 1.0 [MPa] respectively.

$$r = \big(a(T_f - T_{ref}) + b\big)\left(\frac{P}{P_{ref}}\right)^n \tag{6.8}$$

Regression rate information for KNSB, shown in figure 6.2, was found from three sources during the literature review. Fine KNSB [63] by strand-burner tests over a pressure range from 0.101-10.7 [MPa] fired at 21 [°C], Coarse KNSB [6] by strand-burner tests over a pressure range from 0.101-10.4 [MPa] fired at 25 [°C], and coarse KNSB [21] determined over an unknown temperature and pressure range but used in motor designs between 1.5-2.5 [MPa]. Up to the start of thesis the only available burnrate was the value determined by Uitendaal [21] for the Stratos I rocket. What is also apparent is that the

burnrate might not fit Vieille's burn rate law (equation 6.8) over the entire pressure range. Especially rates measured for the fine composition indicate sections with a negative pressure exponent n. During analysis of BEM firing results this would be apparent in a 'kink' in the measured burnrate. It is thus important to evaluate the measured burn rates before fitting.

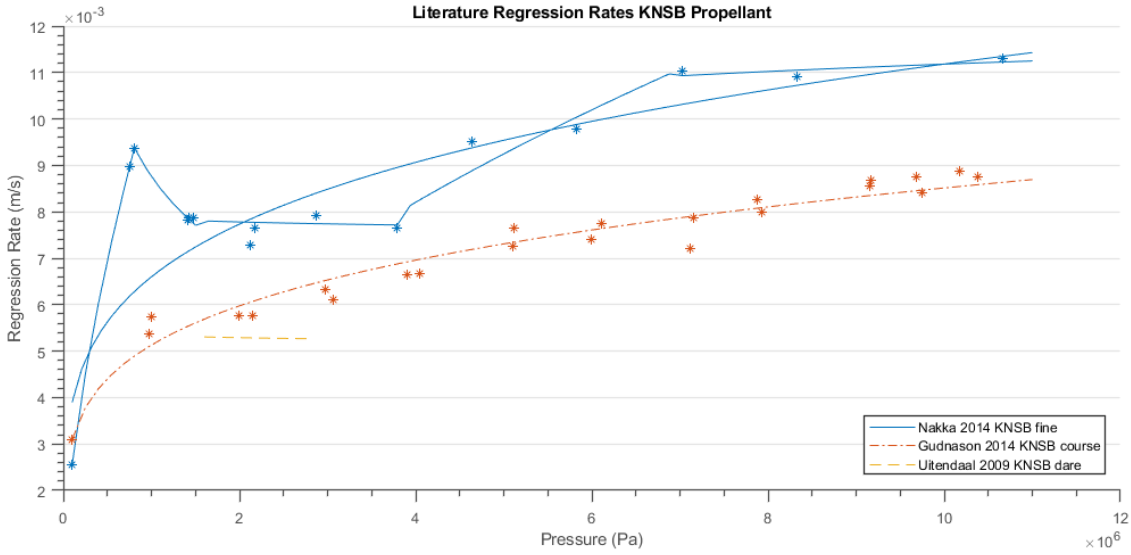

Figure 6.2: Literature Values for fine and coarse KNSB propellant.

Two categories of methods exist for the determination of the instantaneous propellant burnrate from chamber pressure measurements; a thickness over time and mass balance method [4]. With the current BEM design the the mass balance over the motor volume is preferred as it allows determination of the instantaneous burnrate instead of a test averaged value. After analysis of the results equation 6.8 will be fitted to this regression data and from this a temperature dependence will be derived.

6.4.1. Method

Together with the BEM a method was developed to determine the steady regression rate based on chamber pressure measurements, geometrical and mass information of the motor fired. First the method is derived from first principles, afterwards, in section 6.4.2, the sensitivity of the developed method is discussed in a fashion similar to motor performance but is expanded in section 6.4.3 with a sensitivity analysis on the basis of simulated BEM data. To validate the developed algorithm the sensitivity analysis is repeated with data from one of the tests.

When looking at the overall mass balance of the motor, equation 6.9 can be defined for the control volume as shown in figure 6.3 of the chamber up to the nozzle throat excluding the volume occupied by the unburned propellant [16].

$$\frac{dM}{dt} = \frac{d\rho_c V_c}{dt} = \rho_c \frac{dV_c}{dt} + V_c \frac{d\rho_c}{dt} = \dot{m}_{in} - \dot{m}_{out} \tag{6.9}$$

The mass fluxes into and out of the mass balance, m_{in} and m_{out} [kg/s] can be expanded to the following contributions:

1. Propellant regression into the volume, which is described by equation 6.10.

$$\dot{m}_{in} = \rho_p A_b(w) r(P_c, T_0) \tag{6.10}$$

In this equation ρ_p [kg/m^3] is the unburned propellant density, assumed to be uniform as measured, A_b [m^2] is the instantaneous burning surface area as function of the total regressed distance w [m] and $r(P_c, T_f)$ [m/s] is the regression rate of interest in this experiment as function of chamber pressure P_c [Pa], and grain initial temperature T_f [K].

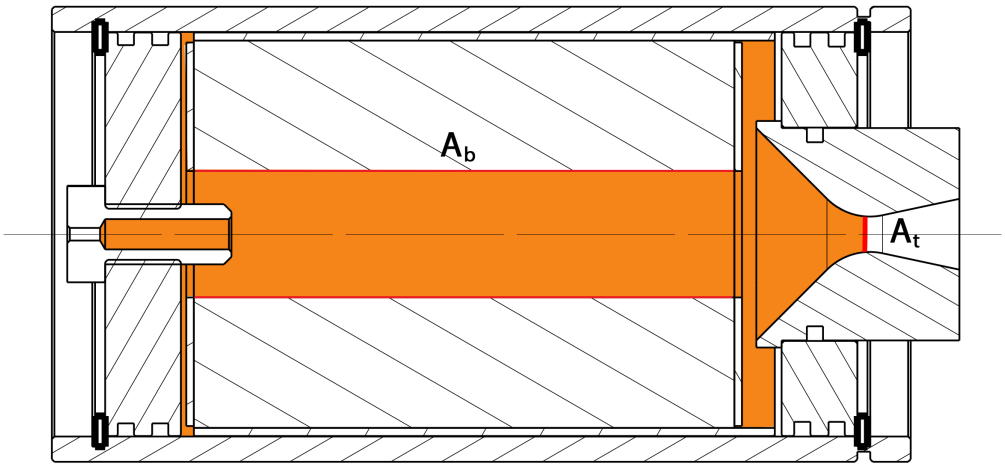

Figure 6.3: BEM control volume as used in the ballistics analysis with active boundaries A_b and A_t. The Control volume considered is shown in orange, rationally symmetric along the BEM longitudinal axis.

2. Nozzle Mass flow out of the control volume described by equation 6.11.

$$\dot{m}_{out} = \frac{P_c A_t(t')}{\eta_b c^*} \tag{6.11}$$

   In this equation P_c is chamber pressure, $A_t(t')$ [m^2] the nozzle throat area, which changes in time denoted by t' [s]. $c^*(P_c)$ and η_b are the characteristic velocity and combustion efficiency in [m/s], [-] respectively. The characteristic velocity used is the value determined for each test as described in previous section. Measurement error in c^* will therefore propagate to a measurement uncertainty in r, a and n.

3. The propellant deposits given as $^{dM_d(t*)}/_{dt}$ [kg/s] which is assumed to accumulate at the end of the burn, similarly to the nozzle area A_t, denoted by a dependency on $t*$.

Equation 6.9 can then be expanded to equation 6.12

$$V_c \frac{d\rho_c}{dt} + \rho_c \frac{dV_c}{dt} = \rho_p A_b(w) r(P_c, T_0) - \frac{P_c A_t(t')}{\eta_b c^*(P_c)} - \frac{dM_d}{dt} \tag{6.12}$$

Typical methods such as described by [62] and [24] further simplify this equation to consider quasi steady state operation including only the mass transfer from nozzle and regression. This results in equation 6.13. With A_b,A_t known (approximately) from the motor design and c^* measured separately or estimated via a chemical analysis program such as RPA. This equation can be used to determine the instantaneous regression rate as function of the measured chamber pressure. This is done with equation 6.14

$$0 = \rho_p A_b(w) r(P_c, T_0) - \frac{P_c A_t(t*)}{c^*} \tag{6.13}$$

$$r(t) = \frac{P_c(t) A_t(t*)}{\rho_p A_b(w) c^*} \tag{6.14}$$

The largest challenge is found in matching the instantaneous burning surface area (through the start and burnout time) and setting the initial burned web thickness at this point. The algorithm written in Matlab [51] follows the structure shown in figure 6.4.

For every time step the instantaneous regression rate $r(i)$ [m/s] is calculated (equation 6.14, subsequently the total regressed length or burned web thickness $w(i+1)$ [m] is updated for the next time step. The differential equations are solved iteratively with a forward Euler method.

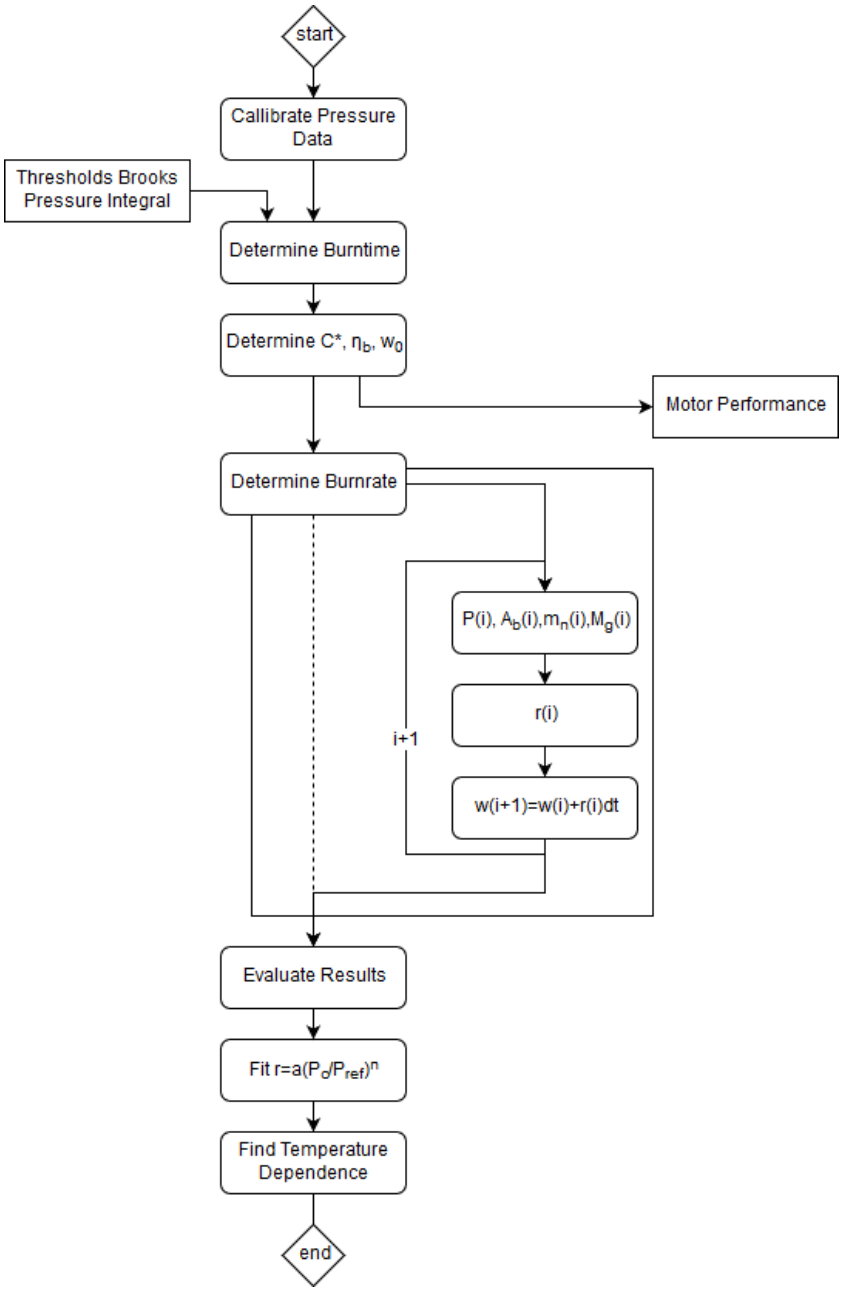

Figure 6.4: Algorithm used in the determination of the steady regression rate.

6.4.2. Sensitivity Discussion

There are several key assumptions that need to be evaluated and possibly tested to assure the calculated regression rate conforms to the actual experiment. These are the various terms in equations 6.12 but also several other less explicit choices that define the result of the analysis. First the various choices are listed and discussed below, subsequently the key choices are evaluated as part of a sensitivity analysis in the next section. Based on this analysis an optimal strategy is chosen.

1. Mass Contributions

   (a) $V_c \cdot d\rho_c/dt$, The unsteady density term can be rewritten to a change in pressure via the ideal gas law as provided in equation 6.15 in which T_c and R denote the chamber gas temperature and specific gas constant respectively. This term describes storage of mass in the control volume due to pressure and density changes. Due to the linear increasing surface area pressure increases constantly during the burn. Analysis of this term showed that the contribution is approximately two orders of magnitude lower than the nozzle mass-flow from equation 6.11, increasing to approximately one order of magnitude lower during start-up and tail-off transients.

$$V_c \frac{d\rho_c}{dt} = \frac{V_c}{RT_c} \frac{dP_c}{dt} \tag{6.15}$$

   (b) $\rho_c \cdot dV_c/dt$, the unsteady volume term describes the change in control volume due to the regression of the propellant. As the volume change is primarily due to the regression of the propellant grain it can be rewritten in terms of instantaneous burning surface area and regression speed shown in equation 6.16. This term is a full two orders of magnitude lower than the nozzle mass flow from equation 6.11.

$$\rho_c \frac{dV_c}{dt} = \rho_c A_b(w) \frac{dw}{dt} = \rho_c A_b(w) r(Pc, T_0) \tag{6.16}$$

   (c) dM_d/dt, the mass deposits due to incomplete ejection of combustion products from the chamber. It is likely that these deposits only accumulate at the end of the burn time and is thus expected to have only a limited effect on the instantaneous regression rate.

   Analysis of test results show that all contributions are a factor 2 smaller within the region of interest ($V_c \cdot d\rho_c/dt$ is one order of magnitude smaller at the end of the test during burnout). This supports the choice of using the simplification 6.14 for the analysis.

2. Constants and Variables

   (a) $A_b(w)$ [m^2] the instantaneous burning surface area of an end inhibited bates grain can be described by equation 6.17. This assumes that the central port burns radially outward until burnout and that the outside, front and end of the grain remain inhibited during this time. The main challenge is in assuring that the instantaneous surface area coincides with the right time. A shift in time (via w) will cause over or under estimation of the actual propellant regression rate. 6.16.

$$A_b(w) = [2\pi(R_0 + w)L_0]_{w=0}^{w=R_e-R_0} \tag{6.17}$$

   (b) V_0 [m^3], the initial chamber volume is chosen as the volume up to the nozzle throat minus that occupied by the propellant grain, a small amount of additional volume is present in the pressure sensor standoff tube which is neglected. The control volume is shown in orange in figure 6.3. Analysis of the drawings indicate an initial free volume of $9.8 \cdot 10^{-5}$ [m^3] with a 107 [mm] long grain occupying an additional $3 \cdot 10^{-3}$ [m^3]. The uncertainty in the initial volume can thus be largely discarded with respect to the volume liberated by the regressing grain.

   (c) η_b, c^*, R, T_c [-,m/s,J/kgK,K] the characteristic velocity, specific gas constant and combustion temperature are obtained from chemical analysis by a program such as RPA [50]. Although these values can be taken as constants, chemical equilibrium calculations show (see appendix A) that combustion properties do shift slightly over the pressure ranges of interest (i.e. from 909 [m/s] at 2 [MPa] to 911 [m/s] at 6.895 [MPa]. A larger uncertainty is with respect to the assumed combustion efficiency. Lacking a better alternative the test average value, $\bar{c_x^*}$ [m/s] will be used during the test.

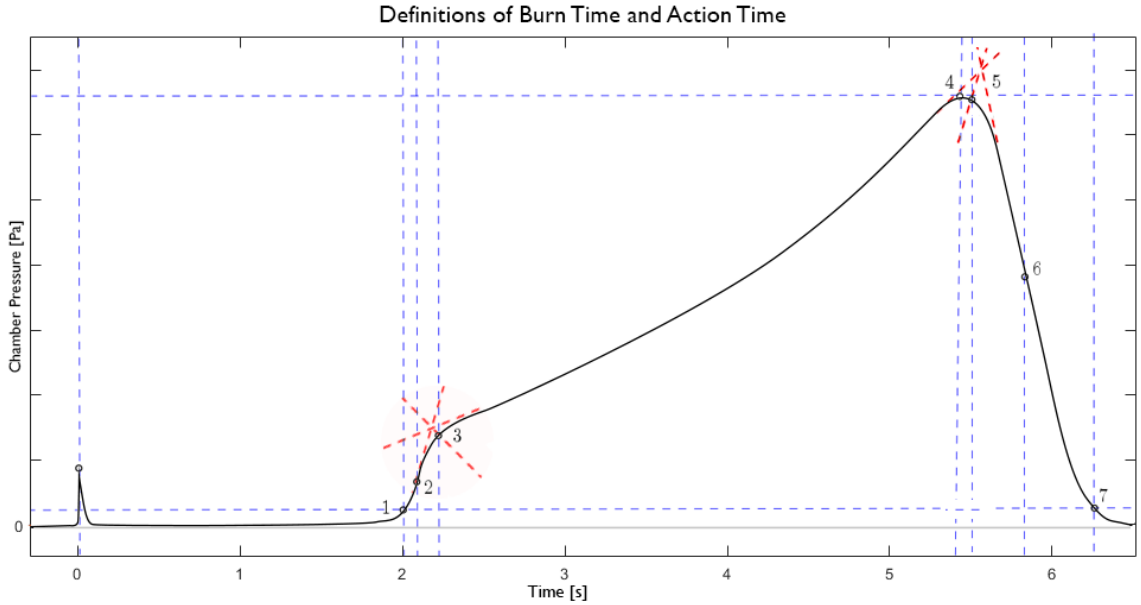

Figure 6.5: Various burn time criteria adapted from [4] for the BEM.

(d) A_t [m^2], the nozzle throat area was discussed in section 6.3.2. A first estimate also for the regression rate is that no slag buildup occurs during the test. Alliteratively deposits can form as function of the nozzle mass flow. As with the mass balance method from equation 6.13 estimates for mass flow are directly available, the nozzle contraction is modelled with a linear approximation as function of expelled propellant. This has a stronger physical justification than linear growth with time. For this study, to keep it simple, a constant initial throat area is assumed.

(e) t_b [s] the start and burnout time motor sees different definitions used in industry [4]. The effect of this choice affects the regression rate estimate primarily through the instantaneous values of A_t and A_b. In applying these criteria two key requirements need to be met. First the chosen criteria needs to reflect the physical process involved, secondly a suitable algorithm needs to be available to select the start time. Based on [5] (page 9), the following candidates are considered and shown in figure 6.5.

i. *Constant P or a % of P_{max}, 10% typical*. Note: use design $P_{max} = 7.5$ [Mpa] for consistency. see fig 6.5 point 1,7
ii. *Tangent-Bisector* see fig 6.5 point 3,5, not used as it relies on subjective operator judgement.
iii. *Brimhall* $d^2P/dt^2 = 0$ or a maximum dP/dt during tail off.
iv. *Brooks' Pressure integral*
v. *Hessler-Glick* from the midpoint of the first perceptible rise to the last sustained rise (for neutral pressure traces) to a negative step of d^2P/dt^2, not used due to a more difficult to implement code.

The chosen method is Brook's Pressure integral shown in equation 6.19 as it has the lowest sensitivity to noise or the chosen method of filtering, and can be effectively made to ignore the initial pressure spike of the igniter. The end points are chosen such that the transients are omitted completely from the burnrate calculation.

$$t_i \rightarrow Y_i = \frac{\int_{t=0}^{t_i} (P(t) - P_a)\, dt}{\int_{t=0}^{\infty} (P_c(t) - P_a)\, dt} \tag{6.18}$$

$$t_e \rightarrow Y_e = \frac{\int_{t=0}^{t_e} (P(t) - P_a)\, dt}{\int_{t=0}^{\infty} (P_c(t) - P_a)\, dt} \tag{6.19}$$

6.4.3. Sensitivity Analysis

To determine the sensitivity of the method to the user defined and measured inputs, a sensitivity analysis is performed. This analysis is performed on three different data sets: two simulated data sets; as described in section D and one experimental data set: EXC-C-06. The sensitivity is expressed by comparing values for a, n to the numbers provided in the simulation and allow direct verification of the method. For the experimental data set an absolute error is not available, instead the values are compared to the nominal fit.

The input to the sensitivity analysis are variations that can realistically occur or have been measured such as the measurement error on the grain port, which is driven by caliper measurement accuracy, or the standard deviation of the characteristic velocity $\bar{c_x^*}$.

Reference Values								
no	variable	unit	value	change	Sim 1	Sim 2	EXC-C-06	
Reference Point								
	a	[mm/s]	4.0		3.846	3.840	4.161	
	n	[-]	0.3,0.4		0.302	0.398	0.340	
Absolute Initial Error at Reference Point								
	e_a	[%]			3.840	-4.01	NA	
	e_n	[%]			0.66	-0.45	NA	
Sensitvity Analysis								
no	variable	unit	value	change	Sim 1	Sim 2	EXC-C-06	
					e_a ,e_n [%]	e_a,e_n [%]	a [m/s] n [-]	Δ_a, Δ_n [%]
Burntime Criterea								
1	Y_i	[-]	0.04	+0.01	-1.61, -4.39	-1.85, -3.56	4.181, 0.337	0.5, -0.85
2	Y_e	[-]	0.85	-0.01	-3.84, 0.66	-4.01, -0.45	4.161, 0.340	0.0, 0.0
Errors in Initial conditions								
3	$\bar{c_x^*}$	[m/s]	747	-16	-1.54, -1.62	-1.73, -1.90	4.268, 0.333	2.58, -2.05
3	x_0	[mm]	2.2	-0.2	-5.24, 3.00	-5.38, 1.03	4.10, 0.347	-1.46, 2.03
Model Constants								
Grain								
5	ρ_p	[kg/m^3]	1724.3	-86.2	0.68, -2.66	0.46, -2.55	4.355, 0.33	4.68, -2.83
8	Grain Length, L_g	[mm]	106.6	-1	-3.04, 0.09	-3.22, -0.81	4.195, 0.338	0.83, -0.49
9	Grain OD, D_o	[mm]	76.2	+0.5	-3.84, 0.66	-4.01, -0.45	4.161, 0.34	0, 0
10	Grain ID	[mm]	25	+0.5	-5.37, 3.23	-5.45, 1.1	4.094, 0.347	-1.6, 2.23
Nozzle Throat								
11	Initial Diameter	[mm]	7.00	-0.05	-4.84, 3.24	-5.00, 1.22	4.117, 0.347	-1.05, 2.22
12	Final Diameter	[mm]	6.60	+0.1	-1.77, -4.7	-1.95, -3.93	4.250, 0.324	2.15, -4.55
Model Assumptions								
13	Constant Throat	[mm]	6.8	0	-12.46, 23.03	-12.59, 14.04	3.878, 0.388	-6.78, 14.32
14	Fixed Chemistry (P_{ref})	[MPa]	5.0	-1.0	-3.87, 0.69	-4.04, -0.43	4.159, 0.34	-0.03, 0.03

Table 6.3: Test matrix for investigation of the steady burn rate.

From the sensitivity table it can be seen that for the most part the error in burnrate constant is equal to around 4%, and below 0.66% for the burnrate exponent. Sensitivity due to a different starting point $Y(i)$ is considerable while relatively insensitive to the end point. Due to the relatively sharper pressure

rise for the actual tests, the effect is however below 1% for actual tests.

Improvements in accuracy can be gained by improving the accuracy of the c_x^* estimate, for which the prediction accuracy is around 1.2 %. Similarly the sensitivity of the initial regressed distance is relatively large.

Of the model constants deviations of the maximum measurement errors lead predictably to changes of a few percent. The notable exception is nozzle throat where it can be clearly seen that the assumption of a linear throat results in serious measurement deviations. In contrast a change to the reference pressure used to calculate the thermodynamic properties of the exhaust gasses (i.e. γ, R) hardly leads any variation, justifying the current approach.

6.5. Experiment Setup

6.5.1. Ballistics Evaluation Motor

The Ballistic Evaluation Motor (BEM) is shown in figure 6.1. Nominal nozzle dimensions are shown in figure 6.6b. The design justification including design requirements, safety and load analysis, and technical drawings are provided in appendix E. A total of six BEM were build to allow multiple tests on the same day. The BEM was mounted horizontally on a test bench developed in DARE in 2018 [53]. Calibration values can be found in appendix C.

Three nozzles with increasing klemmung were developed to account for the expected difference in propellant burnrate from [63] and [6]. Two nozzles (7.00 [mm] ⌀ and 8.37 [mm] ⌀) were used for all nominal tests. One of the 8.37 [mm] ⌀ nozzles was used for the coarse propellant load test while and a larger 9.57 [mm] ⌀ nozzle for the fine propellant load test.

Thrust measurements were made with a Scaime ZFA 500kg load cell (SN 160898) while pressure was measured with a IFM Electronic gmbh PT5402 pressure sensor mounted on a 30 cm stainless steel standoff tube. For every test an additional thermocouple, mounted directly on the DAQ system, was used to record ambient temperature. As could be concluded from the thermal conditioning experiment (see section 6.6.1 the propellant retains ambient temperatures within approximately 1 hour in outdoor conditions. This was the case for all motors. Data acquisition was set to 1 [kHz] for pressure and thrust and 100 [Hz] for the thermocouples.

Tests were conducted outdoors on a field measuring 50 [m] ×109 [m]. Photo's of the field and experiment setup is shown in figures 6.7a to 6.8b.

6.5.2. Protocol

The experimental protocol is provided in appendix B.4, with field procedures in appendix B.4. For every test day a new copy of field procedures were used, which was updated on several occasions during the thesis.

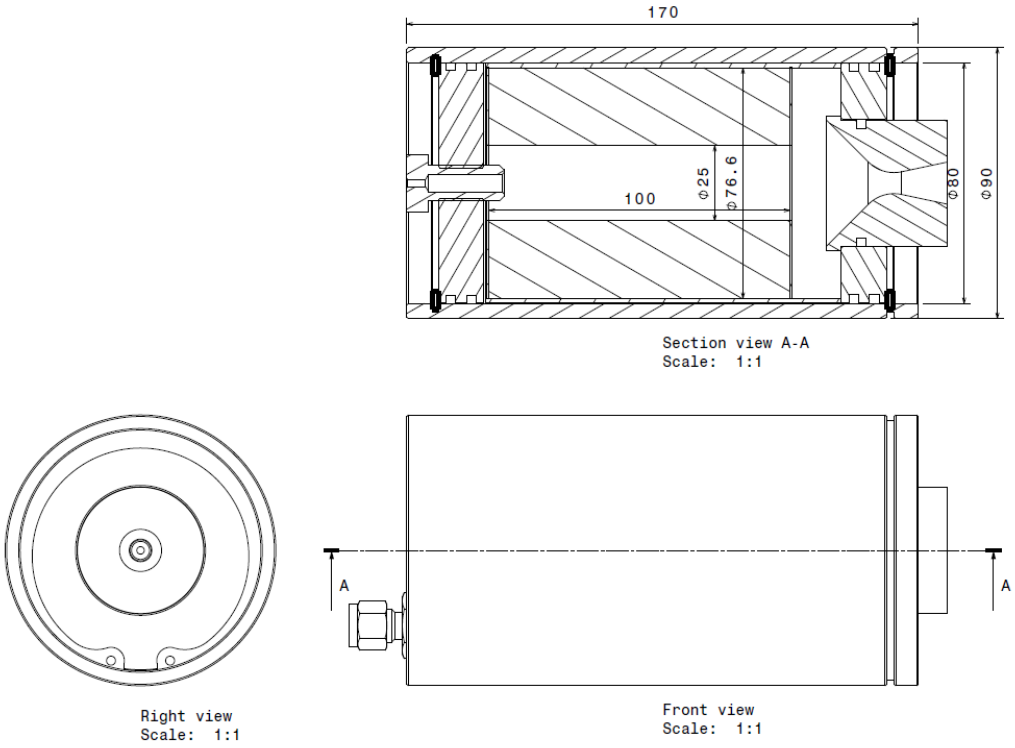

(a) Nominal motor dimensions.

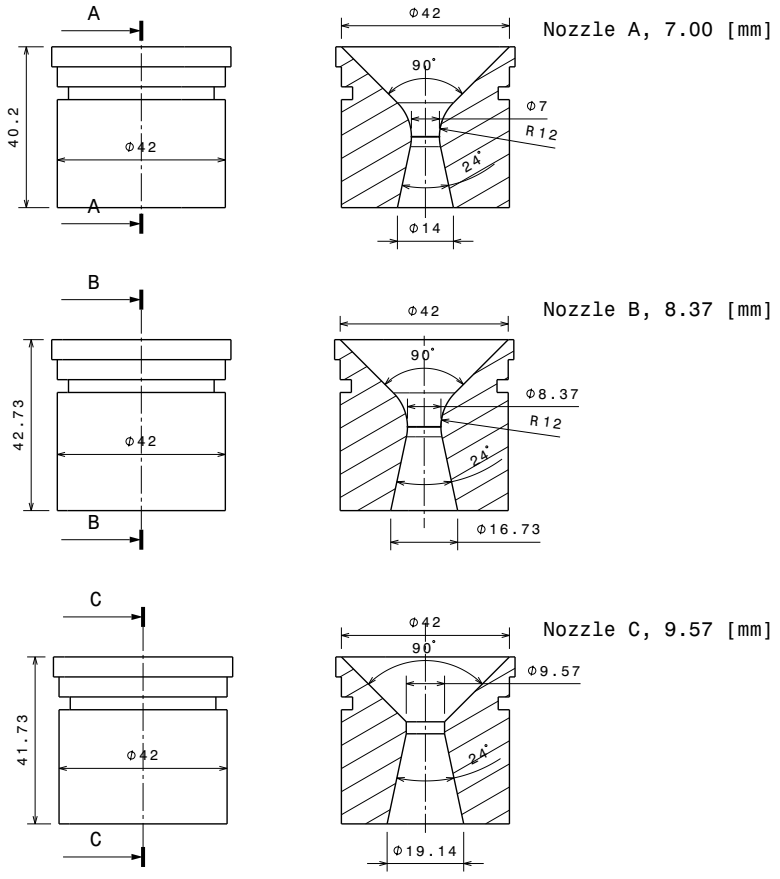

(b) Nozzles used during the steady regression experiments with throat diameters of 7.00 [mm] ∅ (A), 8.37 [mm] ∅ (B) and 9.57 [mm] ∅ (C).

Figure 6.6: Ballistics Evaluation Motor nominal dimensions.

(a) Test field with setup placed under sandbags and shrapnel cover. Behind the setup CP is visible with the author and safety officer (Tobias Knop). Photo taken by Thimo van den Berg.

(b) Detailed view of the experiment setup with C-RIO inside the steel container, firing system (green ammunition box), test bench and sandbags. Firing direction is away from the photographer. Photo taken after firing EXC-C-04.

Figure 6.7: Ballistics Evaluation Motor nominal dimensions.

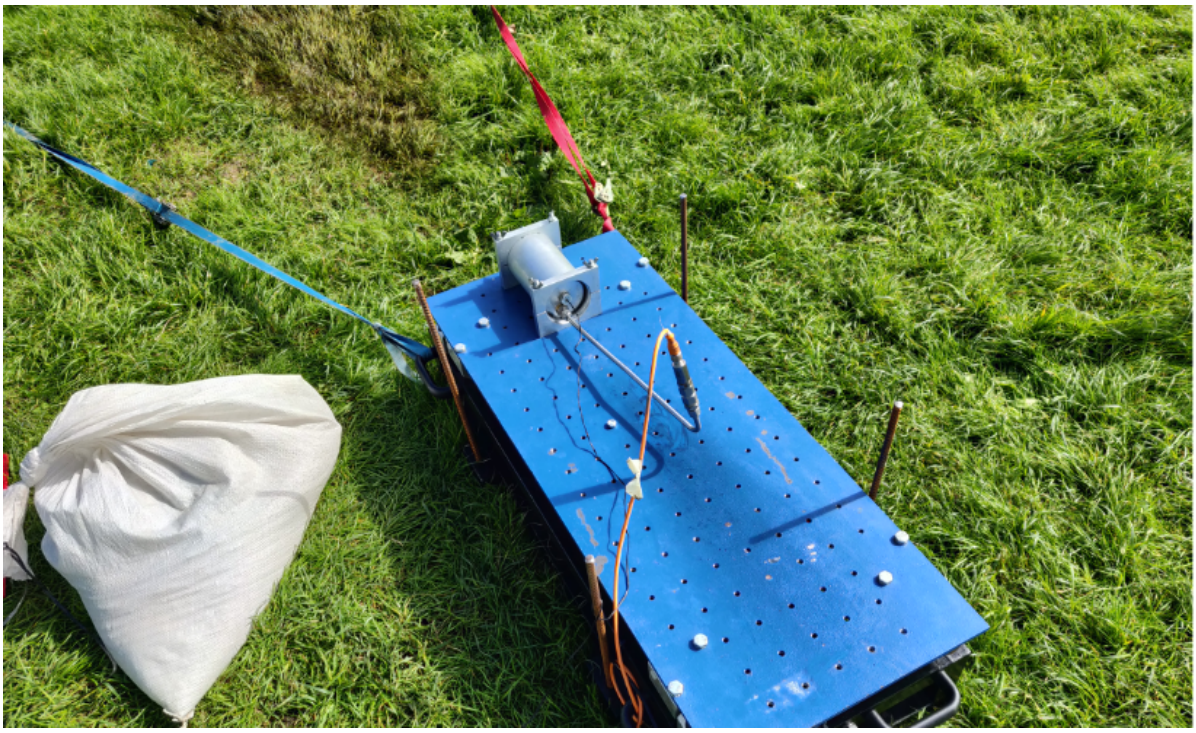

(a) BEM mounted on the test-bench with pressure sensor and igniter mounted (shown post-test of EXC-C-04).

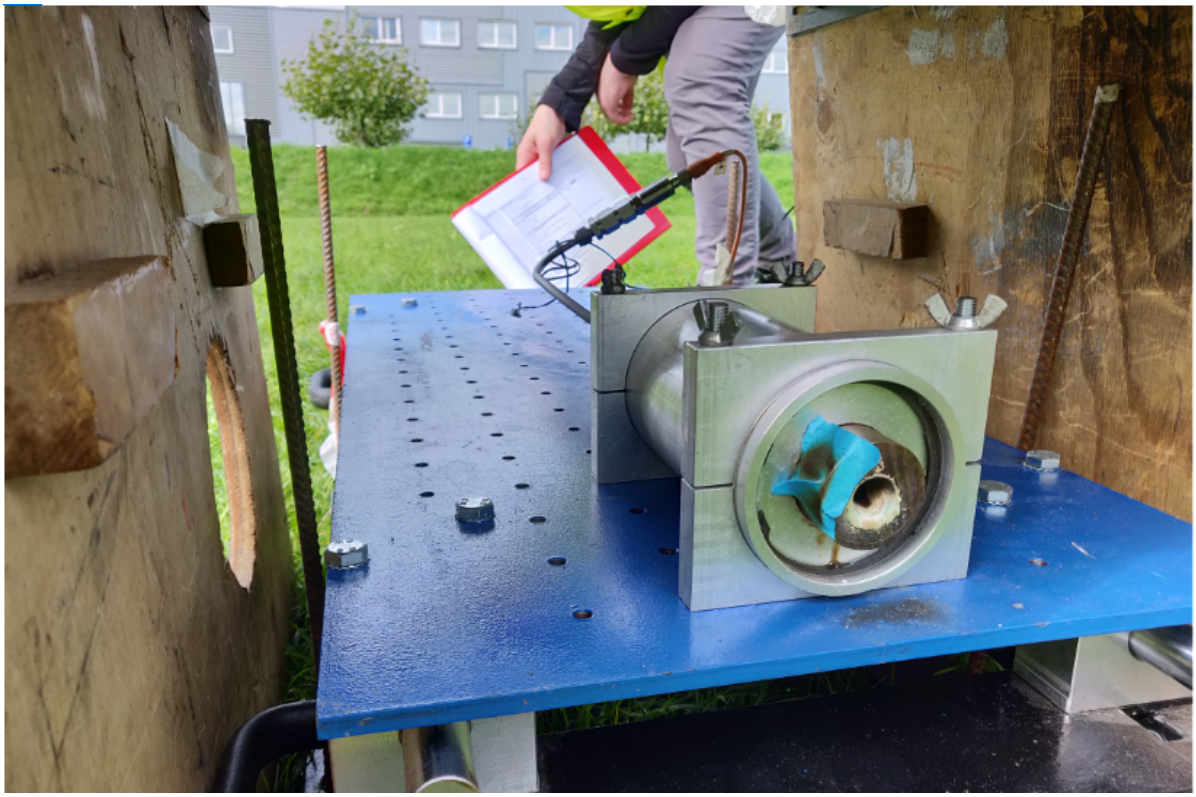

(b) BEM mounted on the test-bench with pressure sensor and igniter mounted (shown post-test of EXC-C-04). Visible are the combustion deposits on the nozzle surface.

Figure 6.8: Ballistics Evaluation Motor nominal dimensions.

6.6. Results

A total of 13 successful BEM tests were completed on test days between 09-09-2018 and 16-01-2018. First the thermal conditioning and the BEM firing results are discussed. Afterwards the configuration measurements and thrust and pressure results are provided. Subsequently in sections 6.7 and 6.8 the motor performance and steady regression rates are calculated for both coarse and fine propellant.

6.6.1. Thermal Conditioning Experiment

With the grains from the experiment described in chapter 4 a thermal conditioning experiment was completed on 18-09-2018. The goal of the test was 1) to verify that the proposed thermal conditioning method worked, 2) to determine the time window available from taking the cold motors out of the conditioning environment up to the moment of firing while not exceeding a grain temperature of 5 [°C], and 3) to ascertain that the grains could handle the thermal shock as this had caused grain failures in the past.

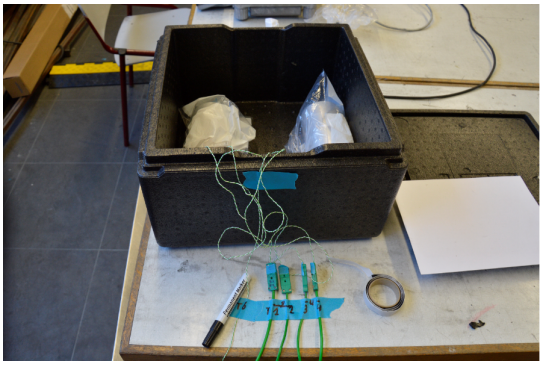

(a) BEM undergoing thermal conditioning with ice. Picture taken before placement of the ice. Motors are protected from moisture with plastic bags.

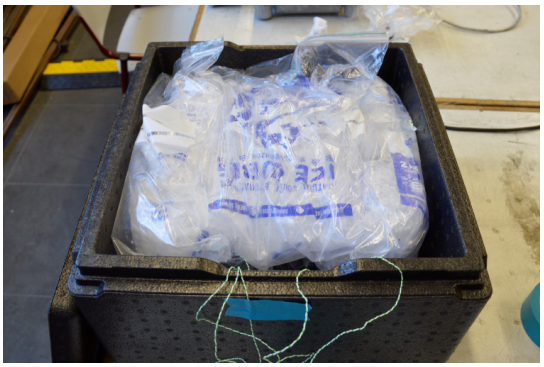

(b) BEM undergoing thermal conditioning with ice. Picture taken before placement of the lid of the conditioning box.

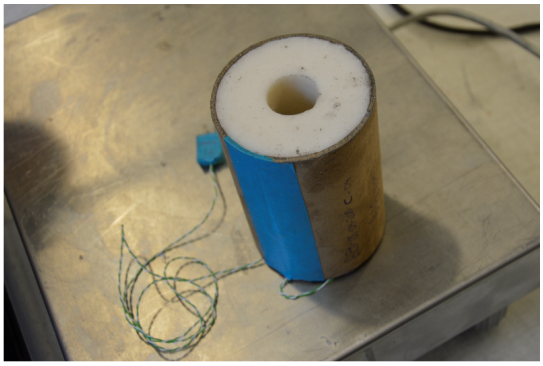

(c) Propellant grain undergoing inspection, embedded thermocouple is visible.

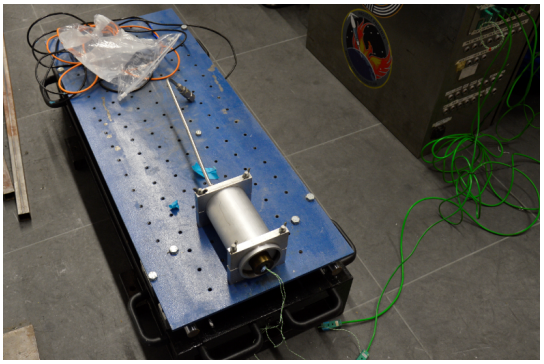

(d) Conditioned grain installed on the test bench. Thermocouples are connected to the DAQ system.

Figure 6.9: Thermal Conditioning Experiment, preparations and execution.

Two grains with embedded thermocouples were installed in motors with additional thermocouples inside the casing at the nozzle bulkhead. The two motors, excluding forward circlips, were stored in a Styrofoam box and cooled down with bags of ice. The motors including the ice are shown in figures 6.9a, 6.9b. Room temperature during the experiment was 23-22 [°C].

The thermal measurements for both runs are shown in figure 6.10. The thermal conditioning of the propellant grains took from 16:41 until 21:20 at which point both motor and grains had attained a steady temperature of 2-3 [°C] while the box reference temperature was at 1-2 [°C]. At 22:46 a first run was performed. Installation procedures, excluding igniter installation were completed after 2 minutes and 55 seconds (denoted by the peak in ambient temperature) at which the casing outside temperature was

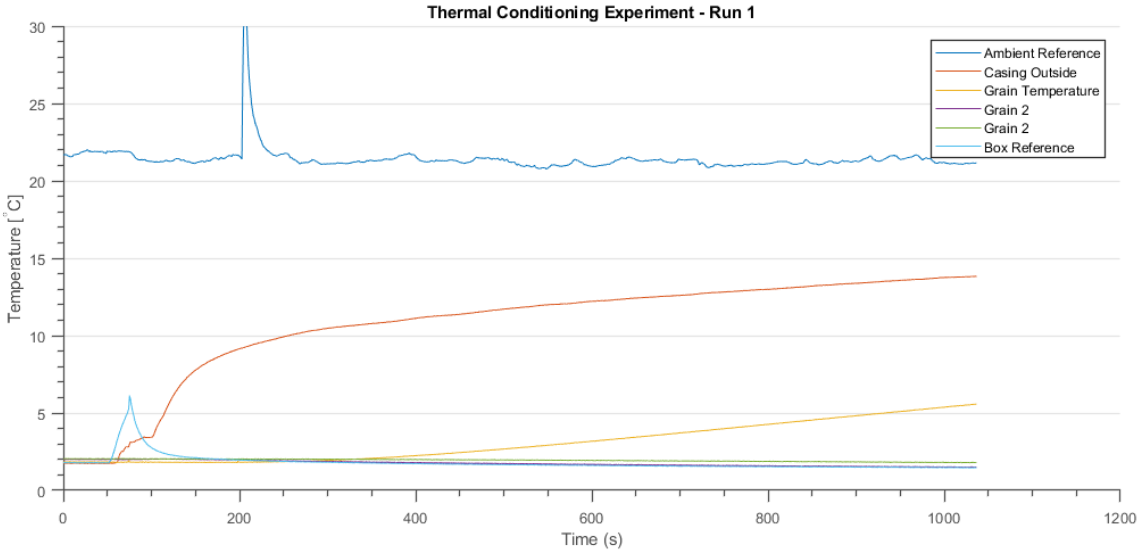

(a) Conditioning Experiment 1.

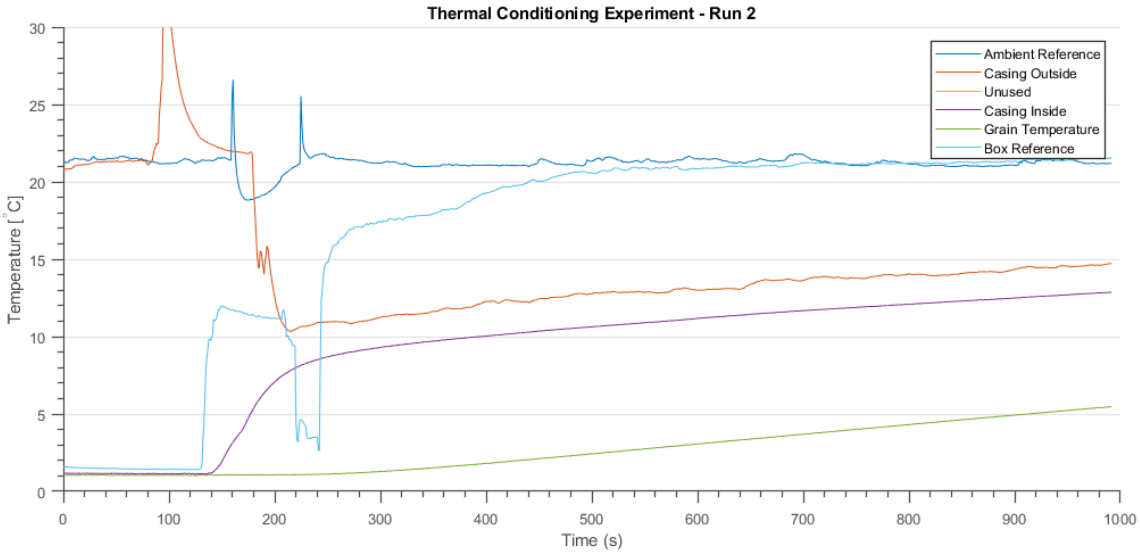

(b) Conditioning Experiment 2.

Figure 6.10: Thermal conditioning experiment, thermal history.

10 [°C], while propellant temperature was 2-3 [°C]. At 23:01 the casing temperature was 14 [°C], while propellant temperature was 5 [°C]. From the start of the experiment until the grain temperature was 5 [°C] took 14.1 minutes. To give the motor more time to come into thermal equilibrium the experiment was repeated the next day with the remaining motor stored overnight in the thermal conditioning box. As an additional thermocouple was available also casing external temperature was measured during this test. Results were similar; the grain had an initial temperature of 1.1 [°C] and became 5 [°C] after 12.83 minutes.

From the thermal conditioning it was established that the developed method for thermal conditioning meets testing objectives (propellant temperature <5 [°C]). Conditioning is best performed over night with the propellant having a resulting thermal gradient of at most 1 [°C]. The time from installation until firing should, conservatively, be below 10 minutes with a larger margin if ambient temperature is lower. Observed thermal lag between the outside of the casing and propellant temperature is 7.5 [°C] allowing a quick estimate of propellant temperature if ambient temperature does not deviate to much from the

conditioning experiment.

Lastly no cracks were found during post inspection of the propellant confirming that conditioned grains can be safely fired. In addition it suggests that the current inhibitor/ grain design does not have the same flaws as some of the motors in the past [56].

6.6.2. Ballistic Evaluation Motor Firing Results

25 Motors were fired on 7 test days between 09-09-2018 and 16-01-2018. Ignition problems resulting in misfires and the Thermal Rocket Propulsion Practical (TRP) resulted in significant changes to the test schedule which took more than double the days initially planned for this experiment. A summary of the performed tests, including misfires is provided in table 6.4. Fine and coarse propellant are numbered chronologically. The test data of the successful tests are further elaborated in subsequent sections.

1. *Data Acquisition Error with Load Cell*
   During transport of the setup to the field the load cell data connection got damaged resulting in an unreliable connection. This resulted in thrust measurement errors for tests EXC-C-05 (fired on 27-05-2019), where the connection failed halfway during the burn, and test EXC-F-11 (fired on 12-01-2019), where no meaningful thrust data was obtained.

2. *Igniter Lead Blowouts*
   Igniter leads were ejected from the igniter bolts of EXC-C-01 and EXC-C-02 (both fired on 09-09-2018) which prompted a small redesign of the igniter based on recommendations from [18].

3. *Coarse KNSB misfires*
   the first test day a single coarse motor misfired (EXC-C-03, igniter configuration (1)). For future motors the ignition primer was increased (igniter configuration (2)), which resolved the issues for the coarse propellant.

4. *Nozzle Ejection*
   An assembly error on motor EXC-C-07 (fired on 20-10-2018) resulted in nozzle blowout during igniter firing. The failure was traced back to incorrect circlip installation at the nozzle resulting in a low speed ejection (components travelled approximately 8 [m] from the test bench without damage to non-consumable hardware or risk to the public (refer to suspension criteria). After this was assured the test campaign was continued with an additional check in the procedures.

5. *Fine KNSB misfires and Ignition Problems*
   As was already previously mentioned consistent misfires occurred for the fine KNSB propellant. First attempts to mitigate the problems focused on simple igniter changes that were believed to increase the chance of successful ignition. These attempts were hampered by long lead times for field reservations (2 weeks) and the availability of only a single motor per day with the low pressure load test configuration. This meant that considerable manpower was necessary for a single attempt at fixing the configuration. A Root Cause Analysis (RCA) was completed at the beginning of October and after another series of misfires (18-10-2018 and 20-10-2018) it was decided to investigate the ignition behaviour directly during a laser ignition experiment. The RCA and ignition experiment is described in chapter 5.

   With the surfactant determined to be the most likely cause of the fine misfires, a new batch of fine propellant grains were produced on 07-01-2019 with a low amount of surfactant (2 drops equal to 0.05 [g/100g]). In the end four motors were successfully fired, EXC-F-11 on the 12-01-2019 and EXC-F-12 to EXC-F-14 on 14-01-2019.

6.6.3. Measurements

The pre-firing measurements results are shown in table 6.5 with firing and post firing results in table 6.6. BEM-ID refers to the Casing number that was used (1-6) during the test, nozzles and bulkheads were cleaned checked and interchanged between motors. Grain geometric measurements are defined in accordance with figure 6.11. All measurements (1-4) are in [mm] $\pm$ 0.05 [mm]. With the exception of the liner length (measurement no. 5) which is measured to within $\pm$ 0.5 [mm] accuracy. Propellant

ID		Experiment Design		Firing Results			
no	test-id	PSD	$P_{c,max}$ [MPa]	Date	T_0 [°C]	P_c [MPa]	notes
1	EXC-C-01	Coarse	1-5.5	09-09-2018	19	3.3	(a,c)
2	EXC-C-02	Coarse	2-7.5	09-09-2018	20	5.6	(c)
3	EXC-C-03	Coarse	2-7.5	09-09-2018	20	Misfire	
4	EXC-C-04	Coarse	2-7.5	09-09-2018	22	7.2	
5	EXC-C-05	Coarse	2-7.5	27-09-2018	25	8.2	(b)
6	EXC-C-06	Coarse	2-7.5	29-09-2018	4(C)	6.9	(d)
7	EXC-C-07	Coarse	2-7.5	20-10-2018	15	Assy	(e)
8	EXC-C-08	Coarse	1-5.5	16-01-2019	7	3.7	(a,f)
9	EXC-C-09	Coarse	2-7.5	16-01-2019	6	6.3	(f)
10	EXC-C-10	Coarse	1-5.5	16-01-2019	6	3.6	(a,f)
11	EXC-C-11	Coarse	2-7.5	16-01-2019	6	6.1	(f)
12	EXC-F-01	Fine	1-5.5	27-09-2018	24	Misfire	
13	EXC-F-02	Fine	1-5.5	29-09-2018	2	Misfire	
14	EXC-F-03	Fine	1-5.5	29-09-2018	2	Misfire	
15	EXC-F-04	Fine	1-5.5	18-10-2018	17	Misfire	
16	EXC-F-05	Fine	1-5.5	18-10-2018	18	Misfire	
17	EXC-F-06	Fine	1-5.5	18-10-2018	20	Misfire	
18	EXC-F-07	Fine	1-5.5	18-10-2018	19	Misfire	
19	EXC-F-08	Fine	1-5.5	20-10-2018	15	Misfire	
20	EXC-F-09	Fine	1-5.5	20-10-2018	16	Misfire	
21	EXC-F-10	Fine	1-5.5	12-01-2019	8	Misfire	
22	EXC-F-11	fine	1-5.5	12-01-2019	8	2.9	(a,b)
23	EXC-F-12	fine	2-7.5	14-01-2019	7	3.9	
24	EXC-F-13	fine	2-7.5	14-01-2019	7	3.7	
25	EXC-F-14	fine	2-7.5	14-01-2019	5	4.1	

notes:

(a) Fired with conservative larger throat.

(b) DAQ Error, no thrust measured.

(c) Igniter leads ejected.

(d) Thermally Conditioned Motor.

(e) Assembly Error which led to ejection of the nozzle.

(f) Fired for the Thermal Rocket Propulsion Practical.

Table 6.4: Test matrix for investigation of the steady burn rate.

diameter specifies the diameter of the grain within the cardboard excluding sorbitol diffusion into the cardboard, this is listed as measurement number 6 in the table.
Cast weight is the weight of propellant cast into the moulds. Final weight specifies the propellant weight of the grain after cleaning, corrected for the cardboard inhibitor tube. From the geometry and

cast weight a propellant density is calculated with some small uncertainty due to sorbitol diffusion into the inhibitor tube. The density ratio, with respect to the ideal propellant density $\rho_{id} = 1841$ [kg/m^3] is provided separately. The last two fields in table 6.5 provide nozzle throat and exit diameters in [mm].
In table 6.6 again test ID and firing date are provided. In addition, under 'propellant' the igniter config-

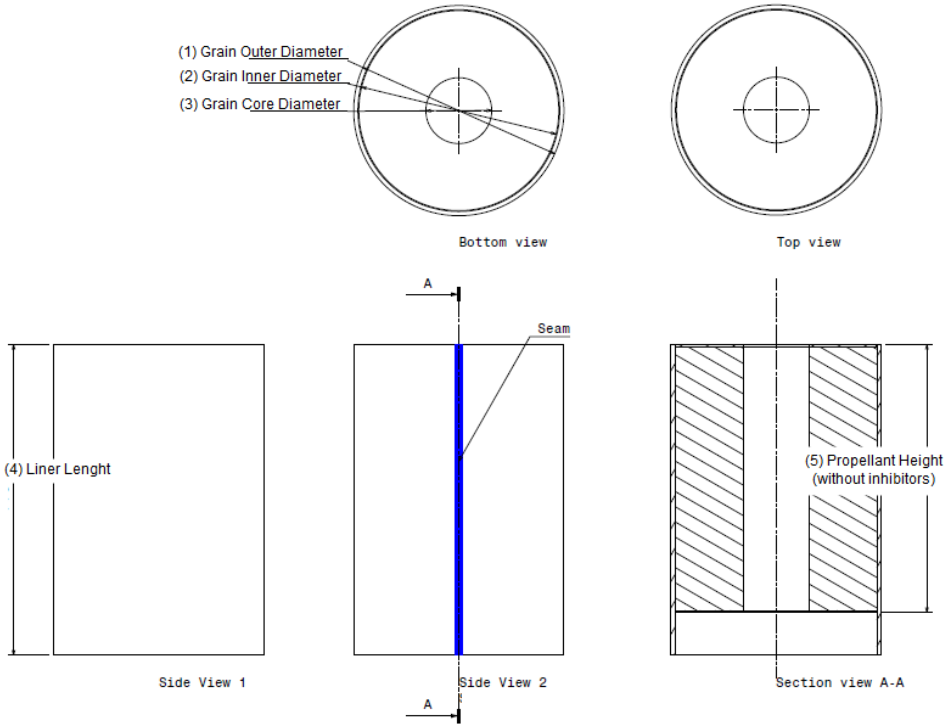

Figure 6.11: Grain Dimensions (1-5) as used in table 6.5.

uration and propellant firing temperature is provided.A (1) denotes the initial 1 [g] of black powder, (2) double amounts of ignition primer, while (3) indicates a test with the Titanium augmented composition (refer to chapter 5 for a more extensive discussion). Test conditions are provided with temperature, averaged from thermocouple readings directly on the C-RIO (2 meters away from the motors) and an indication to the weather conditions.
Loaded and burnout weight relate to the total system weight including pressure sensor, igniter seals and circlips as weighed on the field directly prior to installation and directly after firing. Uncertainty of this weight was ± 5 [g] due to wind influence on the scales. During post test dis-assembly of the motors the chamber residues were separated (roughly) into remaining inhibitor material and burned out propellant residue (such as K_2CO_3). Similar to table 6.5, again nozzle throat and exit diameters are provided, the reduction is due deposits on the nozzle with dimensions averaged from three separate measurements.
Last in table 6.6 are summary numerical values from DAQ measurements: P_{max} [MPa], N_{max} [N], and the burn time t_b [s] and ignition delay t_{id} [s] based on the *Brooks* burn time definition with pressure integral limits at 0.5% and 99 % [4] which is more extensively discussed in section 6.8.

Tests with identical test conditions (nozzle, propellant temperature) showed very similar results which can be clearly established by tests performed for the TRP practical EXC-C-08, EXC-C-09, EXC-C-10 and EXC-C-11 which have peak pressures with a maximum difference of 0.2 [MPa] (3% $P_{c,max}$ and peak thrust with a maximum difference of of 7 % F_{max} [N]. This trend is reflected by the fine composition with a peak pressure variation of $P_{c,max}$ of 0.4 [MPa]. Repeatability is less for tests earlier in the program however this is less representative as results are not corrected for igniter blowouts and the system at that time was still under development. Even so the ambient and cold conditioned test (EXC-C-05 and EXC-C-06) fired on the same day showed almost identical thrust/ pressure behaviour.

Peak pressure for the coarse propellant fired at warmer temperatures agreed very well with the predicted peak pressures while motors fired at cold temperatures achieved lower peak pressures. The fine motors fell significantly short of the design operating pressures with a maximum recorded pressure of 4.1 [MPa].

It proved possible to fire six motors in a single day although due to the misfires a maximum of only 5 motors were ever tested. At the end of the development and assuming only successful tests, the original test schedule could in principle be executed over a total of 2 days. The largest deviations from the test schedule were caused by the misfires as the ignition failure of the single load test resulted in the abort for the day. This reduced the amount of tests to 1 per day with significant overhead due to the time required to pack all equipment and move the equipment between the lab and the field.

Pressure and thrust curves for the coarse propellant motors (EXC-C-01 to EXC-C-11) are shown in figure 6.12b and 6.12a. Pressure and thrust curves for the fine propellant motors are shown in figure 6.13b and 6.13a.

6.6.4. Observations

In preparation for and during the experiment a number of additional observations were made:

1. *Propellant Quality,* was consistent with the previous experiments. Average density of the cast grains was 1755 [kg/m^3] (density ratio of 0.95, based on 10 grains) while fine density was 1776 (density ratio of 0.96, based on 14 grains). Propellant surface quality was uniformly perfect with the exception of the fine grains that were successfully fired. Several superficial defects were visible. However as these surfaces are covered by black silicone glue and cardboard the effective burning surface area remained largely unaffected.

2. *Fine propellant out gassing,* was challenging for the fine composition with only 2 drops, 0.05[g] of surfactant due to the much higher viscosity. This was seen by the lack of boiling of the mixture suggesting the moisture remained trapped in the mixture. This did not however result in measurable density deficiencies (0.95-0.98) for the grains.

3. *Difficulty in applying consistent primer coating.* It proved difficulty to estimating the amount of primer painted on the exposed grain surfaces as the coating was 1-2 grams and could only be measured with a 1 [g] accuracy after drying. Furthermore it was found that upon drying the ignition primer formed cracks and parted from around 10 % of the propellant surface.

4. *Small thrust measurement bias,* can be seen in the thrust measurements for most motors. As the motor was tilted slightly downwards this is explained by the reduction of weight of the motor. The effect was corrected with a linear function with the resulting error «1%.

5. *Test EXC-C-01 to EXC-C-02 igniter blow outs,* occurred on the first two tests (both fired on 09-09-2018). At a pressure of around 3 [MPa] (at 2.13 [s] EXC-C-01 and 2.71 [s] EXC-C-02) the igniter leads were blown out of the motors. The hole had a diameter of 3.2 [mm] ∅ and can be seen as a step decrease in thrust and pressure curves for both tests. As the failure occurred at the forward closure, effectively creating an additional nozzle in the opposite direction, the thrust saw a greater decline than pressure.

6. *Test EXC-C-04,* appears to be an outlier with pressure and thrust behaviour significantly different from the other tests. Based on the pressure/thrust curves EXC-C-04 regression rate values are omitted from the calculations of the test average.

7. *Test EXC-C-08 to EXC-C-11,* were fired with a slightly different inhibitor configuration. The aft cardboard inhibitor disk had a port diameter of 28 [mm] (25 [mm] was nominal). This caused the slightly slower tail-off of the thrust and pressure curves compared to the nominal design as burn through occurred in two steps. But, based on simulations, did not affect the instantaneous burning surface area.

8. *Test EXC-F-1,* showed a deviation in thrust and pressure from 2.5-4 [s] which is likely caused by an unidentified fault in the propellant surface.

Test ID	Firing Date	BEM ID	Grain ID	Grain Dimensions						Prop Weight		Grain Density		Nozzle	
				(1)	(2)	(3)	(4)	(5)	(6)	Cast	Final	ρ	rho/rho_{id}	Throat	Exit
				[mm]	[mm]	[mm]	[mm]	[mm]	[mm]	[g]	[g]	[kg/m³]	[-]	[mm]	[mm]
EXC-C-01	09-09-2018	BEM-2	05/09/2018-C-02	79.9	76.2	24.9	107.6	105.1	0.4	758	756.9	1768	0.96	8.4	16.7
EXC-C-02	09-09-2018	BEM-3	06/09/2018-C-01	80.0	76.3	24.8	107.2	104.5	0.4	758	755.1	1766	0.96	7.0	14.0
EXC-C-04	09-09-2018	BEM-5	05/09/2018-C-03	79.9	76.2	24.8	110.3	107.5	0.4	758	752.0	1716	0.93	7.0	14.0
EXC-C-05	27-09-2018	BEM-1	25/09/2018-C-01	79.9	76.6	24.9	108.9	105.6	0.4	760	755.5	1735	0.94	7.0	14.0
EXC-C-06	29-09-2018	BEM-5	06/09/2018-C-04	79.9	76.2	25.0	109.1	106.6	0.4	748	743.4	1714	0.93	7.0	14.0
EXC-C-08	16-01-2019	BEM-1	07/01/2019-C-01	79.4	76.6	24.9	104.1	99.6	0.4	755	741.8	1807	0.98	8.4	16.7
EXC-C-09	16-01-2019	BEM-2	07/01/2019-C-02	79.3	76.6	25.0	102.7	100.8	0.4	752	740.2	1783	0.97	7.0	14.0
EXC-C-10	16-01-2019	BEM-3	07/01/2019-C-03	79.4	76.6	25.0	105.8	101.4	0.4	755	742.4	1778	0.97	8.4	16.7
EXC-C-11	16-01-2019	BEM-4	07/01/2019-C-04	79.4	76.6	24.8	104.9	102.8	0.4	759	749.6	1769	0.96	7.0	14.0
EXC-F-11	12-01-2019	BEM-1	07/01/2019-F-02	79.8	76.6	24.9	104.4	101.7	0.4	748	742.8	1772	0.96	9.6	19.1
EXC-F-12	14-01-2019	BEM-2	07/01/2019-F-01	80.0	76.6	25.0	105.9	101.8	0.4	762	752.4	1796	0.98	8.4	16.7
EXC-F-13	14-01-2019	BEM-3	07/01/2019-F-03	79.9	76.6	24.9	103.6	101.7	0.4	737	733.0	1750	0.95	8.4	16.7
EXC-F-14	14-01-2019	BEM-4	07/01/2019-F-04	79.5	76.6	25.0	103.8	101.7	0.4	750	732.9	1749	0.95	8.4	16.7

Table 6.5: Pre-firing measurements for steady regression experiment.

Test ID	Firing Date	Propellant		Environment		Motor Weight				Nozzle		Burn Characteristics			
		Ign.	Temp.	Temp.	Cond.	Loaded Weight	Burnout Weight	Inhib. Residue	Prop. Residue	Throat	Exit	P_{max}	F_{max}	t_b	t_{id}
			[°C]	[°C]		[g]	[g]	[g]	[g]	[mm]	[mm]	[MPa]	[N]	[s]	[s]
EXC-C-01	09-09-2018	(1)	18.9	18.9	dry	2418	1694	55	17	7.9	15.2	3.3	255	4.7	4.0
EXC-C-02	09-09-2018	(1)	19.6	19.6	dry	2425	1700	52	26	6.6	13.3	5.6	295	4.1	1.9
EXC-C-04	09-09-2018	(1)	22.1	22.1	dry	2415	1705	53	24	6.7	13.2	7.2	454	3.8	3.8
EXC-C-05	27-09-2018	(2)	25.0	25	dry	2424	1695	59	14	6.7	13.2	8.2	NA	3.6	1.6
EXC-C-06	29-09-2018	(2)	4.0(C)	25	dry	2420	1710	57	19	6.7	20.9	6.9	436	3.7	2.1
EXC-C-08	16-01-2019	(3)	6.5	6.5	dry	2405	1689	52	17	7.9	17.2	3.7	312	4.7	1.5
EXC-C-09	16-01-2019	(3)	6.2	6.2	dry	2408	1680	43	30	6.7	13.7	6.3	381	3.9	1.8
EXC-C-10	16-01-2019	(3)	5.9	5.9	wet	2400	1720	54	14	7.9	17.2	3.6	289	4.7	2.9
EXC-C-11	16-01-2019	(3)	6.0	6.0	wet	2430	1712	40	30	6.7	13.7	6.1	382	3.9	1.6
EXC-F-11	12-01-2019	(3)	8.5	8.5	wet	2404	1694	60	12	8.9	18.3	2.9	NA	4.2	2.3
EXC-F-12	14-01-2019	(3)	7.5	7.5	wet	2440	1721	50	17	7.8	15.1	3.9	308	4.4	2.2
EXC-F-13	14-01-2019	(3)	6.7	6.7	shwr	2414	1680	68	12	7.8	15.8	3.7	303	4.2	2.7
EXC-F-14	14-01-2019	(3)	5.4	5.4	shwr	2421	1720	59	13	7.7	15.8	4.1	330	4.1	1.2

Table 6.6: Post-firing measurements for steady regression experiment.

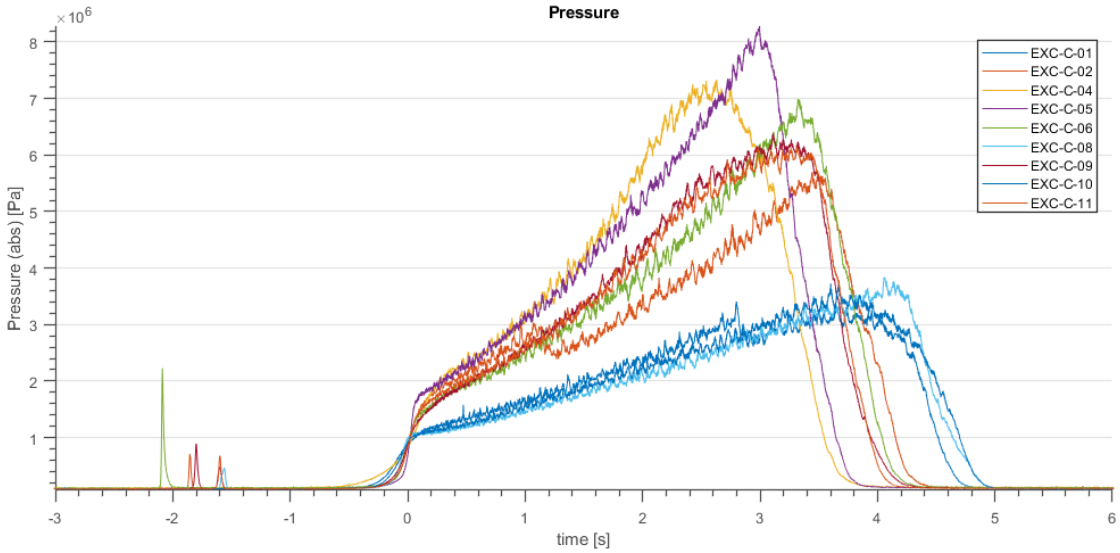

(a) Measured chamber pressure for coarse KNSB propellant.

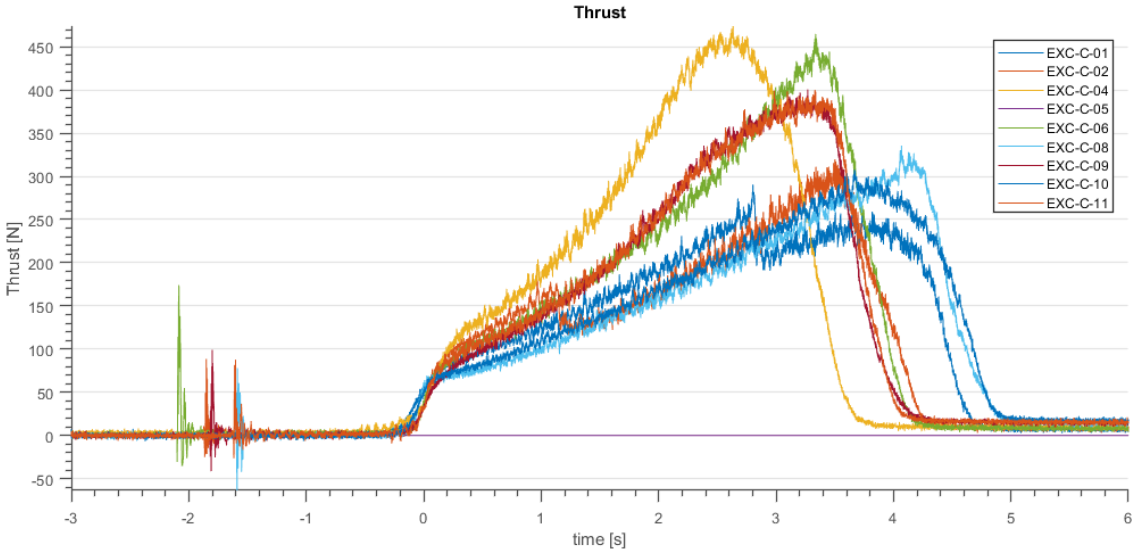

(b) Measured Thrust for coarse KNSB propellant.

Figure 6.12: Thust and pressure traces for coarse KNSB propellant tests.

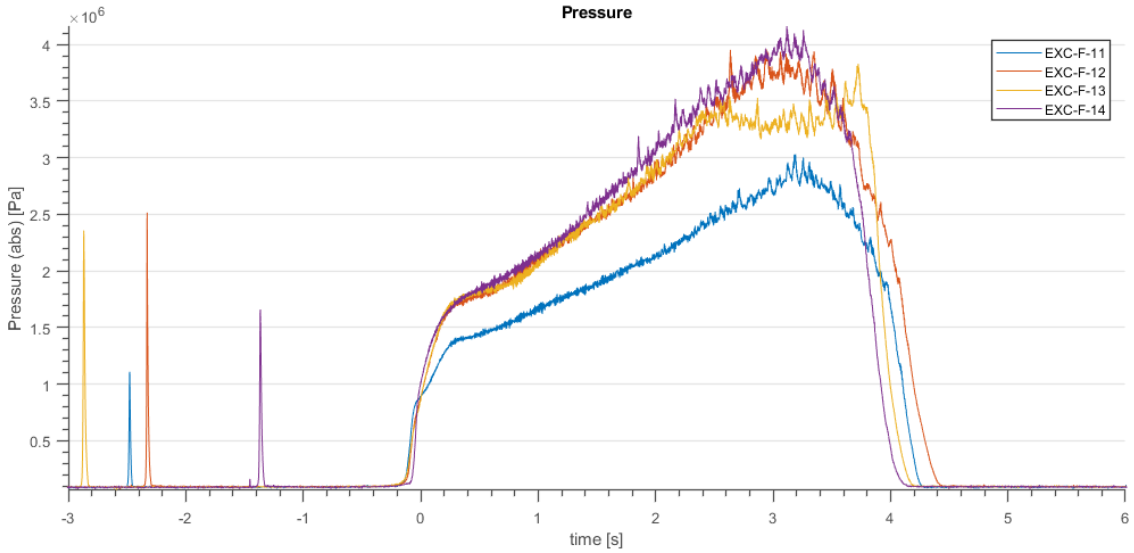

(a) Measured chamber pressure for fine KNSB propellant.

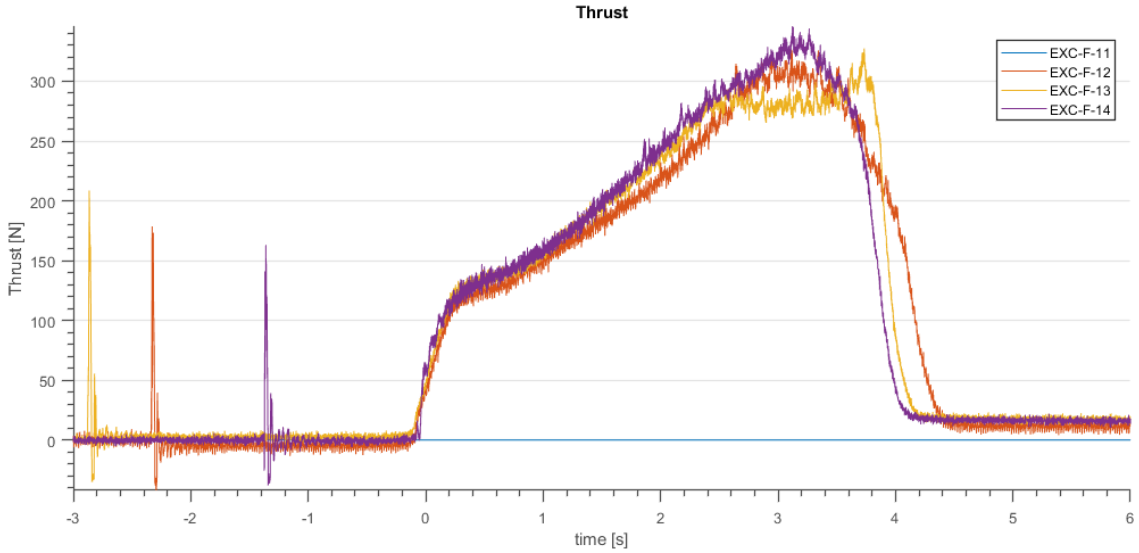

(b) Measured thrust for fine KNSB propellant.

Figure 6.13: Thust and pressure traces for fine KNSB propellant tests.

9. *Ignition Delay,* had large variations. With igniter configuration (1) this was between 1.6-4.0 [s] and was reduced to 1.2-2.9 [s] with the improved compositions.

10. *Nozzle Residues,* were consistently found on all motors (see figure 6.8b) and reduced the effective throat and exit area during the test by as much as 15%. Slag showed an even buildup.

11. *Propellant deposits,* were found in all motors and was typically found as a solid foam at the base of the combustion chamber. The total amount was less in fine motors (average 13.5 [g]) than course (average 21.2 [g]) compositions.

6.7. Analysis - Motor Performance

Determination of the three motor performance indicators c^* [m/s], C_f [-] and I_{sp} [s] is done for all motors where sufficient data was available. Three different conditions are compared in the analysis of results.

- *Ideal Isentropic Performance,* denoted with c^*_{is} [m/s], $C_{f,is}$ [-] and $I_{sp,is}$ [s], calculated using equations 2.2, 2.3 and 2.1 from section 2.1 and 6.3 respectively.
- *Delivered Performance* denoted with c^*_x [m/s], $C_{f,x}$ [-] and $I_{sp,x}$ [s], calculated using equations 6.3, 6.2 with a constant (initial throat).
- *Delivered Performance* denoted with c^*_x [m/s], $C_{f,x}$ [-] and $I_{sp,x}$ [s], calculated using equations 6.3, 6.2 with a linearly varying throat from $At(t=0)$ to $At(t=e)$ over the duration of the test.

The $\bar{I_{sp}}$ and $\bar{c^*_x}$ results for the BEM tests are provided in table 6.9. The mean combustion efficiency is $\eta_b = 0.8769$ [-] with $\sigma = 0.020$ for the course KNSB propellant and $\eta_b = 0.9051$ [-] with $\sigma = 0.013$ for the fine KNSB propellant. This means that a significant relation between KNO_3 PSD was not measured in this experiment. In addition no clear correlation was found between chamber pressure and combustion quality.
With $A_e/A_t = 4$ is is found that the pressure ratio is equal to $P_e/P_c \approx 0.048$. For coarse KNSB $C^0_{f,x}$ is shown in 6.14b. Fine KNSB is shown in figure 6.14a. The deviations upward at the end of the curves coincide at the moment of web burnout and are thus not representative for thrust generated during the nominal burn. A cutoff is introduced based on the Summerfield criteria ($P_e/P_a > 0.45$) [24] and the mean performance $\eta_{F,is}$ compared to the isentropic nozzle coefficients.

The various choices are briefly evaluated:

- *Choice of* ΔM. The averaged mass difference ($\Delta M_1 - \Delta M_2$ for the various tests and the standard deviation of the difference between the two definitions are shown in table 6.7 in the last column the error is shown as percentage of the nominal $M = 758[g]$ propellant grain. Values for the tests respectively are taken from 6.6.

  What is clear from the results is that on average ΔM_1 is 8.5 [g] (coarse) to 11 [g] (fine) larger than the estimate,ΔM_{2+res} which could be explained by a conservative selection between non consumed cardboard and K_2CO_3, or by deposits on the nozzle that were not taken into account. For c^* [m/s] the clean grain weight M_1 will be used as it is more representative for the propellant performance, in addition it avoids most uncertainties (refer to the larger standard deviation) that come with correcting for propellant residues. The effect of this choice results in a factor $1/1.01$ lower estimate for $\bar{c^*_x}$ and is thus limited.

	N [-]	Mean $\Delta M_1 - \Delta M_2$ [g]	Mean $\Delta M_1 - \Delta M_{2+res}$ [g]	[%]	σ_Δ [g]	$\sigma_{\Delta+d}$ [g]
Coarse	N=8	29.7	8.5	1.1	7.5	10.7
Fine	N=4	24.5	11.0	1.4	7.8	11.0

Table 6.7: The difference between cast propellant mass and the fired weight difference.

- *Shifting expansion ratio.* In table 6.8 the variations is shown with typical measured numbers for the nominal nozzles ($R_t = 7.0$ and 8.37 [mm]). As the effect on exit pressure is relatively small, the variation of typically ± 6 [%] leads to $P_e/P_a = \pm 1 \cdot 10^{-3}$ [-] this change is disregarded. The choice for a constant area ratio of 4 [-] appears to be reasonable.
- *Choice for* A_t *[m^2]* As was observed during the tests propellant deposits accumulate on the nozzle. For the smallest nozzle (7⌀ [mm]) this results in a total throat area decrease of approximately 15[%] during the test which agrees with earlier experiences. The average deviation of the measured values to the mean at begin and end is 7.3 [%]. The largest deviation between time based linear assumption and mass flow based approximations (refer to appendix D however is $8.41 \cdot 10^{-7}$ [m^2] or 2.2 [%] (from the time based average nozzle size),with an average deviation of only 1.4 [%]. The effect of this choice is further discussed in the next section.

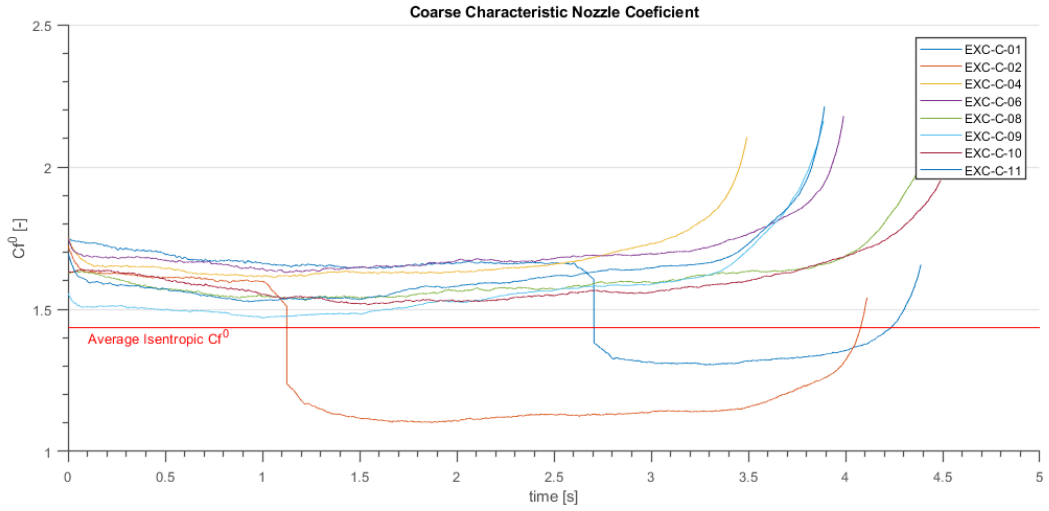

(a) Measured characteristic thrust coefficients for coarse KNSB propellant. Clearly visible are the two igniter leads blown out in tests EXC-C-01 and EXC-C-02.

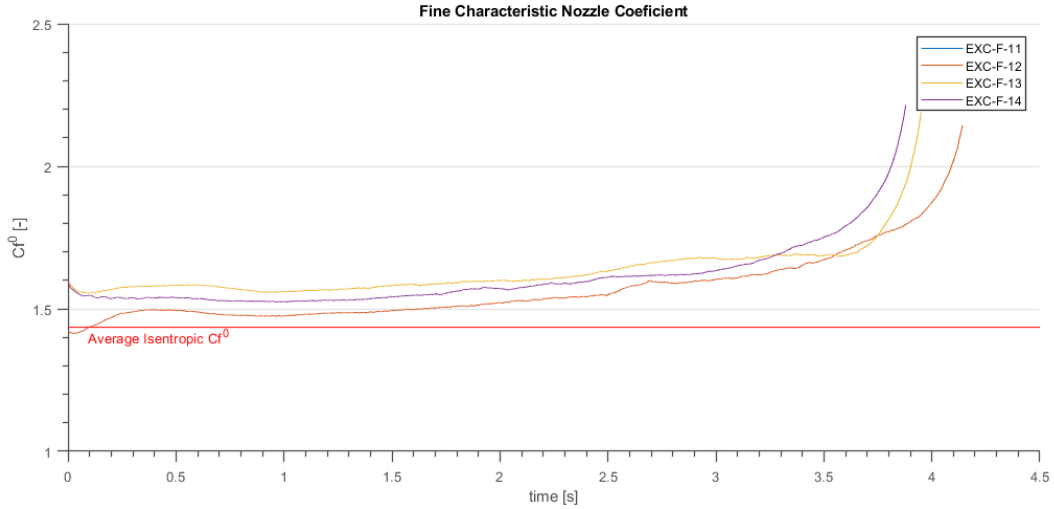

(b) Measured characteristic thrust coefficients for fine KNSB propellant.

Figure 6.14: Characteristic thrust coefficient for BEM tests.

nozzle	R_t [mm]	R_t [mm]	A_e/A_t [-]	P_e/P_c [-]
ignition	7.00	14.00	4.00	0.0492
burnout	6.70	13.50	4.06	0.0483
ignition	8.37	16.73	4.00	0.0492
burnout	7.93	15.75	3.94	0.0503

Table 6.8: Shift in area ratio for both nominal nozzles $R_t = 7.0$ and 8.37 [mm] due to typical material deposits.

ID		Measurements			$\bar{I_{sp}}$		Contant Throat					Linear Throat				
no	test-id	$\bar{P_c}$ [MPa]	I_{tot} [Ns]	ΔM_1 [kg]	$\bar{I_{sp,x}}$ [s]	$\bar{I_{sp,is}}$ [s]	$\bar{c_x^*}$ [m/s]	$\bar{c_{is}^*}$ [m/s]	η_b [-]	$\bar{C_{f,x}^0}$ [-]	$\eta_{f,is}$ [-]	$\bar{c_x^*}$ [m/s]	$\bar{c_{is}^*}$ [m/s]	η_b [-]	$\bar{C_{f,x}^0}$ [-]	$\eta_{f,is}$ [-]
1	EXC-C-01	2.18	793(a)	0.757	107(a)	127	814	908	0.896	1.47	1.024	767	908	0.844	1.55 (a)	1.079
2	EXC-C-02	3.2	715	0.755	97(a)	134	831	910	0.914	1.22	0.85	787	910	0.865	1.28(a)	0.892
3	EXC-C-04	3.98	941	0.752	128	133	790	910	0.868	1.59	1.111	752	910	0.826	1.67	1.164
4	EXC-C-05	4.19	NA(b)	0.755	NA(b)	136	817	910	0.898	NA(b)	NA(b)	777	910	0.854	NA(b)	NA(b)
5	EXC-C-06	3.57	928	0.743	127	134	785	909	0.863	1.62	1.131	747	909	0.821	1.7	1.183
6	EXC-C-08	2.13	794	0.742	109	126	780	908	0.859	1.53	1.064	734	908	0.809	1.61	1.124
7	EXC-C-09	3.6	863	0.74	119	133	788	909	0.866	1.5	1.043	750	909	0.825	1.57	1.092
8	EXC-C-10	2.18	810	0.742	111	127	802	908	0.883	1.52	1.056	755	908	0.832	1.6	1.116
9	EXC-C-11	3.61	877	0.75	119	135	767	910	0.844	1.55	1.078	730	910	0.803	1.62	1.129
10	EXC-F-11	1.98	NA(b)	0.743	NA(b)	127	829	908	0.913	NA(b)	NA(b)	769	908	0.847	NA(b)	NA(b)
11	EXC-F-12	2.57	853	0.752	116	131	829	909	0.912	1.46	1.018	770	909	0.847	1.57	1.095
12	EXC-F-13	2.55	835	0.733	116	131	805	909	0.886	1.52	1.057	746	909	0.821	1.63	1.136
13	EXC-F-14	2.68	842	0.733	117	132	827	909	0.909	1.48	1.03	756	909	0.832	1.61	1.121

notes:

(a) Partially lower thrust due to igniter lead blowout at motor head end.

(b) No thrust data due to load cell failure.

Table 6.9: Test matrix with the total and averaged specific impulse ($I_{tot}, \bar{I_{sp}}$), test average characteristic velocity and combustion quality, $\bar{c_x^*}$, η_b and characteristic thrust coefficient.

6.8. Analysis - Determination of Steady Regression Rate

The most important part of this BEM experiment is to obtain the KNSB burnrate at different propellant temperatures and pressures and comparing those results to the experiment results from [6] and [63] who have done strand burner experiments up to 10 [MPa] for both coarse and fine KNSB respectively.

6.8.1. Steady Regression Rate

Two examples of regression rates and the function fits $r(P_c)$ are provided in 6.15. Both curves provide smooth function fits over the applied pressure ranges justifying a direct fit of the propellant burnrate. As can be seen in EXC-C-02 it is clear that the addition of additional hole at the motor head end due to the igniter blow out is well corrected by a step-wise correction of the klemmung. The burnrate results are shown in table 6.10 with the curves plotted in figure 6.16 for coarse and 6.16 for the fine compositions.

The average burnrate for coarse propellant is best described by equation 6.20 with a standard deviation of $\sigma r = 0.40$ [mm/s]. In this equation P_{ref} is equal to 1 [MPa] and T_{ref} is equal to 273.15 [K]. It is prudent at this point however to define the uncertainty slightly different; all measured regression rates fall between $+1.6\sigma_r$ and $-0.8\sigma_r$ also shown in figure 6.17 as such a margin results in more practical design rules.

$$r_c(T_f, P_c) = (1.55 \cdot 10^{-5}(T_f - T_{ref}) + 4.47 \cdot 10^{-3})\left(\frac{P_c}{P_{ref}}\right)^{0.305} \qquad 1.0\text{[MPa]} < P_c < 8.0\text{ [MPa]} \tag{6.20}$$

For coarse propellant the spread in propellant burnrate exponents is larger than the equivalent spread in regression rate constants as shown by the intercept of the various curves around 1.5 [MPa] (close to the $P_c/P_{ref} = 1$). The variations in burnrate exponents is largest with values between 0.23 (EXC-C-08) and 0.28 (EXC-C-09) of motors fired on the same day. EXC-C-05 and EXC-C-06 on the other hand show excellent reproducability with 0.338 and 0.335 as burnrate exponents respectively.

As can be seen in figure 6.16b the fine propellant the regression behaviour appears more complex and is not described well with a single burnrate exponent. For the section between 2.0 [MPa] to 4.0 [MPa] The average burnrate at a reference temperature of 7.0 [° C] is given with equation 6.21. Standard deviation is $\sigma_r = 0.14$ [mm/s] with all measured regression rates within $\pm 2\sigma_r$ of this margin.

$$r_f(7.0[^\circ\text{C}], P_c) = 6.23 \cdot 10^{-3}\left(\frac{P_c}{P_{ref}}\right)^{0.115} \qquad 2.0\text{[MPa]} < P_c < 4.0\text{ [MPa]} \tag{6.21}$$

6.8.2. Temperature Dependence

As only the coarse propellant was fired over a sufficiently large temperature range to make a meaningful analysis of the temperature dependence possible, only coarse propellant is investigated for its temperature dependence. The determined dependency will then subsequently be used to correct regression rates for the fine propellant, allowing direct comparison with the data from both [6] and [63]. Results for coarse are shown in figure 6.17c. The burn rates corrected for temperature are shown in figure 6.17, indicating a smaller spread of the measured tests. Especially a comparison between EXC-C-05 and the conditioned EXC-C-06 show that the curves effectively overlap.

The temperature dependence of the propellant can then also be described as the more standardised π_K and σ_P coefficients. Typical industry values for solid propellants are between $0.001 > \pi_K > 0.009$ [19] showing a very reasonable comparison to literature values.

$$\sigma_p = \frac{1}{a}\frac{da}{dT_f} = \frac{1.55 \cdot 10^{-5}}{0.00470} = 0.0033\text{ [-]} \tag{6.22}$$

$$\pi_K = \frac{1}{1-n}\sigma_p = \frac{1}{1-0.305}0.0033 = 0.0048\text{ [-]} \tag{6.23}$$

ID		Test Conditions				Speed		Fit	
no	test-id	PSD	T_f	P_{min}	P_{max}	r_{min}	r_{max}	a	n
			[° C]	[MPa]	[MPa]	[mm/s]	[mm/s]	[mm/s]	[-]
1	EXC-C-01	Coarse	18.9	1	3.13	4.737	6.701	4.879	0.259
2	EXC-C-02	Coarse	19.6	1.57	5.5	5.237	7.977	4.725	0.302
3	EXC-C-04	Coarse	22.1	1.95	7.1	6.296	9.871	(4.729)(a)	(0.379)(a)
4	EXC-C-05	Coarse	25.0	1.74	7.97	5.882	9.764	4.799	0.338
5	EXC-C-06	Coarse	16.0	1.51	6.68	5.247	8.606	4.49	0.335
6	EXC-C-08	Coarse	6.5	1.00	3.08	4.887	6.233	4.769	0.23
7	EXC-C-09	Coarse	6.2	1.38	5.56	4.737	8.196	4.255	0.388
8	EXC-C-10	Coarse	5.9	1.00	3.24	4.879	6.316	4.747	0.242
9	EXC-C-11	Coarse	6.0	1.50	5.3	5.234	8.036	4.494	0.347
10	EXC-F-11	Fine	8.5	2.00(b)	2.87	6.569	6.842	6.125	0.103
11	EXC-F-12	Fine	7.5	2.00(b	3.78	6.694	7.246	6.014	0.128
12	EXC-F-13	Fine	6.7	2.00(b	3.38	6.824	7.379	6.258	0.126
13	EXC-F-14	Fine	5.4	2.00(b	3.97	7.006	7.560	6.504	0.105

notes:

(a) Reference only

(b) Fitting Limit

Table 6.10: Burnrate results for coarse and fine KNSB propellant motors.

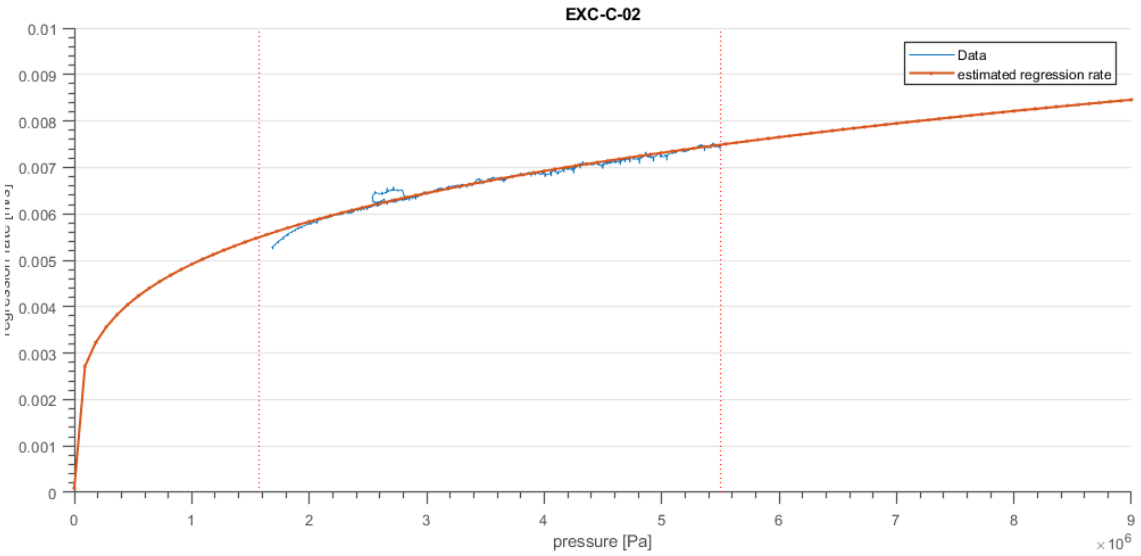

(a) Estimated instantaneous propellant burnrate and burnlaw fit for EXC-C-02, with correction for igniter leads blowout.

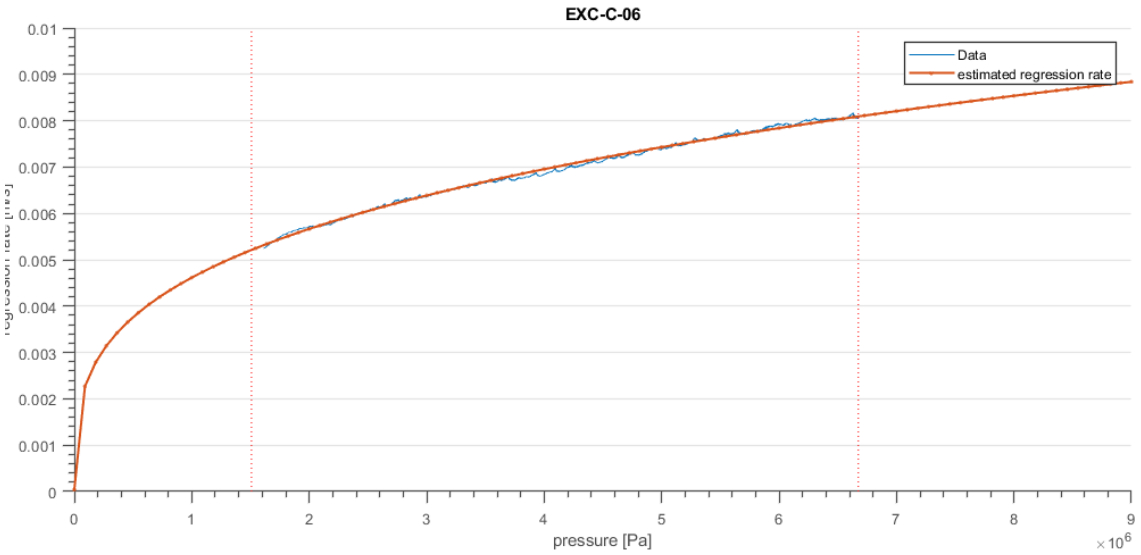

(b) Estimated instantaneous propellant burnrate and burnlaw fit for EXC-C-06.

Figure 6.15: Fit results for EXC-C-02, with klemmung correction for igniter blowout, and EXC-C-06.

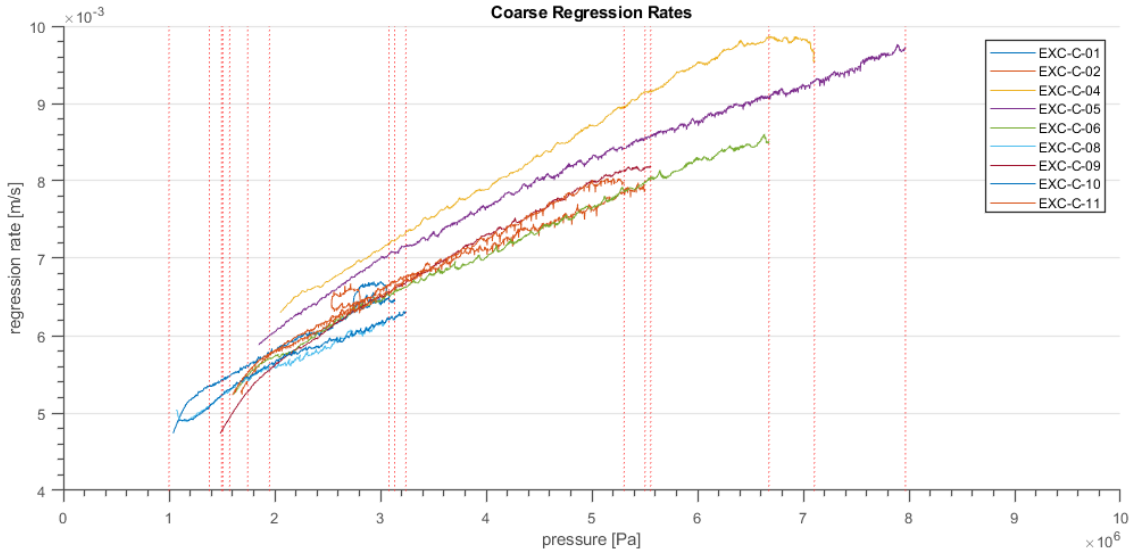

(a) Coarse propellant burn rates estimated with the mass balance method.

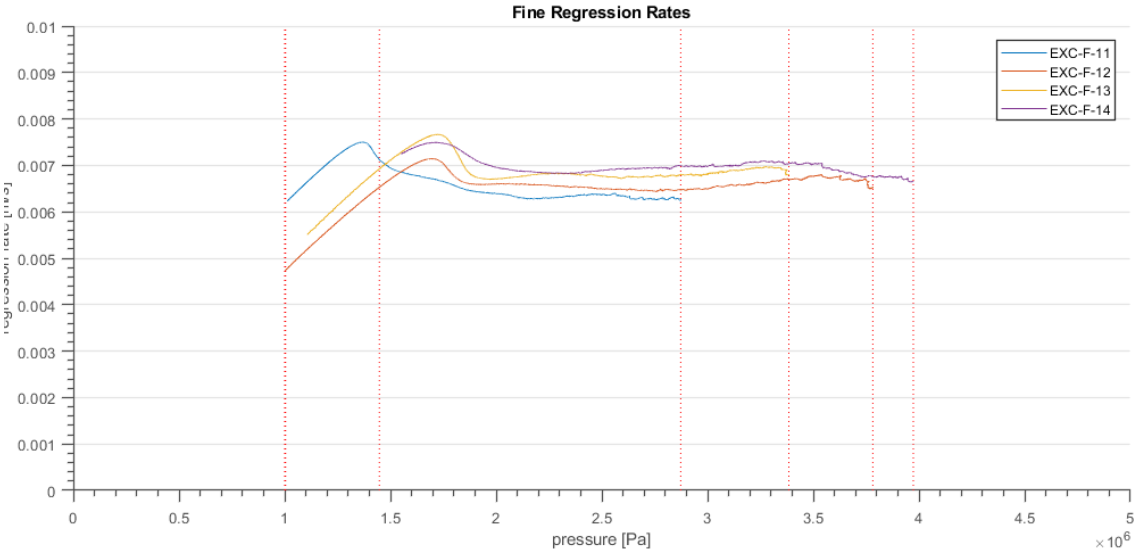

(b) Fine propellant burn rates estimated with the mass balance method.

Figure 6.16: Regression rate results for KNSB propellant.

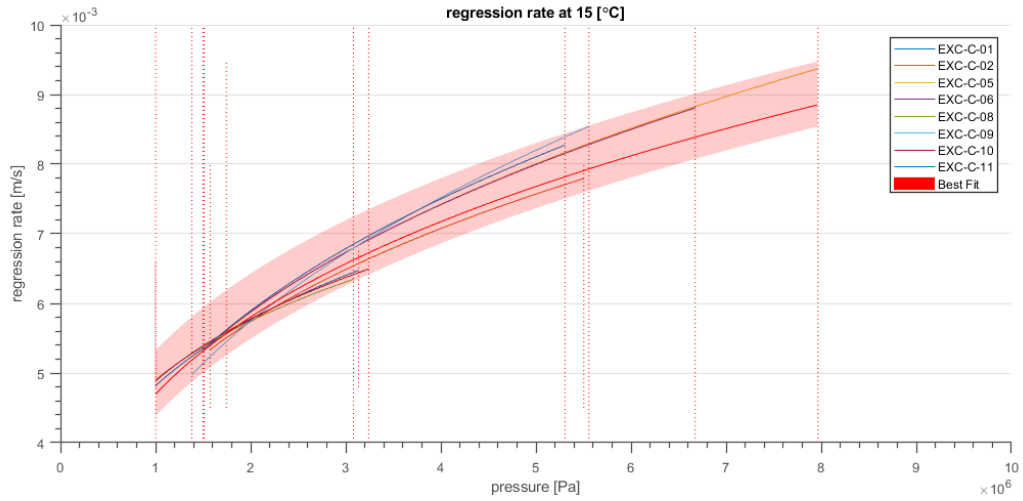

(a) Coarse propellant burn rates corrected for temperature including the regression rate fit and uncertainty.

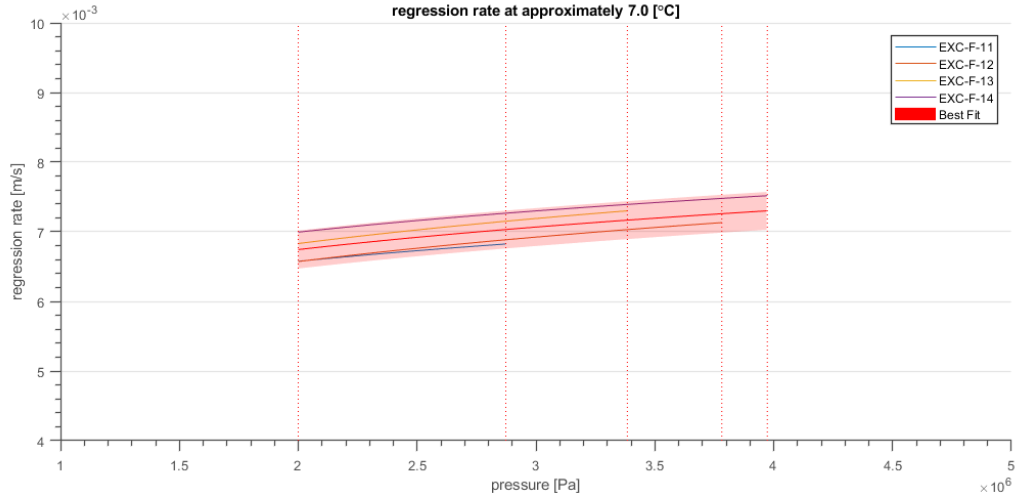

(b) Fine propellant burn rates at an average firing temperature of 7 [° C] with the regression rate fit and uncertainty.

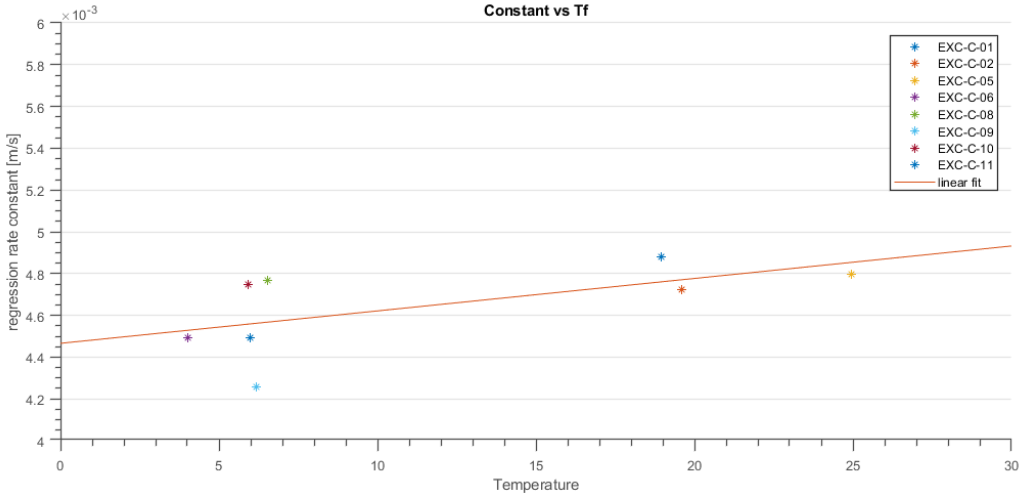

(c) Coarse burnrate constant fitted as function of propellant firing temperature. $a = 1.55 \cdot 10^{-5}(T_f - 273.15) + 4.47 \cdot 10^{-3}$ [m/s]

Figure 6.17: Regression rate temperature results for the BEM experiments.

6.9. Discussion

A total of 25 ballistic evaluation motors were fired which resulted in 13 successful tests. These tests were used to determine the fine and coarse propellant performance and obtain estimates for the propellant regression rates. In addition the developed BEM system, including improved propellant composition were put to the test increasing system maturity.

The results and observations are discussed below, first the improved propellant composition and BEM system are discussed including a discussion of the lessons learned and recommended improvements. Afterwards in section 6.9.2 and in section 6.9.3 the performance and regression rate results are discussed respectively.

6.9.1. BEM for Evaluating Propellant Ballistic Properties

Propellant developed with the improved KNSB propellant was tested using the BEM which was developed for this thesis. As the development of the BEM and the measurement method were developed largely at the same time several development issues arose such as the ignition problems (discussed in the previous chapter) resulting in several configuration changes. With those lessons learned the repeatability, expressed in terms of peak pressure and impulse delivered was found to agree quite well.

Propellant grains produced for this experiment were all of excellent quality compared to the typical DARE propellant used at the start of this thesis. Coarse propellant had a 95% density ratio while the fine composition, even after reduction, had a density ratio of 96%. Of the two grains fired with densities below 95 % one grain showed considerable deviations from the expected behaviour. Although this could be connected also to an error in assembly, this does confirm that 95% is a good threshold for the quality check of propellants. Surfaces for coarse propellant was perfect (defects $< 1\%$ of $A_b(0)$) while fine propellant grains had only minor surface deficiencies which were deemed acceptable. These surface defects were covered by the inhibitor disks glued to the forward and aft propellant surfaces and were deemed non critical. At least on one motor, EXC-F-13, these defects appear to have caused at substantial deviation from the pressures measured by the other motors.

Although this is a considerable improvement of the propellant quality, variation were still measured and most apparent in the large spread of burnrate constants. This could points to potential deficiencies in the propellant formulation, BEM assembly or test error. Based on a comparison motors fired on the same day appear to have a higher repeatability (compare EXC-C-05 and EXC-C-06), the two pairs of motors fired for the TRP Practical (EXC-C-08 to EXC-C-11) and the fine motors (EXC-F-11 to EXC-F-14). This suggests that batch to batch propellant variations and BEM configuration changes such as the change in igniter /ignition primer are the most likely cause of the variations. If the tests up to this point are considered the development period, it is recommended to come to a formalise tests for the BEM motor with a manual that covers the following additional points:

- *Preparation of propellant grains,* including the quality check, but also adhesive bonding of both inhibitor disks and the composition and application of the ignition primer coating. As the amount of coating cannot be accurately measured this remains a point of discussion until a better process is developed.
- *Preparation of igniters,* so that igniter lead blow outs will not occur again (like in the work of [18] and consistent results are obtained between tests.
- *Assembly of the motors,* to assure that motors are build identical between tests and no such guide exists.

Field procedures are very well described and have been sufficiently iterated such that is unlikely that this needs significant improvement. Lastly it was shown that thermally conditioning motors with ice is a feasible way of determining the propellant temperature dependence lacking more expensive industrial equipment. It was demonstrated that a BEM motor could be fired within the time limit without compromising safety or test goals. As the test campaign extended into January the need for thermal conditioning became less, however it does demonstrate the possibility to at least investigate propellant performance for environmental conditions such as might be realistically encountered during a winter

launch campaign.

As extensively discussed the ignition of the fine propellant grains was especially problematic, however even during the last test campaign considerable ignition variation was observed between motors. This could for instance be seen in the variations in ignition delay and differences in pressure spikes at the start of the test. Over the course of motor development the typical ignition delay was reduced from initially 4 [s] (EXC-C-01) to 1.5 [s] (EXC-C-08) through the use of more energetic compositions, however the application of ignition primer proved very difficult to control and prone to flaking. It can thus be concluded that, while this igniter/primer combination might be excellent for launching rockets, it is insufficient for ballistics research where a high repeatability is required. With most commercially used compositions such as $BKNO_3$ [9] out of reach, it is recommended to first investigate ignition primers further by improving on the results obtained in chapter 5, afterwards a redesign of the current igniter would be a good point of improvement for the BEM.

6.9.2. Propellant Performance

BEM motor performance, measured in terms of the characteristic velocity c^* [m/s], thrust coefficient C_f [-] and specific impulse I_{sp} [s] was determined for both coarse and fine propellant. The combustion quality $\eta_{b,c} = 0.8769$ and $\eta_{b,f} = 0.9051$ for fine and coarse KNSB respectively, which is significantly lower than the efficiency reported by other authors ($\eta_{b.f} = 0.95 - 0.99$) [63]. This performance gap is compensated by the very high thrust coefficient $C^0_{f,c} = 1.55$ (coarse) and $C^0_{f,f} = 1.487$ (fine) which is on average $\eta_{f,c} = 1.083$ [-] and $\eta_{f,f} = 1.037$ [-] higher than the isentropic predictions resulting in an overall I_{sp} [s] of up to 128 [s], close to the maximum theoretical I_{sp} of 136 [s] with a progressive burning motor.

When assuming a linearly decreasing throat the effect is even larger. The combustion quality decreases to $\eta_{b,c} = 0.831$ and $\eta_{b,f} = 0.837$ respectively while the characteristic thrust coefficient increases to $C^0_{f,c} = 1.628$ [-] and $C^0_{f,f} = 1.603$ for fine and coarse respectively, which equals a nozzle efficiency of $\eta_{F,c} = 1.133$ and $\eta_{F,c} = 1.118$, well above the theoretical maximum performance.

A clear conclusion is that no increase in combustion quality was measured between coarse and fine KNSB compositions. This is contrary to observations by [63] who suggests an η_b increase of several percent between fine and coarse propellants. Several reasons could be suggested why no relation was found. A potentially longer residence time for the BEM design, due to the large grain port/ to throat ratio, could lead to efficient combustion for both coarse and fine compositions. Alternatively the surfactant could have negatively affected the combustion temperature of the fine but not the coarse propellant grains, similarly resulting in a reduction of the difference.

The measured I_{sp} does not suffer, being among the highest ever measured in DARE and possibly to increase even more if the flow is ideally expanded at higher chamber pressures. From these numbers it can however be concluded that KNSB propellant performance might not be so limited as was expected. At the very least more research is necessary to confirm these findings. The progressive behaviour of the BEM results in considerable changes in chamber pressure which means the nozzle is not optimised for performance. In addition the chemical composition of the chamber changes with pressure. The change in $\bar{c^*}$ is approximately 1-2 % between 2-7.5 [MPa] [50], however in practice the changes also in η_b could be larger than currently expected. A different reason might be found in condensed phase mass fractions in the exhaust, which make up to 40 % of the exhaust products, resulting in higher effective mass flow through the nozzle. A thorough investigation of the condensed phase flow phenomena is an important next step if KNSB propellant performance is further investigated.

To verify the findings from this thesis in terms of KNSB performance it is recommended to test with the BEM using neutral burning grains. This can be achieved by omitting the inhibitor disks glued to the ends of the grains. Alternatively a star shaped mandrel might be developed for the motor, similarly resulting in near neutral burning behaviour but likely with less challenging start up behaviour. Such results would offer more insight into the respective contributions of the mentioned uncertainties, in addition it might confirm I_{sp} performance well above 130 [s], providing an example of the true potential of KNSB propellant.

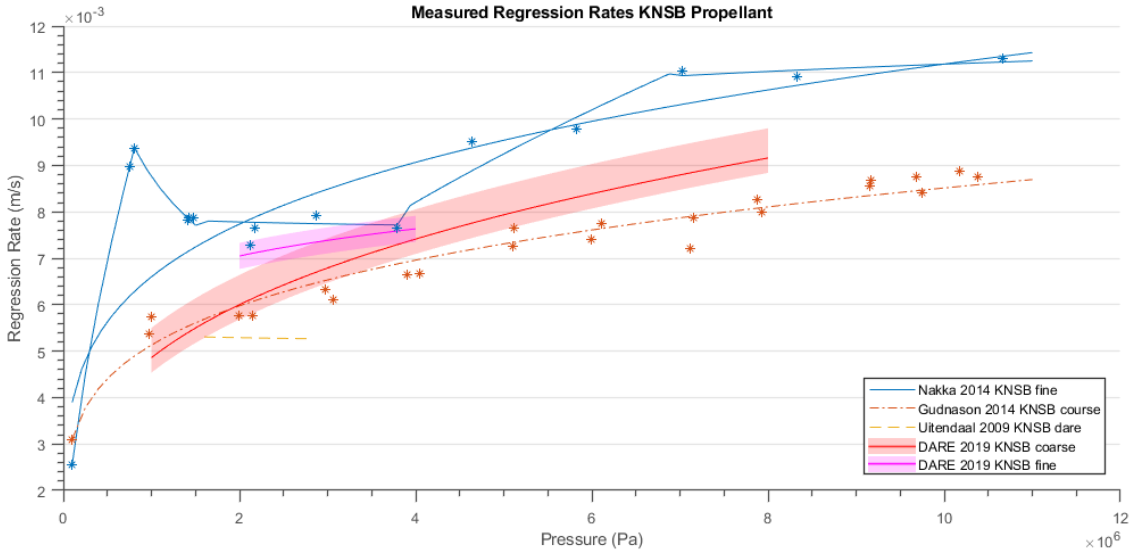

Figure 6.18: Comparison between regression rates from this study and literature values. Regression rates are corrected for propellant temperature (20-25 [°C]) as reported in literature.

6.9.3. Propellant Burnrate Behaviour

The propellant burnrate was measured for both coarse and fine compositions. The result, corrected to the firing temperature reported by [63] and [6] is shown in figure 6.18.

From the results it is clear that, taking into account a temperature correction, the measured burn rates agree reasonably well with the values found in literature. For both coarse and fine propellants the burnrate exponent is smaller (0.305 vs 0.222 [6]) and (0.115 vs -0.013 [63]) while burnrate constants are slightly slower. It is unclear if this is due BEM measurements error, strand burner measurement error or differences in propellant composition. It can however be concluded that compared to [21] a significant improvement is made with respect to the applicable range and pressure dependence of the burnrate.

In literature strand burners are found to be somewhat slower than ballistic evaluation motors due to the difference in thermal environment [19]. The largest uncertainty in the method is to the estimated throat area's during the test. Constant (initial) throat area's were used however the sensitivity analysis already indicated that the difference results in burnrate variations upwards of 15%. This is insufficient to explain the differences in burnrate exponents but the uncertainty is one of the largest encountered for the BEM and warrants further study. Furthermore the method used in this study assumed a constant average value of c^* [m/s] for the calculation of the propellant burnrate which could result in an overestimation of the burnrate exponent. In terms of composition the following variations could explain the observed differences:

- Trace amounts of moisture
- Variations in particle size distributions
- the fine KNSB composition the propellant in this study included a small amount of surfactant which was not present in the composition investigated by [13].

The peak visible in the fine propellant burnrate (between 1-2 [MPa], refer to fig 6.16b) was also present in the work from [63] who reported mesa burning propellant (burnrate with a negative exponent over a short pressure range) with a peak around 1.5 [MPa] and a plateau up to around 4 [MPa]. Although the peak is less pronounced for the fine composition measured in this study.

Scatter in the burnrate constant for coarse KNSB was fairly limited after correction for temperature. The Exponent variation is on the other hand much larger and the largest cause for the variation in propellant burnrate. It was found that reproducability of the BEM tests was considerably better for grains/ motors produced in the same batch. Similar results conclusions can also be drawn for the

measured burn rates. Although this variation is likely not problematic for DARE's day to day activities where slightly larger performance margins are acceptable, it is recommended to still investigate if this variation can be reduced further especially to rule out currently unknown formulation deficiencies.

Besides the configuration changes discussed in the previous section, the observed variations could for instance also be caused by differences in the particle size distributions between batches. When comparing the PSD's for several of the production batches a shift of more than the standard deviation is observed. This could be caused by measurement errors but equally be caused by differences in distributions between bags or even between samples from the top or bottom of a drum. Especially with the now available method for determining the propellant ballistic properties it is recommended to still investigate mixing as a gap in the current propellant formulation.

6.10. Conclusion and Recommendations

In this experiment 25 BEM motors were fired with both coarse and fine KNSB propellants. Significant problems were encountered with motor ignition, especially with the fine composition which led to which resulted in 13 usable data sets (9 for coarse, 4 for fine KNSB).

The BEM motor worked very well meeting all design requirements (see appendix E.2) up to and exceeding the nominal design operating pressure (8.5 [MPa]). An element of the design that did cause significant problems was the sub optimal ignition. Ignition of the fine propellant grains was especially problematic which was the direct motivation for the laser ignition experiment. It must however also be noted that ignition for the other motors was occasionally problematic. This could be seen in the variations in ignition delay and differences in pressure curves for almost identical motors.

In terms or reproducability motors from the same production/ assembly batches showed the highest repeatability. From this it can be concluded that further control of the production and assembly of the BEM are areas where improvements can be made. Although such variations are perhaps less critical for day to day DARE activities it is recommended for scientific study that both the propellant formulation and BEM method are further improved. Area's of improvement for the propellant formulation are ingredient variations, propellant mixing (both of the drums and of the premix). For the BEM system itself the ignition proved to be the most difficult to control. It is recommended to continue research on these characteristics both via laser ignition experiments and BEM firing.

6.10.1. Propellant Performance

BEM motor performance was measured in terms of the characteristic velocity c^* [m/s], thrust coefficient C_f [-] and specific impulse I_{sp} [s]. The values deviated considerably from literature with, on average low characteristic velocities and very high thrust coefficients. Thrust coefficients occasionally exceeded the ideal isentropic predictions suggesting that the current equations are insufficient to describe KNSB performance.

It is recommended that further study is performed on the performance of KNSB propellant as it is currently unknown what theoretical maximum might be achieved. Based on achieved I_{sp} results ($I_{sp,x}/I_{sp,is} = 0.96$, sea level performance upwards of 145 [s] might be possible at high chamber pressures (ideal expansion to sea level conditions at 7 [MPa] $\approx$ 1000 [Psi]. This needs to be studied as it would be a 50% improvement over some motors fired in DARE history.

As the BEM was designed around a progressive burn profile with ideal expansion around 2 [MPa] the system was not optimised for measuring performance. An (approximately) neutral burning grain burning at 6 [MPa] could be easily developed for the BEM allowing a study into motor performance. In addition it would allow validation of the measured propellant regression rates and further confirm the validity of the developed methods.

6.10.2. Propellant Regression Rate

The propellant burnrate was determined for both coarse and fine compositions at varying pressure. In addition a first estimate was obtained for the temperature dependence of the propellant burnrate between 5-25 [°C]. There was still considerable variation between measured burn rates and especially the burnrate exponents, which could ideally be reduced in the future with, as mentioned, improved ignition but also by even more rigorous control of propellant manufacturing and motor assembly.

The coarse propellant burnrate was determined between 1.0 and 8.0 [MPa] with an uncertainty of $\sigma r = 0.4$ [mm/s] while the fine propellant burnrate was determined between 1.0 and 4.0 [MPa] with an uncertainty of 0.14 [mm/s]. The coarse composition agreed quite well with results obtained by [6] at lower pressure but had a burnrate exponent that was considerably higher (0.222 vs 0.305). Similarly the results for the fine composition showed reasonable agreement with the results from [63] although being somewhat slower. Also here the measured burnrate had a higher burnrate exponent (0.115 vs -0.03) over range from 2.0-4.0 [MPa]. These discrepancies could be due to the different measurement

technique, but also be contributed to several assumptions that are still unresolved in the developed method. The most significant is the varying nozzle throat as function of propellant deposits, while the use of a test-average c^* could also contribute to the measurement error. As both result in over prediction of the regression rates during the test this could potentially explain the differences measured.

The fine propellant was tested over a lower temperature range than initially planned. The propellant showed mesa burning behaviour similar to that was predicted by [63]. The lower maximum pressure could in part be explained by the lower firing temperature, but also by the effect of surfactant and residual amounts of moisture that similarly work as burnrate depressants. For future tests at higher ambient temperatures improvements of the measured regression rates are expected and might show a larger portion of the burnrate reported by [63].

The temperature dependence was found to be $\sigma_P = 0.0052$ and $\pi_k = 0.0038$ at a reference temperature of [°C] which is in line with values reported for other propellants. This is further supported by the thermally conditioned test which, when corrected for firing temperature, almost perfectly overlaps with the non conditioned test fired on the same day.

The most important first step is to validate the measured burn rates with neutral burning grains and evaluate if the measured rates agree well with predictions. This might be achieved by modifications to the BEM grains, but could also be achieved with other propulsion developments in DARE. If new evaluation tests are planned it is specifically recommended to produce all grains as one batch and assemble and fire the motors over one day. With the available hardware this would allow tests of 4 ambient grains and 2 conditioned grains. Besides expected improvements in measurement accuracy it could confirm the cause of the observations still observed.

6.10.3. Evaluation of Experiment Goals

The test objectives are the following:

- **PARTIALLY MET***Determination of the steady regression rate for both fine and course KNSB propellant as function of chamber pressure and propellant initial temperature.* Propellant regression rates were determined for both coarse and fine propellant. In addition the temperature dependence of the coarse composition was estimated. The fine composition was tested over a smaller range than planned which could be caused by temperature effects or differences in composition between the propellant used in this thesis, and the propellant used by [63].

  The regression rates still need to be validated in a neutral burning motor to confirm that they can be used for motor development. As such this goal is considered partially met.
- **PARTIALLY MET***Confirmation of the similarity between the propellant from this study and those used by Nakka [63] and Gudnason [6].* Although reasonable agreement was achieved between the determined regression rates, the burnrate exponent was found larger than during tests by [63] and [6]. Validation of the measured values should confirm whether the measurement method needs to be tweaked further or if propellant composition variations caused the difference.
- **MET***Determination of characteristic velocity, thrust coefficient and specific impulse for KNSB propellant.* The propellant performance was measured over the applicable range and was found to be quite reproducible with small variations between tests. These results suggest performance much higher than achieved in DARE is possible but also indicate that isentropic relations are insufficient to describe the performance. This is likely caused by condensed phase flow in the nozzle exhaust.
- **MET***Development and demonstration of an experimental method for determining the propellant steady burnrate.* A method was developed that allows determination of propellant ballistic properties. Recommendations are made to further improve the reproducability of the propellant and BEM system during future tests.
- **MET***Establish, evaluate and suggest improvements for increasing the repeatability of DARE solid rocket motors.* Propellant quality was evaluated during this experiment and propellant quality increased slightly over the coarse of the project. When evaluating the propellant quality it is clear that the 95% density margin provides a suitable criterion. Further formulation improvements study

the effect of mixing as a good candidate for future improvements. In terms of the rocket motors the largest uncertainty is caused by igniter variations, although suitable for rockets, recommendations are made to investigate this area further which could prompt a redesign of the BEM.

7

Conclusion

During this thesis the potassium nitrate-sorbitol propellant was investigated as an alternative, low cost, and safe solid propellant for use in small scale research. It is used extensively in the amateur community but has, in that context, only be investigated by a few enthusiastic amateur researchers without the resources of a professional research lab. DARE is in the unique position that it has access to a considerable amount of tools, measurement equipment and lab space that, although not fully comparable to the resources of a professional dedicated propulsion laboratory, is a considerable improvement in research faculty compared to most part-time rocket designers.

This does not mean that DARE does not have its own challenges that need to be overcome. Several failures in recent years of experimental solid rocket motors show that design of reliable solid rocket motors is a complex undertaking. The inexperience of many team members new to the field of propulsion is both exciting, but also leads to simple mistakes and frequent brain drain. Propulsion research is very much about details, as was also demonstrated by this thesis. The ignition train developed for the BEM motor followed a proven design and wasn't given much thought. Not only has this aspect proven to be one of the hardest problems to solve, but the solution required an approach and additional experiments completely not anticipated during the planning for this thesis.

To provide DARE with an improved propellant formulation the KNSB manufacturing was investigated. In addition a BEM was developed that allows measurement of the propellant ballistic properties. This improves on the default propellant regression rates that were used for SRM design over the past 10 years. The addition of an estimate of the applicable range and measurement uncertainty allows design and manufacture of motors with considerably higher performance than those developed in the past.

As part of the propellant formulation the ingredients were more thoroughly investigated. This resulted in new insight in propellant chemical properties summarised in appendix A), which up to that point had never been sorted out. This resulted in new insight in how KNSB propellant and its ingredients behave and how good quality propellant could be manufactured. Several key solid propulsion concepts were discovered as part of this study that beforehand were never actively considered such as contamination with moisture and the effect of particle size distributions. The improved propellant formulations therefore provides a definitive step up from the KNSB manufacturing method from the past.

7.1. Improved Propellant Quality

This thesis project was set up to provide a step-by-step program to improve the KNSB propellant. The initial focus was in that sense relatively mundane; what steps are necessary to reliably make good quality propellant grains? Even before looking at more complex combustion characteristics or solid rocket motor performance the boundary conditions need to be met. This means suitable control over the manufacturing process of solid propellants and KNSB propellant in particular.

During this thesis propellant density was increased from occasionally below 85% to on average 95% of theoretical. Propellant surface defects have been almost fully eliminated with the improved manufacturing process, developed tooling and quality checks. Where over the last several years the poor propellant quality has led to several large and time consuming test failures, the rejection rate for BEM grains is now well below 1 out of every 10 grains produced. This translates to significant improvements in motor reliability but also significant saving in time and resources.

The conducted experiments focused on several recommended improvements of the manufacturing method which were found in literature and recommendations from other (amateur) researchers. The first experiment focused on several out-gassing strategies. It was found that contamination with moisture was one of the root causes of the low observed propellant densities. As both KNO_3 and Sorbitol are hygroscopic special care needs to be taken to assure contamination is kept minimal. This was completely contrary to expectations as the ingredient sources used in DARE are stored in airtight containers or sealed plastic bags. The hygroscopicity of Sorbitol is most critical as it will take up significant quantities of moisture from the air in relative humidities over 60%. This explains in part why moisture has been such an issue for DARE in contrast to propellant experiments conducted in other drier parts of the world. During the casting experiments it was found that DARE ingredients can have moisture quantities above 1-2% by mass which will result in a 5-10% decrease in propellant density.

Several methods for reducing moisture were investigated; continuous heating, storage with desiccant and application of vacuum. It was determined that simply heating the propellant to the desired temperature for casting, 125 [$\circ$C], was insufficient to effectively reduce the amount of moisture to desirable levels (below 0.25 [%] or better). Almost all moisture could be removed using either the application of vacuum (<10 [mbar]) on the molten propellant premix or by sustained heating. Application of vacuum is the fastest method but requires a suitable vacuum pump and propellant pot. Sustained heating takes approximately twice as long as the application of vacuum but can be the desirable method if a heater with suitable thermostat is available. For DARE a suitable vacuum lid was developed that allows the removal of moisture for up to 6 [kg] of propellant at a time.

Storage with desiccant was tested, but was found to be an ineffective method to remove moisture contamination on the spot. Instead it is recommended to store ingredients with suitable packages of desiccant preventing contamination altogether. Exposure of the propellant ingredients in DARE cannot be ruled out unless the facilities are significantly improved. With proper storage and application of vacuum however KNSB propellant grains can be created with densities in excess of 95%.

The second experiment focused on process control. New casting equipment was designed that would allow for better quality grains with high tolerances and a very low reject rate. This was demonstrated in this thesis. For the BEM propellant grains with a typical length of 105 [mm] the compression could only explain propellant density increase of 0.36-0.8 [%]. This was directly contrary to expectations at the start of the thesis, where compression in the order of 5-10% was considered. The addition of compression does significantly increase propellant surface quality to the point that propellant grains have surface consistencies not unlike plastic. The benefit of preheating of casting moulds was also investigated and it was found that density or quality of the propellant was not significantly improved. It would however be recommended when small propellant grains are manufactured as it can prevent the rapid onset of solidification during the casting process.

It can be concluded that the new, improved manufacturing process works in producing grains that are of excellent quality and that will solve most of DARE's propellant problems. Recommendations are made to improve the formulation further in support of more academic oriented research. The effects of measured propellant variations such as trace amounts of moisture of smaller particle size variations are not currently understood.

7.2. Propellant Ballistic Performance

The subsequent step to improve the propellant quality was the accurate determination of the propellant regression rate. KNSB propellant data was available from the work by *Richard Nakka* [63] and by

Magnus Gudnasson [6] who have both done extensive strand burner testing on KNO_3-sugar propellants including the KNSB composition investigated in this thesis. The steady regression experiment was therefore both an attempt to design a reliable test method for the steady regression rate of KNSB propellants, but also an attempt to validate their findings with measurements in the actual motor environment.

The BEM system was developed together with the necessary measurement tools to determine the propellant regression rates over a large pressure range. Several modifications were made to the BEM system, most notably to the igniter configuration. After several misfires with the fine composition were resolved, a total 13 successful tests were conducted with multiple repetitions of both fine and coarse propellant. It was demonstrated that thermal conditioning is possible for achieving the desired propellant firing temperature. Repeatability between motors was evaluated, stressing the importance of rigorous configuration control of the system, and pointing to future improvements in the DARE propellant formulation.

The misfires encountered with the fine propellant were a large concern over the fall of 2018. An extensive list of solutions was tried in an attempt to get the fine composition to ignite. Ignition of the fine KNSB composition however remained illusive. The large amount of overhead for these BEM tests but also the exhaustion of new BEM igniter concepts forced an approach from a different angle. It proved possible to conduct an ignition experiment with one of the welding lasers at 3ME. This allowed the investigation of propellant ignition directly.

During the experiment 24 samples were fired of which 12 were used to investigate the effect of the added surfactant to the fine composition, In addition 9 tests were done with three different types of ignition primers, to study the difference between coated and uncoated ignition. In conclusion: insight was gained in the flame structure of KNSB propellant with noticeable differences between coarse and fine propellant compositions. It was indeed confirmed that the addition of surfactant, especially at ratios at or above 6 drops, or 0.15 [g] per [100g] propellant adversely affects ignition by inhibiting likely KNO_3 decomposition or mixing of its decomposition products. This was clearly observed in one of the fine KNSB samples that extinguished, even though a significant amount of energy was supplied to the propellant surface. A clear difference between the various ignition primers was not discovered although the KNO_3/Charcoal mixture burned slower which is likely caused by absence of sulphur, which decomposes at relatively lower temperature and works as an ignition catalyst.

The combustion quality $\eta_{b,c} = 0.8769$ and $\eta_{b,f} = 0.9051$ for fine and coarse KNSB respectively, which is significantly lower than the efficiency reported by other authors ($\eta_{b.f} = 0.95 - 0.99$) [63]. This performance gap is compensated by the very high thrust coefficient $C^0_{f,c} = 1.55$ (coarse) and $C^0_{f,f} = 1.487$ (fine) which is on average $\eta_{f,c} = 1.083$ [-] and $\eta_{f,f} = 1.037$ [-] higher than the isentropic predictions resulting in an overall I_{sp} [s] of up to 128 [s], close to the maximum theoretical I_{sp} of 136 [s] with a progressive burning motor. Together c^* and C_f provide a rocket performance only a few seconds shy of the maximum achievable I_{sp}.

The final regression rate was determined for fine and coarse KNSB propellant over the pressure range from 1.0 to 8.0 [MPa] with an uncertainty of $\sigma r = 0.4$ [mm/s] while the fine propellant burnrate was determined between 1.0 and 4.0 [MPa] with an uncertainty of 0.14 [mm/s]. The measured regression rates agreed quite well with the strand-burners results found in literature. Even so, compared to literature performance, the BEM method appears to over-predict the burnrate exponent by a considerable margin compared to the values found in literature. This change could be explained by differences in propellant formulation, but the effect of modelling choices cannot at this point be fully ruled out. The largest effect is likely the deposit of slag during the test constricting the nozzle throat area. Similarly the combustion efficiency could be a function of pressure. The use of an average value could thus lead to the over prediction of the measured burnrate exponents.

To solve these issues it is recommended to validate the regression rates found in this thesis with neutral burning motors. This might be easily achieved by changing the inhibitor configuration of the BEM system that was developed. Alternatively differently shaped mandrels could result in effectively

neutral burning grains, allowing both the investigation of performance at higher pressures and expansion ratios, but also serve as a validation of the BEM method assumptions.

Several additional recommendations need to be made with respect to the measurement of the steady burnrate. With the spread in burn rates still considerable at this time, it is expected that accuracy of the measured burn rates can still be improved. This does mean that configuration management needs to be even stricter than during this study. The large variations in igniter performance is the expected largest contribution, however also the effect of long term storage and mechanical mixing of ingredients is something to strongly.

7.3. A Few Final Words

The propellant investigated in this study is not very good in terms of I_{sp} performance compared to many commercially used propellants. They do however offer the prospecting rocket engineer access to propulsion research that would otherwise require professional equipment and facilities. In DARE solid propulsion has over the years become less of a focus point as hybrid rocket motors offered, on paper, easier access to space. This is related to the fact that most solid rocket propellant research is to a large extend defined by chemical and process engineering. Furthermore casting logistics and safety concerns have hampered to a large part the AP and AN based propellant development. As was also found during this thesis study the lack of fundamental chemical knowledge leads to extensive experiments or precautions that a chemist or lab technician might consider trivial. DARE needs more chemical engineers as this aspect of (solid) rocket propulsion is often overlooked.

Ballistics research is a lot of fun as it involves propellants, rocket motors, lasers and smoke. I would like to make several recommendations to people that consider following up on solid propulsion research. During this thesis already considerable attempts were made to improve process and motor configuration control. It was found that this was still insufficient with a considerable spread in measured burn rates. This could be considered part of the development of the BEM system, and several necessary changes were made to the system over the past months, however using consistent ingredients and performing the characterisation tests such as the determination of the particle size distributions is also a fundamental step in solid propellant formulation. It is thus recommended that for any research that will need even tighter control of the propellant ballistic properties, the constituents are drawn from ingredient lots reserved for the purpose. It should subsequently be reasonably straightforward within DARE's professional network to have such quantities of ingredients mixed professionally. Even at the TU Delft a large amount of measurement equipment is available for free.

Solid propulsion and the KNSB propellant is a workhorse of the DARE society as without it, many of the yearly test flights could not happen. With the results from this thesis it however is clear that much about the propellant is not yet known. It might be possible to fly much higher and faster on a propellant than we currently know. At the same time, it offers a way to develop many essential experimental methods necessary for larger, more advanced, systems. From this it can be concluded that DARE solid propellant still has far to go.

Bibliography

Academic References

[1] AGARD-AR-230. *AGARD-AR-230, Performance of Rocket Motors with Metallized Propellants*. NATO, 1986.

[2] Harry van der Akker and Rob Mudde. *Fysische Transportverschijnselen (3^e druk)*. VSSD, 2008. ISBN 90-407-1204-2.

[3] PL Blinde, FJJ Schrijer, and SJ Powel. Experiments on a hot plume base flow interaction at mach 2. In *8th European Symposium on Aerothermodynamics for Space Vehicles*. TU Delft, 2015.

[4] R.S. Fry, Luigi DeLuca, R Frederick, Guy Gadiot, R Strecker, H.-L Besser, A Whitehouse, J.-C Traineau, D.Ribereau , and J.-P Reynaud. Evaluation of methods for solid propellant burning rate measurement. *Chemical Propulsion Information Agencey Columbia MD*, 7 2002.

[5] R.S. Fry, Luigi DeLuca, R Frederick, Guy Gadiot, R Strecker, H.-L Besser, A Whitehouse, J.-C Traineau, D.Ribereau , and J.-P Reynaud. Solid propellant subscale burning rate analysis methods for u.s. and selected nato facilities. Technical report, NATO Research and Technology Organization (RTO), Advanced Vehicle Technology (AVT), Working Group (WG) 016, 01 2002.

[6] Magnus Mar Gudnason. Characterization of potassium nitrate - sugar alcohol based solid rocket propellants. Master's thesis, DTU Chemistry, 2010. Bachelor Thesis.

[7] Kenneth Kosanke. *Pyrotechnic Chemistry*. Journal of Pyrotechnics Incorporated, 2004.

[8] Kenneth K. Kuo and Martin Summerfield. *Fundamentals of Solid Propellant Combustion*. AIAA, The address, 3 edition, 1984. ISBN 0-915928-84-1.

[9] Francesca Lillo. Srm igniters design and development at avio. In *AIAA Short course Solid Rocket Igniter Technology and Applications*. AVIO, 2006. AIAA Presentation at Solid Rocket Igniter Technology and Applications Short Course.

[10] M. Milos and V. Bozic. Small motor measurement method for determining burning rate of solid rocket propellants. *AIAA 98-3390*, 1998. doi: 10.2514/6.1998-3390.

[11] Olga O. Motsyk. Design of a solid rocket motor for a transonic research vehicle. Master's thesis, Delft University of Technology, 2014.

[12] R.A. Nakka. Solid propellant rocket motor design and testing. Master's thesis, Mechanical Engineering Thesis, Univeristy of Manitoba, 1984.

[13] Richard Nakka. Richard nakka's experimental rocketry web site, 2016. URL `http://www.nakka-rocketry.net/`.

[14] NASA-SP-8075. Solid propellant processing factors in rocket motor design. Technical report, NASA, Lewis Research Center, Cleveland, Ohio 44135, 10 1973.

[15] Martin Olde and Andrei Hutan. Propulsion for a supersonic test vehicle, me46060 engineering optimization final project. Technical report, TU Delft, 2016.

[16] Martin Christiaan Olde. Performance of a potassium nitrate sorbitol rocket motor. Technical Report 1, Delft Univeristy of Technology, Kluyverweg 1, 2629 HS Delft, March 2018. MSc Literature Study.

[17] Martin Christiaan Olde. Performance of potassium nitrate sorbitol solid rocket motors, msc thesis proposal. Technical Report 3, Delft Univeristy of Technology, Kluyverweg 1, 2629 HS Delft, April 2018. Completed for AE4010 Research Methodologies.

[18] Hein Olthof. Design of a solid rocket motor, powered by the newly designed alan-7 propellant. Master's thesis, Delft University of Technology, 2013.

[19] George P. Sutton and Oscar Biblarz. *Rocket Propulsion Elements*. John Wiley & Sons, INC., 4 edition, 2001. ISBN 0-471-32642-9.

[20] George P. Sutton and Oscar Biblarz. *Rocket Propulsion Elements*. John Wiley & Sons, INC., 8 edition, 2010. ISBN 978-0-470-08024-5.

[21] Mark Uitendaal. The stratos rocket: Design, simulation and production of a record breaking rocket. Master's thesis, Delft University of Technology, 2009.

[22] Michael A. Willcox, M. Quin Brewster, K. C. Tang, D. Scott Stewart, and Igor Kuznetsov. Solid rocket motor internal ballistics simulation using three-dimensional grain burnback. *Journal of Propulsion and Power*, pages 575–584, 05 2007. doi: 10.2514/1.22971.

[23] B.T.C. Zandbergen. Some typical solid rocket motors, 2003. Memorandum M-712 (Version 2.0).

[24] B.T.C. Zandbergen. *AE4S01 Thermal Rocket Propulsion Course Reader*. TU Delft, 2.04 edition, 2016.

Engineering References

[25] Wolfram|Alpha: Making the world's knowledge computable, Dec 2018. URL https://www.wolframalpha.com/input/?i=heat+of+fusion+sorbitol. [Online; accessed 12. Dec. 2018].

[26] Sorbitol, Apr 2019. URL https://webbook.nist.gov/cgi/cbook.cgi?ID=C50704&Mask=80#IR-Spec. [Online; accessed 7. Apr. 2019].

[27] Guido Barone, Giuseppe Della Gatta, Daniela Ferro, and Vincenzo Piacente. Enthalpies and entropies of sublimation, vaporization and fusion of nine polyhydric alcohols. *Journal of the Chemical Society, Faraday Transactions*, 86(1):75–79, 1990.

[28] Elliott H. Berger, Rick Neitzel, and Cynthia A. Kladden. Noise navigatortm sound level database, 2016.

[29] Nicoleta Birta, N Doca, Gabriela Vlase, and T Vlase. Kinetic of sorbitol decomposition under non-isothermal conditions. *Journal of Thermal Analysis and Calorimetry*, 92(2):635–638, 2008.

[30] Cirteq Ltd. Cirteq technical manual. Technical report. URL http://www.cirteq.com/data-sheets/. [Online; accessed 9. Apr. 2018].

[31] Micheal Eigen. Blast effect calculation. URL https://www.metabunk.org/attachments/blast-effect-calculation-1-pdf.2578/. [Online; accessed 4. Apr. 2018].

[32] Rolf Hubener. The seeger handbook, a designers handbook. Technical report, Seeger Orbis GmbH, 1984.

[33] ifm electronic gmbh. Pt5402 data sheet. Technical report, Friedrichstraße1, 45128 Essen, 2014. URL https://docs-emea.rs-online.com/webdocs/1336/0900766b813361b1.pdf. Bought via RS Components.

[34] George J Janz. *Molten salts handbook*. Elsevier, 2013.

[35] Akihide Kaizawa, Nobuhiro Maruoka, Atsushi Kawai, Hiroomi Kamano, Tetsuji Jozuka, Takeshi Senda, and Tomohiro Akiyama. Thermophysical and heat transfer properties of phase change material candidate for waste heat transportation system. *Heat and Mass Transfer*, 44(7):763–769, May 2008. ISSN 1432-1181. doi: 10.1007/s00231-007-0311-2. URL https://doi.org/10.1007/s00231-007-0311-2.

[36] Anh S Le and Kathleen Bowe Mulderrig. Sorbitol and mannitol. *FOOD SCIENCE AND TECHNOLOGY-NEW YORK-MARCEL DEKKER-*, pages 317–334, 2001.

[37] David R Lide et al. *CRC handbook of chemistry and physics*. CRC Boca Raton, 2012.

[38] MA Lonappan. Thermal expansion of potassium nitrate. In *Proceedings of the Indian Academy of Sciences-Section A*, volume 41, pages 239–244. Springer, 1955.

[39] Harald Mehling and Luisa F Cabeza. Phase change materials and their basic properties. In *Thermal energy storage for sustainable energy consumption*, pages 257–277. Springer, 2007.

[40] Yuji Nagasaka and A Nagashima. The thermal conductivity of molten nano3 and kno3. *International Journal of Thermophysics*, 12(5):769–781, 1991.

[41] Brentagg Nederland. Brenntag in Nederland - Productcatalogus - Distributeur en Exporteur van Chemicaliën en Grondstoffen, Mar 2019. URL http://www.brenntag.nl. [Online; accessed 25. Mar. 2019].

[42] Ann W Newman, Imre M Vitez, Ronald L Mueller, Chris C Kiesnowski, W Paul Findlay, Chris Rodriguez, Martha Davidovich, and Gary McGeorge. Sorbitol. In *Analytical profiles of drug substances and excipients*, volume 26, pages 459–502. Elsevier, 1999.

[43] NIST. Nist chemistry webbook, nist standard reference database number 69. http://webbook.nist.gov/chemistry/. December 14, 2017.

[44] BRENNTAG N.V. Potassium nitrate pure grade with anti-caking. Technical report, BRENNTAG N.V., 2017. TECHNICAL DATA SHEET.

[45] SS Paulsen. Pressure systems stored-energy threshold risk analysis. Technical report, U.S. Department of Energy, August 2009. URL http://www.chem-eng.utoronto.ca/wp-content/uploads/2015/08/PNNL-18696.pdf. [Online; accessed 4. Apr. 2018].

[46] Pubchem. Sorbitol, Dec 2018. URL https://pubchem.ncbi.nlm.nih.gov/compound/5780#section=Flash-Point. [Online; accessed 13. Dec. 2018].

[47] Michael Steiger, A. Elena Charola, and Katja Sterflinger. *Weathering and Deterioration*, pages 227–316. Springer Berlin Heidelberg, Berlin, Heidelberg, 2011. ISBN 978-3-642-14475-2. doi: 10.1007/978-3-642-14475-2_4. URL https://doi.org/10.1007/978-3-642-14475-2_4.

Software References

[48] Dassault System. Catia v5r21, 2017. URL https://www.3ds.com. Available via TU Delft Software Portal.

[49] Richard Nakka. Srm 2014.xls solid rocket motor performance, 2014. URL https://www.nakka-rocketry.net/softw.html.

[50] Alexander Ponomarenko. Rocket propulsion analysis, rpa v.1.2.9 lite edition, 2017. URL http://www.propulsion-analysis.com/index.htm.

[51] The mathworks, Inc. Matlab 2017b, education edition, 2017. URL https://www.mathworks.com/products/matlab.html.

Additional References

[52] Delft aerospace rocket engineering, website/about, March 2019. URL https://dare.tudelft.nl/about. [Online; accessed 23. Mar. 2019].

[53] Krijn de Kievit, Eoghan Gilleran, Jeije van den Wijngaart, Fabio Kerstens, Kevin Eppenga, Felix Kuhnert, Marco Geurtsen, and Nikita Sirons. Et3056tu: Detailed design report thurst vector minor. Technical report, Delft Aerospace Rocket Engineering, Stevinweg 4, 2628CN, Delft, March 2018.

[54] Leo Deelman. Amateur rocketry blog by leo deelman. https://deelmanl.wordpress.com/. Accessed: 2017-10-12.

[55] Leo Deelman and Jurriaan van de Beek. Making of a kilo grain. Technical report, NERO, 2014. internal production summary and logbook.

[56] Trevor Fradgley. Test report dxs asimov full scale motor test 01. Technical report, DARE, 2017. internal test report.

[57] Rob Hermsen and Karlo Rado. Srp-2016 redesign. Technical report, DARE, 2016. internal test report and measurement data.

[58] Scott Jolley. Amateur rocketry blog by scott jolley. http://www.ajolleyplace.com. Accessed: 2017-10-12.

[59] Stuart Leslie and James Yawn. Proposal for the inclusion of kno3/sugar propellants in the tra experimental rocketry program. Accepted by Tripoli Rocket Association, October 2002. URL http://www.4sightinc.com/stu/docs/SugarPro_Proposal.pdf.

[60] Rick Mashek. Personal communication. facebook, email, 2017.

[61] Olga Motsyk. Personal communication, 2016.

[62] Richard Nakka. Richard Nakka's Experimental Rocketry Site, Jun 2011. URL https://www.nakka-rocketry.net/ptburn.html. [Online; accessed 13. Dec. 2018].

[63] Richard Nakka. Richard nakka's experimental rocketry web site, 2016. URL http://www.nakka-rocketry.net/.

[64] Richard Nakka. Personal communication. email, 2017.

[65] Martin Christiaan Olde. Kalindex propellant overview. Technical report, DARE, 2016. internal document.

[66] Martin Christiaan Olde and Willem van der Lynden. Pressure vessel design guideline. Technical Report 1, Delft Aerospace Rocket Engineering, Stevinweg 4, 2628CN, Delft, 12 2017.

[67] Martin Christiaan Olde, Thimo van den Berg, and Katy Blyth. Knsb casting and trimming, general casting version version 3. Technical Report 1, Delft Aerospace Rocket Engineering, Stevinweg 4, 2628 CN Delft, February 2018.

[68] Hein Olthof. Kalindex production, storage and handling. Technical report, DARE, 2011. internal production guidelines.

[69] SS2S. Sugar shot to space project website. https://www.sugar-shot.org, 2015. website not anymore in use.

[70] Jurriaan van de Beek. Amateur rocketry blog by juriaan van den beek. http://www.verticallimits.nl, 2010-2017. Accessed: 2017-10-12.

Appendixes

A

Potassium Nitrate-Sorbitol Propellant Chemistry Reference

One of the issues encountered during work on KNO_3 Sorbitol (KNSB) propellant was a lack of propellant thermophysical data both of the combustion products and of the used ingredients. In this appendix these collected properties are listed. As in this entire thesis the used composition is assumed to be 65% KNO_3 to 35% Sorbitol by mass. Section A.1 gives combustion properties, regression rates and mechanical properties of the propellant. Section A.2 gives the general thermodynamic and material properties of Potassium Nitrate. In addition some numbers are provided about the interaction of moisture with KNO_3. In the subsequent section, A.3, similar information is given for Sorbitol.

A.1. Combustion Properties

In table A.1 the combustion properties are provided. This consists primarily of analysis and results made in the Rocket Propulsion Analysis-program (RPA)[50]. Provided are two cases with combustion pressures of 2 and 6.895 [MPa] (1000 [Psi]). Assumed is ideal expansion to 0.1 [MPa]. I_{sp} is calculated with isentropic relations from chamber conditions as determined by RPA [50]. This was done to allow comparison with the performance for condensed phase flow (which is significant). Vacuum I_{sp} is then calculated using the same expansion ratio but without back pressure (vacuum conditions). In the second half of the table the regression rates are given as determined by [6] and [63] based both on strand burner experiments at room temperature. These relations, together with the individual measurement points are also shown in figure A.1.

Of particular interest in the combustion products is Potassium Carbonate (K_2CO_3) which, based on chemical equilibrium, constitutes over 40% of the condensed products in the exhaust. Performing no expansion work, these particles significantly reduce theoretical performance. Material properties such as density or viscosity as function of temperature of pure K_2CO_3 can be found (similar to KNO_3) in Janz [34]. This also includes surface tension data for calculation of the Weber number (relevant for droplet size estimation).

Property	Unit	Value	Note	Source
Ingredients				
O/F	[-]	1.858		
KNO_3	[%]	65	by mass	
Sorbitol	[%]	35	by mass	
Theoretical, ideal expansion at $P_a = P_e = 0.1$ [MPa], infinite combustion chamber				
P_c	[MPa]	2.0	absolute	
A_e/A_t	[-]	4.11	Optimal expansion ratio	
I_{sp}	[s]	110		[16]
$I_{sp,VAC}$	[s]	129	$P_a = 0$ [MPa]	[16]
c^*	[m/s]	909		[50]
T_c	[K]	1576		[50]
γ	[-]	1.137	Gas Only	[50]
R	[kJ/kgK]	0.2102		[50]
C_p	[kJ/kgK]	2.5217	Gas Only	[50]
C_s	[kJ/kgK]	1.537	Condensed Phase	[43]
X	[-]	0.423	Condensed Phase Mass Fraction	[50]
Theoretical, ideal expansion at $P_a = P_e = 0.1$ [MPa] infinite combustion chamber				
P_c	[MPa]	6.895	absolute, (1000 [Psi])	
A_e/A_t	[-]	10.76	Optimal expansion ratio	
I_{sp}	[s]	126		[16]
$I_{sp,VAC}$	[s]	141	$P_a = 0$ [MPa]	[16]
c^*	[m/s]	911		[50]
T_c	[K]	1600		[50]
γ	[-]	1.137	Gas Only	[50]
R	[kJ/kgK]	0.209		[50]
C_p	[kJ/kgK]	2.0466	Gass Only	[50]
C_s	[kJ/kgK]	1.537	Condensed Phase	[43]
X	[-]	0.436	Condensed Phase Mass Fraction	[50]
Regression Rate Constants Coarse KNO_3, 330 [μm] average PSD				
a	[mm/s]	5.132	23-26 [°C], see fig A.1	[6]
n	[-]	0.222		[6]
P_{ref}	[MPa]	1.0		
Regression Rate Constants fine KNO_3, 60-125 [μm] average PSD				
a	[mm/s]	6.60	21 [°C], see fig A.1	[49],[63]
n	[-]	0.229		[49],[63]
P_{ref}	[MPa]	1.0		

Table A.1: KNSB baseline propellant properties

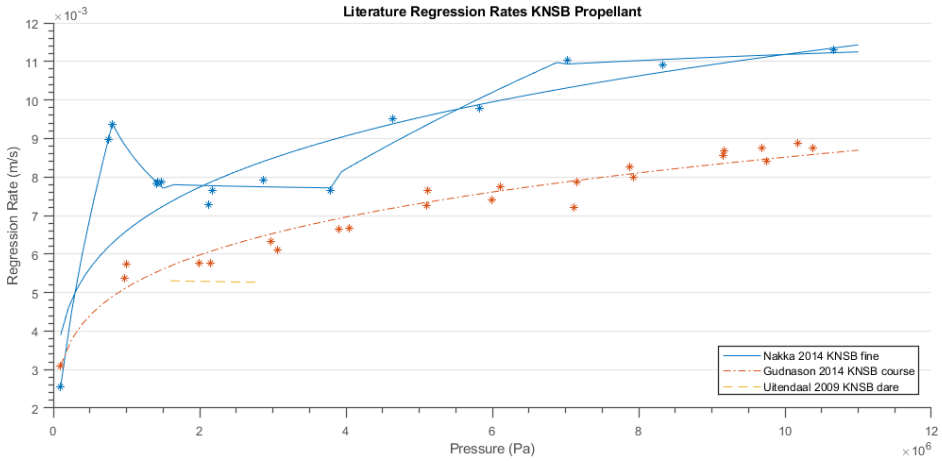

Figure A.1: Burnrate data for KNO_3-Sorbitol Propellant with fine and coarse KNO_3 PSD

A.2. KNO3 Material Properties

Potassium Nitrate, Niter, KNO_3 is a white crystalline solid at room temperature. It is not combustible by itself however, as it is a oxidizing agent, can react vigorously with a fuel. KNO_3 is used extensively in the food industry for which it is obtainable in granulated form. When used in KNSB propellant it is generally inert during production as it has a melting point significantly above that of Sorbitol. A boiling point is not readily known as KNO_3 will decompose into KNO_2 and oxygen at 400 [°C].

KNO_3 is reported to be hazardous in case of skin contact (irritant), of eye contact (irritant), of ingestion, of inhalation (lung irritant). Prolonged exposure may result in skin burns and ulcerations. Over-exposure by inhalation may cause respiratory irritation. In practice when working with KNO_3 it suggested to limit contact with the skin. With small Particle Size Distributions (PSD) it is further recommended to prevent the particles to get airborne in addition to the normal PPE such as simple dust masks and eye protection.

In table A.2 the physical data is provided for KNO_3. The point of fusion (melting point), T_f, decomposition point, T_d are provided. Note that decomposition of KNO_3 occurs before the boiling point. Subsequently the thermal capacity, heats of formation and heat of fusion is provided. Lastly the density and thermal conductivity are given for both solid and liquid phases. In the liquid phase the density can be calculated with equation A.1 where Tm is fusion temperature and constants are as provided in the table.

$$\rho(T) = \rho_m - k_\rho(T - T_m) \tag{A.1}$$

The interaction of moisture between KNO_3 is relatively limited with a critical relative humidity (CRH) above 90% between 0-30 [°C] below which KNO_3 will not readily take up moisture.

Property	Unit	Value	Note	Source
General Properties				
Formula	[-]	KNO_3	Crystalline, at room conditions	
M_{mol}	[g/mol]	101.103		[37]
Thermal Events				
T_d	[°C]	400	Decomposition ($KNO_3 \rightarrow KNO_2$+O)	
T_b	[°C]	NA	(decomposes, see above)	
T_f	[°C]	337	Fusion Temperature	[37]
T_{au}	[°C]		Auto Ignition Temperature	
T_{flash}	[°C]		Flash Point	
Thermodynamic Properties from STP				
C_p	[kJ/kgK]	953.5		[37]
$\Delta_f G^o$	[kJ/kg]	-3905.9		[37]
$\Delta_f H^o$	[kJ/kg]	-4892.0		[37]
Q_f	[kJ/kg]	-	Heat of fusion	
Mass and Transport Properties				
ρ_s	[kg/m³]	2109	Crystalline STP	[37]
α	[1/K]	228x10^{-6}	Volumetric Thermal Expansion Coefficient (Crystalline KNO_3) at STP	[38]
$\rho_l(T)$	[kg/m³]	1865	373-457[°C] see eq. A.1	[37]
k_ρ	[kg/m³ °C]	0.723	see eq. A.1	[37]
k	[W/mK]	0.5	solid,	[46]
k	[W/mK]		liquid, 349<T<438 [°C]	[40]
Interaction With Moisture				
CRH	[%]	97.0	0 [°C] Deliquescence humidities	[47]
CRH	[%]	93.7	20 [°C]	[47]
CRH	[%]	88.9	40 [°C]	[47]

Table A.2: KNO_3 Thermophysical Properties

A.3. Sorbitol Material Properties

Sorbitol is a poly-alcohol that is extensively used as an artificial sweetener but has seen significant research also as a pharmaceutical ingredient. It has a low melting point at 110-115 [°C] which is lowered via hydration to around 95 [°C]. Table A.3 provides similar material properties as table A.2. [29] does report a partial decomposition when sorbitol is heated to above 250 [°C] in an oxygen environment. In contrast to KNO_3 the substance also has a quantified boiling point T_b. The last temperature is the glass transition temperature which for pure sorbitol is -9 [°C] or lower in its hydrated form. It is generally found that the KNSB propellant retains rubbery for around 12-24 hours after casting and cooling to room temperature. After this time the propellant becomes brittle (crystaline?). It is unknown what theory describes this process.

The thermal conductivity for solid and liquid sorbitol was not found in any reliable source which is

why, values for Erythritol are provided. Erythritol is a sugar alcohol similar to sorbitol but with a carbon chain of 4 instead of 6. Moisture interaction of sorbitol is critical as it will attract significant amounts of moisture in low relative humidities. The Critical relative humidity is around 60% at room temperature. The moisture isotherms for various industrial sources of sorbitol are further shown in figure A.2 [42]. EMC [-] is defined via equation A.2, P [%] is the percent moisture dry basis in the sample.

$$EMC = \frac{P}{P + 100} \cdot 100 \tag{A.2}$$

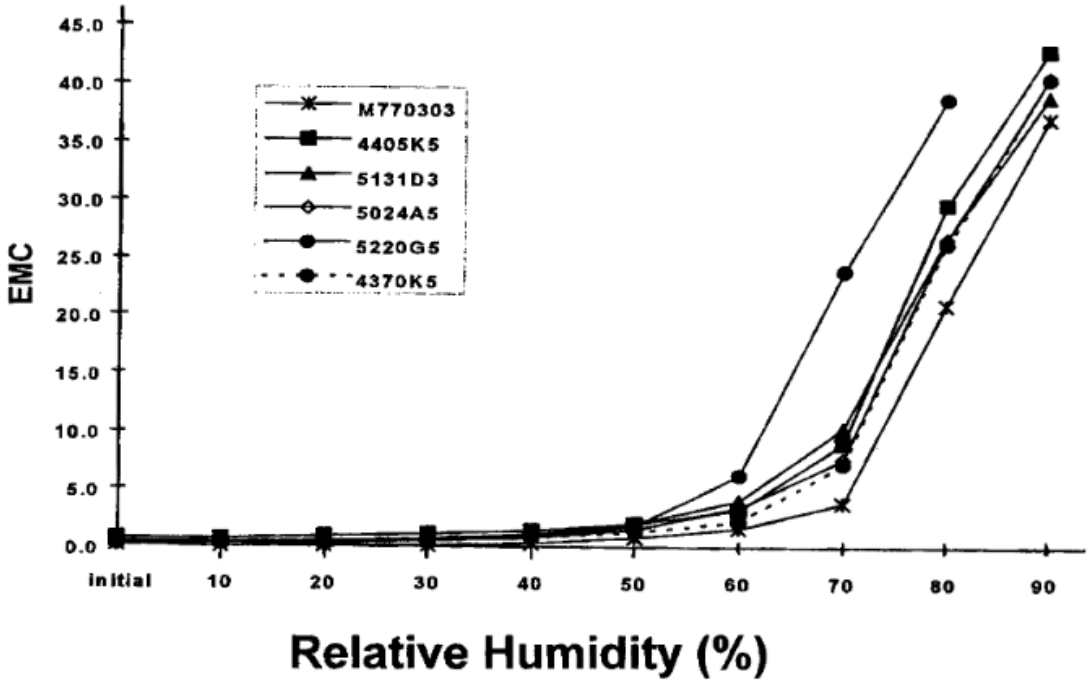

Figure A.2: Sorbitol moisture uptake (EMC) as function of relative humidity at room temperature.

Property	Unit	Value	Note	Source
General Properties				
Formula	[-]	$C_6H_14O_6$	Solid at STP	
M_{mol}	[g/mol]	182.171		[37]
Thermal Events				
T_b	[°C]	295	(167 at 10 mbar)	[25, 37]
T_d	[°C]	250	Partial decomposition with oxygen	[29]
T_f	[°C]	111	(95 for hydrate), Temperature of Fusion	[37]
T_g	[°C]	-9	Glass Transition Temperature	[37]
T_{au}	[°C]	420	Auto Ignition Temperature	[46]
T_{flash}	[°C]	>100	Flash Point, non-flammable oxidizer	[46]
Thermodynamic Properties from STP				
C_p	[kJ/kgK]	1.213-1.325	Crystaline Solid	[27, 46]
C_p	[kJ/kgK]	1.844	Liquid	[27]
C_p	[kJ/kgK]	1.032	Gaseous	[27]
$\Delta_f G^o$	[kJ/g]			
$\Delta_f H^o$	[kJ/kg]	7430.98		[43]
Q_f	[kJ/kg]	110-154.0	Heat of fusion (one is likely hydrated)	[25, 35]
Q_E	[kJ/kg]	727	Heat of Evaporation	
Mass and Transport Properties				
ρ_s	[kg/m³]	1489 1542	STP, dependent on crystal form	[25, 37]
$\rho_l(T)$	[kg/m³]			[37]
k_ρ	[kg/m³K]			[37]
k	[W/m²K]	0.733	!Erythritol!,solid,	[39]
k	[W/mK]	0.326	!Erythritol!,liquid	[39]
α	[1/K]		Volumetric Thermal Expansion Coefficient	[38]
Interaction With Moisture				
CRH	[%]	60	20 [°C] Deliquescence humidities	[42]

Table A.3: Sorbitol Thermophysical Properties

B

Experiment Protocols

The experiment protocols were developed for the experiments described in this thesis. These protocols were developed as part of the planning and execution of the experiment and assured that all relevant measurements and steps were taken.

B.1. Experiment Part A: Out-gassing Experiments

The experiment protocol is based on the casting procedures as found in [68] and expanded to meet test objectives. Part A describes the preparation of the premix and the introduction of moisture contamination into the propellant. Part B details the sample preparation used during this experiment. Part C-F subsequently describes the various out gassing methods applied to the different propellant samples. Part G describes the post test inspection of the experiment.

All weights are determined at +/-0.5 [g] accuracy unless otherwise noted.

Part A: Premix Preparation

Step-A1 Gather all equipment from the list (refer to appendix B.3).

Step-A2 Set up equipment in casting room.

Step-A3 Confirm a bucket of water and fire extinguisher are near the entrance.

Step-A4 Confirm all equipment is set up correctly and general preparations [68] are complete.

Start of work with energetic materials.

Step-A5 Gather 2g samples of raw ingredients (KNO_3 and Sorbitol).

Step-A6 Prepare 3 kg of premix as outlined in [68].

Step-A7 Thoroughly mix the propellant for 15 minutes so that a homogeneous mixture is obtained.

Step-A8 Weight empty storage containers, note down tare weight, check they are properly labelled.

Step-A9 Divide premix over empty storage containers to create 3, 1 kg batches.

Step-A10 Weigh filled storage containers, note down weight.

Prepare Moisture Contamination

Step-A11 Measure the required amount of water (25 gram and 50).

Step-A12 Weigh small containers with kitchen paper note down tare weight.

Step-A13 Transfer water to small container with kitchen paper.

Step-A14 Place small containers in storage containers.

Step-A15 Close storage containers.

Step-A16 Note down time.

Step-A17 Note down any observations.

Storage containers are now stored for at least 24 hrs.

Step-A18 Clean up equipment.

Part B: Sample Preparation

Step-B1 Gather all equipment from the list.

Step-B2 Set up casting equipment in casting room.

Step-B3 Make a bucket of water and fire extinguisher are near the entrance.

Start of work with energetic materials. To be repeated for containers EXA-00-1, EXA-00-2, EXA-25 and EXA-50

Step-B4 Weigh filled storage containers, note down weight.

Step-B5 Note down any observations.

Step-B6 Open storage container, remove small container.

Step-B7 Check consistency of premix, make photos.

Step-B8 Note down any observations.

Step-B9 Weigh small container with kitchen paper, note down weight.

Step-B10 Thoroughly mix large container so that a homogeneous mixture is obtained.

Step-B11 Weight empty storage containers, note down tare weight, check they are properly labelled.

Step-B12 Divide premix over empty sample containers to create 4x 250 g batches. (small differences due to losses or moisture are expected.

Step-B13 Weigh small containers, note down weight.

Part C: Application of Vacuum *To be repeated for samples from containers EXA-00-1, EXA-00-2, EXA-25 and EXA-50*

Step-C1 Check that vacuum chamber and vacuum pump are working.

Step-C2 Check that casting equipment is ready.

Step-C3 Check that casting moulds are ready and correctly labelled.

Step-C4 Weigh the empty mould.

Step-C5 Weigh the empty pot.

Step-C6 Pour the premix into the pot.

Step-C7 Weigh again, and note down starting weight and current time.

Step-C8 Start heating the sample.

Step-C9 When the mixture is fully molten (125 ± 2 [° C]), remove from stove.

Step-C10 Weigh the pot, note down weight and current time.

Points C11 and C12 are to be repeated 3 times unless no difference is measured.

Step-C11 Apply vacuum for 1 minute.

Step-C12 Weigh the pot, note down weight and current time.

Step-C13 Reheat the propellant to 125 ± 2 [° C].

Step-C14 Cast the propellant into one of the moulds, apply plunger.

Step-C15 Note down weight of casting mould + propellant.

Step-C16 Note down any observations.

Step-C17 Clean equipment for next propellant batch.

Part D: Continued Heating *To be repeated for samples from containers EXA-00, EXA-25 and EXA-50*

Step-D1 Check that casting equipment is ready.

Step-D2 Check that casting moulds are ready and correctly labelled.

Step-D3 Weigh the empty mould.

Step-D4 Weigh the empty pot.

Step-D5 Pour the premix into the pot.

Step-D6 Weigh again, and note down starting weight and current time.

Step-D7 Start heating the sample.

Step-D8 When the mixture is fully molten (125 ± 2 [° C]), remove from stove.

Step-D9 Weigh the pot, note down weight and current time.

Points D10 and D11 are to be repeated 3 times unless no difference is measured.

Step-D10 Heat the propellant for an additional 2 minutes. Makes sure propellant does not exceed 130 [° C].

Step-D11 Weigh the pot, note down weight and current time.

Step-D12 Reheat or let the propellant cool to 125 ± 2 [° C].

Step-D13 Cast the propellant into one of the moulds, apply plunger.

Step-D14 Note down weight of casting mould + propellant.

Step-D15 Note down any observations.

Step-D16 Clean equipment for next propellant batch.

Part E: Storage with Desiccant *To be repeated for samples from containers EXA-00, EXA-00-2, EXA-25 and EXA-50*

Step-E1 Clean the storage containers and fill with desiccant (Calcium Chloride).

Step-E2 Weigh the storage box, note down weight.

Step-E3 Place Sample container inside storage box.

Storage containers are now stored for at least 24 hrs.

Step-E4 After approx 8 hours, weigh again, and note down weight and current time.

Step-E5 After approx 16 hours, weigh again, and note down weight and current time.

Step-E6 After approx 24 hours, weigh again, and note down weight and current time.

Containers are removed from storage.

Step-E7 Check that casting equipment is ready.

Step-E8 Check that casting moulds are ready and correctly labelled.

Step-E9 Weigh the empty mould.

Step-E10 Weigh the empty pot.

Step-E11 Pour the premix into the pot.

Step-E12 Weigh again, and note down starting weight and current time.

Step-E13 Start heating the sample.

Step-E14 When the mixture is fully molten (125 ± 2 [° C]), remove from stove.

Step-E15 Weigh the pot, note down weight and current time.

Step-E16 Cast the propellant into one of the moulds, apply plunger.

Step-E17 Note down weight of casting mould + propellant and current time.

Step-E18 Note down any observations.

Step-E19 Clean equipment for next propellant batch.

Part F: Control Group *To be repeated for samples from containers EXA-00, EXA-25 and EXA-50*

Step-F1 Check that casting equipment is ready.

Step-F2 Check that casting moulds are ready and correctly labelled.

Step-F3 Weigh the empty mould.

Step-F4 Weigh the empty pot.

Step-F5 Pour the premix into the pot.

Step-F6 Weigh again, and note down starting weight and current time.

Step-F7 Start heating the sample.

Step-F8 When the mixture is fully molten (125 ± 2 [° C]), remove from stove.

Step-F9 Weigh the pot, note down weight and current time.

Step-F10 Cast the propellant into one of the moulds, apply plunger.

Step-F11 Note down weight of casting mould + propellant.

Step-F12 Note down any observations.

Step-F13 Clean equipment for next propellant batch.

Part G: Post Test Inspection *The samples are let to cure for at least 24 hours. Make sure samples are not mixed up during cleaning.*

Step-G1 Check that equipment is ready.

Step-G2 Remove the propellant from the moulds.

Step-G3 Clean samples with paper (remove grease).

Step-G4 Make sure samples are properly labelled.

Step-G5 Check samples according to QA criteria (see section 4.2.1

Step-G6 Note down any observations.

Step-G7 Weigh all samples, note down weight.

Step-G8 Measure physical dimensions of samples.

For inspection the grains are now cut with a saw in line with BEM-QA-2.2_1 (see section 4.2.1. This can be done at a later time.

Step-G9 Apply tape to side of sample

Step-G10 Cut grain in three pieces.

Step-G11 Inspect propellant for flaws.

Step-G12 Note down any observations.

Step-G13 Clean up equipment.

Step-G14 Dispose of samples in bucket of water.

B.2. Experiment Part B: Compression Experiments

This casting procedure follows the general casting procedures outlined in [68]. For brevity only the specific experiment steps are provided. Part A describes the setup preparation, Part B describes the casting of the propellant grains for the casting experiment. Part C describes the propellant inspection and quality measurements.

Part A: Setup Preparation

Step-A1 Gather all equipment from the list.

Step-A2 Set up casting equipment in casting room.

Step-A3 Place a bucket of water and fire extinguisher near the entrance.

Step-A4 Confirm all equipment is set up correctly and general preparations [68] are complete.

Step-A5 Confirm that DAQ system (CRIO + thermocouple module) are set up correctly and working.

Step-A6 Prepare casting moulds, 6 without, 4 with cardboard liners.

Step-A7 Prepare four moulds with thermocouples for compression experiment and for thermal conditioning experiment.

Step-A8 Make sure that casting Moulds and Liners (if applicable) are properly labelled.

Step-A9 Weigh the empty moulds, note down weights.

Step-A10 Place 2 moulds in oven, set temperature to 100 [° C].

Start of work with energetic materials.

Step-A11 Gather 2g samples of raw ingredients (KNO_3 and Sorbitol).

Step-A12 Prepare 2 kg of premix as outlined in [68].

Part B: Propellant Manufacturing

Step-B1 Thoroughly mix the propellant for 15 minutes so that a homogeneous mixture is obtained.

Step-B2 Note down time.

Step-B3 Note down any observations.

Step-B4 Weigh the pot, note down weight and current time.

Start heating of propellant mixture

Step-B5 When the mixture is fully molten (125 ± 2 [° C]), remove from stove.

This step is modified in line with the most effective method from experiment part A: out-gassing strategies.

Step-B6 Weigh the pot, note down weight and current time.

Step-B7 Retrieve heated moulds, store in Styrofoam box.

Start of propellant casting, to be repeated for all moulds.

Step-B8 Place mould on scales

the following two steps are only applicable for grains with embedded thermocouples.

Step-B9 Connect thermocouples to DAQ, start acquisition.

Step-B10 Turn on time-lapse camera.

Step-B11 Cast 250 gram of premix into one of the moulds, apply plunger.

Compression is only applied after all grains have been cast.

Step-B12 Apply initial compression of 700 N. Confirm compression distance with calipers (K=156 [N/mm]≈ 4.5 [mm]. Note down compression distance and time.

Step-B13 Confirm DAQ system is working correctly and that time-lapse camera can measure grain compression.

The samples are let to cure for at least 24 hours.

Part C: Post Test Inspection *The samples are let to cure for at least 24 hours. Make sure samples are not mixed up during cleaning.*

Step-C1 Check that equipment is ready.

Step-C2 Remove the propellant from the moulds.

Step-C3 Clean samples.

Step-C4 Make sure samples are properly labelled.

Step-C5 Check samples according to QA criteria (see section 4.2.1).

Step-C6 Note down any observations.

Step-C7 Weigh all samples, note down weight.

Step-C8 Measure physical dimensions of samples.

For inspection EXB grains are now cut with a saw in line with BEM-QA-2.2_1 (see section 4.2.1. This can be done at a later time. Make sure thermocouples are not damaged.

Step-C9 Apply tape to side of sample

Step-C10 Cut grain in three pieces.

Step-C11 Inspect propellant for flaws.

Step-C12 BEM Grains are stored for later use.

Step-C13 Note down any observations.

Step-C14 Clean up equipment.

Step-C15 Dispose of samples in bucket of water.

B.3. Experiment Part A/B: Equipment List

Adapted from [67] and [68].

Safety Items

- 2 fire extinguishers
- 2 buckets of water
- 1 (per person) pair of safety glasses per person
- 1 (per person) lab coat
- 2 pairs of leather gloves
- 1 roll of red-white tape
- 2 Safety no entrance signs

Tools

- 2 sets of Casting procedures
- 2 clipboards
- 1 Stanley Knife
- 1 Small Tarp
- 1 White plug box
- 1 pair of Scissors
- 1 Permanent Marker
- 2 pens
- 1 scourer (schuurspons)
- 1 unit Bearing Grease
- 1 pair of calipers
- 1 set of scales (25 kg, 1 gram resolution)
- 1 infrared Thermometer

Casting Equipment

- 1 Heating plate
- 2-4 cooking pots (sufficiently large)
- 2-4 wooden stirring spoons
- 3 silicone place-mats
- 2 glass bowls

Consumables

- 5 sheets of A3 Paper
- 1 roll wide crepe-tape
- 1 roll of duct-tape
- 1 box of Latex Gloves
- 1 roll of blue cleaning paper/ toilet paper
- 1 roll of garbage bags

Experiment Specific Items

- 1 Experiment Protocol
- 3 clean sample containers
- 1 vacuum pan + lid + O-ring
- 1 vacuum pump
- 9 small storage containers (Xenos)
- 10 Casting Jigs
- 1 Thermal (pizza) conditioning box
- 1 Box of (fresh) desiccant
- 3 boxes of premix with water (25 g/kg, 50 g/kg)
- 1 drum of course KNO_3
- 1 drum of Sorbitol
- 1 camera for time-lapse
- 1 good camera (phone) for making pictures

B.4. Experiment Part C: Steady Regression Experiments

B.4.1. Thermal Conditioning Experiment

Part A: Experiment Preparation

Step-A1 Gather all equipment from the item list.

Step-A2 Ensure DAQ system is working.

Propellant Handling will now start.

Step-A3 Unpack Propellant grains.

1. Inspect all propellant grains.
2. Weigh all propellant grains.
3. Confirm thermocouple numbering.
4. Note down grain and BEM combinations.

Step-A4 Confirm ambient thermocouple is attached to DAQ system, confirm readout.

Step-A5 Connect all thermocouples to DAQ system, confirm readout.

Step-A6 Disconnect all thermocouples from DAQ system. (except ambient)

Step-A7 Install propellant grains into BEM's excluding nozzle circlip. Route thermocouple leads through nozzles.

Step-A8 Install external thermocouple to casing with metal tape after cleaning with Acetone.

Step-A9 Place loaded BEM inside plastic bags, apply tape to opening with thermocouple leads.

Step-A10 Connect all thermocouples to DAQ system, confirm readout.

Step-A11 Start logging temperature data.

Differentiate here between hot and cold conditioning. If cracking is heard during experiment note down applicable BEM and mark the time.

Step-A12 Place grains inside Styrofoam box. Apply plastic bags with ice around BEM's or turn on heater.

Step-A13 Apply Lid to Styrofoam box.

Cool down starts.

Part B: Conditioning Experiment *Once grains have achieved near uniform temperature T<5 [°C] the conditioning experiment can continue.*

Step-B1 Assure that test bench and equipment is ready.

Step-B2 Confirm that temperature is within the experimental range (15<T<25 [°C]).

Step-B3 Stop logging data with DAQ with low sample rate.

Step-B4 Start logging temperature data. (i.e. new file with higher sample rate.)

Follow Installation procedures as for BEM testing (see part C of section B.4.2.

Step-B5 Assure that thermocouples are re-attached as soon as possible during installation.

Step-B6 Mark time in DAQ when ready for testing.

Wait until grain has returned to temperatures significantly outside testing range.

Step-B7 Stop logging data with DAQ.

Part B is repeated for all grains.

Part C: Post Test Evaluation

Step-C1 Disassemble BEM's.

1. Inspect all hardware.
2. Inspect all propellant grains (especially for cracks or liner separation)
3. Weigh all propellant grains.

Step-C2 Store Propellant grains

Step-C3 Clean and store BEM's.

Step-C4 Note down time.

End of Experiment

B.4.2. Ballistic Evaluation Motor Testing

Part A: Experiment Preparation (Laika)

Step-A1 Gather all equipment from the item list.

Step-A2 Look up weather conditions

Step-A3 Ensure DAQ system is working.

Step-A4 Perform all calibration tasks (load cell, pressure sensor(s)).

Step-A5 Unpack Propellant grains.

1. Inspect all propellant grains.
2. Weigh all propellant grains.
3. Measure all propellant grains.

Step-A6 Coat all grains with ignition primer.

Step-A7 Weigh all propellant grains. Note: wait until ignition primer is thoroughly dried. This is done to get a mass estimate of the amount of primer.

Conditioned BEM's can be taken from refrigerator or oven close to installation

Step-A8 Install BEM end caps BEM. Place tape over pressure opening.

Step-A9 Measure nozzle throat and exit diameter.

Step-A10 Install Propellant grain in BEM, write down combination grain and BEM.

Step-A11 Install nozzle in BEM. Note: without the circlip.

Step-A12 Weigh entire BEM assembly.

Step-A13 Apply thermocouples to outside of casing for conditioned BEM's.

Step-A14 Store BEM's.

Step-A15 Confirm temperature of Styrofoam boxes.

Part B: Field setup (Fels field) *Arrive at fellowship field and unpack equipment.*

Step-B1 Install test bench.

Step-B2 Confirm test bench is horizontal to within 0.5 [°] or better.

Step-B3 Mark time.

Step-B4 Confirm DAQ system is operational by pushing load cell and checking pressure and temperature readout.

Step-B5 Confirm Ignition system is operational by doing a mock firing sequence.

Step-B6 Confirm temperature of conditioned BEM's, confirm amount of ice remaining.

Confirm with safety officer that it is ready for testing.

Part C: Firing (Fels field) *To be repeated for all BEM tests.*

Step-C1 Assure correct procedures are used.

Step-C2 Mark time.

Step-C3 In case of conditioned test: turn on camera. Make sure the test-ID is visible on the the test setup.

Step-C4 Make sure all tools are at hand.

Step-C5 Unpack BEM, confirm BEM ID.

Step-C6 Weigh entire BEM assembly.

Step-C7 Install BEM on test bench.

Step-C8 Install pressure sensor, confirm reading.

Start Safety Critical Operations

Step-C9 Install nozzle circlip.

Step-C10 Install Igniter.

Step-C11 In case of normal test: turn on camera. Make sure the test-ID is visible on the the test setup.

Step-C12 Retreat to CP.

Step-C13 Turn on DAQ, confirm logging.

***** ***Motor Firing*** *****

Step-C14 Wait 1 minute post test.

End Safety Critical Operations

Step-C15 Stop DAQ logging.

Part D: Post Test Evaluation I (Fels field)

Step-D1 Return to setup.

Step-D2 turn off camera.

Step-D3 Inspect Setup.

Step-D4 Disassemble BEM from setup.

Step-D5 Weigh entire BEM assembly.

Step-D6 Note down any observations.

Restart Part C if additional tests. Otherwise clean up and return to Laika lab.

Part E: Post test Evaluation II (Laika)

Step-E1 Unpack toolboxes.

Step-E2 Disassemble BEM's

1. Write down BEM ID.
2. Inspect all casings, note down observations.
3. Disassemble BEM, collect slivers/ deposits.
4. Split slivers/ deposits into inhibitor material/ propellant material.
5. Weigh slivers/ deposits.
6. Measure nozzle throat and exit diameter. Note: including deposits, make fotos.

Step-E3 Clean BEM hardware.

Step-E4 Measure nozzle throat and exit diameter.

Step-E5 Store BEM hardware.

Step-E6 Clean other equipment.

Step-E7 Clean lab.

Other items are for record keeping.

Step-E8 Write down any important events or considerations.

Step-E9 Scan used procedures.

Step-E10 Obtain video files from camera, clear camera memory.

Step-E11 Obtain DAQ data files, confirm data has been logged properly, clear DAQ memory.

End of experiment

B.4.3. Firing Procedures

x

Ballistics Evaluation Motor, Ambient test

MC-EXC-PROC-1_6

Test date	14-01-2019
Version	6

Test day code	20190114-BEM-06
Associated project	MC Thesis Project

Information: The TC reads out this checklist, the TO performs all operations and the OSO has an observer role and absolute authority over stopping activities due to safety concerns. Make sure all calibration is done before start of the procedures. Never walk directly behind the exhaust area of the motor. Thermally conditioned tests have to be fired within 15 min after getting the motor from the box so that grain temp is below <5°C however sooner is better.

Test Conductor (TC)	Martin Olde
Test Operator (TO)	
Operational Safety Officer (OSO)	Jeije Van Wijngaard
Approving Safety Officer	

TU DELFT SAFETY PHONE NUMBER
+31 (0)15 27 81226

TU DELFT POWER NUMBER
+31 (0) 15 27 82777

Abbreviations:

TC	Test Conductor
OSO	Operational Safety Officer
TO	Test Operator
CP	Command Post
DAQ	Data AcQuisition
CRIO	Magic Data acquisition Computer that converts sensor input to data files
BEM	Ballistics Evaluation Motor, system under test.

Part A: System Check

Checkboxes	ID	Action to be performed	Comments
	A 1	Clear the area, only OSO, TC, TO are allowed on location	
	A 2	Turn of phones	
	A 3	Check to make sure everyone in danger area is wearing eye protection and labcoats/coveralls	
	A 4	Verify if primary key of ignition system is in possession of Operational Safety Officer	The key from Lucifer/ Or RIO safe/arm
	A 5	Make sure the area is secure	
	A 6	Make sure a bucket of water and a fire extinguisher are placed 10m away from the setup	
	A 7	Confirm distances to CP, spectators, location of red white ribbon tape	27 meters to nearest spectator
	A 8	Make sure the testbench is secured on the ground	Check by hand; Make sure 4 metal rods are inserted in the ground properly
	A 9	Make sure tension straps are tight	Check by hand; Make sure 2 metal rods are inserted in the ground properly
	A 10	Make sure sandbags are positioned correctly around the testbench	
	A 11	Make sure 3 sandbags are in line with nozzle failure	
	A 12	Make sure the testbench is securely assembled by checking the bolts	
	A 13	Make sure Boombox can be moved into possition easily	
	A 14	Make sure the bench is electrically grounded to the pegs in the legs of the testbench	Use multimeter
		DAQ system chechout (can be run in paralel to A22-A31 if neccecary)	
	A 15	Turn on RIO	
	A 16	Confirm with CP that CRIO is connected and opperational	
	A 17	Visually check that all sensors are connected to the data acquisition system	There should be three sensors (load cell, pressure sensor, thermocouple)
	A 18	Confirm with CP that a testrun can be performed	
	A 19	Start Data acquisition and let run for 1 minute	
	A 20	Confirm with CP that data acquisition can be stopped	
	A 21	Confirm with CP that data file was correctly written (confirm filename and size of data file)	
		Launchbox checkout	
	A 22	turn on launchboxes, arm launch boxes. Key to gabriel	
	A 23	Connect multimeter to ignition leads, measure voltage	0 volt
	A 24	Request CP to do a firing sequence, counting down via the radio	12 Volt at t=0, kick the testbench
	A 25	Confirm with CP that if ignition test was a succes	
	A 26	Turn Gabriel to safe, key to OSO	
	A 27	Make sure no parts are in the way of the motor exhaust	
	A 28	Make sure no parts rest on elements measured by the load cell	
	A 29	Make sure cables running on the ground are not a trip hazard	
	A 30	Take photos of testbench, CP, firing line, closeup of RIO and cables.	Good overview photos, and several detailed shots
	A 31	Checkout complete	

System state:
The system is now checked out and ready for operation

Part B1: Pyrotechnics Ambient Conditions

Checkboxes	ID	Action to be performed	Comments
	B1 1	Acquire the pyrotechnics for the current test	Motor with both bulkheads inserted, nozzle snapring is missing
	B1 2	Weigh entire motor on large Scales,	BEM, snapring, pressure tube and pressure sensor, igniter
		Motor pre firing weight	
		BEM 1= motor no. _____, mass= _____ gr.	
		BEM 2= motor no. _____, mass= _____ gr.	
		BEM 3= motor no. _____, mass= _____ gr.	
		BEM 4= motor no. _____, mass= _____ gr.	
		BEM 5= motor no. _____, mass= _____ gr.	
		BEM 6= motor no. _____, mass= _____ gr.	
	B1 3	Take foto of BEM on scales	
	B1 4	Mount engine onto test bench	
	B1 5	Connect the pressure sensor to the endcap with dowdy seal, tighten	
	B1 6	Connect the cable to the pressure sensor, confirm a proper readout	
	B1 7	Take foto of BEM	Closeup and field of view
	B1 8	Confirm testbench is ready, tools are at hand	Multimeter, tape, key no 19, clamps undone, with 4 winged nuts available
	B1 9	OSO Confirm that BEM is propely constrained	Check engine on thrustbench by pulling on engine
	B1 10	Install Snapring in Forward Bulkhead	
	B1 11	OSO Confirm that igniter can be placed	
	B1 12	Confirm that igniter is shunted	
	B1 13	Insert igniter into the motor with dowdy seal, tighten	M12, need Key no. 19. be carefull with igniter leads.
	B1 14	Place shrapnell box and apply sandbags around the setup	
	B1 15	Confirm that Lucifer is on and safe	
	B1 16	Wrap igniter leads around metal peg	
	B1 17	Move away from the engine as far as igniter leads allow	
	B1 18	Check that there is 0V on the igniter lines with the multimeter	
	B1 19	Un-shunt the igniter cables	
	B1 20	Connect the igniter wires to Lucifer igniter cable	
	B1 21	Wrap tape around igniter leads so they cant short	
	B1 22	Turn on any camers and start recording	
	B1 23	OSO turns Lucifer to arm, OSO takes key	
	B1 24	Run away in a controlled and distinctive manner	
	B1 25	Take photo of field	

System state:
The system is armed at the test site and is awaiting an ignition pulse from CP.

Part C1: Motor Firing Ambient Conditions

Checkboxes	ID	Action to be performed	Comments

Checkboxes	ID	Action to be performed	Comments
	C1 1	Verify that the test area surroundings are clear	
	C1 2	Confirm people on corners of fellowship field are in position	
	C1 3	Confirm parkinglot is clear	
	C1 4	Confirm filename is correct	
	C1 5	Confirm Pressure sensor is configured correctly	
	C1 6	Confirm Loadcell is configured correctly	
	C1 7	Confirm Thermocouple is connected correctly	
	C1 10	Confirm parkinglot is clear	
	C1 11	OSO confirm that countdown can start	
	C1 12	Start data Acquisition	
	C1 13	Loudly anounce start of countdown	
	C1 14	Start countdown from T-15 seconds	
	C1 16	At T-0 seconds, ignition via Gabriel	
		The motor now fires for between 3 – 6 seconds.	
	C1 16	At T+45 seconds, stop DAQ acquisition	
	C1 17	CP: Safe Data file	
	C1 18	Write down	
		Estimate Peak Pressure achieved from labview	
		BEM 1= motor no. _____, Pressure _____ Mpa, time _____:_____	
		BEM 2= motor no. _____, Pressure _____ MPa, time _____:_____	
		BEM 3= motor no. _____, Pressure _____ MPa, time _____:_____	
		BEM 4= motor no. _____, Pressure _____ MPa, time _____:_____	
		BEM 5= motor no. _____, Pressure _____ MPa, time _____:_____	
		BEM 6= motor no. _____, Pressure _____ MPa, time _____:_____	
	C1 18	After waiting for 1 minute, OSO and TC inspect the test area post test.	
	C1 19	Turn Lucifer to safe, turn cameras off	
	C1 20	Remove sandbags and boombox	
	C1 21	OSO Confirm system is secured, spectators can approach the system	
	C1 22	Take photos	Setup, nozzle, both bulkheads, anything else of interest
	C1 23	Warn people motor is still hot	
	C1 24	Undo clamps, dissconnect igniter	
	C1 25	Weigh Entire motor on scales	
		Motor Burnout Weight	
		BEM 1= motor no. _____, mass= _____ gr.	
		BEM 2= motor no. _____, mass= _____ gr.	
		BEM 3= motor no. _____, mass= _____ gr.	
		BEM 4= motor no. _____, mass= _____ gr.	
		BEM 5= motor no. _____, mass= _____ gr.	
		BEM 6= motor no. _____, mass= _____ gr.	
	C1 22	Store motor to the side to cool down completely	Setup, nozzle, both bulkheads, anything else of interest
	C1 26	When Cool, store motor in sealable bag to prevent moisture damage to deposites	

Part D: Post Test

Checkboxes	ID	Action to be performed	Comments
	D 1	Clean up, stow all equipment. Pick up any trash	Take care when handling engine or thrust bench. They may still be hot; and are certainly dirty.
	D 2	Verify that the test area surroundings are clear	
	D 3	Move equipment back to workshop.	
	D 4	Put away all of the tools and equipment in their proper places.	
	D 5	Clean the engine casings immediately after the test; do not leave engine casings un-cleaned as it will corrode and ruin the parts. Oil any steel components.	
	D 6	Download and save data from the datalogger. Write short test report & include data in it.	
	D 7	Copy and save any photos and videos from the DARE cameras. Delete the photos from the cameras.	

B.5. Experiment Part D: Ignition Experiments

x

Laser Ignition Testplan

MC-EXC-PROC-2_1

Test date	10/12/2018
Version	1

Test day code	20181210-IGN-01
Associated project	MC Thesis Project

Information: The TC reads out this checklist, the TO performs all operations and the OSO has an observer role and absolute authority over stopping activities with pyrotechnics due to safety concerns. Laser is only operated by TECH, who will observe laser safety and is end responsible for the room.

Test Conductor (TC)	Martin Olde
Operational Safety Officer (OSO)	Jeije van den Wijngaart
Technician	Jurriaan van Slingerland

TU DELFT SAFETY PHONE NUMBER
+31 (0)15 27 81226 (112 on internal phones)

Abbreviations:

TC	Test Conductor
OSO	Operational Safety Officer
TECH	Technician

Part A: Preperations

Checkboxes	ID	Action to be performed	Comments
	A 1	Make sure workspace is clean, tools are at hand	
	A 2	Check to make sure everyone in danger area is wearing required PBM	safety Shoes: laser glasses are at hand
	A 3	Install camera's, sample holder with doublesided tape	
	A 4	Check that thermal camera is setup correctly together with laptop	
	A 5	Check that go-pro is set up correctly	
	A 6	Check that JVC cam is set up correctly	
	A 7	Check that fire extinguisher is at hand and in a logical location	
	A 8	Check that setup and sample holder is placed correctly	
	A 9	Take photos of testbench, Room and camera setup	Good overview photos, and several detailed shots
	A 10	Preperations complete	

System state:
Setup Complete

Part B: System Checkout and Laser Callibration

Checkboxes	ID	Action to be performed	Comments
	B 1	Makes sure thermal paper and allignment equipment is at hand	
	B 2	Check that Techician is available to allign optical elements	
	B	Discuss allignment plan with Technician, discuss laser safety	
	B 3	Allign optics with pilot laser to sample center	**Unknown in laser goggles neccecary for this**
	B 4	Measure distance to optics such that focus point alligns with test plane.	see cheat sheet
	B 5	Retract focal plane by X mm to achieve desired beam width at sample surface.	see cheat sheet
	B 6	Place thermal paper at sample ignition plane	
	B 7	**Check Laser Safety: safety glasses and door interlock**	
	B 8	**10 ms pulse at 50 W; repeat if neccecary to get suitable image**	
	B 9	**Confirm laser off**	
	B 10	Check spot width with callipers	16mm+/- 0.5
	B 11	*If neccecary: Retract focal plane by additional required amount*	see cheat sheet
	B 12	*If neccecary: Repeat procedure from B5*	
	B 13	Take photos of testbenh setup with final allignment	
	B 14	System Checkout and allignment complete	

System state:
The system is armed at the test site and is awaiting an ignition pulse from CP.

Part C: Laser Power Level Callibration

Checkboxes	ID	Action to be performed	Comments
	C 1	Put on safety glasses/ laser glasses for handling pyrotechnics	
	C 2	Make sure cleaning equipement and tools are at hand	
	C 3	Acquire pyrotechnics for current test	
	C 4	Place 1/2 size sample in fixture, check height with respect to fixture base	(sample is a little shorter than nominal)
	C 5	Write down room temperature	
	C 6	*if neccecary: Callibrate sample emmisivity in thermal camera*	
	C 7	Check thermal camera is ready for recording	
	C 8	Write down time	See Lab Notes sheet.
	C 9	Take photos of sample in fixture	
	C 10	**Check Laser Safety: safety glasses and door interlock**	
	C 11	Confirm with Technician that experiment can start	
	C 12	Turn on JVC camera	
	C 13	Trigger thermal camera	
	C 14	**100 ms pulse at 50 W**	
	C 15	**Confirm laser off**	
	C 16	Turn JVC camera off	
	C 17	Write down notes	
	C 18	Determine Sample surface temperature increase	
	C 19	Determine Desired power level to reach 400 °C in about 1 second for Coarse KNSB	Estimated Decomposition Temperature
	C 20	Check thermal camera is ready for recording	
	C 21	Write down time	See Lab Notes sheet.
	C 22	Take photo of sample in fixture	
	C 23	**Check Laser Safety: safety glasses and door interlock**	
	C 24	Confirm with Technician that experiment can start (power and duration)	
	C 25	Turn on JVC camera	
	C 26	Trigger thermal camera	
	C 27	**10 second pulse at predetermined (see C19) power level SAMPLE BURNS FOR UP TO 3 Seconds**	Check if 10 seconds makes sense
	C 28	**Confirm laser off**	
	C 29	Turn JVC camera off	
	C 30	Take photos of setup	
	C 31	Write down notes	
	C 32	Clean Setup	Stealwool, brush and cloth
	C 33	*if nececary: adjust power level*	If ignition takes significantly more or less than 1 second
	C 34	Repeat from C3 for Sample (if neccecary) B,C,D.	
	C 35	End of Power Level Callibration	

Part D: Ignition Test Uncoated Samples

Checkboxes	ID	Action to be performed	Comments
	D 1	Acquire the pyrotechnics for the current test	
	D 2	Check setup is ready, tools are at hand	
		To be repeated for all samples in table	
	D 3	Acquire pyrotechnics for current test	
	D 4	Place sample in fixture	
	D 5	Check Setup is ready	
	D 6	Check thermal camera is ready for recording	

Checkboxes	ID	Action to be performed	Comments
	D 7	Write down time	See Lab Notes sheet.
	D 8	Take photo of sample in fixture	
	D 9	**Check Laser Safety: safety glasses and door interlock**	
	D 10	Confirm with Technician that experiment can start	
	D 11	Turn on JVC camera	
	D 12	Call out test number for JVC camera	
	D 13	Trigger thermal camera	
	D 14	**10 second pulse at predetermined (see C19) power level** **SAMPLE BURNS FOR UP TO 3 Seconds**	Check if 10 seconds makes sense
	D 15	**Confirm laser off**	
	D 16	Turn JVC camera off	
	D 17	Take photo of fixture	
	D 18	clean sample fixture	
	D 19	Write down notes	See Lab Notes sheet.
	D 20	*if neccecary: Recycle to point D3*	
	D 21	Ask for feedback on experiment from technician write down	See Lab Notes sheet.
	D 22	End of Experiment	

Part D: Post Test

Checkboxes	ID	Action to be performed	Comments
	E 1	Take group picture	
	E 2	Vigourously thank technician	
	E 3	Clean up, stow all equipment. Pick up any trash	
	E 4	Vigourously thank technician	
	E 5	Move equipment back to workshop.	
	E 6	Put away all of the tools and equipment in their proper places.	
	E 7	Copy and save any photos and videos from the DARE cameras. Delete the photos from the cameras.	

C

Sensor Calibration

C.1. Load cell Calibration

Calibration of the Scaime ZFA 500kg (sn 160898) load cell was performed on 13/01/2019 with the test bench mounted horizontally on the D:Dream welding table. A total of six weights were suspended over a pulley mounted on the test bench superstructure to assure that calibration could be performed with the bench mounted horizontally. The load cell was preloaded with a small spring mounted under the test bench which is also present in the field. The DARE DAQ system was used which included the National Instruments Compact RIO, the sensors and modules as mentioned in section 6.5. The load cell response [mV] was measured and is shown in figure C.1.

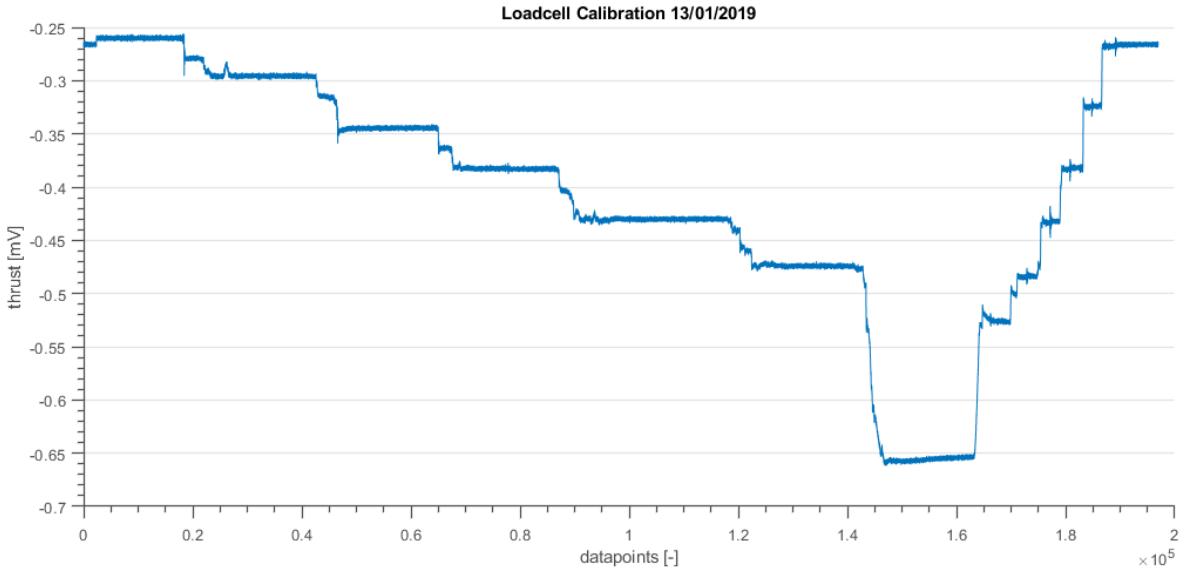

Figure C.1: Calibration measurement in measured [mV].

The calibration weights used were measured with the Metler Toledo FNR 225594 scales with a resolution of 1 [g] and are provided in table C.1. The voltage was averaged over approximately $15{\cdot}10^3$ values per measurement instance. A linear and quadratic fit was made of these seven data points. It was found that the linear fit, see equation C.1, provided the best results with a standard deviation of 5.4 [N] (approximately 0.7% of the measurement range). The quadratic fit, see equation C.2, produced marginally worse results with a standard deviation of 6.0 [N], (approximately 0.8% of the calibrated measurement range). Both fits and the measurement points from table C.1 are shown in figure C.2. The linear calibration is used in this report. Note that, as the test bench cannot be mounted exactly horizontal and spring tension might vary, the zero level needs to be adjusted between tests.

Table C.1: Load cell loaded weight [kg] and [N] and measured response in [mV]

step	weight [kg]	Force [N]	Response [mV]
0	0	0	-0.2600
1	7.996	78.41	-0.2957
2	15.998	156.89	-0.3446
3	23.979	235.15	-0.3828
4	31.984	313.66	-0.4301
5	40.002	392.29	-0.4741
6	73.902	724.73	-0.6557

$$F_N[\text{N}] = -1815.0 \cdot [\text{mV}] + -465.59 \tag{C.1}$$

$$F_N[\text{N}] = -31.254 \cdot [\text{mV}]^2 + -1843.7 \cdot [\text{mV}] - 471.62 \tag{C.2}$$

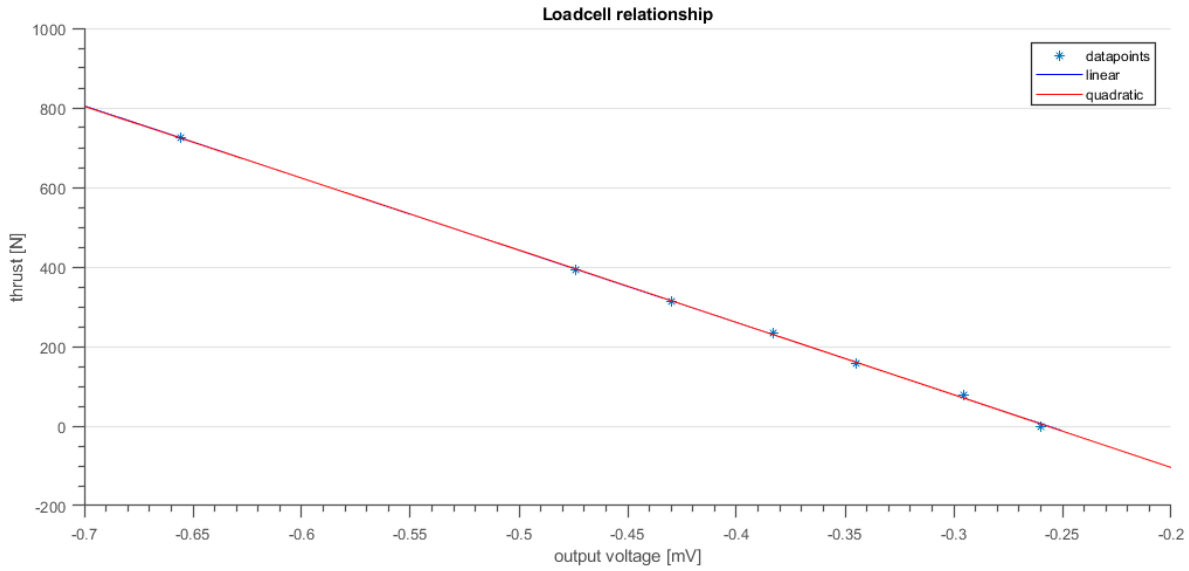

Figure C.2: Linear and quadratic fits with the calibration points showing good linear behaviour.

C.2. Pressure Sensors

Pressure sensors are of the type PT5402 procuced by IFM Electronic gmbh [33]. The pressure sensor is current based with a 4-20 [mA] analogue output. Output pressure (relative) is given in equation C.3

$$P[\text{Pa}] = (6250 \cdot [\text{mA}] + -25) \cdot 10^5 \tag{C.3}$$

Measurement accuracy = 0.25% of the measurement range from 1-100 bar.

D

Internal Ballistics Software Model

To simulate behaviour and performance of a core burning ballistics evaluation motor a simple, single control volume, simulation was written. First the equations are provided in section D.1, subsequently two burning surface area models are provided. In the last section two reference cases are generated that are used in the analysis of the steady regression rate (refer to section 6.7).

The model was created in Matlab[51].

D.1. Equations

D.1.1. Balance Equations

The model is based on a mass balance over the gas volume inside the motor up to the nozzle throat. Mass flow from the burning areas is provided in equation D.1, Mass flow through the nozzle in equation D.2, the burn rate r integrated over time yields the total regressed length w given in equation D.3.

$$\dot{m} = \rho_p A_b(w) r = \rho_p A_b(w) a \left(\frac{P_c}{P_{ref}} \right)^n \tag{D.1}$$

$$\dot{m} = -\frac{P_c A_t}{\eta_b c^*} \tag{D.2}$$

$$w = \int_{t_0}^{t} r dt \tag{D.3}$$

Chamber pressure, equation D.4, is derived from a simple mass balance over the internal gas volume, assuming instant and complete ignition and uniform gas temperature and pressure. Data for the propellant and engine performance is taken from appendix A.

$$\frac{dP}{dt} = \frac{RT_c}{V(t)} \left(\rho_p A_b(w) r(P_c) - \left(\frac{P_c A_t}{\eta_b c^*} \right) \right) - \frac{P_c}{V_c} \frac{dV_c}{dt} \tag{D.4}$$

With P_c chamber pressure, t time, RT_C the product of specific gas constant and chamber temperature, ρ_p the unburned propellant density respectively, A_b and A_t the (instantaneous) burning surface area and nozzle throat area, and $c^*$the characteristic velocity, an empirical propellant property.

The engine delivers thrust through the acceleration of the exhaust gasses. Thrust can be calculated from mass flow $\dot{m}$, chamber pressure, exhaust pressure and atmospheric pressure, P_c, P_e, P_c shown in equation D.5. v_e is the exhaust velocity that is derived from isentropic flow equations [24]. In equations D.5 and D.6,D.7 X, c_s and c_p are further provided by the mass fraction of condensed products, and the specific heat for condensed and gaseous products respectively. As can be seen in equation D.5 atmospheric pressure P_a has a small effect on the delivered thrust by providing back pressure to the system, however due to the progressive profile of the BEM this contribution is larger than for typical

neutral burning system.

$$F_t = \dot{m} v_{eff} = \eta_F \dot{m} v_e + (P_e - P_a)\, A_e \tag{D.5}$$

$$v_e = \sqrt{2\left[X c_s + (1-X) c_p\right] T_c \left(1 - \left(\frac{Pe}{Pc}\right)^m\right)} \tag{D.6}$$

$$m = \frac{R}{(X/(1-X))\, c_s + c_p} \tag{D.7}$$

Combined the balance equations for the simulation tool are the following:

$$\frac{dw}{dt} = r(P_c) \tag{D.8}$$

$$\frac{dV_c}{dt} = r\,(P_c)\, A_b(w) \tag{D.9}$$

$$\frac{dP}{dt} = \frac{RT_c}{V(t)} \left(\rho_p A_b(w) r(P_c) - \left(\frac{P_c A_t}{c^*}\right)\right) - \frac{P_c}{V_c}\frac{dV_c}{dt} \tag{D.10}$$

D.1.2. Burning Surface Area and Transient Approximation

$A_b(w)$ is calculated from basic grain geometry. The instantaneous ignition of the full burning surface area results in a relatively simple geometrical equation provided in equation D.12. Including the start up transient is more challenging as the flame-spreading rate or thermodynamic processes inside the motor are not understood. A full description of these transients would require at minimum a 1D gas model with 3D grain burn-back [22] including a transient thermal model connected to 1D heat equations of the propellant surface.

$$0 < w < R_g - R_{port} \qquad Ab = 2\pi(R_{port} + w) L_g \tag{D.11}$$

$$else \qquad A_b = 0 \tag{D.12}$$

A compromise is however possible that, through an implicit assumption of the (upstream) propellant flame-spreading speed and the geometrical starting point of combustion, does still allow a simple mathematical description of grain burn back. The two cases are shown in figure D.1. With igniter impingement and heating from the ignition primer to mainly happen at the nozzle end of the grain this is the most logical starting-point of ignition. If the flame spreading rate is further assumed to be linear $v_f = \lambda_f \cdot r$ with the steady regression rate r [mm/s] this results in a conical burning surface area definition as provided in D.17 with only one free additional parameter, $lamda_f$ or the equivalent cone angle α.

$$0 < w \leq L_g \tan\alpha \qquad Ab = \frac{\pi(2R_p + w)w}{\sin\alpha} \tag{D.13}$$

$$L_g \tan\alpha < w \leq R_g - R_{port} \qquad Ab = (R_p + w)\frac{2\pi L_g}{\cos\alpha} - \pi L_g^2 \frac{\tan\alpha}{\cos\alpha} \tag{D.14}$$

$$R_g - R_{port} < w \leq R_g - R_p + L_g \tan\alpha \qquad Ab = \frac{\pi(R_g + x)(R_g - x)}{\sin\alpha} \tag{D.15}$$

$$x = R_p + w - L_g \tan\alpha \tag{D.16}$$

$$else \qquad A_b = 0 \tag{D.17}$$

The two area curves for the nominal BEM grain ($D_{port} = 25$ [mm], $D_g = 76,4$ [mm], $L = 107$ [mm]) with a flame spreading constant of $\lambda_f = 1/\sin(\alpha) = 1/\sin(1°)$ is shown in figure D.2. It was verified that the integrated total grain volume is conserved for both cases and matches the analytic grain volume. In addition it was verified that $\lim \alpha \to 0$ again yields equation D.12.

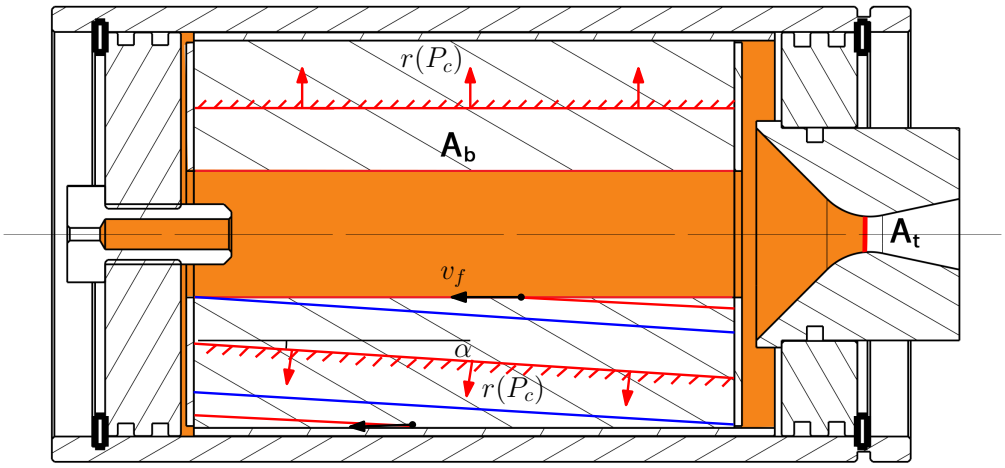

Figure D.1: Two burn back models with perfect instantaneous ignition shown in the upper half and finite flame spreading v_f from the nozzle end shown in the lower half.

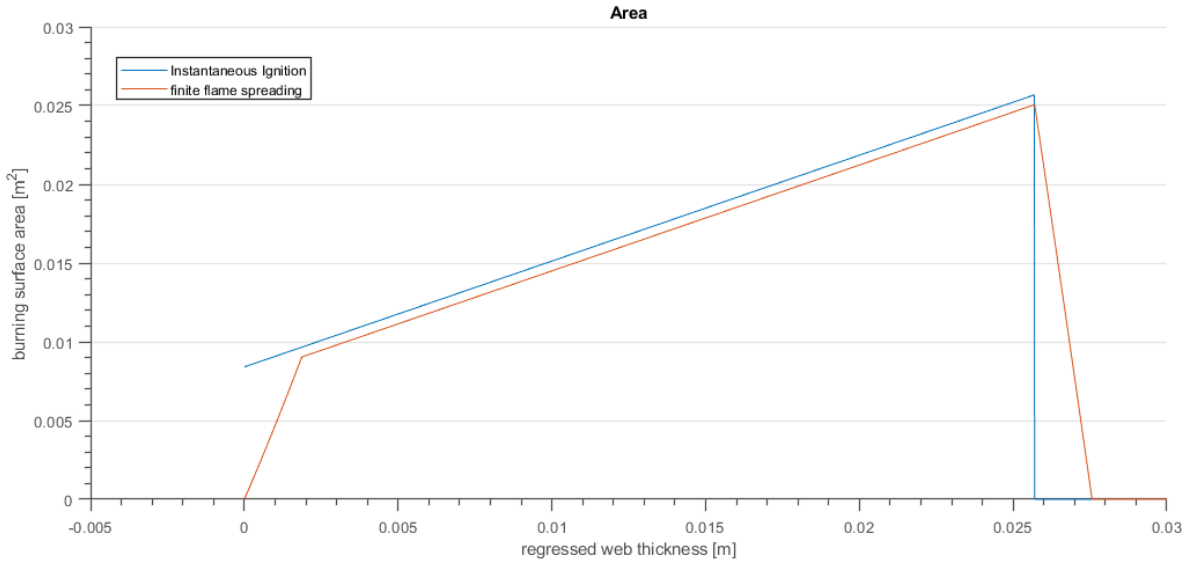

Figure D.2: Resulting burning surface area for two burn back models with perfect instantaneous ignition and finite flame spreading $v_f = \lambda_f r = 1/\sin(1°)r$.

D.2. Simulation Results

With some and tweaking η_b η_F, a and n (the combustion and nozzle quality, and burnrate constants respectively) the thrust and pressure curves can be matched well with experimental results. Pressure and Thrust data is shown in figures D.3 and D.4 respectively. A 3 degree ignition angle equivalent to $\lambda_f r(P_c) = 19.1 r(P_c)$ results in the best match with tail-off behaviour found in experiments.

What is clear from the simulation results is that, although the tail-off behaviour is relatively well matched by the $3\circ$ the start up transient is much steeper than what is simulated. This could be explained by several factors. First of during the first ignition pulse the propellant surface is heated significantly which could significantly increase the burnrate of the propellant locally. A second reason could be the

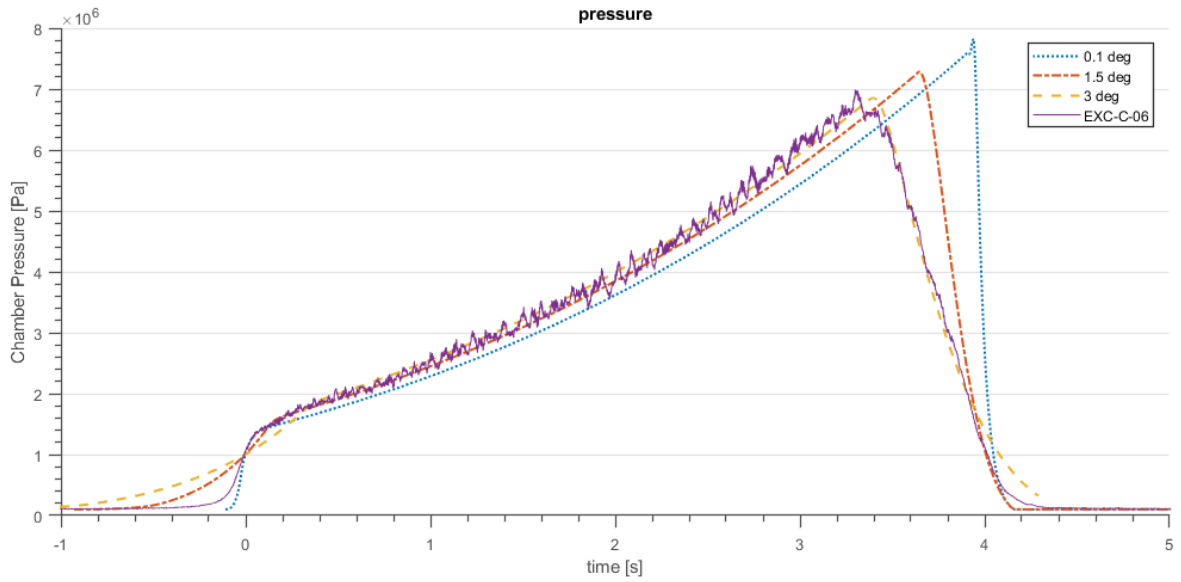

Figure D.3: Measured and simulated pressure data for EXC-06-C with varying ignition angle.

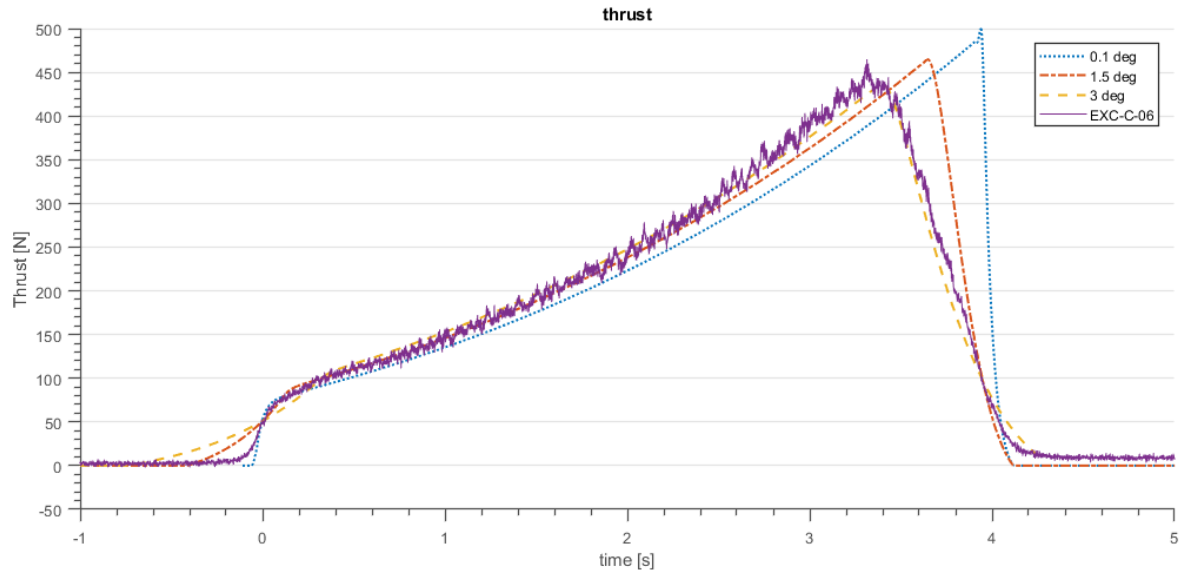

Figure D.4: Measured and simulated thrust data for EXC-06-C with varying ignition angle.

assumed burnrate not being representative for propellant behaviour below 1-1.5 [MPa]. Thirdly Lastly the assumed instantaneous burning surface area might not be accurate resulting in a more pronounced initial pressure built up.

The simulation case data generated from the 3° case with varying burnrate is shown in figure D.5 and D.6. This data set (geometrical data, mass data) is used for tailoring the experimental method as discussed in section 6.8. Selected cases are generated with the burn rates are provided in equations D.19 (all S.I. Units) with and without added noise.

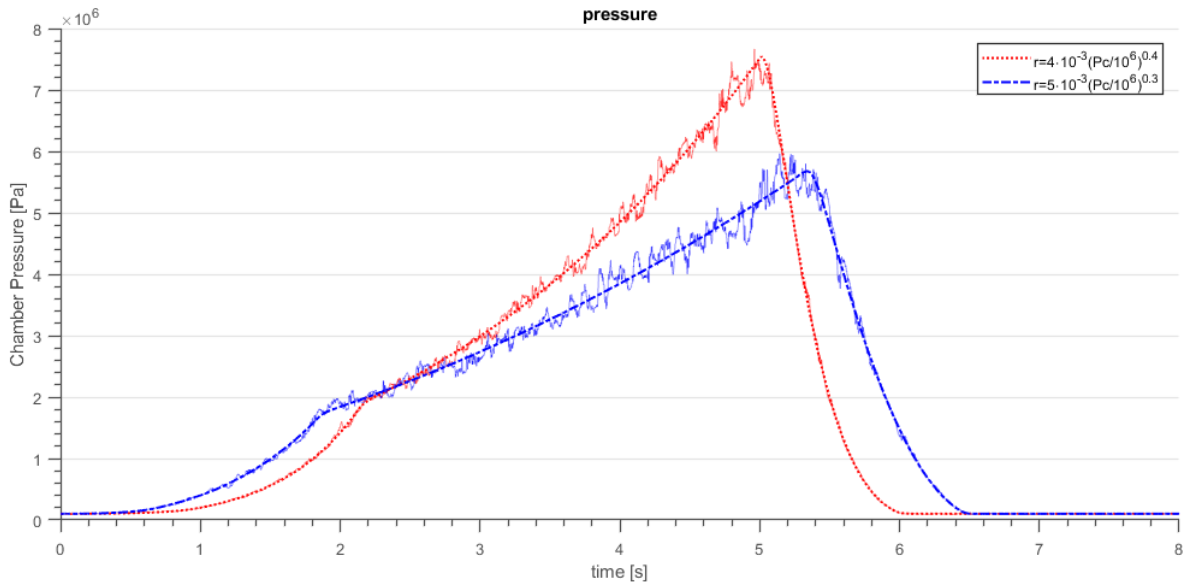

Figure D.5: Simulated pressure data with two different burn rates given in equation D.19.

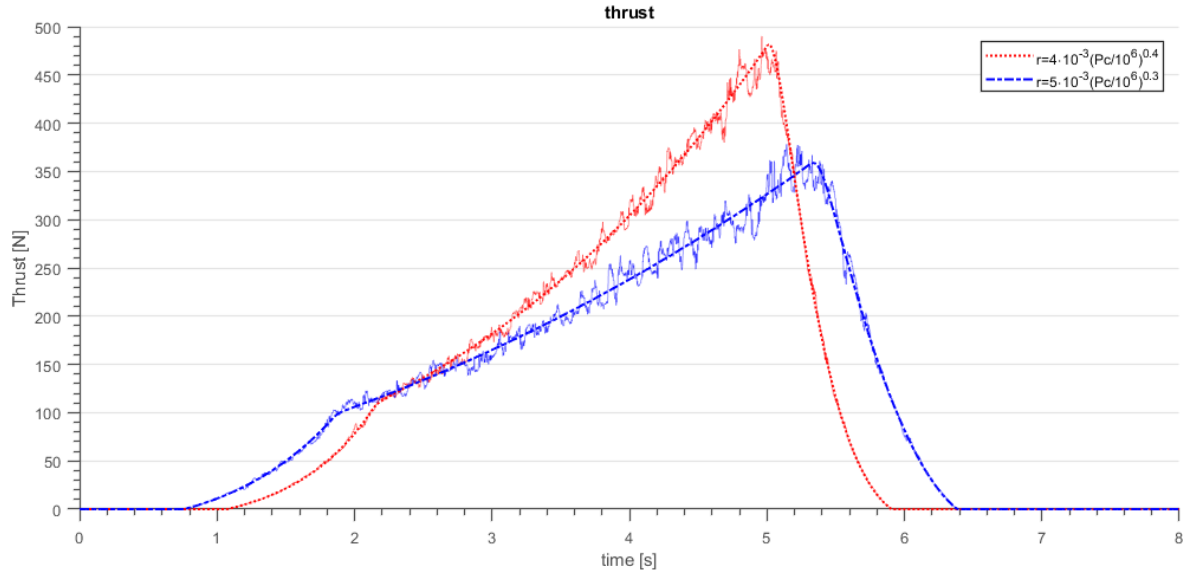

Figure D.6: Simulated thrust data with two different burn rates given in equation D.19.

$$r_1 = 4 \cdot 10^{-3} \left(\frac{P_c}{1 \cdot 10^6} \right)^{0.4} \quad \text{[m/s]} \tag{D.18}$$

$$r_2 = 4 \cdot 10^{-3} \left(\frac{P_c}{1 \cdot 10^6} \right)^{0.3} \quad \text{[m/s]} \tag{D.19}$$

E

Ballistics Evaluation Motor

This chapter describes the ballistics evaluation motor (BEM) design used for the determination of the steady regression rate of Potassium Nitrate Sorbitol (KNSB) during the thesis project of the author. The design was created using Catia V5R21[48].

The design is based on the design described in [4, 5] and [10]. It allows testing the regression rate over a larger pressure range with a linear increasing klemmung. This allows more rapid evaluation of the propellant burnrate as function of pressure and propellant initial temperature. The BEM should be safe and reusable. Furthermore a significant number of tests needed to be completed (refer to 5) within a minimum number of days. These constraints and practical considerations needed to be included in the design. Lastly this BEM design is the first DARE SRM design that will use circlips (dutch: zegering) instead of the - DARE standard- radial bolts, therefore specific attention is paid to its structural design.

This chapter consists of 9 sections. First a brief design description will be provided in section E.1, design requirements will be provided in E.2. The general design will be provided in section E.1-E.7 which includes preliminary simulations, safety analysis and design failure mode analysis. Subsequently, in chapter E.8, a requirement verification matrix is provided which shows the design meets it design requirements. Detailed design drawings and production photos can be found at the end in section E.9.

E.1. BEM Design Summary

An overview of the BEM design is shown in figure E.1. The design was created in 4 steps outlined below. This report will follow roughly the same structure, however it must be noted that the design effort is highly iterative process.

1. First the ballistic design was created using *srm2014.xlsx* [49] for both course and fine KNSB to achieve the desired operating pressure range. (refer to BEM-PERF-1_1).
2. The design was iterated to favourable casing dimensions such that the required material was available of the shelf.
3. The safety limits of the system were evaluated; although the BEM design is reasonably generic it does need to be fired at the fellowship within the framework of the MSc thesis project.
4. The detailed design of all mechanical connections and interfaces. This included the detailed the technical drawings.
5. The test bench interfaces and tooling such as the casting moulds were designed.
6. The structural design was validated with a tensile load test, this led to the final selection of the external groove depth.

The final BEM design is shown in figure E.1. Total NEM for an ideal KNSB propellant grain ($\rho = 1841$ [kg/m^3]) of 10 [cm] length is 0.758 [kg]. More detailed assembly and production drawings are provided in the appendix E.9.

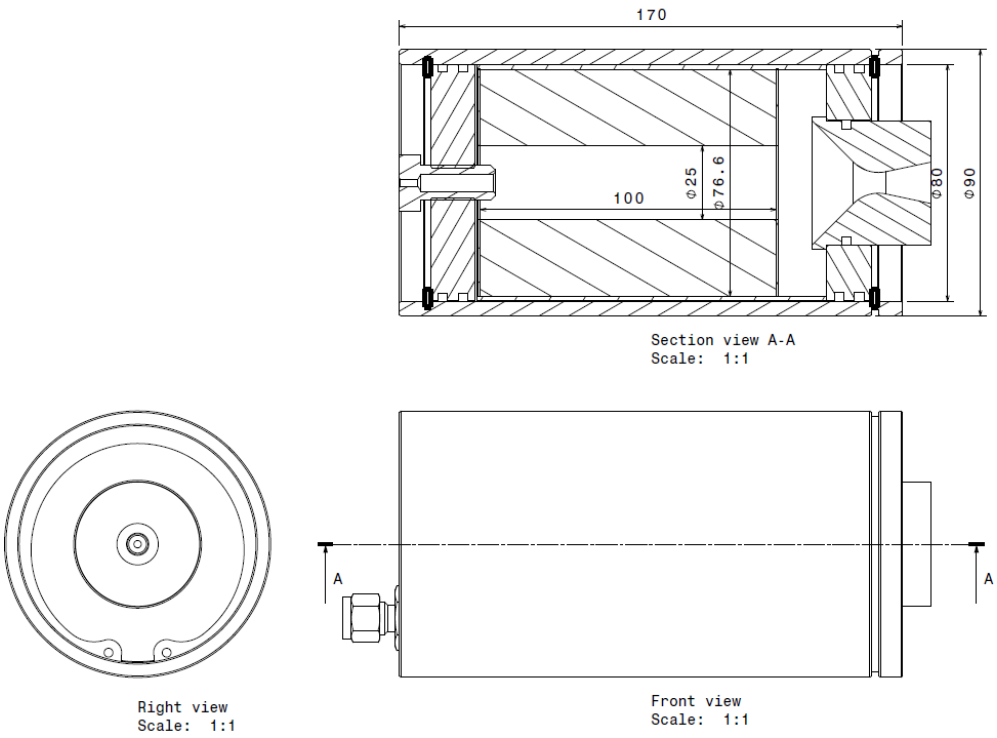

Figure E.1: The design of the BEM (version 2) with rough dimensions.

E.2. Design Requirements

The Ballistics evaluation motor (BEM) is based on the design recommended by [4] based on setups found in industry. This design is shown in figure E.2. Design recommendations are the following:

1. Propellant mass should be at least 300-400g to achieve sufficient accuracy and comparability.
2. The design shall use cartridge loaded grains for easy cleaning and fast changeover.
3. The design shall utilise an exchangeable nozzle throat insert.

From DARE safety several requirements are applicable. With respect to the pressure vessel design they are as listed in [66]. In addition several requirements are stated with respect to the handling of pyrotechnics. Although generally these requirements are not thoroughly documented in DARE as systems differ to much for universal application. When applicable for this setup they will be provided explicitly.

E.2.1. Requirement Identifier Strategy

The requirement numbering strategy is provided below. The identifiers in this document are briefly explained below:

BEM-SAFE-2.2_1

BEM refers to the system under design. The second code (SAFE) refers to the category of requirements, a short list of categories is provided below. The subsequent number (2.2) refers to the number with children listed after a dot. _1 refers to ID version. Requirements without category (e.g. BEM-1.2) are system requirements. MoV refers to method of validation; A=Analysis, S= Simulation (Matlab, Python, CFD etc.),R= Review (external), T=Testing.

- SAFE: safety requirements as defined in collaboration with the DARE safety board.
- FUNC: Functional requirements

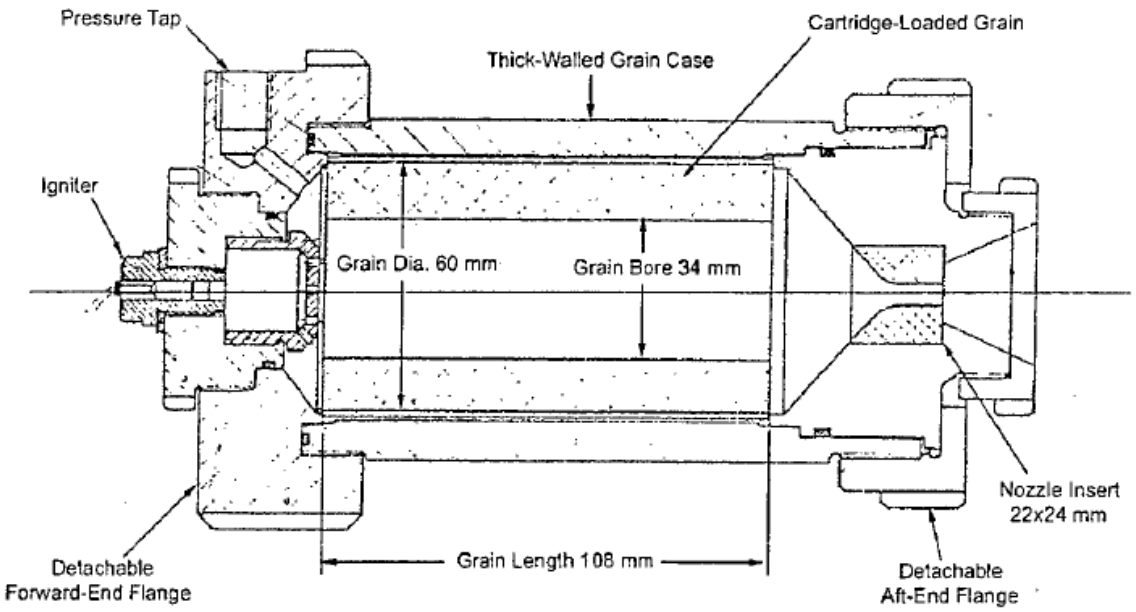

Figure E.2: Design of a typical BEM from Fry et al.

- PERF: Performance requirements

The text in italics provide some clarification or additional information with respect to the requirements.

E.2.2. Ballistics Evaluation Motor Design Requirements

System Requirements

Identifier	Parent	Requirement	MoV
BEM-1_1		The BEM shall allow the determination of KNSB propellant regression speed at varying pressure and temperature *i.e. general purpose of the device as determined in the MSc literature study [16]*	A
BEM-2_1		The BEM shall meet DARE safety requirements *i.e. be safe for students to work with.*	A,R
BEM-3_1		The BEM shall meet budget requirements as specified in [MC-MNT-DOC-4_1] *i.e. meet all financial constraints as defined in the thesis budget*	A

Table E.1: BEM system requirements.

E.2.3. Safety Requirements

Identifier	Parent	Requirement	MoV
BEM-SAFE-1_1	BEM-2_1	The BEM design shall pass the DARE safety review *As well as can be practically determined by review from the DARE safety board, the system shall not cause an unacceptable risk to:* • *The general public* • *DARE personnel* • *3d party property* • *DARE critical property (i.e. DAQ systems)*	A,R
BEM-SAFE-2_1	BEM-2_1	The system shall allow for an arm and disarm procedure while installed on the test bench *Igniter installation shall be reversible while the system is constrained*	A,R
BEM-SAFE-3_1	BEM-2_1	The BEM shall be compatible with the DARE firing system *i.e. use squibs, and the DARE launch boxes for ignition.*	A,R
BEM-SAFE-4_1	BEM-2_1	Risks associated with failure of the system due to over pressurization shall be constrained to the test area *i.e. the safety radius shall be explicitly evaluated and this distance shall fit within the available space*	A,R
BEM-SAFE-5_1	BEM-2_1	The BEM design shall follow the DARE pressure vessel design guidelines as provided in sub requirements 5.1-5.3 *e.g. requirements with respect to used safety factors etc.*	A,R
BEM-SAFE-5.1_1	BEM-SAFE-5_1	The BEM shall include a design failure mode *The pressure at failure is input to BEM-SAFE-5_1*	A,T
BEM-SAFE-5.2_1	BEM-SAFE-5_1	The design failure mode shall be between 1.5 to 2 times the MEOP, other failure modes shall be above 2 times MEOP *To assure a descent safety margin but also to limit the maximum pressure at failure*	A,T
BEM-SAFE-5.3_1	BEM-SAFE-5_1	Yield of structural elements shall not occur below 1.25 MEOP (equal to about 85% of the design failure mode) *To assure full re-usability of the hardware in case of over pressurization*	A,T
BEM-SAFE-6_1	BEM-2_1	Propellant shall meet minimal quality criteria as defined in I *To assure the minimal risk of system malfunctions due to propellant faults.*	A,T

Table E.2: BEM safety requirements.

E.2.4. Functional Requirements

Identifier	Parent	Requirement	MoV
BEM-FUNC-1_1	BEM-1_1	The regression rate shall be determined by measuring pressure and system temperature during the test	A
BEM-FUNC-2_1	BEM-1_1	Nominal operating pressures are defined 2-7.5 [MPa] at at nominal operating conditions *i.e. propellant pressure range of interest shall be between 2-7.5 [MPa]*	A
BEM-FUNC-3_1	BEM-1_1	The BEM shall be compatible with the minor test bench *i.e. the test bench as described in [53].*	A
BEM-FUNC-4_1	BEM-1_1	The BEM shall be compatible with general DARE experimental practices and facilities. These are: • Outdoor • Non-Permanent Setup *i.e. outside on the fellowship field, with a removable setup*	A
BEM-FUNC-5_1	BEM-1_1	Nominal operating conditions are defined in the outdoors, between 0 to 30 [°C] at sea level *i.e. temperature range to be tested*	A
BEM-FUNC-6_1	BEM-1_1	Re-usability of the system shall be considered *i.e. it should be efficiently cleaned, and use easy reloads for using again.*	A
BEM-FUNC-7_1	BEM-1_1	Nozzle inserts shall be replaceable *i.e. to allow it to be used in future systems as well*	A
BEM-FUNC-8_1	BEM-1_1	Propellant shall meet grain acceptance criteria *i.e. Meet minimal standards on propellant density and surface defects to assure behaviour is approximately as expected.*	

Table E.3: BEM functional requirements.

E.3. Nozzle Design

Although not its primary function, the system is also going to be used for the determination of motor performance (thrust is measured via the test-bench). As such the nozzle should be designed with some consideration. In addition the two propellant variants to be tested with the BEM have slightly different regression characteristics. As such the nozzles will be tailored to the propellant specifically. This results in two custom nozzles for both cases.

Based on literature the nozzle longitudinal radius of at least two times the nozzle throat radius [16]

was selected. In addition the nozzle divergence half angle shall be 12 [°] conform recommendations by [63]. As over-pressure in a nozzle is easier to predict than under pressure due to flow separation effects, the expansion ratio is picked as optimum for the lower pressure ratio requirement (BEM-FUNC-2_1), in addition this results in the shortest nozzle for the application. This is results in an expansion ratio of 4.

Lastly, from a manufacturing constraint it is recommended to not create nozzles with throat diameters smaller then 6 mm as this would pose limits on CNC tooling available in the D:Dreamhal

E.4. Proposed Ballistic Design

The BEM has two main operating modes: 1) with an end and externally inhibited grain to produce a linearly progressive burn-profile and 2) with only the exterior of the grain inhibited (BATES grain) resulting in a nearly flat burn profile. Independent of the propellant, the klemmung K (geometrical ratio A_b/A_t) is given for both cases. In the remainder of this document the end inhibited grain will be the default configuration conform the experiments described in chapter 6.

For the end inhibited grain, assuming constant throat area:

$$\frac{K_{max}}{K_{min}} = \frac{A_t}{A_t}\frac{L \cdot 2 \cdot \pi \cdot R_e}{L \cdot 2 \cdot \pi \cdot R_i} = \frac{1 \times 10^{-1} \cdot 2 \cdot \pi \cdot 3.83 \times 10^{-2}}{1 \times 10^{-1} \cdot 2 \cdot \pi \cdot 1.25 \times 10^{-2}} = \frac{2.4 \times 10^{-2}\ [\mathrm{m}^2]}{7.85 \times 10^{-3}\ [\mathrm{m}^2]} = 3.045\ [\text{-}] \tag{E.1}$$

For the standard BATES grain with also the ends burning this ratio is given in equation E.2, the initial, maximum and final (minimum) areas are given for the flat burn profile.

$$K_x = \frac{A_b(x)}{A_t} = \frac{2 \cdot \pi \left((R_e^2 - (R_i + x)^2 + (L - 2x)(R_i + x)\right)}{A_t} \tag{E.2}$$

This results in the following areas throughout the burn.

$$\begin{aligned} A_{b,i} &= 1.61 \times 10^{-2}\ [\mathrm{m}^2] \\ A_{b,max} &= 1.74 \times 10^{-2}\ [\mathrm{m}^2] \\ A_{b,min} &= 1.16 \times 10^{-2}\ [\mathrm{m}^2] \end{aligned} \tag{E.3}$$

For the optimum horizontal burnrate the grain core diameter or grain length could be slightly adapted. Similarly the nozzle throat diameter is highly configurable through separate steel inserts (refer to BEM-FUNC-7_1). This allows tailoring of the design to the specific klemmung needed. As this part is to be a variable feature of this BEM design, the nozzle internal geometry and specifically the throat diameter will be included for the KNSB propellant variations to be used in this MSc thesis study. The nominal nozzle geometry is shown in figure E.3.

E.4.1. Ballistic Simulations

Using *SRM2014.xlsx* [49] a simulation was performed for both fine and course KNSB using burnrate data and densities reported by [6] and [63]. This results in the following graphs. A clear dependency is seen of the burnrate on the pressure contour observed in the figures.

E.4.2. Igniter Design

Conform the requirements the standard ignition system shall be used. This includes a Davey Brickford electric match and gunpowder charge. Although the detailed effects of the amount of blackpowder cannot be currently evaluated it is expected that 1.5 grams, together with 0.5 gram of a nitrocellulose/ blackpowder ignition primer will be sufficient for efficient ignition of the center port. This is equal to the charges used with the SRP motor [16].

Normal installation occurs via a nozzle mounted bag igniter however the small size of the nozzle throat (7 mm) makes this in practical. Instead a bolt mounted igniter design was chosen with the squib glued into a custom M12 Bolt.

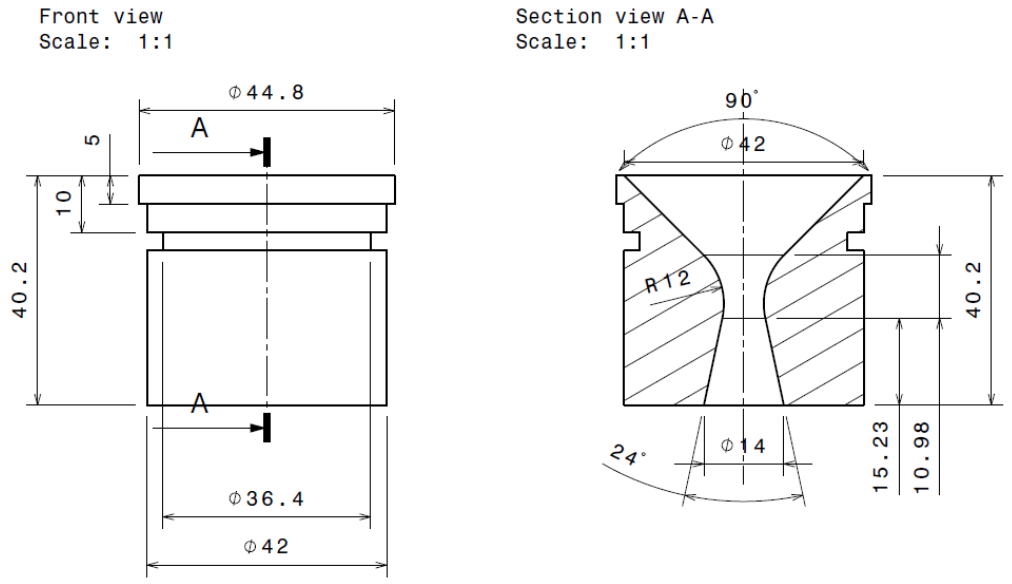

Figure E.3: Nozzle nominal geometry for a 7 mm throat and expansion ratio of four.

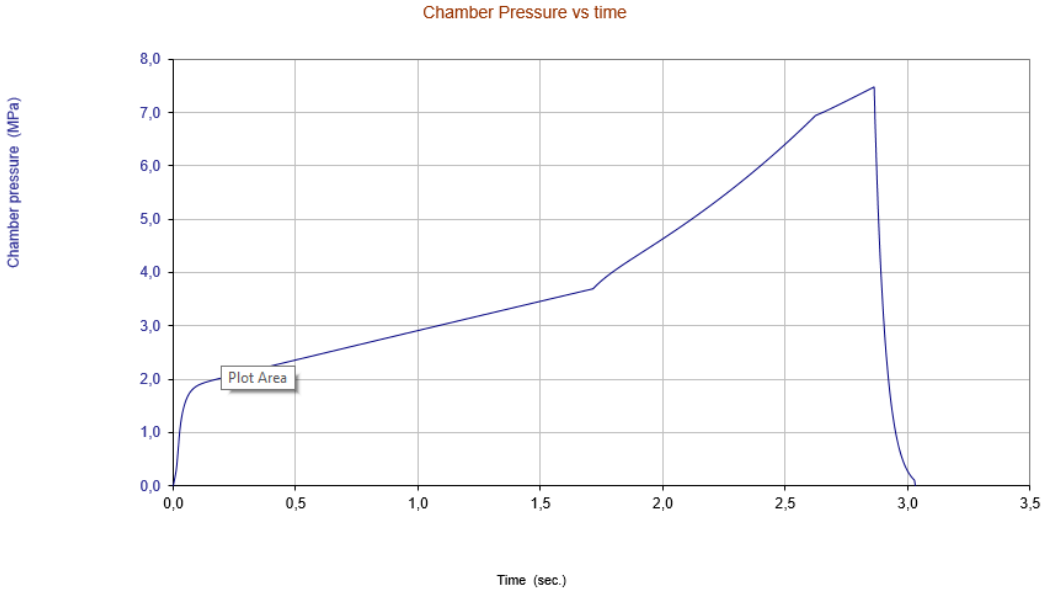

Figure E.4: Simulation using *SRM2014.xlsx* for the nominal case of fine KNSB propellant with an 8.37 mm throat. Chamber Pressure in MPa.

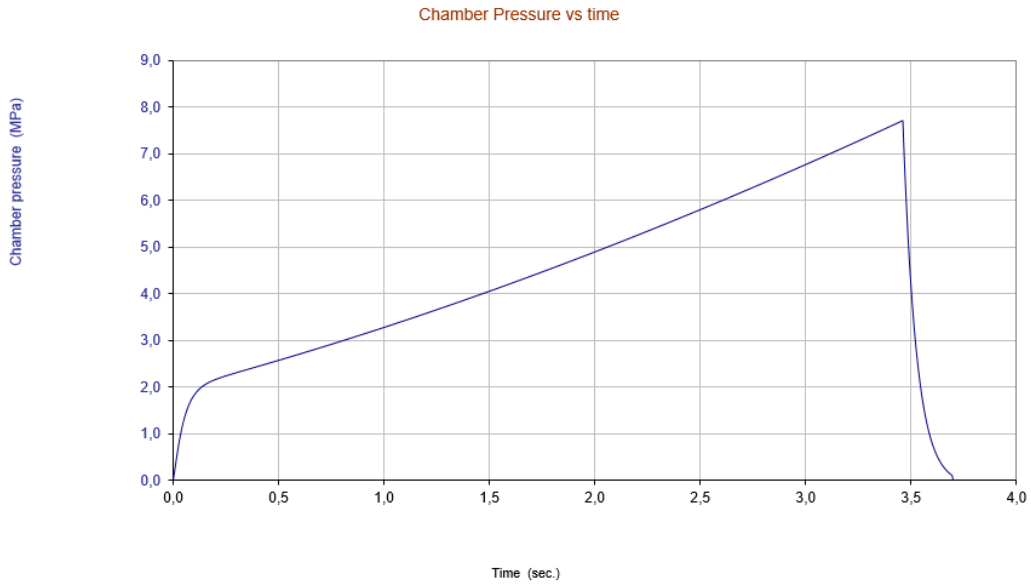

Figure E.5: Simulation using *SRM2014.xlsx* for the nominal case of course KNSB propellant with a 7.01 mm throat. Chamber Pressure in MPa.

E.5. Minimum Safety Measures

Conform the requirements BEM-SAFE-4_1, BEM-SAFE-5_1 an analysis is performed of the required safety distance and shrapnel protection around the system. First the failure scenarios will be described including the applicable theory. Subsequently these scenarios will be evaluated. In the last section the recommendations will be provided. The identified hazards are the following:

1. Pressure wave Hazard
   In case of a sudden over pressurization and failure of the pressure vessel, the energy contained in the pressure vessel is rapidly released to the atmosphere. This creates a pressure wave that can potentially be a risk to people, test equipment or property.
2. Shrapnel Hazard
   In case of sudden failure of the system, parts of the system can be rapidly accelerated away from the system. This shrapnel can be a risk to people, test equipment or property.

E.5.1. Pressure Wave Hazard

Theory

The common way of estimating the required safety distance is the calculation of the systems equivalent amount of TNT. For TNT equivalent mass several empirical relations exist that provide shock wave pressure and duration as a function of the distance to the system. The amount of energy contained in the system assuming isentropic expansion of an ideal gas is given in equation E.4 [45].

$$E_{baker} = \frac{P_{burst} V}{\gamma - 1}\left[1 - \left(\frac{P_{atm}}{P_{burst}}\right)^{\frac{\gamma-1}{\gamma}}\right] \tag{E.4}$$

Subsequently the TNT equivalent mass is calculated through equation E.5. One kilogram of TNT equals 4.184 [MJ] of released energy.

$$M_{TNT,eq} = \frac{E_{baker}}{E_{TNT}} = \frac{E_{baker}}{4.184x10^6} \tag{E.5}$$

The last step is calculating the minimum safety distance for a surface detonation of the equivalent mass of TNT. Using this in the pressure wave equation from [31] the safe distance where a maximum pressure difference of 0.05 [kg/cm^2] occurs will be calculated. Experiments have shown that this is the threshold pressure below which the risk to buildings (windows), surrounding personnel and equipment is acceptable. Note that ΔP is in units of [atm] [31].

$$\Delta P_{atm} = 0.95\frac{(M_{TNT,eq})^{1/3}}{r} + 3.9\frac{(M_{TNT,eq})^{2/3}}{r^2} + 13.0\frac{(M_{TNT,eq))}}{r^3} \tag{E.6}$$

An alternative limit can be imposed by looking at sound limits. Typically these are provided in [DB] for periodic signals. Compared to explosions a firearm (at 1 [m]) or firecracker (at 3 [m]) typically generates sound levels of around 150 [dB] [28]. Above 140 dB hearing damage might occur and hearing protection is needed when firing firearms. The translation to the sound pressure level in [dB] is subsequently done via equation E.7. $P_{ref} = 20$ [μPa] is the decibel reference level. Note that for fireworks a maximum sound level of 156 [dB] at 2 meters is accepted in the Netherlands.

$$I_{dB} = 20\log\left(\frac{\Delta P_{rms}}{P_{ref}}\right) \tag{E.7}$$

Assumptions

To make a quantitative evaluation possible several assumptions need to be made. These are outlined below.

- Failure pressure is the maximum design operating pressure of 7.5 [MPa] multiplied with the design safety factor of 1.5. This yields a rupture pressure of 11.25 [MPa]. Failure with the design safety factor of 2 yields a rupture pressure of 15 [MPa].
- Maximum system volume is defined by a 80 [mm] $\varnothing$, 150 [mm] length cylindrical pressure vessel for a total volume of 7.54×10^{-4} [m^3]

- At system rupture the maximum internal volume is filled with hot exhaust gasses $\gamma = 1.13$ [16] at the design failure pressure. As KNSB propellant does not detonate, the situation at burnout with all propellant consumed is most conservative.
- The system fails instantaneously, and creates an isentropic, hemispherical pressure wave.
- Ambient pressure is equal to 10^5 [Pa].

Results

Based on the above equations a calculation tool was written. The results are shown in figure E.6 and E.7. What can be seen is that structural damage from the blast wave in the case of full system failure will be limited to a few meters around the setup. The DARE DAQ is located inside a very rigid box and as such is expected to easily survive at about 3-5 meters from the setup.

Minimum acceptable distance with respect to hearing damage is 27 meters however as the gradient at that distance is not very steep it is recommended to keep spectators at least 50 meters away for a sufficient margin. Operators at 27 meters should wear hearing protection.

Note that the equations assume instantaneous pressure release, isentropic expansion and a perfect non-absorbing ground. In addition failures due to cracks occur typically at the start of the burn where the gas volume is less than half of the final, conservative volume used in calculation. This means that the expected failure of the system is likely to be significantly lower and is thus a conservative margin. Additionally, increasing the rupture pressure to 15 [MPa] increases the distances only marginally as such the calculated values are considered.

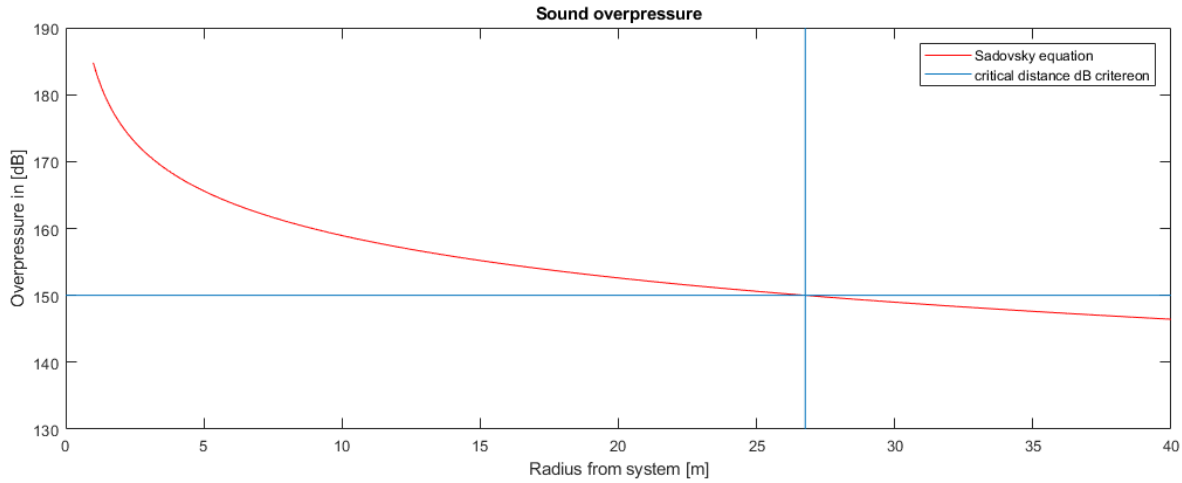

Figure E.6: Maximum sound intensity as function of distance from the setup. Critical distance for 150 dB, similar to the firecracker at 3 meter.

E.5.2. Shrapnel Hazard

Shrapnel formation is challenging as ejected components can reach velocities in the order of 30 [m/s]. For a poorly designed pressure vessel this shrapnel can move in unpredictable directions.

For DARE this is mitigated in the following way. An example of the setup with sandbags in place is shown in figure E.8.

- Using a well defined failure mode, in this case nozzle blowout that defines the direction of any shrapnel.
- Using several sandbags downstream of the nozzle to catch any debris.
- Using a wooden shrapnel box to cover the setup. This will catch any debris in other directions.
- Using several sandbags around the setup to weigh down the shrapnel box.

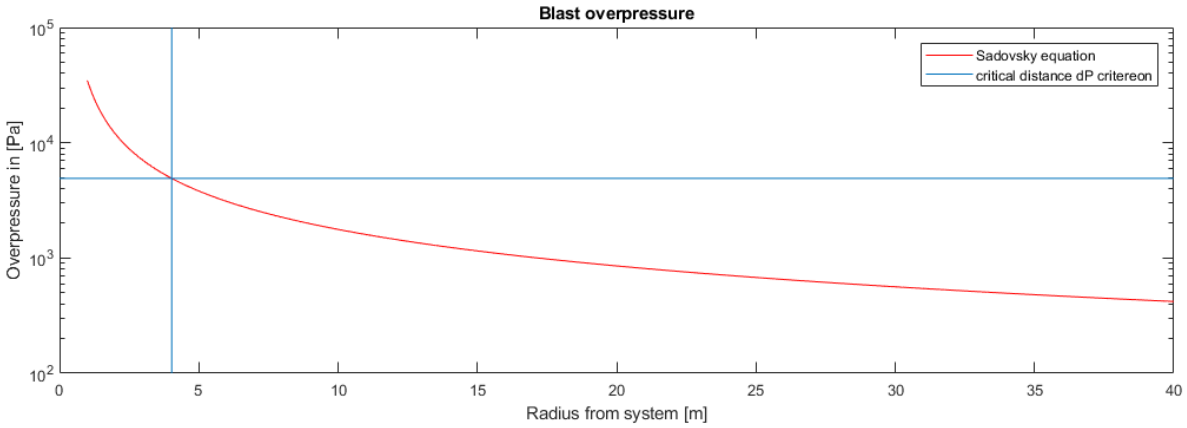

Figure E.7: Maximum pressure as function of distance from the setup. Critical distance is 0.05 [kg/m^2] below which structural elements like windows will not get damaged.

Figure E.8: Figure of an SRP test done on 21-12-2017. Shown are the shrapnel box, sandbags around the setup and downstream of the nozzle.

E.5.3. Conclusion

The main risk to safety are pressure wave and shrapnel caused in the event of pressure vessel rupture. The pressure wave was considered quantitatively, the shrapnel hazard addressed qualitatively. These evaluations were conservative considering worst case scenarios.

With respect to the pressure wave hazard the critical assumptions are: the lack of damping from sandbags and cover, instantaneous pressure release, maximum gas volume, ideal isentropic relations and the lack of a directional effect. It is therefore expected that the actual sound level in case of failure is at least 10 dB lower. Increasing the failure pressure to 15 [MPa] (compared to 11.25 [MPa]) has a marginal effect on the recommended distances. The calculated values are provided below. A minimum safety perimeter is proposed based on experiences from gunfire safety where sound levels above 140 dB are considered problematic with respect to hearing damage. therefore, based on the calculations, testing personnel should stay at least 27 meters away from the setup and wear hearing protection. Spectators should be at least 50 meters away from the setup. Furthermore the firing axis should be tangential to the operators and spectators. All The applicable distances are summarized in table E.4.

Level	ΔP [Pa]	Distance [m]
Damage to Structures and windows	4.9×10^3 (0.05 [kg/m^2])	4
Maximum Acceptable Noise Level Operator with hearing protection	6.23×10^2 (150 [dB])	27
Recommended Distance Spectators	3.32×10^2 (145 [dB])	50

Table E.4: Summary of critical safety distances for the BEM system.

The shrapnel hazard is more difficult to analyze. Standard DARE practises are recommended with a shrapnel box and sandbags. The design failure mode is nozzle blow out, for this purpose a sandbag is placed 6 meters downstream of the nozzle. No people should be within the cone extended by the nozzle and shrapnel box.

Considering the very conservative margin and the fact that it comprises a critical failure scenario, not nominal operation, it is expected that with the following recommendations the BEM system can be used safely.

E.6. System Structural Design

Below is a description of the BEM structural design of the pressure vessel. This includes definition of the load cases, material values used in the calculations and the resulting safety margins. The expected maximum operating point is 7.5 [MPa] conform the BEM-PERF-1_1. The design safety margin is to the lowest failure mode shall be 1.5-2 times this value in accordance with BEM-SAFE-5_1.

The design will use thin wall pressure vessel calculations to obtain values for the pressure vessel. The Circlips will be calculated through the DIN 472 Handbook provided by Seeger Orbis GmbH [32].

As the stress concentrations are difficult to predict, the groove depth is chosen as a nominal value only. A tensile test (refer to section E.6.3) will validate the design load and determine the final depth of the external groove.

E.6.1. Material Properties

Material properties for the AW-6060 T66 casing as specified by `AluminiumOpMaat.nl`. The rings are defined according do DIN 472 and supplied through Jeveka. The applicable documentation is found in [30].

E.6.2. Failure Mode Analysis

The required load case is a pressure of $1.5 - 2$ times the operating pressure of 7.5 [MPa]. This results in the following load case:

$$\begin{aligned} P_{load,min} &= 1.5 \cdot 7.5 \times 10^6 \rightarrow 112.5\text{[bar] lower limit} \\ P_{load,max} &= 2 \cdot 7.5 \times 10^6 \rightarrow 150\text{[bar] upper limit} \end{aligned} \tag{E.8}$$

The failure modes that are considered are:

1. Chamber Radial Failure
   Radial failure of a thin walled pressure vessel is given in equation E.9.

$$\begin{aligned} P_{max} &= \frac{\sigma_x \cdot t}{R} = \frac{1.60 \times 10^8 \cdot 5 \times 10^{-3}}{4.0 \times 10^{-2}} \rightarrow 200 \text{ [bar] yield} \\ P_{max} &= \frac{\sigma_u \cdot t}{R} = \frac{2.15 \times 10^8 \cdot 5 \times 10^{-3}}{4.0 \times 10^{-2}} \rightarrow 269 \text{ [bar] ultimate} \end{aligned} \tag{E.9}$$

Property	symbol	Value	Unit	Source
Yield Stress	σ_x	160	[MPa]	Nedal Aluminium datasheet
Ultimate Stress	σ_u	215	[MPa]	Nedal Aluminium datasheet
Nominal Wall Thickness	t	5	[mm]	
Inner Radius	R	40	[mm]	
Circlip Groove Depth	t_i	2	[mm]	
Circlip Groove width	s	2.5	[mm]	
Collar to groove depth Ratio	n/t	4	[-]	see [32] p. 38
External Groove depth	t_e	1.75	[mm]	initial -nozzle side only
External Groove depth	t_e	2	[mm]	final -nozzle side only

Table E.5: Aluminium AW-6060 T66 Casing and 80mm x 2.5 mm Circlip specifications.

2. Chamber Axial Failure
First the nominal casing failure is provided. Subsequently both CirClips grooves are calculated, both the wall thickness at the forward closure and the wall thickness at the nozzle closure.

(a) Nominal Axial Failure
Axial failure of a thin walled pressure vessel is given in equation E.10.

$$\begin{aligned} P_{max} &= \frac{2 \cdot \sigma_x \cdot t}{R} = \frac{2 \cdot 1.60 \times 10^8 \cdot 5 \times 10^{-3}}{4.0 \times 10^{-2}} \rightarrow 400 \text{ [bar] yield} \\ P_{max} &= \frac{2 \cdot \sigma_u \cdot t}{R} = \frac{2 \cdot 2.15 \times 10^8 \cdot 5 \times 10^{-3}}{2 \cdot 4.0 \times 10^{-2}} \rightarrow 538 \text{ [bar] ultimate} \end{aligned} \tag{E.10}$$

(b) Axial Failure at forward CirClip
At the forward Circlip the wall thickness is reduced by the groove depth of $t_i = 2$ [mm] to $t = 3$ [mm]. Similar equations apply. Stress concentrations will be considered in more detail in section E.6.3.

$$\begin{aligned} P_{max} &= \frac{2 \cdot \sigma_x \cdot t}{R} = \frac{2 \cdot 1.60 \times 10^8 \cdot 3 \times 10^{-3}}{4.0 \times 10^{-2}} \rightarrow 240 \text{ [bar] yield} \\ P_{max} &= \frac{2 \cdot \sigma_u \cdot t}{R} = \frac{2 \cdot 2.15 \times 10^8 \cdot 3 \times 10^{-3}}{4.0 \times 10^{-2}} \rightarrow 322 \text{ [bar] ultimate} \end{aligned} \tag{E.11}$$

(c) Axial Failure at aft CirClip (design failure mode)
At the aft CirClip, near the nozzle, an additional external notch is present to lower the failure load to the required value. This notch is $t_e = 1.75$ [mm] deep resulting in a total wall thickness of only $t = 1.25$ [mm]. Not considering stress concentrations this results the following failure loads. As stated before stress concentrations will be considered in more detail in section E.6.3.

$$\begin{aligned} P_{max} &= \frac{2 \cdot \sigma_x \cdot t}{R} = \frac{2 \cdot 1.60 \times 10^8 \cdot 1.25 \times 10^{-3}}{4.0 \times 10^{-2}} \rightarrow 100 \text{ [bar] yield} \\ P_{max} &= \frac{2 \cdot \sigma_u \cdot t}{R} = \frac{2 \cdot 2.15 \times 10^8 \cdot 1.25 \times 10^{-3}}{4.0 \times 10^{-2}} \rightarrow 134 \text{ [bar] ultimate} \end{aligned} \tag{E.12}$$

3. Circlip Groove Failure
   Besides the axial failure of the groove also the groove itself can fail as specified in the technical documentation [32]. This failure is due to plastic deformation of the groove edge and needs to be modified for the values provided by [30] as the groove material is aluminium instead of steel. A_p and A_N are the port and groove area respectively [m^2] given in equation E.13. q is a constant defined by the collar to groove depth length ratio. For collars larger than $4t_i$ this is equal to 1.

$$\begin{aligned} A_P &= \pi R^2 = \pi(4.0 \times 10^{-2})^2 = 5.027 \times 10^{-3} \text{ [m}^2\text{]} \\ A_N &= \pi\left((R + t_i)^2 - R^2\right) = \pi\left((4.2 \times 10^{-2})^2 - (4.0 \times 10^{-2})^2\right) = 5.152 \times 10^{-4} \text{ [m}^2\text{]} \end{aligned} \tag{E.13}$$

$$\begin{aligned} P_{max} &= \frac{F_N}{A_P} = \frac{\sigma_x \cdot A_N}{q \cdot A_P} = \frac{1.60 \times 10^8 \cdot 5.152 \times 10^{-4}}{1 \cdot 5.027 \times 10^{-3}} \rightarrow 164 \text{ [bar] yield} \\ P_{max} &= \frac{F_N}{A_P} = \frac{\sigma_x \cdot A_N}{q \cdot A_P} = \frac{2.15 \times 10^8 \cdot 5.152 \times 10^{-4}}{1 \cdot 5.027 \times 10^{-3}} \rightarrow 220 \text{ [bar] ultimate} \end{aligned} \tag{E.14}$$

4. Circlip Failure
   Failure of the Circlip occurs primarily due to conical deformation. This can be calculated via equation E.15. Ψ is defined in [32] for an 80 [mm] ring to be 0.25 The factor $h = 0.3 + 0.002d_1$ [mm] for sharp cornered faces gives $0.3 + 0.002 \cdot 80$ [mm] = 0.46 [mm]. K is the spring constant and equal to 241000 [N mm]. This results in the following equation:

$$P_{max} = \frac{F_R}{A_P} = \frac{\Psi \cdot K}{h \cdot A_P} = \frac{0.25 \cdot 2.41 \times 10^5}{0.46 \cdot 5.027 \times 10^{-3}} \rightarrow 261 \text{ [bar] yield} \tag{E.15}$$

E.6.3. Structural Design Validation

The calculation of the failure modes is done without explicit evaluation of the stress concentrations and or friction effects. Two solutions could be used to evaluate these: a FEM analysis of the grooves, and mechanical testing of the final connection on the D:Dream Tensile test bench. This will allow careful evaluation of the required external groove depth to meet the required failure pressure.

The FEM analysis is very dependent on the achieved groove chamfers. This requires careful analysis of the mesh and convergence to eliminate unrealistic results. Additionally production tolerances are difficult to fully analyze in FEM. As such experimental determination is the preferred testing mode.

As the failure of the pressure vessel is significantly higher than the failure of the groove itself it is proposed that the tensile test completely replaces the hydrostatic test campaign typically done in DARE to meet requirement BEM-SAFE-5_1. This allows more rapid evaluation of the failure mode with shorter lead times.

Validation Test Design

The test article is shown in figure E.9 and consists of a short tank with two closures bolted to the machine. One side has an external groove. The depth of this groove will be varied during the test to verify both the nominal failure load without notch as well as with the groove at the specified design limit. After a first test the center M12 bolt was increased to M20 Nominally for increased strength. Five tests were performed. Two tests on a chamber section without external groove, 3 on chambers with external grooves of varying depth. Both the yield requirement and final rupture loads were investigated. One of the chambers is shown in figure E.10. The machine is a Zwick 1484 Tensile Test bench rated to 200 [kN]. First the load was applied to 100 [bar], or 51 [kN] and investigated. Subsequently the parts were tested to failure.

Validation Test Results

The yield requirement was met. At 51 [kN] no damage or yielding of structural components was measured apart from some minor scratches of the closure surface. The chamber can thus easily be loaded to 100 [bar].

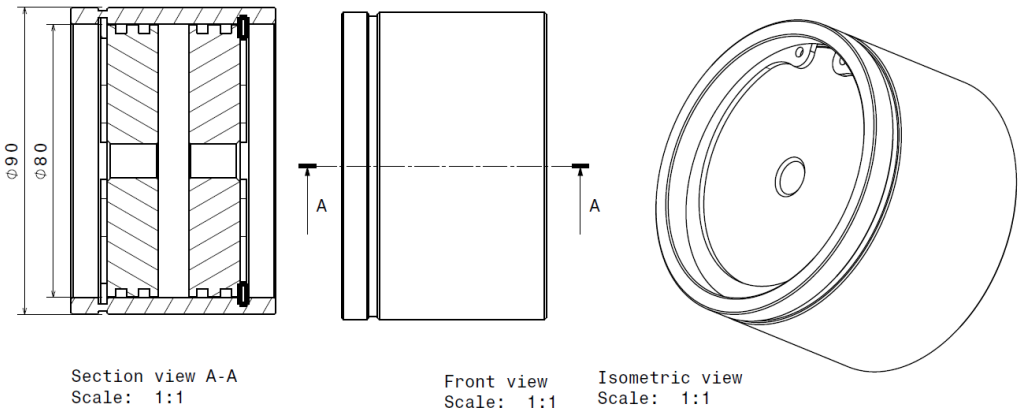

Figure E.9: The test setup to validate failure load of the groove connection.

Figure E.10: One of the failed chambers inside the test setup.

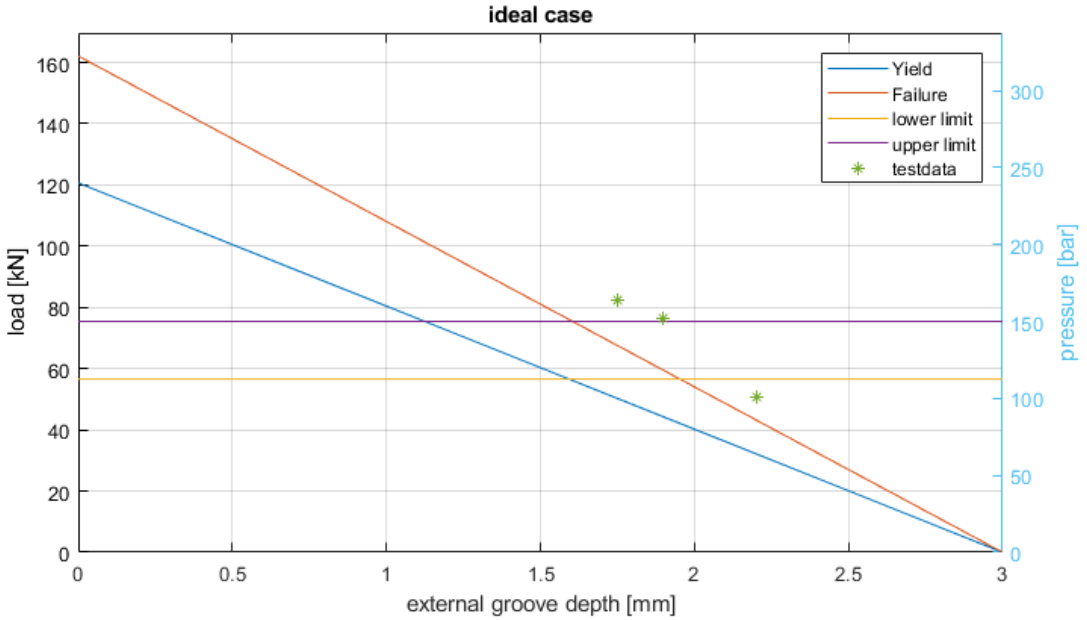

Figure E.11: Predicted failure load and test results with original properties.

Subsequent failure tested was less clear as parts exhibited a higher failure load than expected based on the ideal material properties. The 1.75 [mm] groove failed at 82.599 [kN], significantly above the 150 [bar], 76 [kN] limit. Subsequent chambers were tested with deeper grooves and failed at 58 (2.2 [mm] groove) and 76 [kN] (1.8 mm groove) respectively. This confirmed the trend. Results including the predicted (ideal) performance are shown in figure E.11.

These results are highly counter intuitive as the failure mode was as predicted but occurred at loads higher than considered theoretically possible. It was suggested that this was due to the wrong type of aluminium being used, however consultation with the company made that unfeasible. Additional reasons might be the reference on the surface of the casing being slightly larger than 5 mm, friction in the system or possible misalignment of the closures.

To select the final recommended groove depth it is proposed to extrapolate from current data as this is deemed the best representation of reality. The prediction with adapted load constants is shown in figure E.12. Selecting a failure point between the two pressure limits yields an optimal groove depth of 2 [mm]. This value was used in the system.

E.6.4. Failure Mode Summary

In the table below are the various failure modes and the calculated values. The design failure mode is highlighted in blue. As can be seen there is sufficient margin between the various failure modes to assure axial failure at the nozzle closure. The wall thickness at the nozzle retaining ring is a critical dimension and as such should be made with relatively high tolerances. This shall be explicitly checked after construction of the chambers.

E.7. Interfaces

Several interfaces need to be explicitly considered. These are briefly referred to below.

- Pressure sensor In accordance with requirement BEM-FUNC-1_1 a pressure sensor shall be included in the system. This, A Swagelock RS-4 adapter has a $^1/_4$ BSP thread and is placed in the forward closure.
- Temperature sensor In accordance with requirement BEM-FUNC-1_1 a temperature sensor shall be included in the system. This sensor is taped to the structure using metal tape, optimal locations

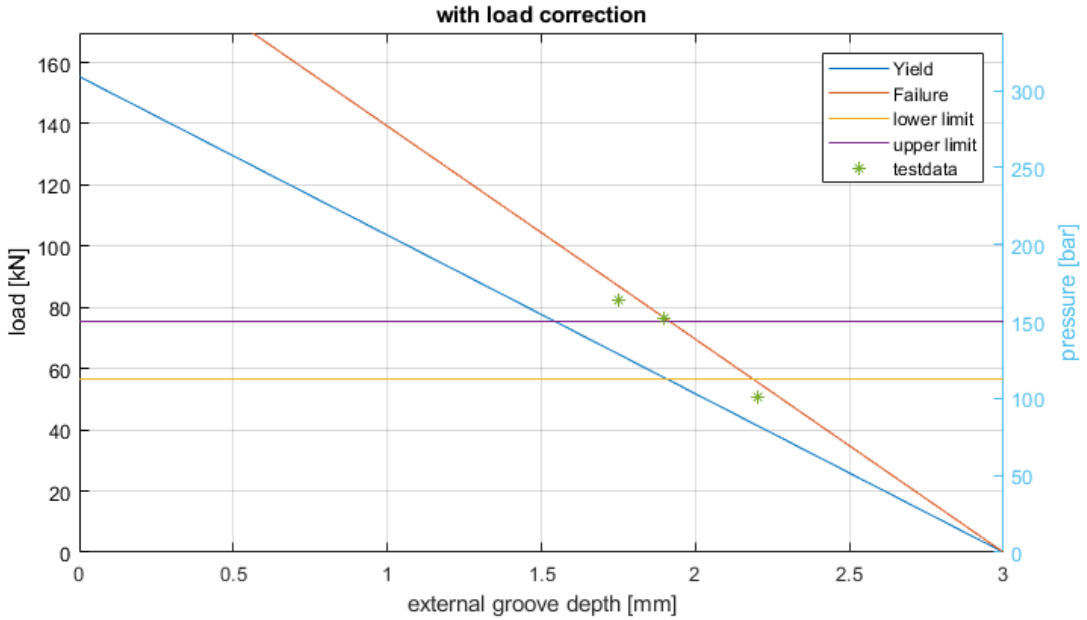

Figure E.12: Predicted failure load and test results with original properties.

Mode	Yield [bar]	Ultimate [bar]	yield [%]	ultimate [%]	MEOP [-]
Chamber Radial Failure	200	269	200	200	2.67
Chamber Axial Failure	400	538	400	400	5.33
Forward Groove Axial Failure	240	322	240	240	3.2
Aft Groove Axial Failure	100+	140	100	100	1.86
Circlip Groove Failure	164	220	164	164	2.93
Circlip Failure	261	na	237	na	316

Table E.6: Summary of the analytic failure mode analysis.

will be determined during a thermal conditioning test.

- Test bench in accordance with requirement BEM-FUNC-2_1 the system needs to fit on the minor test bench (refer to [53]. This achieved through two clamps and a fixture for thrust. The test bench with motor is shown in figure E.13. The two clamps allow fast installation of the system. A detailed drawing of the setup is provided in section E.9.

E.8. Requirement Verification Table

captionBEM requirements verification table.

Identifier	Parent	Requirement	MoV
BEM-1_1		The BEM shall allow the determination of KNSB propellant regression speed at varying pressure and temperature	A

Continued on next page

Table E.7 – continued from previous page

Identifier	Parent	Requirement	MoV
		Similar in design to designs from [10] and [4]. In accordance with test plan from 6. All Functional requirements are met.	
BEM-2_1		The BEM shall meet DARE safety requirements	A,R
		All Safety Requirements are met, or awaiting review. Assessment of system safety included and in line with DARE practices.	
BEM-3_1		The BEM shall meet budget requirements as specified in [MC-MNT-DOC-4_1]	A
		Total costs from MC-MNT-DOC-4_1 within budgeted costs. Accepted by treasurer.	
BEM-SAFE-1_1	BEM-2_1	The BEM design shall pass the DARE safety review	A,R
		Accepted for testing in July 2018	
BEM-SAFE-2_1	BEM-2_1	The system shall allow for an arm and disarm procedure while installed on the test bench	A,R
		Met, design in line with standard DARE procedures	
BEM-SAFE-3_1	BEM-2_1	The BEM shall be compatible with the DARE firing system	A,R
		Met, design in line with standard DARE procedures	
BEM-SAFE-4_1	BEM-2_1	Risks associated with failure of the system due to over pressurization shall be constrained to the test area	A,R
		Analysis performed, with appropriate distances and protective measures the system can be operated safely at the fellowship field	
BEM-SAFE-5_1	BEM-2_1	The BEM design shall follow the DARE pressure vessel design guidelines	A,R
		Sub requirements are met	
BEM-SAFE-5.1_1	BEM-SAFE-5_1	The BEM shall include a design failure mode	A,T
		Nozzle shear out is design failure mode (refer to section (E.6) 40% margin by design to next failure mode.	
BEM-SAFE-5.2_1	BEM-SAFE-5_1	The design failure mode shall be between 1.5 to 2 times the MEOP, other failure modes shall be above 2 times MEOP	A,T
		Design failure at 100 (yield) 134 (ultimate), stress concentrations expected to slightly lower this value, to be confirmed with testing. Other failure modes well above 2 times MEOP.	
BEM-SAFE-5.3_1	BEM-SAFE-5_1	Yield of structural elements shall not occur below 1.25 MEOP (equal to about 85% of the design failure mode)	A,T
		Yield of first mode at 100 bar, above 1.25 MEOP (9.4 [MPa])	

Continued on next page

Table E.7 – continued from previous page

Identifier	Parent	Requirement	MoV
BEM-FUNC-1_1	BEM-1_1	The regression rate shall be determined by measuring pressure and system temperature during the test *Provisions for pressure sensor and temperature sensors on the system.*	A
BEM-FUNC-2_1	BEM-1_1	Nominal operating pressures are defined between 2-7.5 [MPa] at at nominal operating conditions *Simulations with two types of KNSB propellants provide steady regression between 2-7.5 [MPa] with fixed nozzle geometries.*	A
BEM-FUNC-3_1	BEM-1_1	The BEM shall be compatible with the minor test bench *Design in accordance with minor test bench. Adapter discussed provided in section E.7, drawings available in this report*.	A
BEM-FUNC-4_1	BEM-1_1	The BEM shall be compatible with general DARE experimental practices • Outdoor • Non-Permanent Setup *By design.*	A
BEM-FUNC-5_1	BEM-1_1	Nominal operating conditions are defined in the outdoors, between 0 to 30 [°C] at sea level *Selected materials are compatible, additional care taken with propellant grains and thermal shocks, confirmed with thermal conditioning experiment*	A
BEM-FUNC-6_1	BEM-1_1	Re-usability of the system shall be considered *By design, replaceable nozzles and cartidge loaded grains.*	A
BEM-FUNC-7_1	BEM-1_1	Nozzle inserts shall be replaceable	A
		By design	
BEM-FUNC-8_1	BEM-1_1	Propellant shall meet grain acceptance criteria *i.e. Meet minimal standards on propellant density and surface defects to assure behaviour is approximately as expected.*	

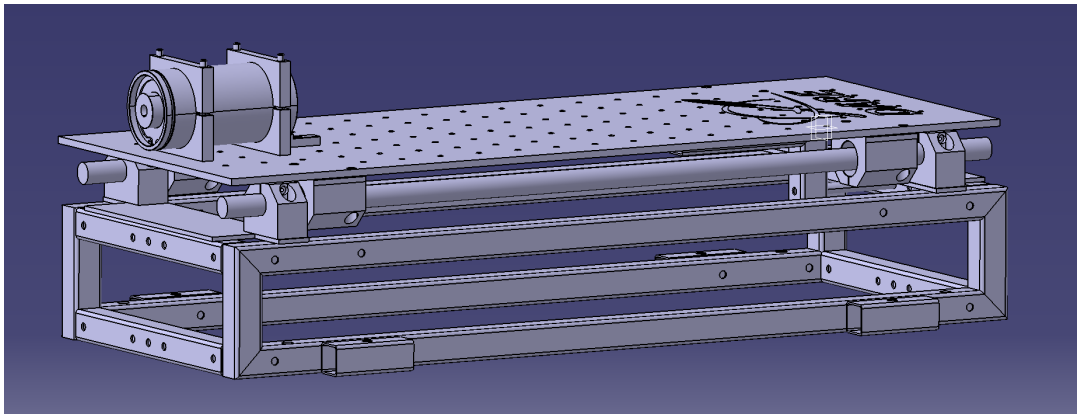

Figure E.13: Breadboard test bench developed during the thrust vectoring minor with the BEM mounted.

E.9. Design Drawings

E.9.1. Parts List

The parts list for a single BEM is provided in table E.8.

Part ID	Name	Dimensions [mm]	Material	Supplier
BEM-C001_1	Casing	90 OD x 80 ID x 180	AW 6060-T66	Aluminiumopmaat.nl
BEM-C002_1	Forward Closure	80 OD x 15	AW 6060-T66	Aluminiumopmaat.nl
BEM-C003_1	End Closure	80 OD x 15	AW 6060-T66	Aluminiumopmaat.nl
BEM-C004_1	Nozzle	50 OD x 42		PMB shop
BEM-C005_1	Snap ring 2x	80 OD x 2.5		Jeveka/ Cirteq
BEM-G001_1	Grain	80 OD x 100	KNSB	Safety
BEM-G002_1	Inhibitor Tube	69.8 OD x 76.6 (ID) x 150	Cardboard	stells.co.uk
BEM-G002_1	Inhibitor disk (2x)	97.8 OD x 1.5	Cardboard	BK

Table E.8: BEM parts list

E.9.2. Technical Drawings

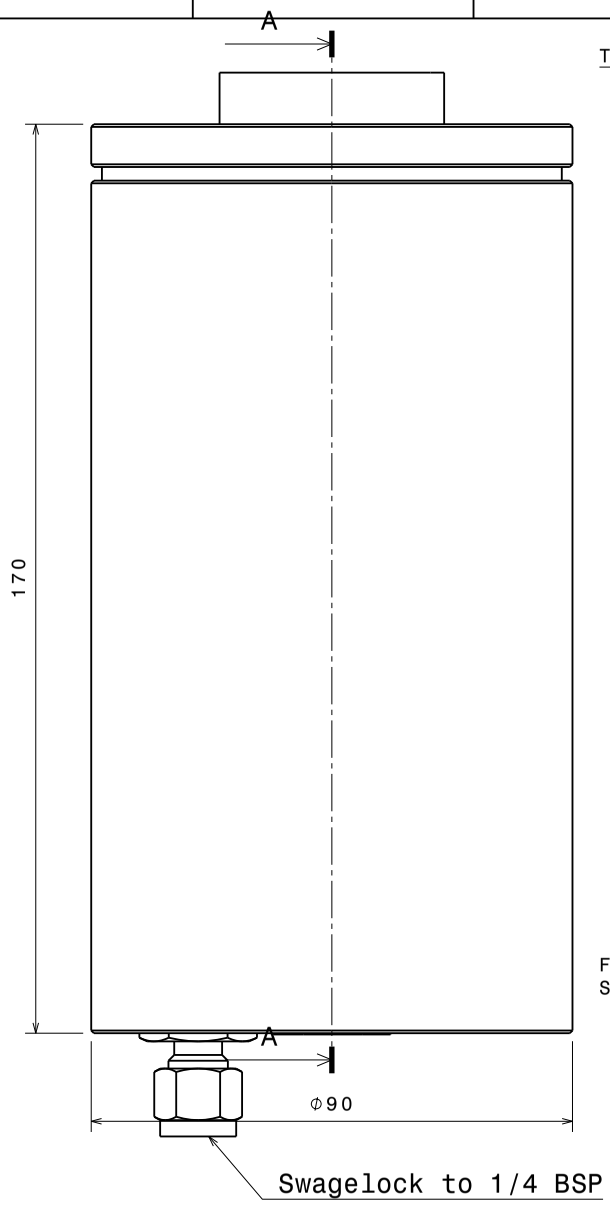

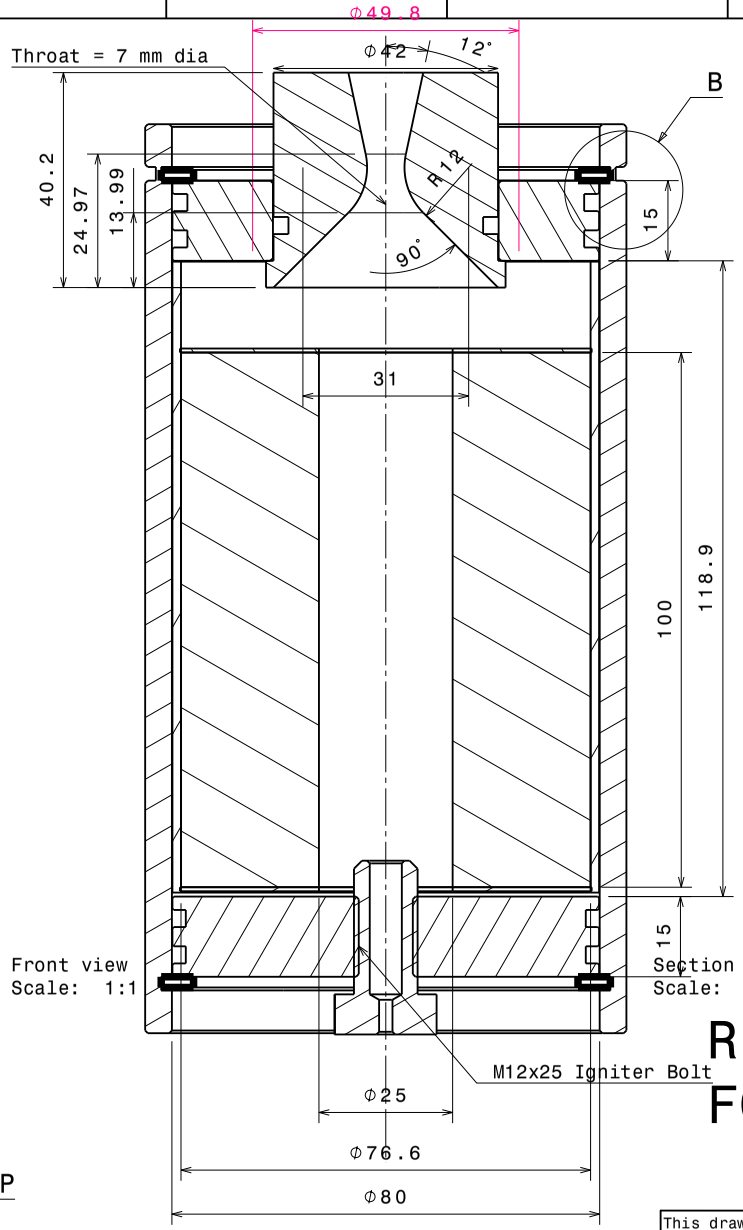

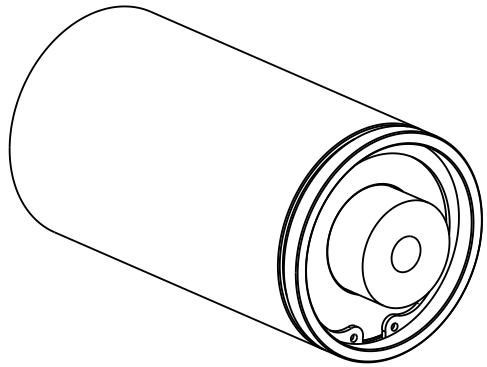

Isometric view
Scale: 1:2

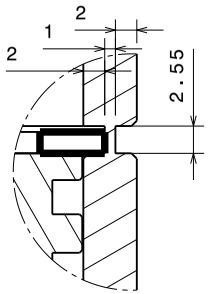

Detail B
Scale: 2:1

REFERENCE DRAWING NOT FOR PRODUCTION

DARE
Delft Aerospace Rocket Engineering

Drawing version	DRAWING TITLE			
V2.0	MC-HDW-DRAW-1_2 BEM Assembly			
SHEET 1/1	SIZE A3	DRAWN BY MC	DATE 04/04/2018	SCALE 1:1

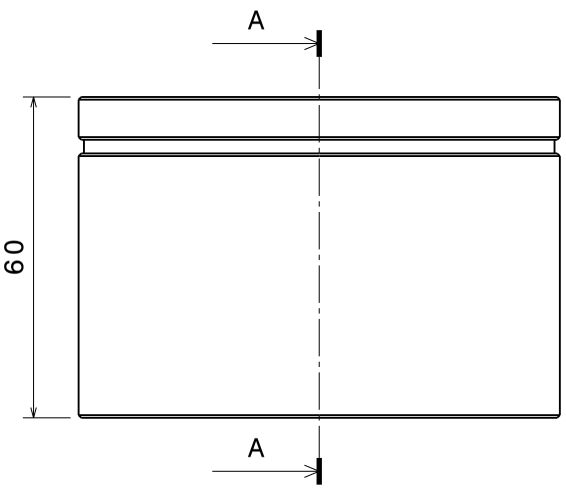

Front view
Scale: 1:1

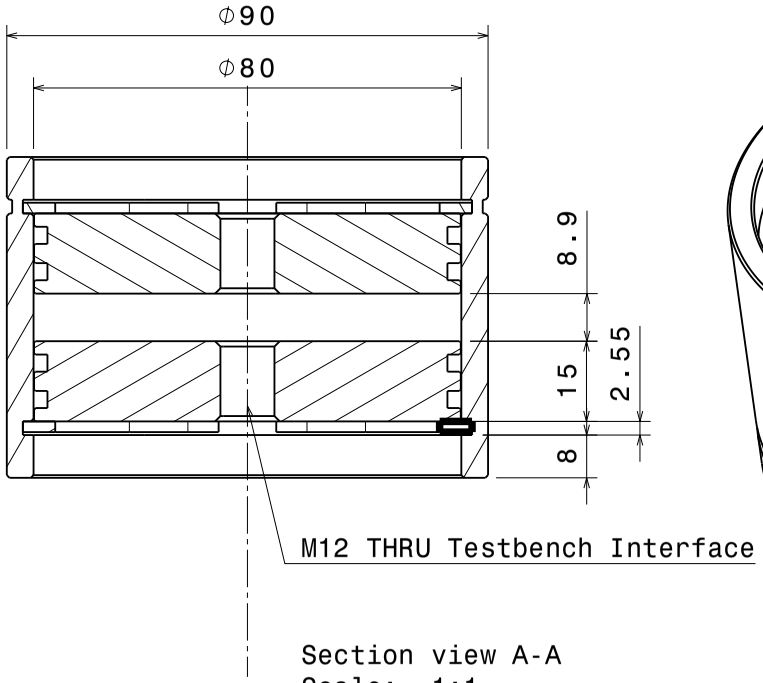

Section view A-A
Scale: 1:1

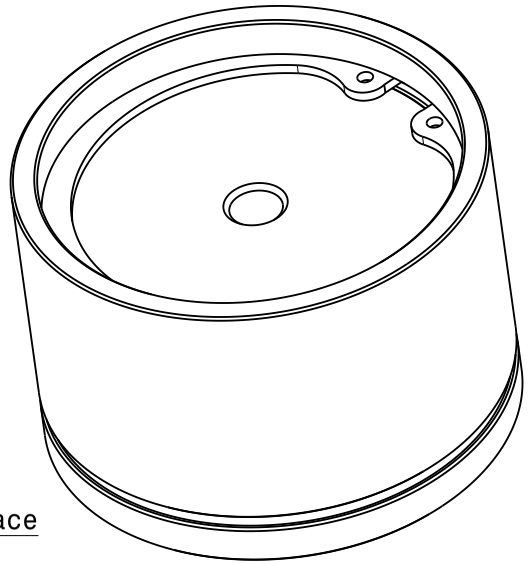

Isometric view
Scale: 1:1

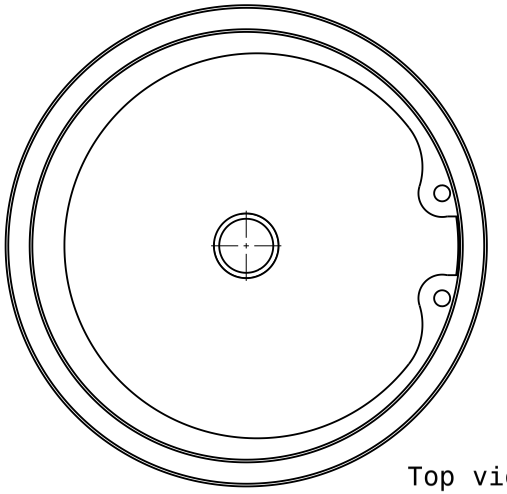

Top view
Scale: 1:1

REFERENCE DRAWING NOT FOR PRODUCTION

DARE
Delft Aerospace Rocket Engineering

Drawing version	DRAWING TITLE			
V2.0	MC-HDW-DRAW-2_2 BEM Tensile Test			
SHEET 1/1	SIZE A3	DRAWN BY MC	DATE 16/04/18	SCALE 1:1

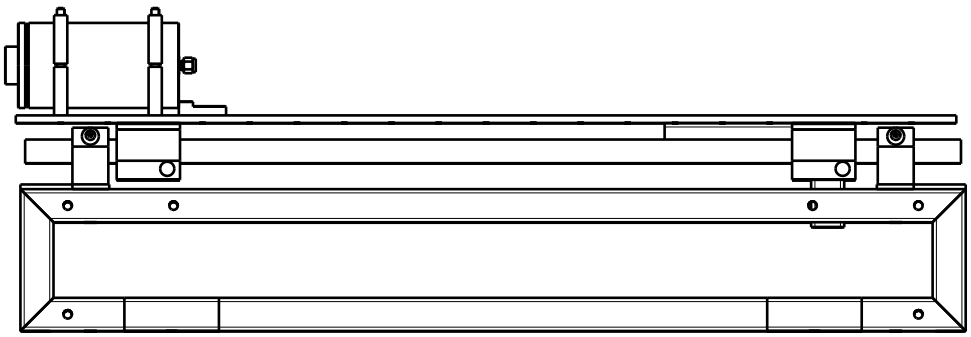

Front view
Scale: 1:8

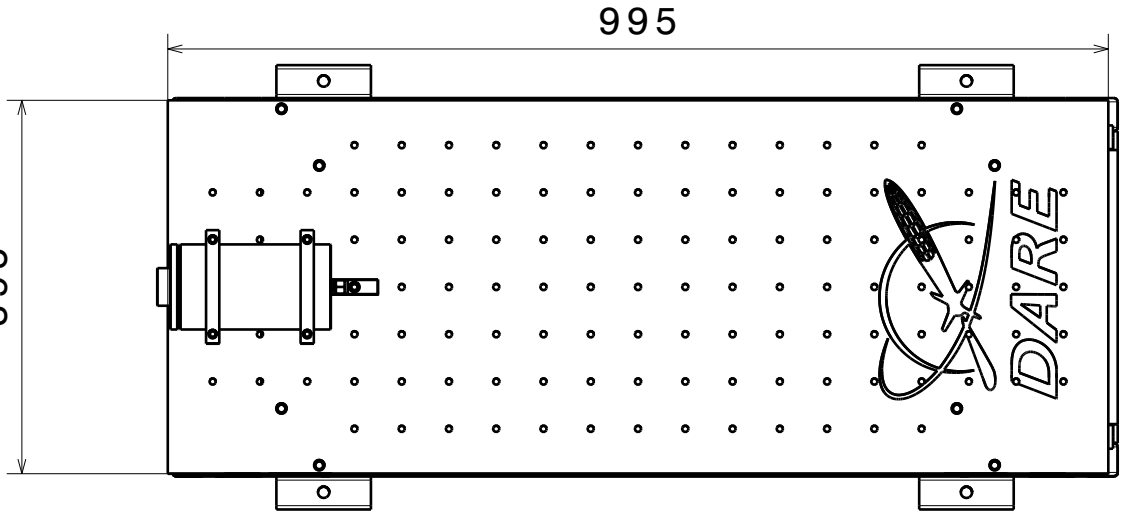

Top view
Scale: 1:8

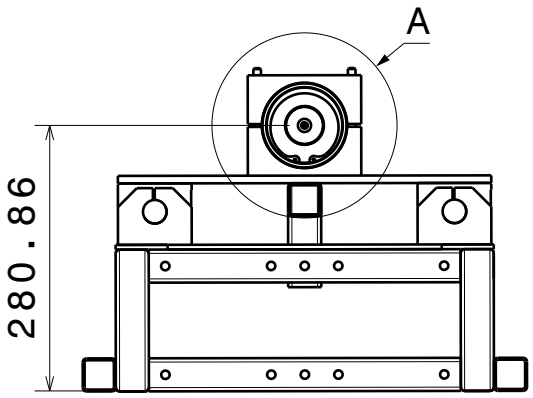

Side View
Scale: 1:8

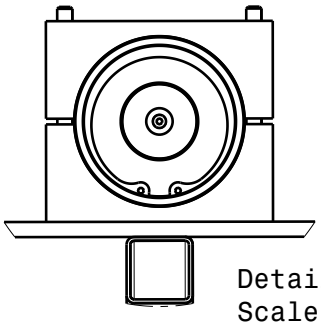

Detail A
Scale: 1:4

Testbench Interface
For Reference Only

DARE
Delft Aerospace Rocket Engineering

DRAWING TITLE: BEM Testbench Assy			
DRAWING ID: MC-HDW-DRAW-14_1		DATE: 10/05/18	
DESIGNED BY: F Kuhnert/MC Olde		CHECKED BY:	
SIZE: A3	SHEET: 1/1	SCALE: 1:1	WEIGHT [kg]: 1.0
MATERIAL: Various		TOLERANCES (UNLESS STATED OTHERWISE): +/- 0.05mm	

E.9.3. Manufacturing Drawings

Front view
Scale: 1:2

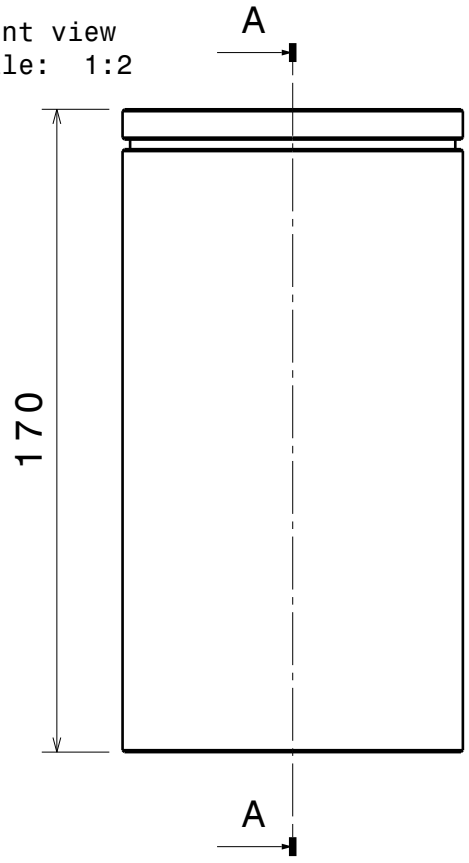

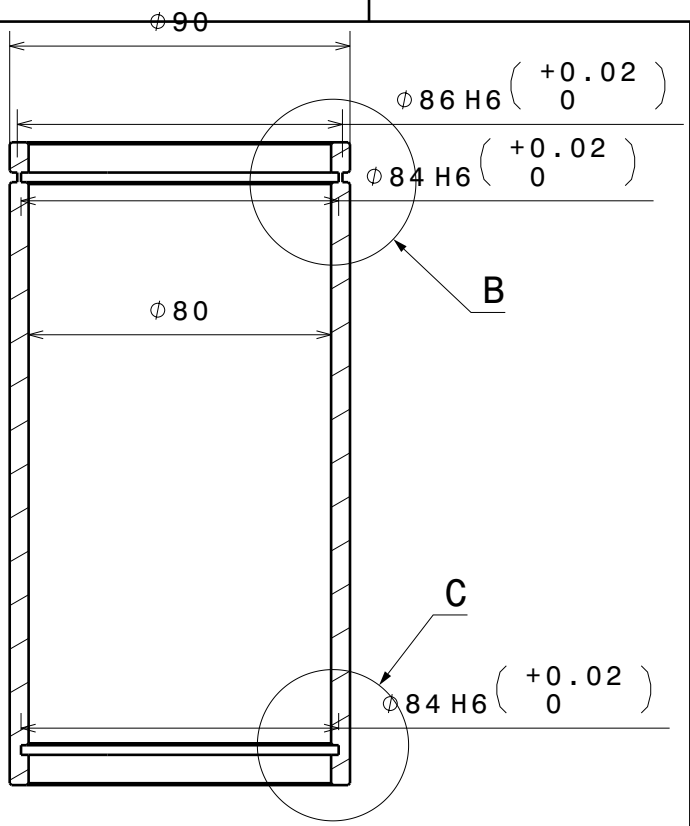

Section view A-A
Scale: 1:2

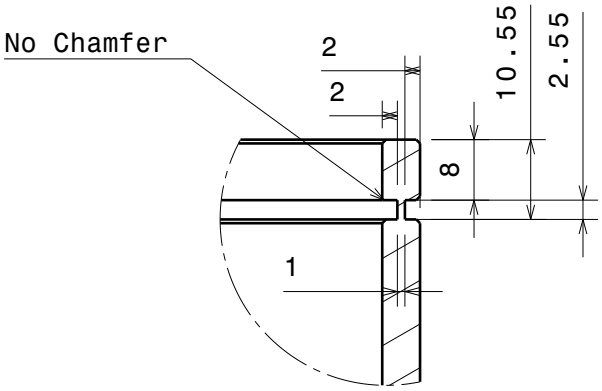

Detail B
Scale: 1:1

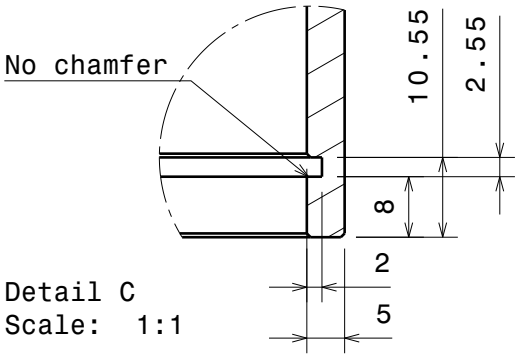

Detail C
Scale: 1:1

Break all edges
Unless stated otherwise

DARE
Delft Aerospace Rocket Engineering

DRAWING TITLE: BEM Casing			
DRAWING ID: MC-HDW-DRAW-4_2		DATE: 03/05/18	
DESIGNED BY: MC Olde		CHECKED BY:	
SIZE: A3	SHEET: 1/1	SCALE: 1:1	WEIGHT [kg]: 1.0
MATERIAL: Alu. 6060		TOLERANCES (UNLESS STATED OTHERWISE): +/- 0.05mm	

Front view
Scale: 1:1

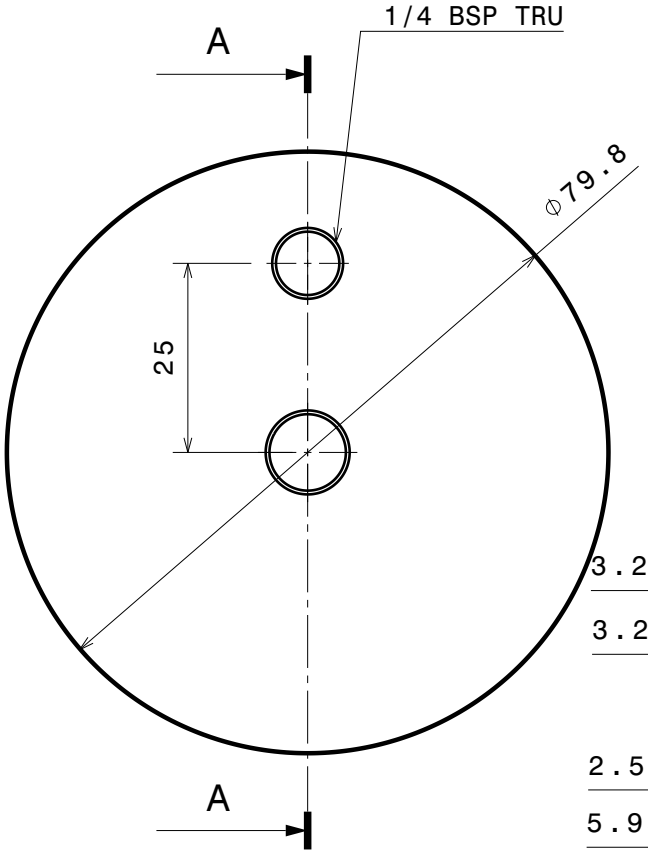

Left view
Scale: 1:1

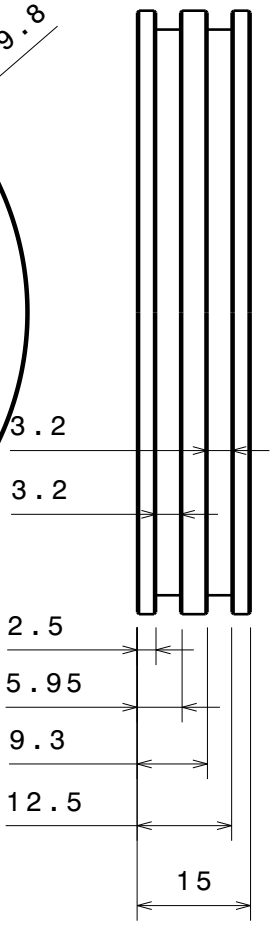

Section view A-A
Scale: 1:1

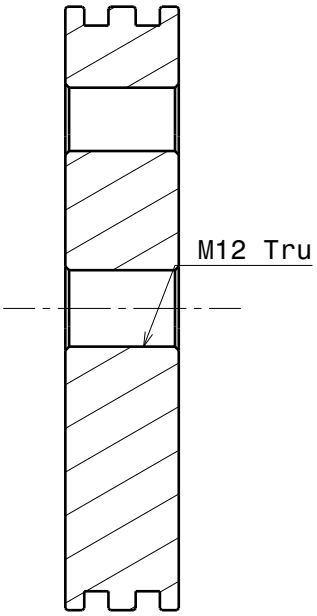

Break All Edges

DARE
Delft Aerospace Rocket Engineering

DRAWING TITLE: BEM FWD Closure			
DRAWING ID: MC-HDW-DRAW-5_2		DATE: 03/05/18	
DESIGNED BY: MC Olde		CHECKED BY:	
SIZE: A3	SHEET: 1/1	SCALE: 1:1	WEIGHT [kg]: 1.0
MATERIAL: Alu. 6060		TOLERANCES (UNLESS STATED OTHERWISE): +/- 0.05mm	

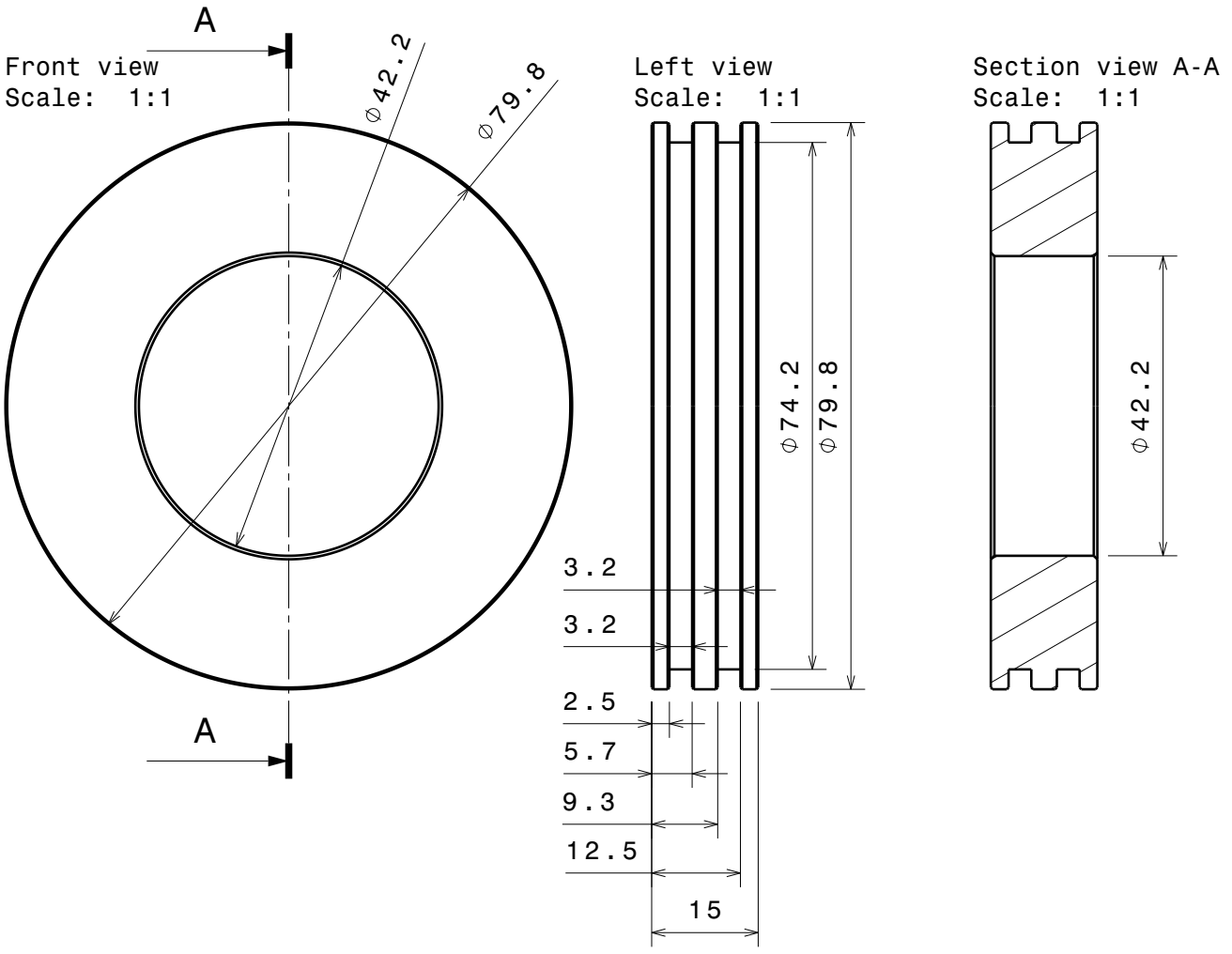

Break all edges

DARE
Delft Aerospace Rocket Engineering

DRAWING TITLE: BEM AFT Closure			
DRAWING ID: MC-HDW-DRAW-6_2		DATE: 03/05/18	
DESIGNED BY: MC Olde		CHECKED BY:	
SIZE: A3	SHEET: 1/1	SCALE: 1:1	WEIGHT [kg]: 1.0
MATERIAL: Alu. 6060		TOLERANCES (UNLESS STATED OTHERWISE): +/- 0.05mm	

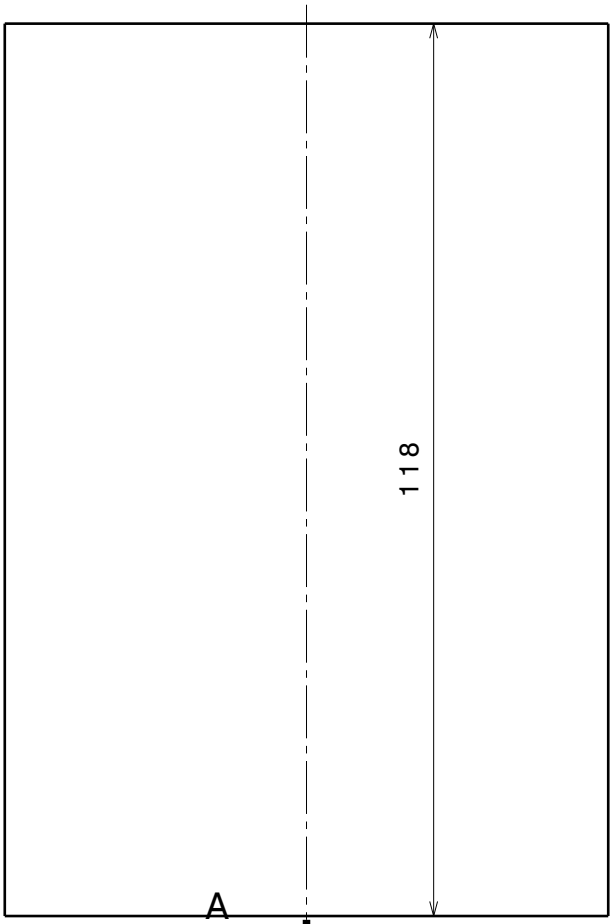

Bottom view
Scale: 1:1

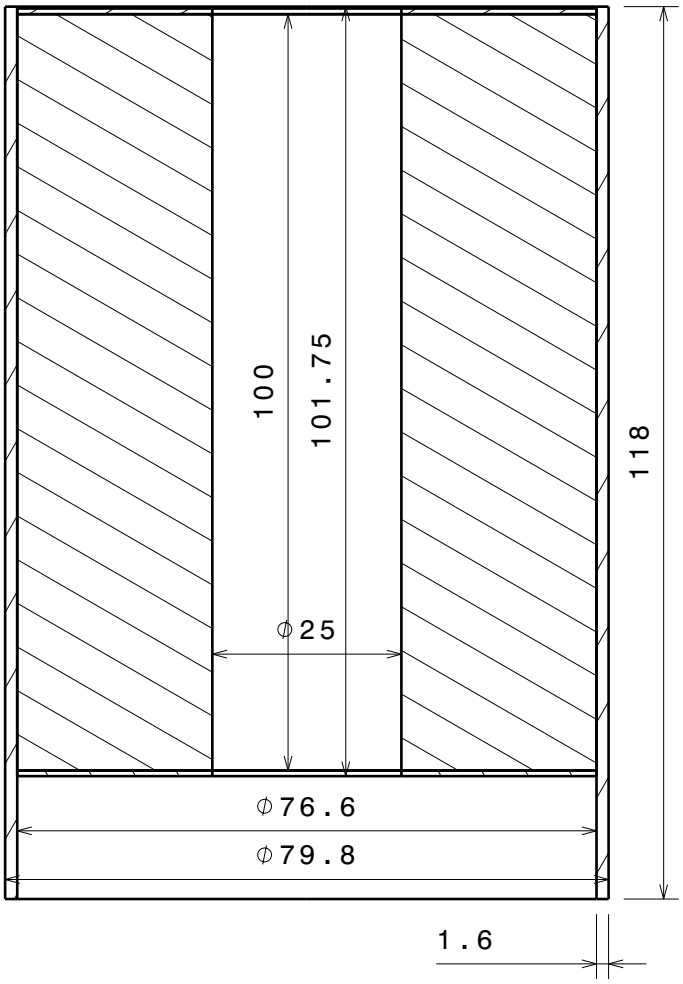

Section view A-A
Scale: 1:1

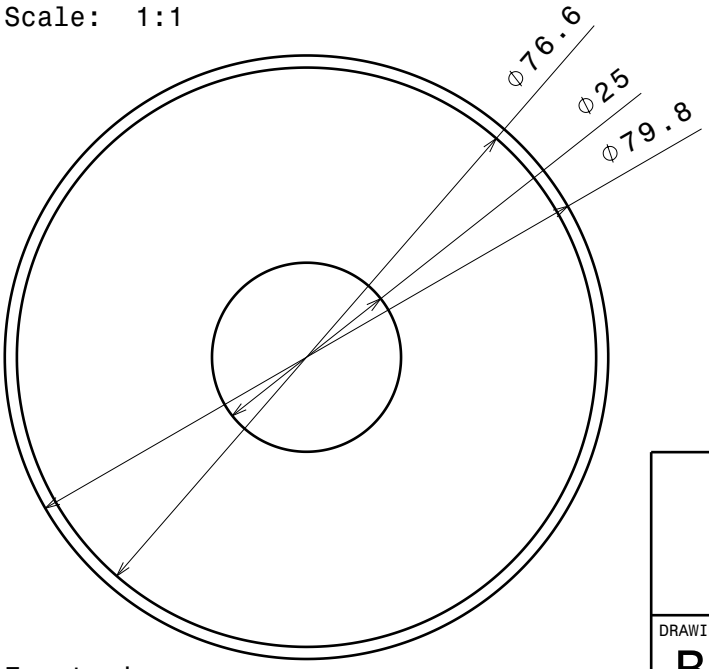

Front view
Scale: 1:1

DARE
Delft Aerospace Rocket Engineering

DRAWING TITLE: BEM Grain Assy	
DRAWING ID: MC-HDW-DRAW-7_2	DATE: 03/05/18
DESIGNED BY: MC Olde	CHECKED BY:
SIZE: A3 SHEET: 1/1	SCALE: 1:1 WEIGHT [kg]: 1.0
MATERIAL: KNSB + Cardboard	TOLERANCES (UNLESS STATED OTHERWISE): +/- 0.05mm

Front view
Scale: 1:1

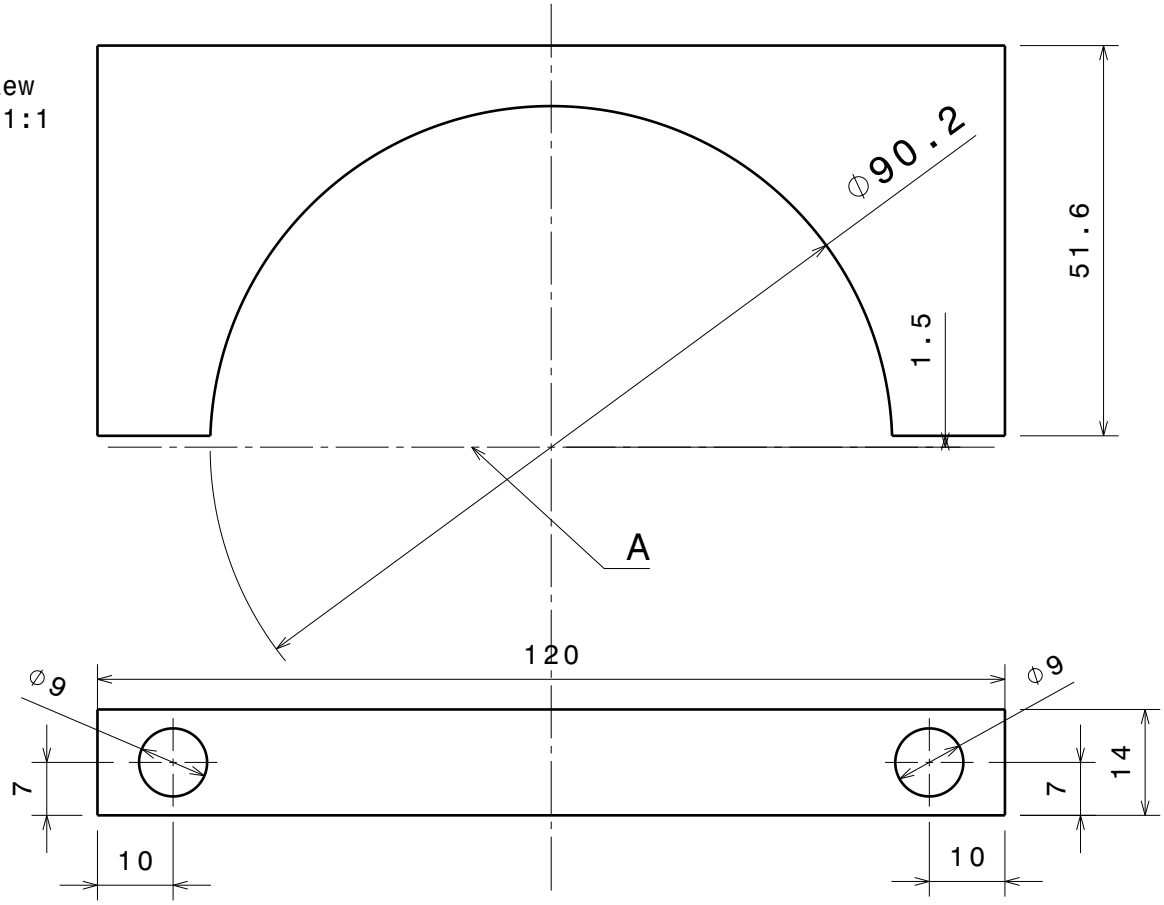

Top view
Scale: 1:1

Production Note: Create connected pairs, then cut allong A

DARE
Delft Aerospace Rocket Engineering

DRAWING TITLE: BEM BenchClamp			
DRAWING ID: MC-HDW-DRAW-15_1		DATE: 10/05/18	
DESIGNED BY: MC Olde		CHECKED BY:	
SIZE: A3	SHEET: 1/1	SCALE: 1:1	WEIGHT [kg]: NA
MATERIAL: AL 6060		TOLERANCES (UNLESS STATED OTHERWISE): +/- 0.5mm	

Front view
Scale: 1:1

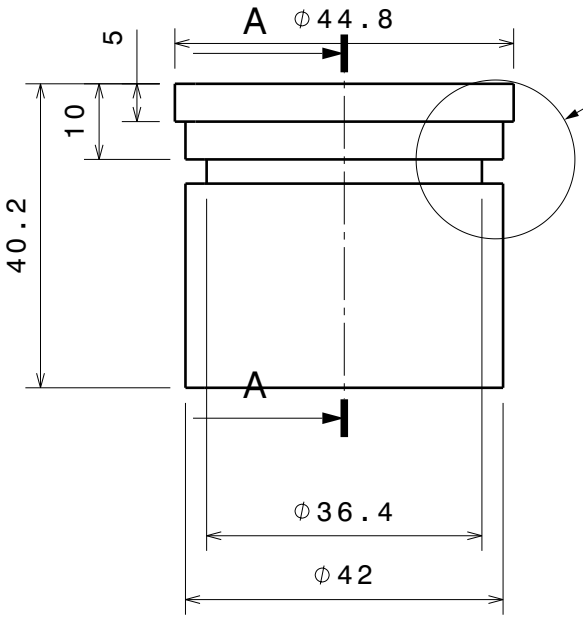

Section view A-A
Scale: 1:1

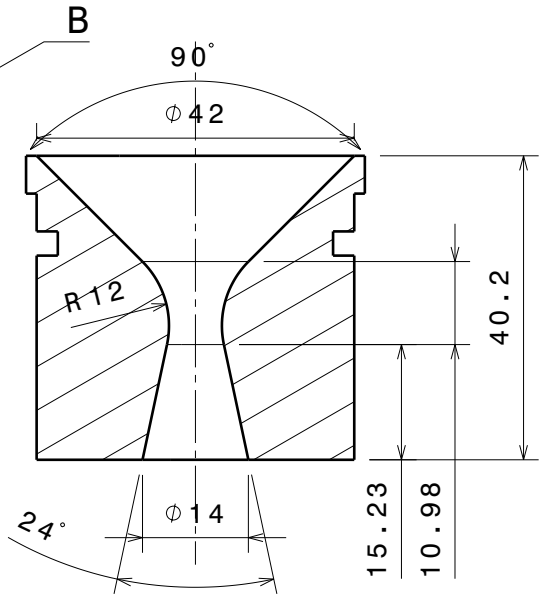

Top view
Scale: 1:1

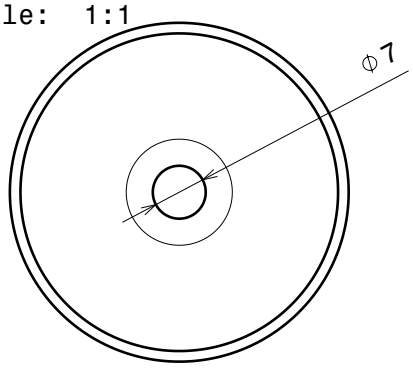

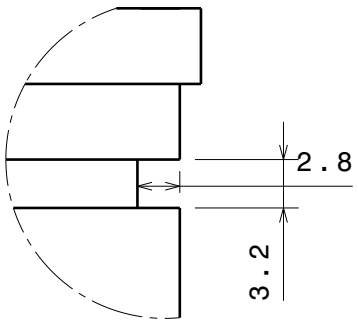

Detail B
Scale: 2:1

Break All Edges

DARE
Delft Aerospace Rocket Engineering

DRAWING TITLE: BEM Nozzle A			
DRAWING ID: MC-HDW-DRAW-17_2		DATE: 22/05/18	
DESIGNED BY: MC Olde		CHECKED BY:	
SIZE: A3	SHEET: 1/1	SCALE: 1:1	WEIGHT [kg]: NA
MATERIAL: TBD Steel		TOLERANCES (UNLESS STATED OTHERWISE): +/- 0.5mm	

Front view
Scale: 1:1

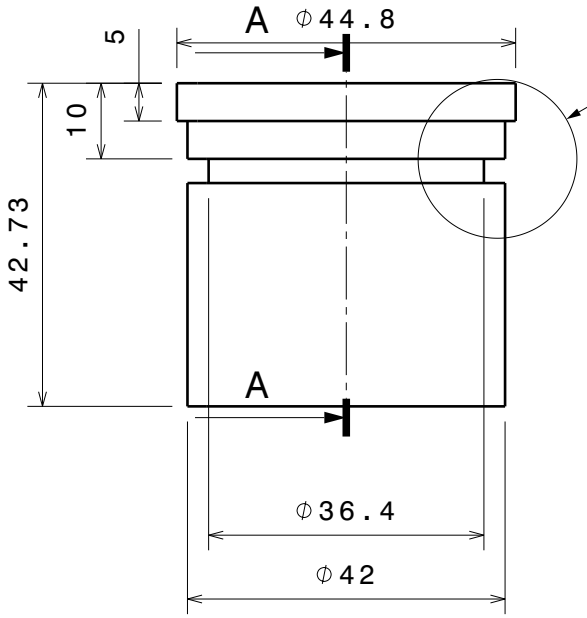

Section view A-A
Scale: 1:1

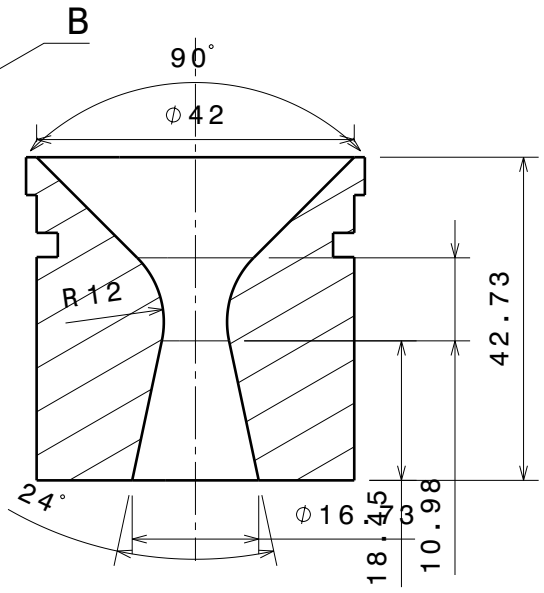

Top view
Scale: 1:1

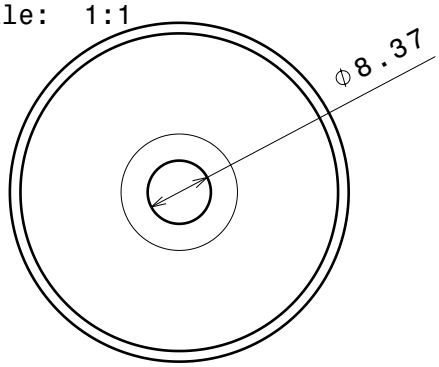

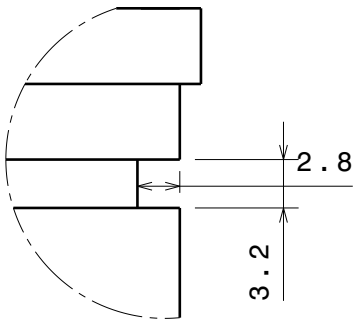

Detail B
Scale: 2:1

Break All Edges

DARE
Delft Aerospace Rocket Engineering

DRAWING TITLE: BEM Nozzle B			
DRAWING ID: MC-HDW-DRAW-18_1		DATE: 22/05/18	
DESIGNED BY: MC Olde		CHECKED BY:	
SIZE: A3	SHEET: 1/1	SCALE: 1:1	WEIGHT [kg]: NA
MATERIAL: TBD Steel		TOLERANCES (UNLESS STATED OTHERWISE): +/- 0.5mm	

F

Casting Equipment

Several recommendations were made in the MSc Literature study [16] to achieve improved propellant quality and improved propellant density. KNSB propellant is produced relatively easily, compared to AP/AN based propellants, by heating a powder mixture of Sorbitol and KNO_3 to above the melting temperature of sorbitol and casting the relatively viscous mixture in casting moulds. The design of the casting moulds is based on similar work from [60] and [55]. The most important technical recommendations with respect to mould design are the following:

- The propellant should be pressurized after casting the mixture. Work from[60] and [64] suggest mechanical compression in the order of 25 Psi or around 1.7 bar to give good results.
- The casting jig should be heated prior to casting as this prevents rapid setting of the propellant on contact with the cold moulds. This is explicitly mentioned [63] for smaller sized grains (few hundred grams).

Furthermore, in support of the thermal conditioning experiment (refer to chapter 6) and casting experiment (refer to 4), it will be necessary to measure temperature of the propellant during production. This will be done through the use of embedded thermocouples. Two Casting Jigs will be specifically adapted for this purpose. The width of a thermocouple wire (RS Pro Type K) is 1.5 [mm] diameter.

F.1. Design Summary

The design of the casting jigs is based around the grain design from previous chapter. The following aspects need to be taken into consideration specifically:

- Shrinkage of the propellant. The KNSB mixture shrinks by around 15-25% when it cools down from the casting temperature around 125 [°C] to room temperature. The casting Jigs and inhibitor tubes need to be able to accommodate this.
- Compression. To make sure the propellant grain becomes an consistent, high density product it needs to be compressed mechanically. This is done with a plunger and a spring. The mean compression should reach around 25 [Psi] or 1.7 [bar] of pressure [16]
- Tooling removal. Experiences in DARE have shown that removing the coring rods can be greatly simplified if provisions are made for removing the coring rods. Other authors have used slightly tapered moulds however straight mandrels are also used.
- Ideal BATES grain length. The ideal bates grain length for a almost perfectly flat response is 127 [mm] casting Jigs should accommodate this.

The casting jig is shown in figure F.1, the parts list is provided in table F.2.

The spring was selected based on the following equations. To limit the total length of the setup the spring was selected with a slightly lower length. This means that it needs to be re-tightened twice during the curing process.

$$S_{min} = \frac{L}{0.75} = \frac{0.1}{0.75} - 0.1 = 3.3 \times 10^{-2} \text{ [m]} \tag{F.1}$$

$$\begin{aligned} F_{min} &= P \cdot \pi(R_e^2 - R_i^2) = 1.7 \times 10^5 \cdot 4.12 \times 10^{-3} \approx 700 \text{ [N]} \\ &= K \cdot x = 2.1 \times 10^4 \text{ [N/m]} \cdot 3.3 \times 10^{-2} \text{ [m]} \end{aligned} \tag{F.2}$$

The final spring properties are shown in table F.1, and has a significantly higher spring constant. To

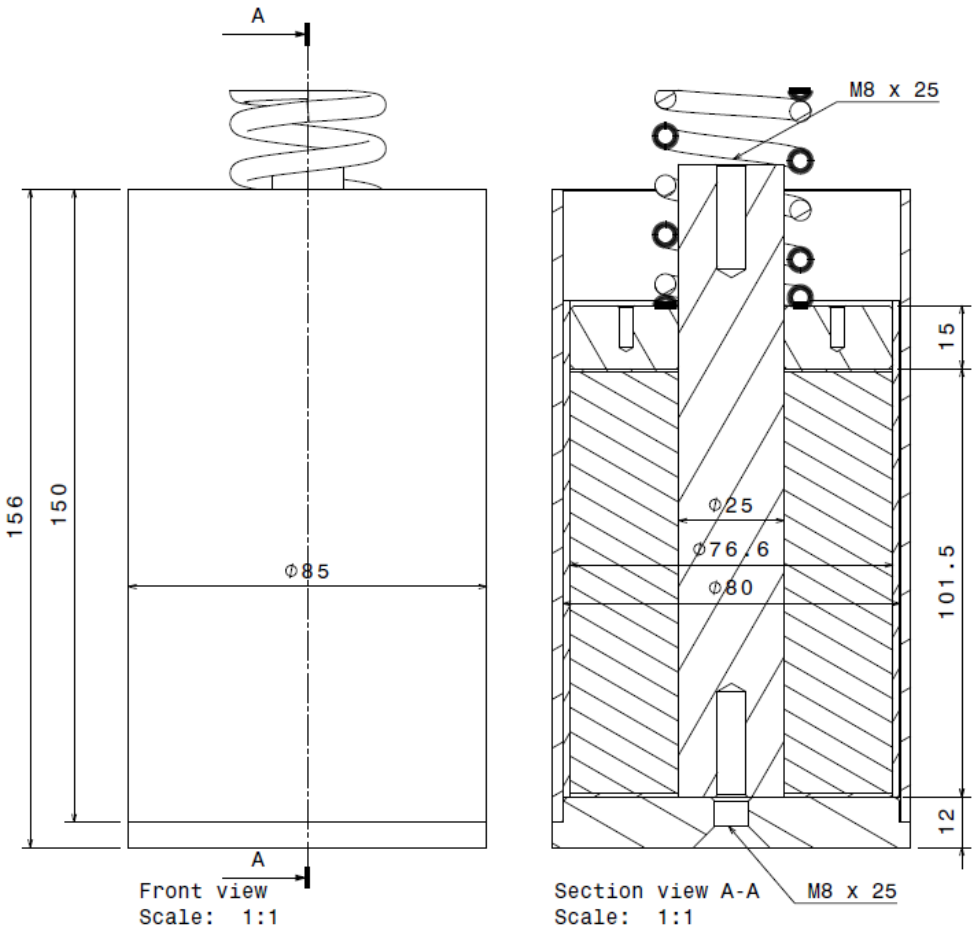

Figure F.1: The design of the BEM (version 2) with rough dimensions.

obtain a spring force of 700 N compression needs to be only:

$$F_{min} = 700 \text{ [N]} = 156 \cdot 4.48 \text{ [mm]}. \tag{F.3}$$

This can be measured with a caliper from the washer holding the spring to the plunger surface. A slightly higher spring load would be recommended initially.

OD [mm]	ID [mm]	L_0 [mm]	L_{min} [mm]	$F_{50\%}$ [N]	K [N/mm]
50,0	25,0	64,0	32	2496	156.0

Table F.1: Selected Spring Properties (product F24114100500064 from `jeveka.com`)

F.2. Design Drawings

F.2.1. Parts List

Part ID	Name	Dimensions [mm]	Material	Supplier
BEM-J001_1	Casting Tube	84 OD x 80 ID x 150	AW 6060-T66	`Aluminiumopmaat.nl`
BEM-J002_1	Casting Base	85 OD x 12	AW 6060-T66	`Aluminiumopmaat.nl`
BEM-J003_1	Coring Rod	25 OD x 150	AW 6060-T66	`Aluminiumopmaat.nl`
BEM-J004_1	Plunger	80 OD x 15	AW 6060-T66	`Aluminiumopmaat.nl`
BEM-J005_1	Spring	50 OD x 25 ID x 64	Steel	`jeveka.com`

Table F.2: BEM parts list

F.2.2. Technical Drawings

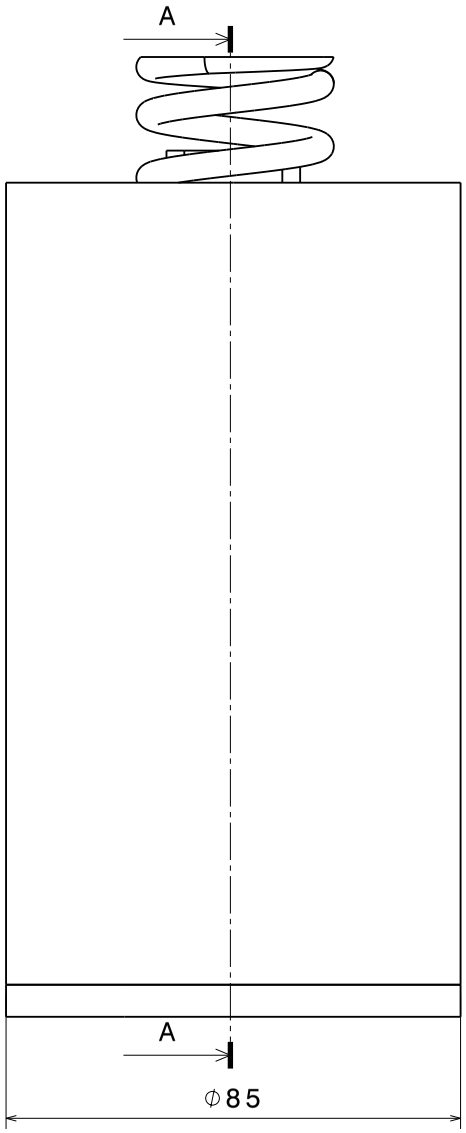

Front view
Scale: 1:1

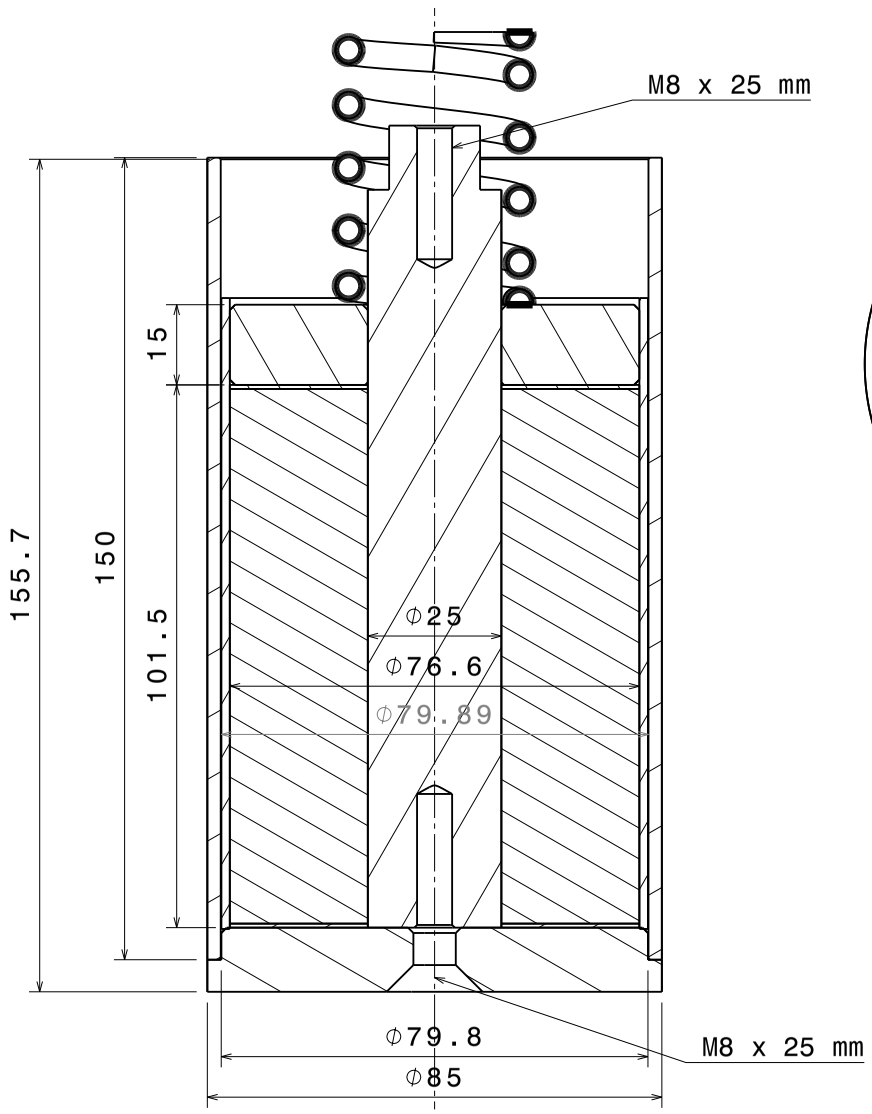

Section view A-A
Scale: 1:1

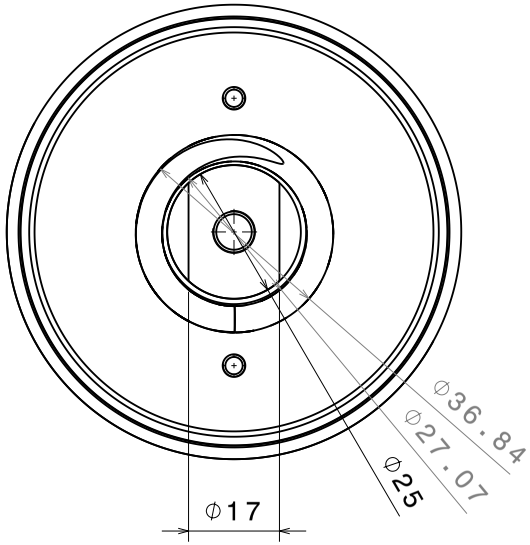

Side view
Scale: 1:1

DARE
Delft Aerospace Rocket Engineering

Drawing version: V1.0	DRAWING TITLE: MC-HDW-DRAW-3_1 BEM Casting Jig			
SHEET: 1/1	SIZE: A3	DRAWN BY: MC	DATE: 17/04/18	SCALE: 1:1

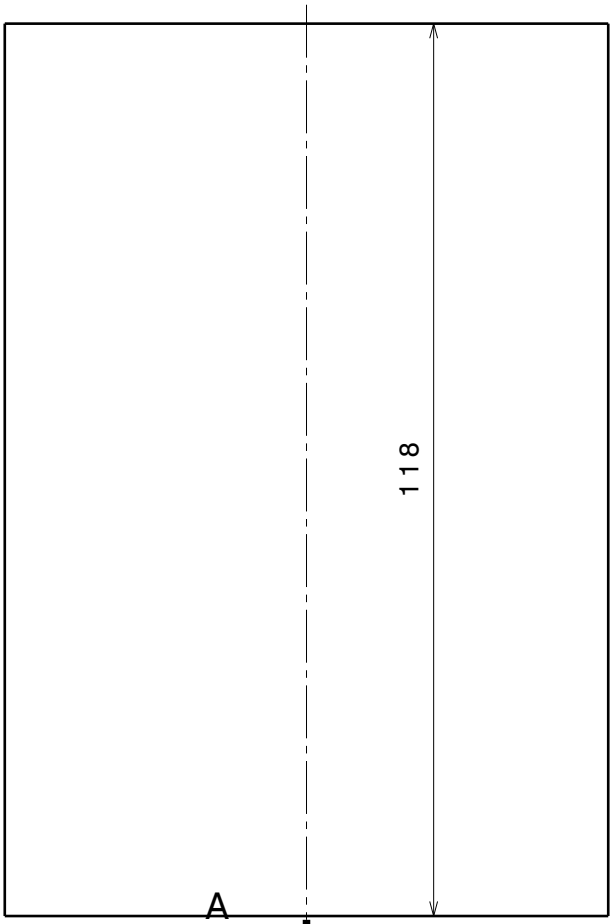

Bottom view
Scale: 1:1

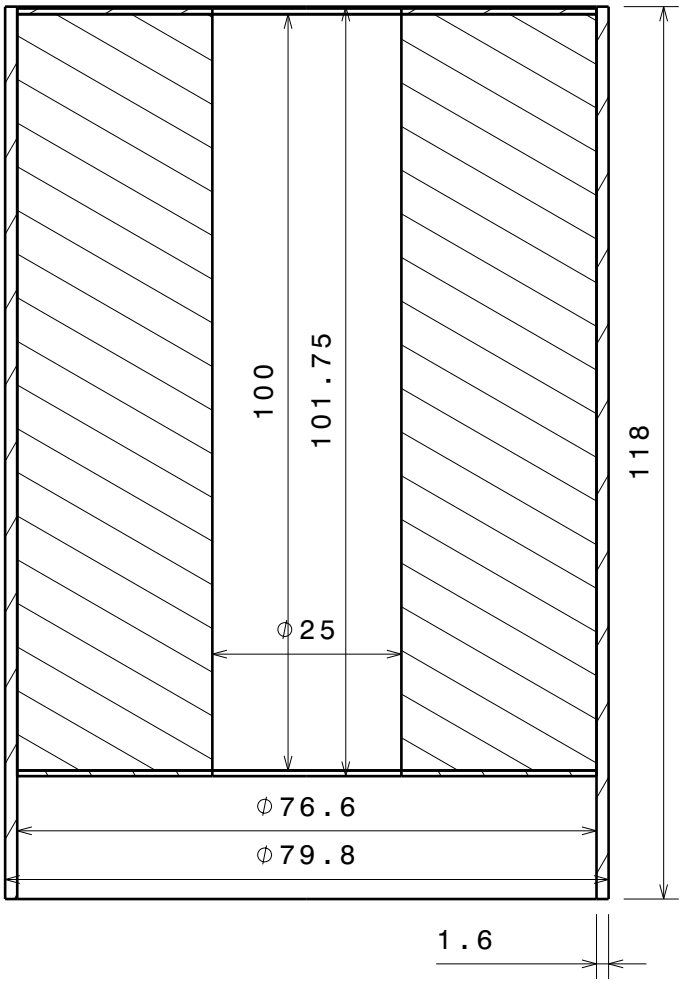

Section view A-A
Scale: 1:1

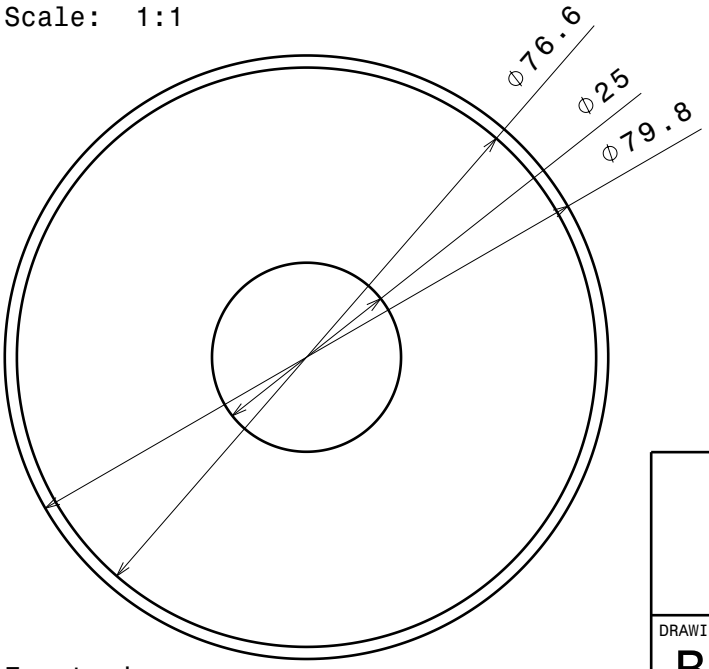

Front view
Scale: 1:1

DARE
Delft Aerospace Rocket Engineering

DRAWING TITLE: BEM Grain Assy	
DRAWING ID: MC-HDW-DRAW-7_2	DATE: 03/05/18
DESIGNED BY: MC Olde	CHECKED BY:
SIZE: A3 SHEET: 1/1	SCALE: 1:1 WEIGHT [kg]: 1.0
MATERIAL: KNSB + Cardboard	TOLERANCES (UNLESS STATED OTHERWISE): +/- 0.05mm

F.2.3. Manufacturing Drawings

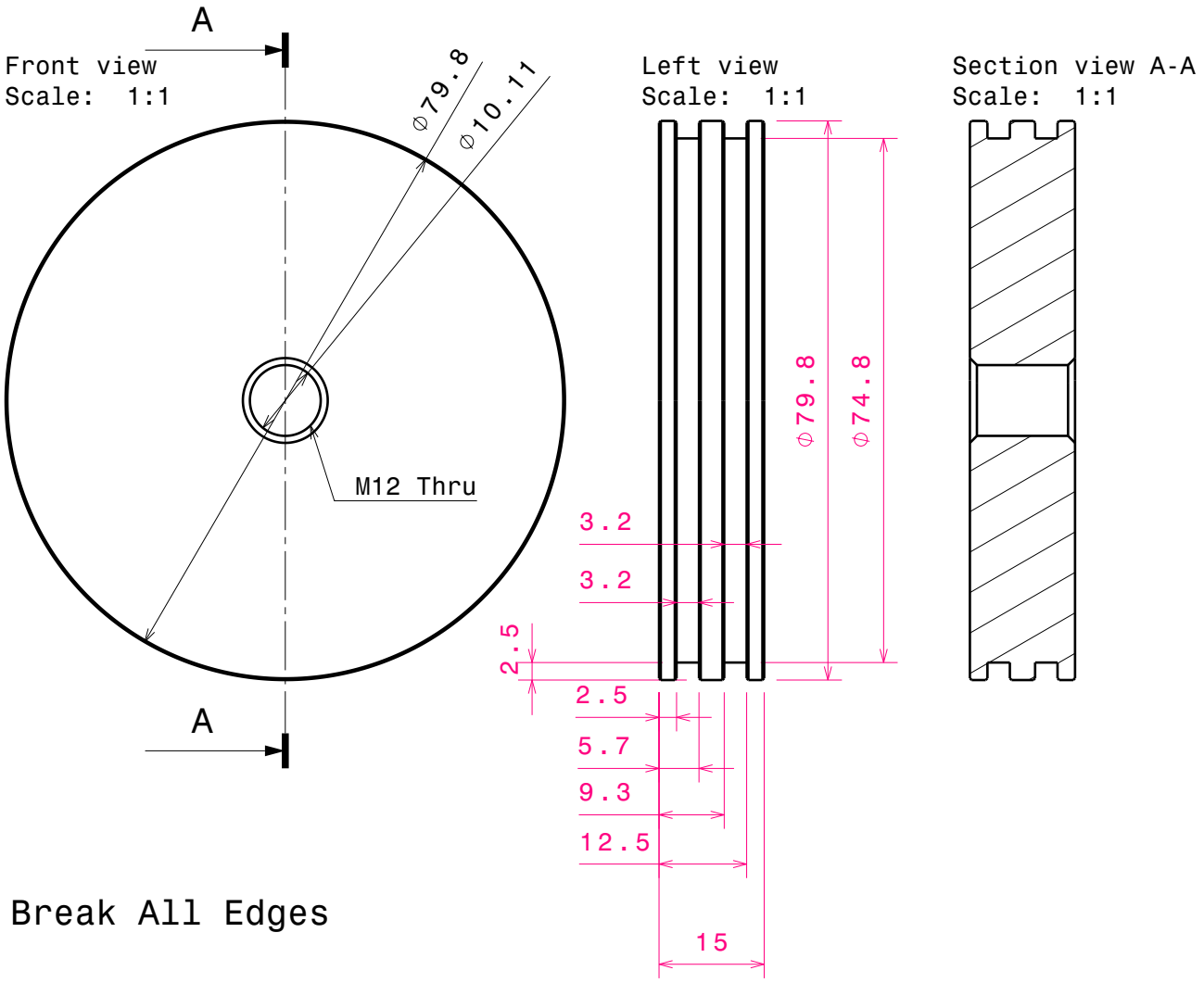

Break All Edges

DARE
Delft Aerospace Rocket Engineering

DRAWING TITLE: BEM tensile closure			
DRAWING ID: MC-HDW-DRAW-9_1		DATE: 03/05/18	
DESIGNED BY: MC Olde		CHECKED BY:	
SIZE: A3	SHEET: 1/1	SCALE: 1:1	WEIGHT [kg]: 1.0
MATERIAL: Alu. 6060		TOLERANCES (UNLESS STATED OTHERWISE): +/- 0.05mm	

Front view
Scale: 1:1

Break All Edges

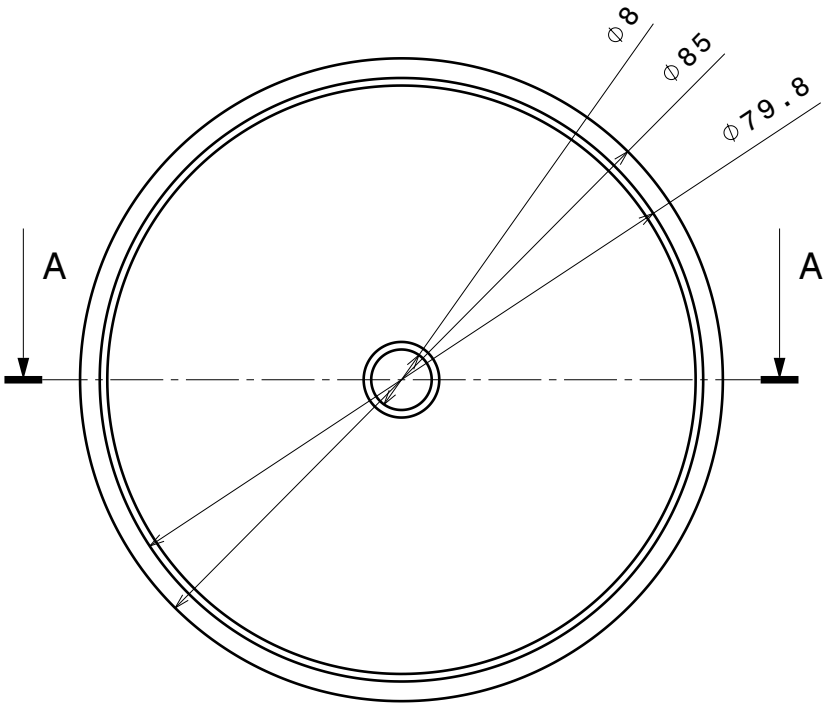

Top view
Scale: 1:1

8mm Thru, Countersunk
Check Bolt fitting

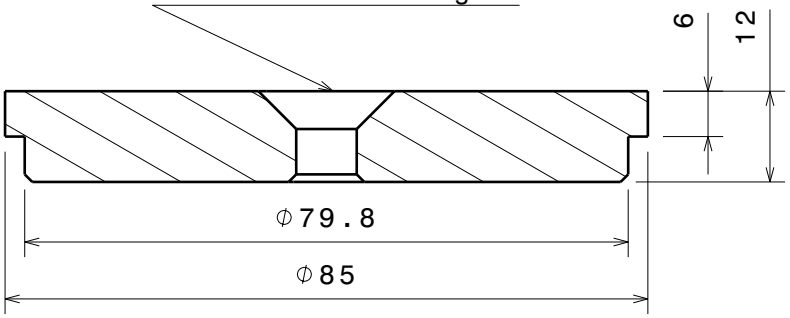

Section view A-A
Scale: 1:1

DARE
Delft Aerospace Rocket Engineering

DRAWING TITLE: BEM Casting Jig Base			
DRAWING ID: MC-HDW-DRAW-11_1		DATE: 03/05/18	
DESIGNED BY: MC Olde		CHECKED BY:	
SIZE: A3	SHEET: 1/1	SCALE: 1:1	WEIGHT [kg]: 1.0
MATERIAL: Alu. 6060		TOLERANCES (UNLESS STATED OTHERWISE): +/- 0.05mm	

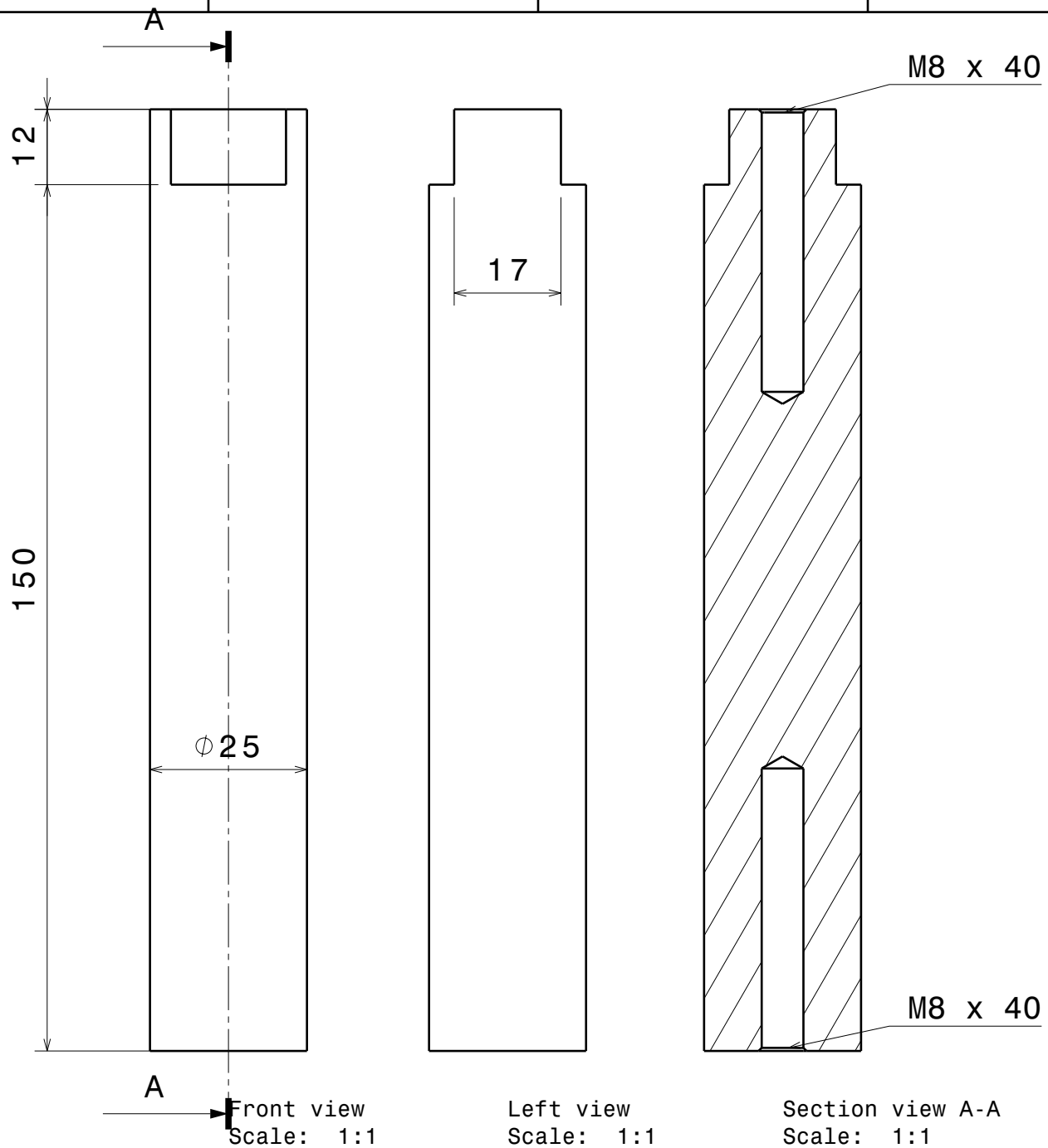

Front view
Scale: 1:1

Left view
Scale: 1:1

Section view A-A
Scale: 1:1

Break All Edges

DARE
Delft Aerospace Rocket Engineering

DRAWING TITLE: BEM Casting Jig Rod			
DRAWING ID: MC-HDW-DRAW-12_1		DATE: 03/05/18	
DESIGNED BY: MC Olde		CHECKED BY:	
SIZE: A3	SHEET: 1/1	SCALE: 1:1	WEIGHT [kg]: 1.0
MATERIAL: Alu. 6060		TOLERANCES (UNLESS STATED OTHERWISE): +/- 0.05mm	

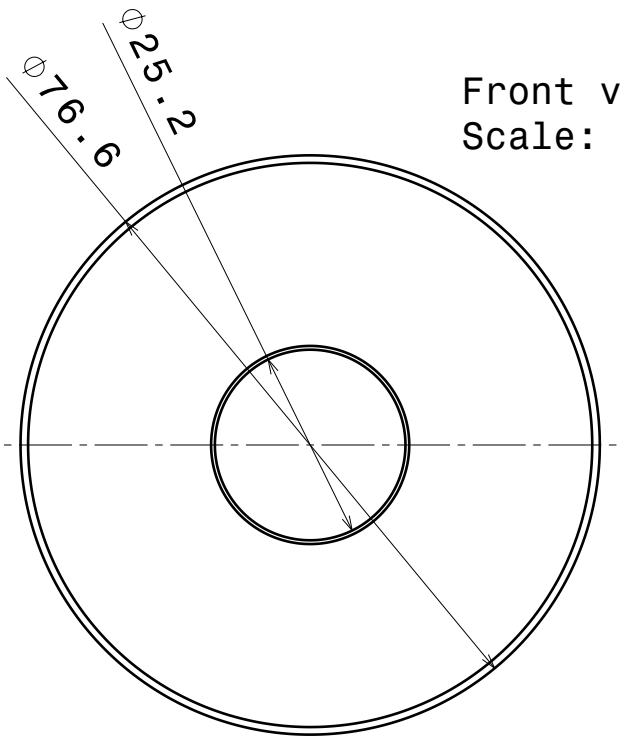

Front view
Scale: 1:1

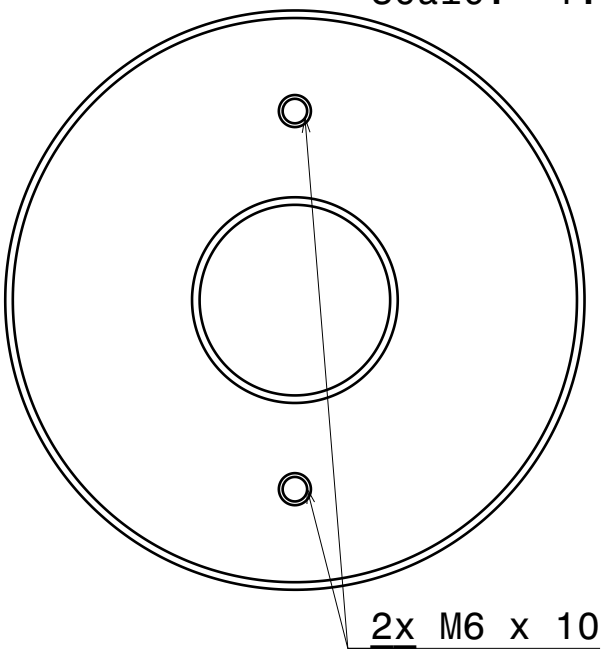

Rear view
Scale: 1:1

Break All Edges

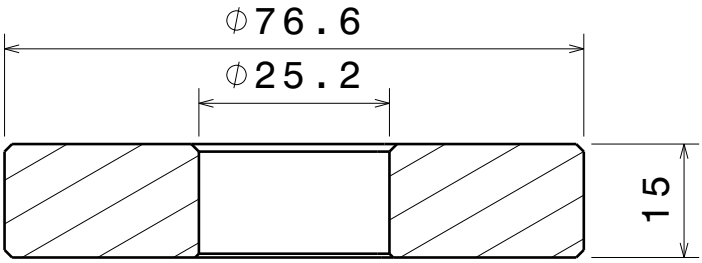

Section view A-A
Scale: 1:1

DARE
Delft Aerospace Rocket Engineering

DRAWING TITLE: BEM Casting Jig Plunger			
DRAWING ID: MC-HDW-DRAW-13_1		DATE: 03/05/18	
DESIGNED BY: MC Olde		CHECKED BY:	
SIZE: A3	SHEET: 1/1	SCALE: 1:1	WEIGHT [kg]: 1.0
MATERIAL: Alu. 6060		TOLERANCES (UNLESS STATED OTHERWISE): +/- 0.05mm	